Exhibit P

UNITED STATES DISTRICT COURT
FOR THE EASTERN DISTRICT OF TEXAS
MARSHALL DIVISION

TQ DELTA, LLC, *Plaintiff,* v. **COMMSCOPE HOLDING COMPANY, INC., COMMSCOPE INC., ARRIS US HOLDINGS, INC., ARRIS SOLUTIONS, INC., ARRIS TECHNOLOGY, INC., and ARRIS ENTERPRISES, LLC** *Defendants.*	CIV. A. NO. 2:21-CV-310-JRG (Lead Case)
TQ DELTA, LLC, *Plaintiff,* v. **NOKIA CORP., NOKIA SOLUTIONS AND NETWORKS OY, and NOKIA OF AMERICA CORP.,** *Defendants.*	CIV. A. NO. 2:21-CV-309-JRG (Member Case)

OPENING EXPERT REPORT OF MARK R. LANNING ON THE INVALIDITY OF THE ASSERTED CLAIMS OF THE FAMILY 10 PATENTS
(U.S. PATENT NOS. 9,154,354; 8,937,988)

TABLE OF CONTENTS

Page

I. INTRODUCTION

1. My name is Mark Lanning. I have been asked by CommScope Holding Company, Inc., CommScope Inc., ARRIS US Holdings, Inc., ARRIS Solutions, Inc., ARRIS Technology, Inc., and ARRIS Enterprises, LLC (collectively, "CommScope") and Nokia of America Corporation, Nokia Corporation, and Nokia Solutions and Networks, Oy (collectively, "Nokia") (together, "Defendants") to provide this report in connection with the above-captioned District Court action.

2. Specifically, I have been asked to give expert opinion and testimony regarding whether claim 10 of U.S. Patent No. 9,154,354 ("the '354 Patent") and claim 16 of U.S. Patent No. 8,937,988 ("the '988 Patent") are valid or invalid. I understand these patents are referred to as "the Family 10 Patents."

3. My report is based on the information that is currently available to me. My analysis is ongoing. As I discover new material, or as new material is presented to me, I may continue to review such material. As a result, I reserve the right to modify or supplement my opinions, as well as the basis for my opinions, based on the nature and content of the documentation, data, proof and other evidence or testimony that the Plaintiff or its experts may present or based on any additional discovery or other information provided to me or found by me in this matter. I also reserve the right to present exhibits and demonstratives as appropriate to help demonstrate and explain my opinions if I am asked to testify at trial.

II. BACKGROUND AND QUALIFICATIONS

4. I have summarized in this section my educational background, work experience, and other relevant qualifications. A detailed curriculum vitae showing more of my credentials is attached to this report as Appendix A. I have extensive development and network design

experience in the field of electrical and optical transmission systems, the Public Telephone Switching Network (PSTN) and cellular networks.

5. I am currently the president of two active consulting companies: Telecom Architects, Inc. and Reticle Consulting, LLC. I have over 40 years of experience in a wide variety of communication technologies including, but not limited to, different types of circuit-switched and packet-switched networks, cellular networks and their components, advanced cellular network based services, Public Switched Telephone Network ("PSTN") networks, local loop connection equipment including xDSL systems, VoIP networks, Advanced services that use Intelligent Networking ("Advanced Intelligent Network" or "AIN") network elements, and various signaling protocols (e.g., Signaling System 7 ("SS7") and Integrated Digital Services Network ("ISDN")).

6. Since 1995, I have also provided second generation (2G) and third generation (3G) Code Division Multiple Access (CDMA) network architecture and equipment design and implementation consulting services to companies such as Nextel. While consulting for Nextel, which has since become part of Sprint, as one of the network architects for its iDEN network, one of my responsibilities was the design for its packet switched and SONET transmission networks that were used to carry the voice and data of the cellular network and all the VoIP traffic for its dispatch network. At the time, Nextel's packet-switched network was one of the largest in the U.S.

7. I have developed software for many types of computer systems ranging in size from large scale distributed computer systems that used hundreds of computers down to a single personal computer. I have also used many different types of operating systems and programming

languages, including creating software applications that interfaced with operating systems for at least: process creation and scheduling; memory management; and inter-process communication.

8. My experience that is specifically relevant to the report began in 1985 when I was hired by Telinq, Inc. (now part of ADC Telecommunications, Inc.) as their director of software development and was later promoted to vice president of hardware and software development. Telinq initially focused on the development of high-speed digital multiplexers and analyzers for DS1, DS3 TDM transmission systems and later built SONET multiplexing equipment. This hardware consisted of multiple microprocessors for operation and control and custom designed high-speed gate arrays for the signal processing and multiplexing functions.

9. Beginning in 1991, I have been responsible for the design and implementation of multiple packet-switched networks and their required interfaces to circuit-switched networks. Examples of these networks are British Telecom in the U.K. and Nextel in the U.S.

10. I also have gained additional experience in my role as an expert regarding the implementation, configuration, installation, and operation of many of the same or similar types of accused devices that are at issue in this case. Specifically, these cases are:

- Cisco Systems, Inc. vs. Alcatel USA, Inc. and Alcatel S.A. A case regarding switching, optical (SONET) transmission and cross connect systems;
- Ciena Corporation vs. Nortel Networks Inc. A case regarding SONET, ATM, TDM and Packet Switching equipment and packet network routing methods;
- QPSX Developments 5 Pty Ltd. v. Ciena Corporation et al. A case regarding statistical multiplexing of data in high-speed digital communication networks;
- Alberta Telecommunications Research Centre (TR Labs) vs. AT&T Corporation. A case regarding TDM and SONET transmission in high-speed transmission networks; and
- Genband U.S. LLC v. Metaswitch Networks Ltd and Countersuit. Multiple cases that involved many different types of local loop and network equipment that are used in DSL, packet, voice and high-speed transmission networks.

11. In addition to my experience listed above, for at least the past ten years, in connection with my consulting work and otherwise, I have worked extensively with the 3G, 4G and 5G network standards and their associated equipment and protocols including through my study of each new release of these standards, technical books and trade publications and by evaluating the functionality of many different types of network equipment, mobile devices, baseband chipsets and literally thousands of cellular oriented patents.

12. I am a member of the Institute of Electrical and Electronics Engineers (IEEE), including the IEEE Standards Association. I am also a member of the Association for Computing Machinery (ACM). I was also a member of the American National Standards Institute (ANSI) T1 and T1X1 standard groups responsible for the definition and standardization of the Advanced Intelligent Network (AIN) and Signaling System 7 (SS7) protocol. The relevant parts of the standards created by these two groups was incorporated by the CCITT for the international SS7 standard.

13. I received a B.S. in Computer Science from SMU in 1983.

14. A complete list of cases in which I have testified at trial, hearing, or by deposition within the preceding five years is provided in my curriculum vitae, which is attached as Appendix A to my report.

15. Based on my education and experience, I believe I am qualified to render the opinions set forth here.

III. COMPENSATION

16. I am being compensated for my work on this litigation at my customary hourly rate of $550 per hour, plus reasonable expenses. I have received no additional compensation of any kind for my work on this case. No part of my compensation is dependent on the conclusions that I reach or the outcome of this case.

IV. DOCUMENTS AND OTHER MATERIALS RELIED UPON

17. My opinions are based on my years of education, research and experience, as well as my investigation and study of the relevant materials.

18. In developing my opinions, I have considered the ’988 and ’354 Patents, the file histories for the ’988 and ’354 Patents, the parties’ claim construction briefing and the Court’s claim construction order, and other documents specifically identified in this report, in their entirety, even if only portions of these documents are discussed herein as an exemplary fashion. For instance, I may rely on sections of referenced documents in addition to those referenced in this report, and may create slides or demonstratives that add detail to the matters discussed below to provide support for my opinions expressed herein. For convenience, a list of documents I have relied upon is attached hereto as Appendix B.

19. Additionally, I have considered my own experience and expertise concerning the knowledge of a person having ordinary skill in the relevant art during the timeframe of the claimed priority date of the Family 10 Patents. I have reviewed information generally available to, and relied upon by, a person having ordinary skill at the time of the alleged invention.

20. I was told to assume the time of the alleged invention is April 18, 2000, the date on which the earliest-filed provisional application, No. 60/197,727, was filed. I am also informed, however, that once an accused infringer has introduced sufficient evidence to put at issue whether there is prior art alleged to anticipate the claims being asserted, and that prior art is dated earlier than the apparent effective date of the asserted patent claim, the patentee has the burden of going forward with evidence and argument to the contrary.

V. SUMMARY OF OPINIONS

21. Claim 10 of the '354 Patent and claim 16 of the '988 Patent (collectively, "Asserted Claims") are invalid as either anticipated and/or rendered obvious by the prior art cited in this report, as summarized below.

22. It is also my opinion that claim 10 of the '354 Patent and claim 16 of the '988 Patent are invalid as lacking written description and enablement.

23. A summary of my opinions is below:

Claim	Invalid Under	Prior Art
'354 Patent, claim 10; '988 Patent, claim 16	35 U.S.C. § 102	Peeters
'354 Patent, claim 10; '988 Patent, claim 16	35 U.S.C. § 103	Cai in view of Peeters
'354 Patent, claim 10; '988 Patent, claim 16	35 U.S.C. § 103	Kapoor in view of Peeters
'354 Patent, claim 10; '988 Patent, claim 16	35 U.S.C. §§ 102, 103	Chow
'354 Patent, claim 10; '988 Patent, claim 16	35 U.S.C. § 103	Kapoor in view of Chow
'988 Patent, claim 16	35 U.S.C. §§ 102, 103	TNETD8000 User Guide
'354 Patent, claim 10; '988 Patent, claim 16	35 U.S.C. §112	N/A

VI. STATEMENT OF RELEVANT LEGAL PRINCIPLES

24. I am not an attorney and will not offer opinions on the law. I have, however, an understanding of several principles concerning invalidity that I have used in arriving at my stated conclusions in this report.

25. I was requested to consider issues regarding invalidity of the Asserted Claims in this litigation and specifically address the following topics:

- the level of skill of persons who would have worked in the field around the time of the alleged inventions;
- if the claims are invalid as anticipated or obvious; and
- how, if at all, such a person would have understood the meaning and scope of these claims, and thus whether any of the claims are lack written description or enablement.

A. Presumption of Validity

26. I understand that in deciding whether to issue a patent, the U.S. Patent and Trademark Office ("USPTO") examines the patent specification, its claims, and prior art references the examiner finds or the applicant discloses to determine whether the patent application and its claims meet the requirements for patentability.

27. I understand that prior art is defined as including, but not limited to, issued patents, published patent applications, and other printed or electronic publications that were publicly accessible such that a person of ordinary skill exercising reasonable diligence could locate it. I also understand that prior art includes inventions that were known, used, in public use, or on sale in this country. I have also been told that a patent applicant can describe prior art in the "Background of the Invention" section of their patent.

28. I understand that each claim of a patent issued by the USPTO is presumed valid by law. This presumption of validity is overcome, however, if the party seeking to invalidate a claim proves invalidity by clear and convincing evidence, which I understand to mean evidence that convinces you that it is highly probable that the particular proposition is true. I understand that the clear and convincing standard is a higher burden of proof than by a preponderance of the evidence, the latter of which is something that is simply more likely than not.

29. I understand that the first step in determining whether a patent claim is invalid is to properly construe the claims. I also understand that the claims must be construed the same way in determining invalidity (or validity) and non-infringement (or infringement). I further understand that generally a claim should not be limited to a preferred or exemplary embodiment in the specification, but that in certain cases, the scope of the right to exclude may be limited by a narrow disclosure or by positions taken, such as by statements made during the prosecution

history. I also understand the claims must be supported by the specification. Also, to the extent that a patent claims priority to an earlier filed application, a patent claim is only entitled to the priority of an earlier filed application if the claims are fully supported by the disclosure in that earlier filed application.

B. Claim Construction

30. My opinions are based on the Court's constructions and, where the Court did not construe a term, the meaning that term would have had to a person having ordinary skill in the art in light of the specification and the prosecution history at the time of the filing of the earliest priority application.

C. Prior Art

31. Prior art includes any of the following items received into evidence during trial:

- any product or method that was publicly known or used by others in the United States before the date of invention;
- patents that issued more than one year before the filing date of the patent, or before the date of invention;
- publications having a date more than one year before the filing date of the patent, or before the date of invention;
- any product or method that was in public use or on sale in the United States more than one year before the patent was filed; and
- any product or method that was made by anyone before the named inventors created the patented product or method where the product or method was not abandoned, suppressed, or concealed.

32. It is my understanding that in order to qualify as a printed publication within the meaning of 35 U.S.C. § 102, a reference must have been sufficiently accessible to the public interested in the art. Whether a reference is publicly accessible is determined on a case-by-case basis based on the facts and circumstances surrounding the reference's disclosure to members of the public. A reference is considered publicly accessible if it was disseminated or otherwise made available to the extent that persons interested and ordinarily skilled in the subject matter or art exercising reasonable diligence, can locate it.

D. Anticipation Under 35 U.S.C. § 102

33. I have been informed by counsel and understand that a claim is invalid on the basis of anticipation (under 35 U.S.C. § 102) if a single prior art reference discloses, either expressly or inherently, each and every element of the claimed invention. If the single prior art reference fails to disclose even one claim element, it does not anticipate the claim.

34. I understand that, although anticipation cannot be established through a combination of references, additional references may be used to interpret the allegedly anticipating reference by, for example, indicating what the allegedly anticipating reference would have meant to one of ordinary skill in the art. However, for the claim to be anticipated, I understand that these other references must make clear that the missing descriptive matter in the patent claim is necessarily or implicitly present in the allegedly anticipating reference, and that it would be so recognized by one of ordinary skill in the art.

35. It is also my understanding that a claim is invalid if the claimed invention was known or used by others in the United States, or was in public use or on-sale before the critical date.

36. Consistent with what I noted above regarding the burden of proof, I have written this report with the understanding that anticipation must be shown by clear and convincing evidence.

37. A single prior art reference may anticipate without disclosing a feature of the claimed invention if such feature is necessarily present, or inherent, in that reference.

38. Under the principles of inherency, if the prior art necessarily functions in accordance with or includes the claimed elements, it anticipates. However, the prior art reference must necessarily include the non-disclosed element. Mere probabilistic inherency, or the

presence of an unrecognized de minimis quantity of a claimed substance in the prior art, cannot anticipate a later patent or patent application.

39. A prior art reference alleged to be anticipatory must also enable one of ordinary skill in the art to make the claimed invention without undue experimentation. There is a rebuttable presumption that prior art patents are enabled.

40. In my opinions below, when I say that a person of ordinary skill would understand, readily understand, or recognize that an element or aspect of a claim is disclosed by a reference, I mean that the element or aspect of the claim is disclosed explicitly to a person of ordinary skill in the art.

E. Obviousness Under 35 U.S.C. § 103

41. I further understand that a claimed invention is not patentable under 35 U.S.C. § 103 if the differences between the invention and the prior art are such that the subject matter as a whole would have been obvious at the time the invention was made to a person having ordinary skill in the art to which the subject matter pertains.

42. I understand that a claim can be found invalid as obvious if the design incentives or market forces provided a reason to make an adaptation, and the invention resulted from the application of the prior knowledge in a predictable manner. I understand that a claim can be found invalid as obvious if the claim would have been obvious because the substitution of one known element for another would have yielded predictable results to one of ordinary skill in the art at the time of the invention. I understand that a claim can be found invalid as obvious if the claim would have been obvious because the technique for improving a particular class of devices was part of the ordinary capabilities of a person of ordinary skill in the art. I understand that a claim can be found invalid as obvious if the claim would have been obvious because a particular known technique was recognized as part of the ordinary capabilities of one skilled in the art. I

understand that a claim can be obvious in light of a single reference, without the need to combine references, if the elements of the claim that are not found in the reference can be supplied by the common sense of one of skill in the art.

43. In evaluating whether a claim would have been obvious, I have also considered the following factors:

- Whether the Plaintiff has identified a reason that would have prompted a person of ordinary skill in the art to combine the requirements or concepts from the prior art in the same way as in the claimed invention;
- Whether the claimed invention applies a known technique that had been used to improve a similar device or method in a similar way; and
- Whether the claimed invention would have been obvious to try, meaning that the claimed innovation was one of a relatively small number of possible approaches to the problem with a reasonable expectation of success by those skilled in the art.

44. I understand that it is important to be careful not to determine obviousness using hindsight because many true inventions can seem obvious after the fact. Obviousness is determined from the position of a person of ordinary skill in the art at the time the claimed invention was made, and it is improper to consider what is known today or what is learned from the teaching of the patent. It is improper to use the ’988 and ’354 Patents as a road map for selecting and combining prior art.

45. The ultimate conclusion of whether a claim is obvious should be based on a determination of the following factual issues:

- The level of ordinary skill in the art that someone would have had at the time the claimed invention was made;
- The scope and content of the prior art;
- The differences, if any, that existed between the claimed invention and the prior art; and
- Secondary considerations or objective evidence of non-obviousness.

46. Secondary considerations or objective evidence of non-obviousness include the following:

- Commercial success of a product due to the merits of the claimed invention;
- A long-felt, but unsolved, need for the solution provided by the claimed invention;
- Unsuccessful attempts by others to find the solution provided by the claimed invention;
- Copying of the claimed invention by others;
- Unexpected and superior results from the claimed invention;
- Acceptance by others of the claimed invention as shown by praise from others in the field of the invention or from the licensing of the claimed invention; and
- Disclosures in the prior art that criticize, discredit, or otherwise discourage the claimed invention and would therefore tend to show that the invention was not obvious.

47. I have written this report with the understanding that obviousness must be shown by clear and convincing evidence.

F. Enablement and Written Description Under 35 U.S.C. § 112, ¶ 1

48. I understand that a patent must contain an enabling disclosure. The specification must contain a written description of the invention, and of the manner and process of making and using it so as to enable a person skilled in the art to make and use the invention. Because patents are presumed valid, lack of enablement must be proven by clear and convincing evidence.

49. Enablement is not precluded where a reasonable amount of routine experimentation is required to practice a claimed invention, however, such experimentation must not be undue. Whether a disclosure requires undue experimentation is not a single, simple factual determination, but rather is a conclusion reached by weighing many factual considerations.

50. In determining whether a disclosure requires undue experimentation, I understand that the relevant considerations can include:

- the quantity of experimentation necessary;
- the amount of direction or guidance presented;
- the presence or absence of working examples;
- the nature of the invention;
- the state of the prior art;
- the relative skill of those in the art;
- the predictability of the art; and

- the breadth of the claims.

51. Not every one of these factors need to be considered.

52. While the existence of a working example of the invention in the specification may be considered as one of many factors of sufficient enablement, working examples are, however, not required to satisfy the enablement requirement. Compliance with the enablement requirement does not turn on whether examples are disclosed in an application so long as the invention is otherwise disclosed in an enabling manner. Indeed, the importance of working examples may vary with the predictability of the art. Unlike in unpredictable arts, such as the biological, chemical, and pharmaceutical fields, the presence of a single embodiment may enable a broad claim when a more predictable art is in question, such as software design.

53. Elements and examples in the specification do not generally limit what is covered by the claims. A specification need not enable a perfected, commercially viable embodiment absent a claim element to that effect.

54. The enablement requirement is separate and distinct from the description requirement.

55. I understand that a patent must comply with a written description requirement by conveying with reasonable clarity to those skilled in the art that, as of the priority date sought, the inventor was in possession of the alleged invention, namely that the inventor had invented each feature that is included as a claim element. I have been informed that I am not to look for verbatim descriptions of the claim elements in the earlier-filed applications. Instead, I understand that the written description doctrine requires the disclosure of an application to adequately describe the invention so that a person of ordinary skill in the art can recognize that the patentee actually invented what is claimed in the patent at the time of filing. In other words, the question is whether

a person of ordinary skill in the art would have understood the inventors to have possessed the invention being claimed based on what is described in the application when it is filed. The disclosure may be either express disclosure (i.e., constituting text, figures, and other descriptive materials) or inherent. A disclosure is inherent if a person of ordinary skill in the art would have understood that the claimed subject matter is necessarily present in the material described in the application. I understand that the written description inquiry looks to the figures and the originally-filed claims in addition to the descriptive text of the application.

56. I also understand that the written description inquiry is not an inquiry into what would have been obvious over what is actually disclosed in the application. The question is not what a person of ordinary skill in the art could have made based on the teachings of the application. Instead, the inquiry focuses on what was described and how a person of ordinary skill in the art would have understood the disclosure.

VII. LEVEL OF SKILL IN THE ART

57. I am informed and understand that the claims of a patent are judged from the perspective of a hypothetical construct involving a "person of ordinary skill in the art." The "art" is the field of technology to which the patent is related. I understand that the purpose of using the viewpoint of a person of ordinary skill in the art is for objectivity. I understand that a person of ordinary skill in the art is presumed to know and be familiar with all of the relevant art in the field at the time of invention.

58. I was also asked to provide an opinion regarding the skill level of a person of ordinary skill in the art of the Family 10 Patents. I considered several factors, including the types of problems encountered in the art, the solutions to those problems, the pace of innovation in the field, the sophistication of the technology, my experience as a person who worked in the art prior to the Family 10 Patents' priority date, and the education level of active workers in the field.

59. At the time of the alleged invention, a person having ordinary skill in the art would have would have had a bachelor's degree in electrical or computer engineering and 5 years of experience in telecommunications or a related field, a Master's degree in electrical engineering and 2-3 years of experience in telecommunications or a related field, or a Ph.D. in electrical engineering with 1-2 years of experience in telecommunications or a related field.

60. I understand that TQ Delta proposes that a person of ordinary skill in the art "would have had a bachelor's degree in electrical engineering with 2-3 years of experience in DSL communication systems." Dkt. No. 124-12 at ¶20.

61. The Defendants' proposed level of ordinary skill in the art is the more appropriate level because it more accurately reflects the educational level of workers in the field. I believe that at least five years of experience in this field, without a master's degree, more accurately reflects the level work experience that workers in the field would have typically had that would be tasked to solve the problem presented by the '988 and '354 Patents. However, it is not uncommon for workers in the field of telecommunications or a related field to have a variety of technical degrees. Additional education might substitute for some of the experience, and substantial experience might substitute for some of the educational background.

62. Nevertheless, I was a person of ordinary skill in the art as of April 18, 2000, under either proposed definition. And my opinions express below are accurate and applicable under either level of ordinary skill in the art.

VIII. BACKGROUND OF THE TECHNOLOGY

A. Relevant Terminology

63. I am not intending to modify the Court's constructions in any way in this section but am simply providing basic definitions for the relevant terms used in the Family 10 Patents and the prior art documents referenced in this report.

245. As discussed above in § XII.A.1.j, and incorporated herein, Peeters also discloses claim 10.g. Thus, Cai in view of Peeters further discloses claim 10.g.

246. Consequently, claim 10 would have been obvious to a person having ordinary skill in the art in view of Cai and Peeters.

3. U.S. Patent No. 6,516,027 to Kapoor et al. ("Kapoor") in View of Peeters

247. Kapoor in view of Peeters renders obvious each element of claim 10 of the '354 Patent.

a. Brief Description of Kapoor

248. U.S. Patent No. 6,516,027 to Kapoor et al. ("Kapoor") is titled "A Method and Apparatus for Discrete Multitone Communication Bit Allocation," and claims a priority date of February 18, 1999. Kapoor issued on February 4, 2004 from a patent application that was filed on February 18, 1999, and therefore constitutes prior art to the '354 Patent under 35 U.S.C. §102(e).

249. Kapoor discloses "[a] method and apparatus for allocating bits to subchannels in a discrete multitone environment." Kapoor at Abstract. In particular, the method disclosed in the patent "employs the use of precalculated and prestored look-up tables which take into account a desired bit error rate, signal to noise ratio gap for particular coding scheme, and gain scaling factor." *Id.* Kapoor describes techniques to determine "bit allocation values calculated based on different margins, different $P_e/2$[6] error rates, and different coding gains." *Id.* at 8:39-42.

250. As noted above in §IX.A.1 Kapoor, Kapoor was considered by the examiner during the prosecution history. The examiner, however, failed to consider Kapoor in view of

[6] Kapoor defines $P_e/2$ as the "symbol error rate per dimension and uses it interchangeably with the Bit Error Rate (BER)." Kapoor at 5:41-47.

Peeters. As discussed below, claim 10 of the '354 Patent is rendered obvious by Kapoor in view of Peeters.

b. Brief Description of Peeters

251. I provided a brief description of Peeters above. *See supra*, §XII.A.1.a, which I incorporate by reference here.

c. Motivation to Combine Teachings of Kapoor With Teachings of Peeters

252. A person having ordinary skill in the art would have been motivated to combine the teachings of Kapoor with the teachings of Peeters as recited in claim 10 of the '354 patent and would have had a reasonable expectation of success in making the combination.

253. Both Kapoor and Peeters are directed to improving the performance of DMT systems. Kapoor's objective is to provide bit loading (i.e., the allocation of bits to subcarriers) techniques that improve on existing bit loading algorithms. *See, e.g.*, Kapoor at Abstract, 3:7-4:21. Peeters is directed to allocating data elements to sets of carriers. Peeters at 2:3-5. Peeters is used in ADSL applications but can also be implemented in other transmission systems. *Id.* at 7:54-57, 3:47-58, claim 11.

254. The disclosures of Peeters are complementary to those of Kapoor, and it would have been obvious to a person having ordinary skill in the art to combine them. For example, Kapoor states that prior art bit loading algorithms "do not support a bit allocation method which allows different subchannels to operate at different bit error rates or margins," but that it would be "desirable to have a method which can allocate bits to subchannels based on a desired bit error rate, and further to be able to allow subchannels to operate at different bit error rates." Kapoor at 4:8-10, 17-21. Kapoor describes that its techniques allow different subchannels to "have bit allocation values calculated based on different margins, different $P_e/2$ error rates, and different

coding gains. . . ." *Id.* at 8:39-42. Kapoor thus discloses that different margins can be used on different subchannels. But Kapoor does not describe in detail how to determine what the different margins on the different subchannels should be. Accordingly, a person having ordinary skill in the art would have sought references addressing how to determine what the different margins on different subchannels should be.

255. A person having ordinary skill in the art would thus have been motivated to add the method of Peeters to the communication devices of Kapoor, and would have found it trivial to do so. More specifically, Kapoor describes reducing the measured SNR of each subchannel by the difference between the margin and the coding gain (i.e., by the quantity γ_margin-γ_coding), and then determining the bit allocation and gain scaling values using the resulting reduced measured SNR values. *See, e.g.,* Kapoor at 7:43-10:46. Based on the teachings of Peeters, a person having ordinary skill in the art would have been motivated to use Peeters' method of grouping subsets of carriers together and assigning certain data to the respective subsets of carriers. *See e.g.,* Peeters at 3:16-24. A skilled artisan would have found this modification trivial, particularly because Kapoor discloses that different margins can be used for different subchannels, and Peeters discloses allocating data elements to different sets of carriers.

256. Thus, a person having ordinary skill in the art would have had a strong expectation of success in combining Peeter's teachings (e.g., allocating data elements to different sets of carriers) with Kapoor's bit allocation procedures that allow the noise margin, error probability, and coding gain to vary from subchannel to subchannel.

a. Claim 10

257. Kapoor in view of Peeters discloses each element of claim 10 of the '354 Patent.

b. Claim 10.pre "A multicarrier communications transceiver operable to:"

258. I understand that CommScope and Nokia do not concede that the preamble is limiting. To the extent that the preamble is limiting, Kapoor discloses Claim 10.pre "A multicarrier communications transceiver operable to."

259. Kapoor details a method and apparatus for discrete multitone communication bit allocation. Kapoor at Title. Kapoor relates to a discrete multitone modulation ("DMT") communication system. "The present invention relates to data communications, specifically to an apparatus and method for allocating bits among carrier tone subchannels (bins) in a discrete multitone modulation (DMT) communication system." *Id.* at 1:7-11.

260. Kapoor also discusses SNR gaps that depend on the modulation and coding used in a transmitter. "The detail behind the derivation of this equation is described below. Recall that the SNR gap depends on the type of modulation and coding used in a transmitter as well as the target bit error rate (BER). This same expression can be rewritten in order to express the SNR required to achieve a particular number of bits per subchannel. Because this expression must hold after bit allocation has been completed, gain scaling should be done at the transmitter to ensure that the received SNR in the i subchannel corresponds to b_i bits in that Subchannel." *Id.* at 3:58-67.

261. Moreover, the method and apparatus operates over a computer, that connects with a DSL network interface and a DTE interface. "Data terminal equipment interface 16 and DSL network interface 20 are used **to send and receive data to and from data terminal equipment and a DSL network**, respectively." *Id.* at 6:13-16; *Id.* at Figure 2.

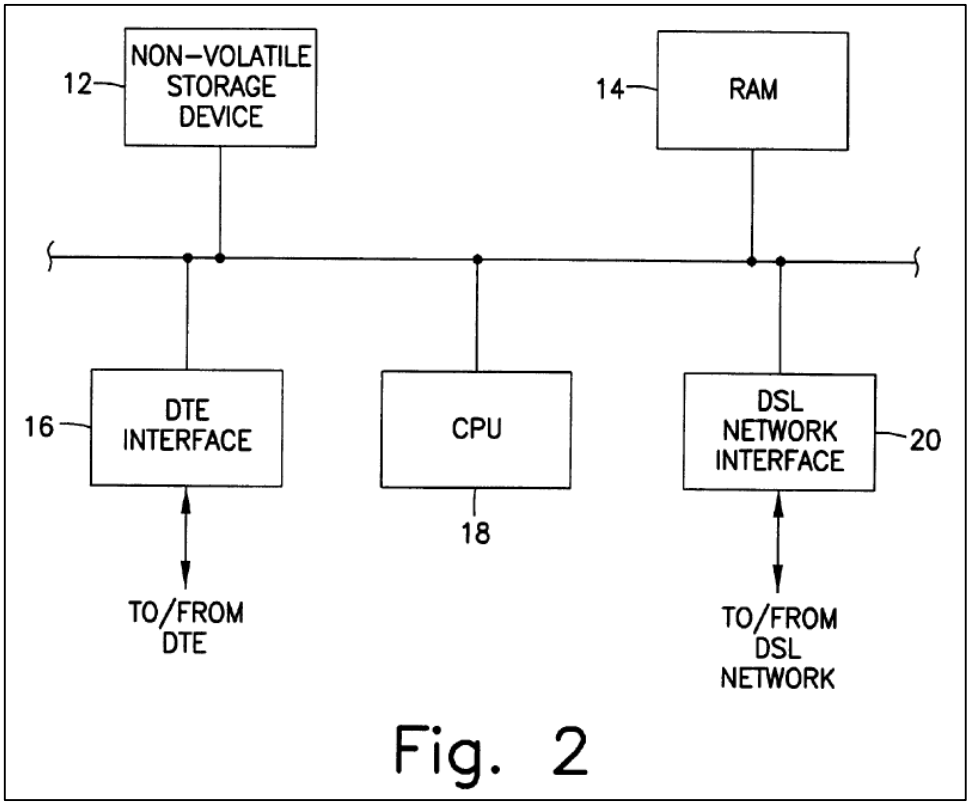

Id. at Fig. 2.

262. Thus, Kapoor discloses the preamble of claim 10, to the extent it is limiting.

263. I explained above (*see supra*, § XII.A.1.c), Peeters also discloses the preamble of claim 10, to the extent it is limiting. I incorporate that explanation by reference here.

264. Thus, Kapoor in view of Peeters further discloses claim 10.pre.

c. Claim 10.a "receive a multicarrier symbol comprising a first plurality of carriers"

265. Kapoor discloses claim 10.a "receive a multicarrier symbol comprising a first plurality of carriers."

266. Kapoor discloses receiving a multicarrier symbol. "Subsequent DMT multicarrier modulation equipment made use of digital signal processing techniques including Fast Fourier Transforms and Inverse Fast Fourier Transforms. Digital signal processing allowed a single DMT

communication device to be used to modulate all subchannels, thereby improving reliability and lowering the cost of communications." *Id.* at 2:7-13.

267. Kapoor discloses a plurality of carriers. "A preferred approach is to load each subchannel based on the individual transmission characteristics of that subchannel. Better subchannels, should carry more information than poorer quality subchannels. This allows an efficient use of the communication channel resources." *Id.* at 2:16-20. The indication of multiple subchannels means there are a plurality of carriers. The underlying invention in Kapoor allows for SNR ratios are measured for each plurality of subchannels in a communication system, which is consistent with having a plurality of channels with different SNR ratios as disclosed in the '354 Patent.

268. In accordance with this method, the stored table is comprised of a plurality of minimum signal-to-noise ratio values and a corresponding plurality of respective bit values, the minimum signal-to-noise ratio values being determined in accordance with a maximum allowable gain scaling factor, wherein the signal-to noise ratio values also correspond to the plurality of respective bit values. It is another object of the present invention to provide a method of allocating bits to a plurality of transmission subchannels in a communication system, in which a measuring step measures a signal-to-noise ratio for each of the plurality of transmission subchannels. An adjusting step adjusts the measured signal-to-noise ratio in accordance with an SNR-margin and a coding gain. *Id.* at 4:32-46.

269. Moreover, different pluralities of carriers are grouped in Kapoor via the different subchannels which each group having different bit allocation values. "Similarly, the process can be repeated to create a set of tables for a different SNR gap for a different line coding technique (step 30). Different subchannels therefore, can each have bit allocation values calculated based

on different margins, different $P_e/2$ error rates, and different coding gains, subject to the quantity of tables stored in the communication device 10." *Id.* at 8:36-42.

270. Kapoor discloses at least two pluralities of carriers in Fig. 5 shown below and its associated text. Specifically, Figure 5 shows two different tables for carrier bit allocation based on the target BER for the carrier. The top table provides the required SNR_{vec} and SNR_{maxvec} values for allocations of different bits based on a target BER of 10^{-7}. The bottom table provides the same information but for a target BER of 10^{-8}. Thus, the bottom table defines a first plurality of carriers with a first plurality of bits based on a more stringent BER. The top table defines a second plurality of carriers with a second plurality of bits based on a less stringent BER. Kapoor describes that the two highlighted rows below for a 5-bit allocation require different SNR margins with:

> For example, in the ANSI Tl.413ADSLstandard Gmin=0.75 and Gmax=l.33 (±2.5 dB). SNRmaxvec tables for Pe/2 of 10^{-7} and 10^{-8} with the SNRmaxvec columns scaled by 1.33 are shown in FIG. 5. For example, the SNRmaxvec value for Pe/2 of 10^{-7} and a bit allocation of 5 bits corresponds to 2.9320e + 02 divided by 1.33, equalling 2.2045e+02. As a comparison, the same bit allocation of 5 bits yields an SNRmaxvec value for Pe/2 of 10^{-8} of 2.5516e + 02.

Id. at 8:20-24.

271. Therefore, Kapoor discloses both a first and second plurality of carriers.

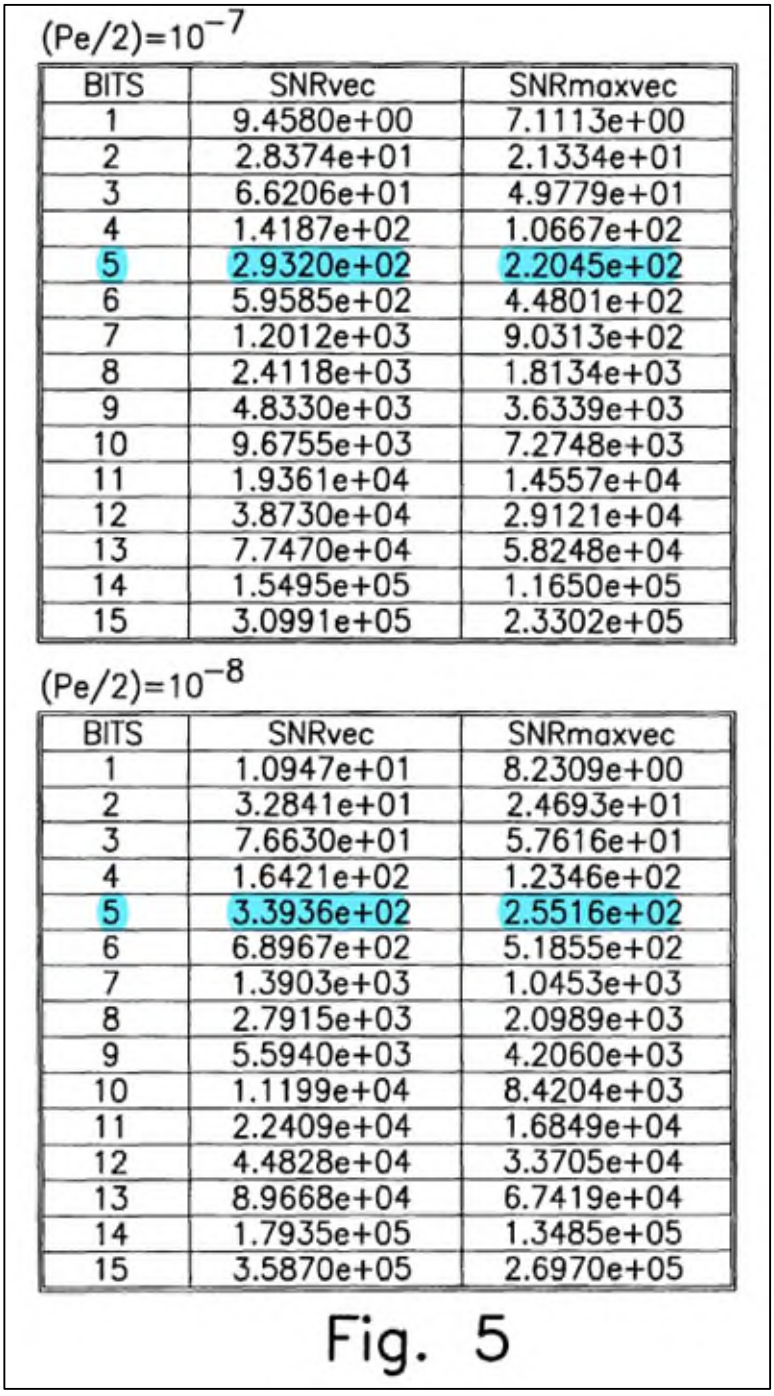

$(Pe/2)=10^{-7}$

BITS	SNRvec	SNRmaxvec
1	9.4580e+00	7.1113e+00
2	2.8374e+01	2.1334e+01
3	6.6206e+01	4.9779e+01
4	1.4187e+02	1.0667e+02
5	2.9320e+02	2.2045e+02
6	5.9585e+02	4.4801e+02
7	1.2012e+03	9.0313e+02
8	2.4118e+03	1.8134e+03
9	4.8330e+03	3.6339e+03
10	9.6755e+03	7.2748e+03
11	1.9361e+04	1.4557e+04
12	3.8730e+04	2.9121e+04
13	7.7470e+04	5.8248e+04
14	1.5495e+05	1.1650e+05
15	3.0991e+05	2.3302e+05

$(Pe/2)=10^{-8}$

BITS	SNRvec	SNRmaxvec
1	1.0947e+01	8.2309e+00
2	3.2841e+01	2.4693e+01
3	7.6630e+01	5.7616e+01
4	1.6421e+02	1.2346e+02
5	3.3936e+02	2.5516e+02
6	6.8967e+02	5.1855e+02
7	1.3903e+03	1.0453e+03
8	2.7915e+03	2.0989e+03
9	5.5940e+03	4.2060e+03
10	1.1199e+04	8.4204e+03
11	2.2409e+04	1.6849e+04
12	4.4828e+04	3.3705e+04
13	8.9668e+04	6.7419e+04
14	1.7935e+05	1.3485e+05
15	3.5870e+05	2.6970e+05

Fig. 5

Id. at Fig. 5 (annotated).

272. Kapoor discloses receiving a multicarrier symbol. "Data terminal equipment interface 16 and DSL network interface 20 are used to send and receive data to and from data terminal equipment and a DSL network, respectively." *Id.* at 6:13-16.

273. Thus, Kapoor discloses claim 10.a.

274. I explained above (*see supra*, § XII.A.1.d), Peeters also discloses claim 10.a. I incorporate that explanation by reference here. Thus, Kapoor in view of Peeters further discloses claim 10.a.

d. Claim 10.b "and a second plurality of carriers"

275. Kapoor discloses claim 10.b "and a second plurality of carriers."

276. Different pluralities of carriers are grouped in Kapoor via the different subchannels which each group having different bit allocation values. "Similarly, the process can be repeated to create a set of tables **for a different SNR gap** for a different line coding technique (step 30). Different subchannels therefore, **can each have bit allocation values calculated based on different margins**, different $P_e/2$ error rates, and different coding gains, **subject to the quantity of tables stored in the communication device 10**." *Id.* at 8:36-42.

277. Kapoor discloses at least two pluralities of carriers in Figure 5 shown below and its associated text. Specifically, Figure 5 shows two different tables for carrier bit allocation based on the target BER for the carrier. The top table provides the required SNR_{vec} and SNR_{maxvec} values for allocations of different bits based on a target BER of 10^{-7}. The bottom table provides the same information but for a target BER of 10^{-8}. Thus, the bottom table defines a first plurality of carriers with a first plurality of bits based on a more stringent BER. The top table defines a second plurality of carriers with a second plurality of bits based on a less stringent BER. Kapoor describes that the two highlighted rows below for a 5-bit allocation require different SNR margins with:

> For example, in the ANSI Tl.413ADSLstandard Gmin=0.75 and Gmax=l.33 (±2.5 dB). SNRmaxvec tables for Pe/2 of 10^{-7} and 10^{-8} with the SNRmaxvec columns scaled by 1.33 are shown in FIG. 5. For example, the SNRmaxvec value for Pe/2 of **10^{-7} and a bit allocation of 5 bits corresponds** to 2.9320e + 02 divided by 1.33, equalling 2.2045e+02. As a comparison, the same bit allocation of 5 bits yields an SNRmaxvec value for Pe/2 of **10^{-8}** of 2.5516e + 02.

Id. at 8:20-24.

278. Thus, Kapoor discloses claim 10.b.

279. I explained above (*see supra*, §XII.A.1.e), Peeters also discloses claim 10.b. I incorporate that explanation by reference here.

280. Thus, Kapoor in view of Peeters further discloses claim 10.b.

e. Claim 10.c "receive a first plurality of bits on the first plurality of carriers using a first SNR margin;"

281. Kapoor discloses claim 10.c "receive a first plurality of bits on the first plurality of carriers using a first SNR margin."

282. The Court has construed "SNR margin" as "a parameter used in determining the number of bits allocated to each of a plurality of carriers, where the value of the parameter specifies an extra SNR requirement assigned per carrier in addition to the SNR required to maintain a specified bit error rate (BER) for the communication link at a specified bit allocation." Claim Construction Memorandum and Order (Dkt. No. 169) at 116.

283. Kapoor meets the Court's definition for SNR Margin. Kapoor describes the "SNR gap" or "margin" as "the amount of additional signal-to-noise ratio in excess of the minimum required to achieve a given performance level for a particular type of modulation scheme with a particular SNR gap." Kapoor at 2:21-27.

284. Further, the "SNR gap is a function of a chosen probability of transmission error and the modulation and coding techniques. The SNR gap measures the inefficiency of the transmission method with respect to the best possible performance, assuming an additive white Gaussian noise channel. The SNR gap is often constant over a wide range of transmission rates which may be transmitted by the particular modulation coding technique. The channel capacity refers to the maximum data rate capable of being transmitted on a particular channel. The

optimum line coding technique has a SNR gap of zero dB. Although such an optimum line code requires infinite decoding/encoding delay and is infinitely complex, it has become practical at typical Digital Subscriber Line (DSL) speeds to implement modulation methods to achieve SNR gaps as low as 1-2 dB. Therefore, one factor to be considered during the bit allocation process is the transmission quality of each subchannel, in order to maximize the bit allocation for each subchannel." *Id.* at 2:21-45.

285. For the SNR required to maintain a specified BER, Kapoor discloses: "the SNR gap depends on the type of modulation and coding used in a transmitter as well as the target bit error rate (BER)." *Id.* at 3:59-61. "The need for an SNR margin factor is motivated by the presence of unforeseen additive noise impairments. It represents the additional noise power in dB that would be required to increase the $P_e/2$ rate to the specified value, for example, 10^{-7}." *Id.* at 7:47-51.

286. Kapoor further describes how the SNR margin is used in connection with bit allocation:

> The processing unit controls functions which **measure a signal-to-noise ratio** for each of the plurality of transmission subchannels, **adjust the measured signal-to noise ratio** in accordance with an **SNR-margin** and a coding gain, generate a plurality of signal-to-noise ratio difference values, select a bit allocation value for each of the plurality of transmission subchannels, **the bit allocation value corresponding to one of the plurality of signal-to-noise ratio difference values**, determine a gain scaling factor for each of the plurality of transmission subchannels, and store each of the bit allocation values and the gain scaling factors as one or more data structures in the memory.

Id. at 5:1-12.

287. These SNR margins have a corresponding bit value as disclosed in Kapoor. "In accordance with this method, the stored table is comprised of a plurality of minimum signal-to-noise ratio values and a **corresponding plurality of respective bit values**, the minimum signal-to-noise ratio values being determined in accordance with a maximum allowable gain scaling

factor, wherein the signal-to-noise ratio values also correspond to the plurality of respective bit values." *Id.* at 4:32-39.

288. Thus, Kapoor discloses claim 10.c.

289. I explained above (*see supra*, §XII.A.1.f), Peeters also claim 10.c. I incorporate that explanation by reference here.

290. Thus, Kapoor in view of Peeters further discloses claim 10.c.

f. Claim 10.d "receive a second plurality of bits on the second plurality of carriers using a second SNR margin;"

291. Kapoor discloses claim 10.d "receive a second plurality of bits on the second plurality of carriers using a second SNR margin."

292. I incorporate by reference my analysis for claim elements 10.pre, 10.a, 10.b, and 10.c.

293. The plurality of subchannels in Kapoor show that the reference discloses that each of the subchannels (carriers) have a separate SNR margin and that each subchannel has a different bit allocation value.

294. Kapoor describes that the two highlighted rows below for a 5-bit allocation require different SNR margins with:

> For example, in the ANSI Tl.413ADSLstandard Gmin=0.75 and Gmax=l.33 (±2.5 dB). SNRmaxvec tables for Pe/2 of 10^{-7} and 10^{-8} with the SNRmaxvec columns scaled by 1.33 are shown in FIG. 5. For example, the SNRmaxvec value for Pe/2 of 10^{-7} and a bit allocation of 5 bits corresponds to 2.9320e + 02 divided by 1.33, equalling 2.2045e+02. As a comparison, the same bit allocation of 5 bits yields an SNRmaxvec value for Pe/2 of 10^{-8} of 2.5516e + 02.

Id. at 8:20-24.

295. Therefore, Kapoor discloses both a first and second plurality of carriers.

$(Pe/2)=10^{-7}$

BITS	SNRvec	SNRmaxvec
1	9.4580e+00	7.1113e+00
2	2.8374e+01	2.1334e+01
3	6.6206e+01	4.9779e+01
4	1.4187e+02	1.0667e+02
5	2.9320e+02	2.2045e+02
6	5.9585e+02	4.4801e+02
7	1.2012e+03	9.0313e+02
8	2.4118e+03	1.8134e+03
9	4.8330e+03	3.6339e+03
10	9.6755e+03	7.2748e+03
11	1.9361e+04	1.4557e+04
12	3.8730e+04	2.9121e+04
13	7.7470e+04	5.8248e+04
14	1.5495e+05	1.1650e+05
15	3.0991e+05	2.3302e+05

$(Pe/2)=10^{-8}$

BITS	SNRvec	SNRmaxvec
1	1.0947e+01	8.2309e+00
2	3.2841e+01	2.4693e+01
3	7.6630e+01	5.7616e+01
4	1.6421e+02	1.2346e+02
5	3.3936e+02	2.5516e+02
6	6.8967e+02	5.1855e+02
7	1.3903e+03	1.0453e+03
8	2.7915e+03	2.0989e+03
9	5.5940e+03	4.2060e+03
10	1.1199e+04	8.4204e+03
11	2.2409e+04	1.6849e+04
12	4.4828e+04	3.3705e+04
13	8.9668e+04	6.7419e+04
14	1.7935e+05	1.3485e+05
15	3.5870e+05	2.6970e+05

Fig. 5

Id. at Fig. 5 (annotated).

296. The processing unit controls functions which measure a signal-to-noise ratio for each of the plurality of transmission subchannels, adjust the measured signal-to noise ratio in accordance with an SNR-margin and a coding gain, generate a plurality of signal-to-noise ratio difference values, select a bit allocation value for each of the plurality of transmission

subchannels, the bit allocation value corresponding to one of the plurality of signal-to-noise ratio difference values, determine a gain scaling factor for each of the plurality of transmission subchannels, and store each of the bit allocation values and the gain scaling factors as one or more data structures in the memory. *Id.* at 5:1-12.

297. A plurality is construed as meaning more than one, thus, there is a second plurality of bits on a second plurality of carriers which uses a second SNR margin.

298. Thus, Kapoor discloses claim 10.d.

299. I explained above (*see supra*, §XII.A.1.g), Peeters also claim 10.d. I incorporate that explanation by reference here.

300. Thus, Kapoor in view of Peeters further discloses claim 10.d.

g. Claim 10.e "wherein the first plurality of carriers is different than the second plurality of carriers,"

301. Kapoor discloses Claim 10.e "wherein the first plurality of carriers is different than the second plurality of carriers."

302. Kapoor discloses that a subset of channels differ from a different subset of channels such that it constitutes different carriers. Although the above description is directed to a bit allocation process in which all subchannels are analyzed and bits allocated, an alternative embodiment exists in which the bit allocation process is completed for a subset of subchannels, with the process not being completed for the remaining subchannels. For example, when the communication device has completed its training sequence and is operating in 'showtime', line degradation might lower the signal-to-noise ratios for certain subchannels such that the bit allocation process might need to be executed, and the bit allocation forwarding table and the gain scaling table updated to reflect the new bit allocations for the selected subchannels. "[T]he bit allocation process is completed for a subset of subchannels, with the process not being completed

for the remaining subchannels. . . . line degradation might lower the signal-to-noise ratios for certain subchannels such that the bit allocation process might need to be executed, and the bit allocation forwarding table and the gain scaling table updated to reflect the new bit allocations for the selected subchannels." *Id.* at 11:35-42. Here, where the process is completed for a set of subchannels and not for the other set of subchannels, it then follows that there is a difference in the first plurality of carriers versus the second plurality of carriers.

303. Thus, Kapoor discloses claim 10.e.

304. I explained above (*see supra*, § XII.A.1.h), Peeters also discloses claim 10.e. I incorporate that explanation by reference here.

305. Thus, Kapoor in view of Peeters further discloses claim 10.e.

h. Claim 10.f "wherein the first SNR margin is different than the second SNR margin,"

306. Kapoor discloses claim 10.f "wherein the first SNR margin is different than the second SNR margin." I incorporate by reference by analysis for claim element 10.d.

307. "Within this inventive system and method, a framework is provided which also supports the use of different $P_e/2$ rates and SNR margins for different subchannels in a communication line, and a process for allocating bits and gain scaling less than the entirety of subchannels." *Id.* at 11:51-55. As stated in Kapoor, different SNR margins can be used for different subchannels.

308. Thus, Kapoor discloses claim 10.f.

309. I explained above (*see supra*, § XII.A.1.i), Peeters also discloses claim 10.f. I incorporate that explanation by reference here.

310. Thus, Kapoor in view of Peeters further discloses claim 10.f.

i. Claim 10.g "and wherein the first SNR margin provides more robust reception than the second SNR margin."

311. Kapoor discloses claim 10.g "and wherein the first SNR margin provides more robust reception than the second SNR margin."

312. Kapoor discloses the contrast between SNR margins such that one can determine which is more robust. "Once an SNR_{vec} and SNR_{maxvec} table has been stored for a particular number of bits, the process can be repeated to create a table for a different BER (step 28). Similarly, **the process can be repeated to create a set of tables for a different SNR gap** for a different line coding technique (step 30). Different subchannels therefore, can each have bit allocation values calculated based on different margins, different $P_e/2$ error rates, and different coding gains, subject to the quantity of tables stored in the communication device 10." *Id.* at 8:34-42.

313. Moreover, Kapoor discloses that "because multiple tables corresponding to different $P_e/2$ values can be predetermined and stored, it is possible to allocate bits and establish gain scaling values for different subchannels using different P/2 values for those subchannels. For example, a $P_e/2$ value of 10^{-7} can be used to determine bit allocation and gain scaling for some subchannels, and a $P_e/2$ value of 10^{-8} can be used for the remaining subchannels. Of course, there is no limit to the number of different $P_e/2$ values which can be used, subject only the quantity of SNR tables stored in the communication device." *Id.* at 10:36-46.

314. Thus, Kapoor discloses claim 10.g.

315. I explained above (*see supra*, § XII.A.1.j), Peeters also discloses claim 10.g. I incorporate that explanation by reference here.

316. Thus, Kapoor in view of Peeters further discloses claim 10.g. Consequently, claim 10 would have been obvious to a person having ordinary skill in the art in view of Kapoor and Peeters.

4. Peter Sienpin Chow, *Bandwidth optimized digital transmission techniques for spectrally shaped channels with impulse noise,* STANFORD UNIVERSITY (May 1993) ("Chow")

317. The Chow reference anticipates and/or renders obvious each element of claim 10 of the '354 Patent.

a. Brief Description of Chow

318. *Bandwidth optimized digital transmission techniques for spectrally shaped channels with impulse noise* was published by Peter Sienpin Chow in conjunction with Stanford University in May 1993 ("Chow"). Chow was published in May 1993, and therefore constitutes prior art to the '354 Patent. The Chow reference recognizes that "[i]n order to reliably transmit and receive the highest data rate possible through such non-ideal channels, every components of the communication system needs to be optimized." Chow at Abstract. In particular, the dissertation focuses on optimization of the system transmission bandwidth via use of a multicarrier system using the Discrete Multitone modulation. *Id.*

319. I understand that the Chow reference was publicly available and thus is prior art. *See* Appendix C.

b. Claim 10

320. Claim 10 of the '354 Patent is anticipated and/or rendered obvious by Chow.

c. Claim 10.pre "A multicarrier communications transceiver operable to:"

321. I understand that CommScope and Nokia do not concede that the preamble is limiting. To the extent that the preamble is limiting, Chow discloses Claim 10.pre "A multicarrier communications transceiver operable to."

322. Chow applies "a **Discrete Multitone transceiver**, with optimized transmission bandwidth, to these three potential DSL applications." Chow at 78. Chow also discloses "[a] detailed description of the ADSL transmission environment is presented, and results of computer simulation on the performance of a DMT transceiver for ADSL are given." *Id.* at 79. Chow also presents "result of computer simulation on the performance of a DMT transceiver for ADSL." *Id.* at 79.

323. Figure 3.1 of Chow, copied below, is a block diagram of a DMT transmitter, and Figure 3.2, also copied below, is a block diagram of a DMT receiver. Thus, Chow discloses a multicarrier communications transceiver that includes both a transmitter and a receiver.

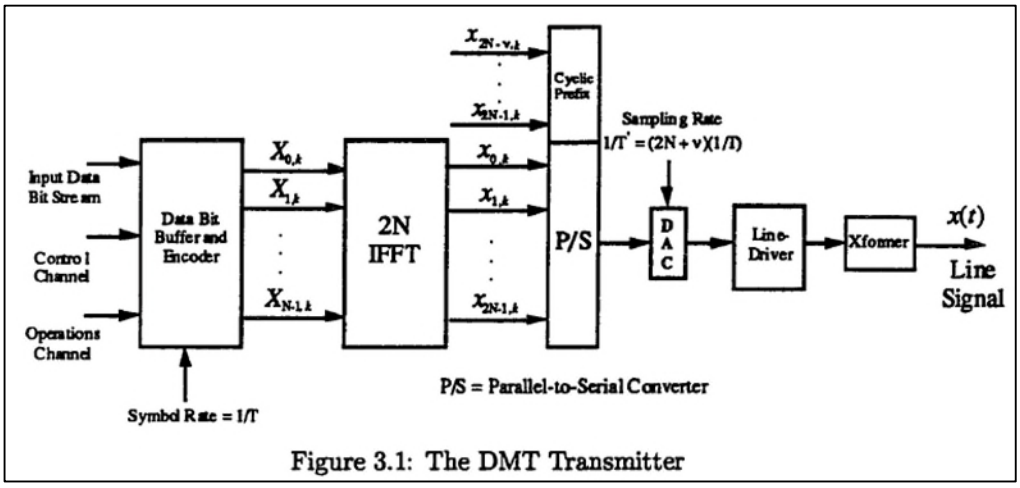

Figure 3.1: The DMT Transmitter

Id. at Fig. 3.1.

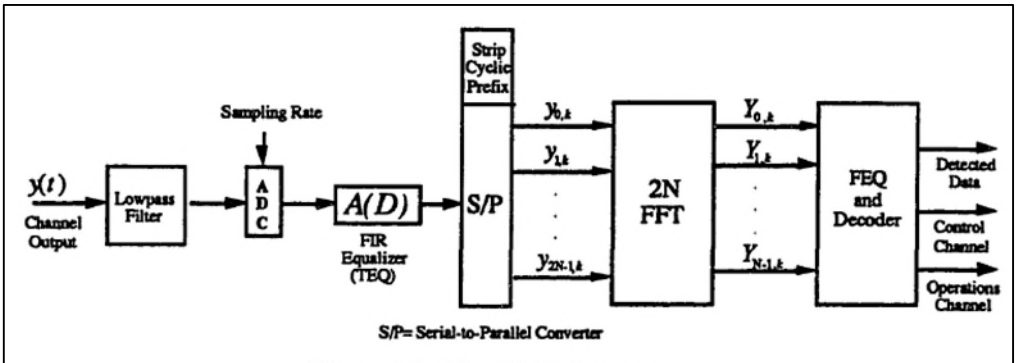

Figure 3.2: The DMT Receiver

Id. at Fig. 3.2

324. Chow also discloses studying a DMT transceiver: "We studied the effect of increasing the transmit power of the DMT transceiver, holding constant the system blocklength at 512 and VHDSL crosstalk coupling at KNEXT = 2×10^{-15} and KFEXT x d = 2.4×10^{-19}. Figure 5.18 shows the achievable throughputs as a function of transmit power for various signaling rates." *Id.* at 107. "Assuming that the crosstalker uses the same signaling strategy and power level as the DMT transceiver, as the transmit power increases the crosstalk noise level increases by the same proportion, and the overall SNR remains constant." *Id.* at 107-08.

325. Chow contains further references use of a DMT system, including an "emphasis . . . on impulse noise mitigation strategies designed specifically for a multicarrier modulation system (in particular, a DMT transceiver for ADSL), we will first briefly review some of the single-carrier, impulse noise mitigation methods that have been proposed in the literature for the sake of completeness." *Id.* at 123-24.

326. Chow also recognizes the benefits of a multicarrier system over a single carrier system. Benefits mentioned include benefits that are specifically contemplated in the '354 Patent, including reduction of interference by distributing over multiple carriers as opposed to a single carrier:

> Fortunately for a multicarrier DMT transceiver, superior impulse noise immunity relative to a single-carrier system is inherent due to its block processing nature. For the ideal case of a true impulse noise occurrence that corrupts only one time domain sample, the total energy of the noise pulse is then spread evenly over every carrier, so in the case of a DMT system implemented with a length 512 FFT, its impulse noise threshold will be approximately 10 log10(512) = 27.1 dB higher than a corresponding single-carrier system. In reality, however, impulse noise occurrences may last for significantly longer than a single sample period at the ADSL sampling rates. As a result, additional protection is necessary to ensure satisfactory system performance. We will now turn our attention to a number of impulse noise mitigation strategies designed specifically for a DMT transceiver. To evaluate the performance of the various impulse noise mitigation strategies discussed in the remainder of this chapter, we make use of the set of canonical loops proposed in [57] for ADSL transceiver evaluation.

Id. at 126.

327. Moreover, Chow recognizes that different carriers of a DMT transceiver can use different margins. "If the DMT transceiver can adaptively learn the spectral shape of the impulse noise and there is sufficient extra margin available, then the extra margin can be placed intelligently on those tones most susceptible to errors due to impulse noise." *Id.* at 151.

328. Chow contemplates the same benefits as disclosed in the '354 Patent, namely the presence of a multicarrier transceiver and how the multicarrier system has increased benefits over a single carrier system:

> In Chapter 6, we examined the characteristics and studied the effects of impulse noise on a DMT system operating over an ADSL transmission environment. We proposed a number of impulse noise mitigation strategies designed specifically for a DMT transceiver that exploit both time and frequency domain characteristics of impulse noise and provide side information to the decoder for erasure declarations. Furthermore, we presented a soft decision, multicarrier, error control technique that continuously adapts both the transmitter and the receiver during normal system operation and adjusts the target system performance margin on a subchannel-by-subchannel basis. Lastly, we tested our proposed impulse noise mitigation schemes through computer simulation and found them to be quite effective in reducing the damage of impulse noise.

Id. at 164-65.

329. Thus, it is my opinion that Chow discloses and/or renders obvious the preamble of claim 10, to the extent it is limiting.

d. Claim 10.a "receive a multicarrier symbol comprising a first plurality of carriers"

330. Chow discloses and/or renders obvious that the multicarrier communications transceiver is operable to receive a multicarrier symbol comprising a first plurality of carriers.

331. Figure 1.1 of Chow, copied below, is a block diagram of a digital communication system that uses multicarrier modulation and includes a receiver that is operable to receive a multicarrier symbol.

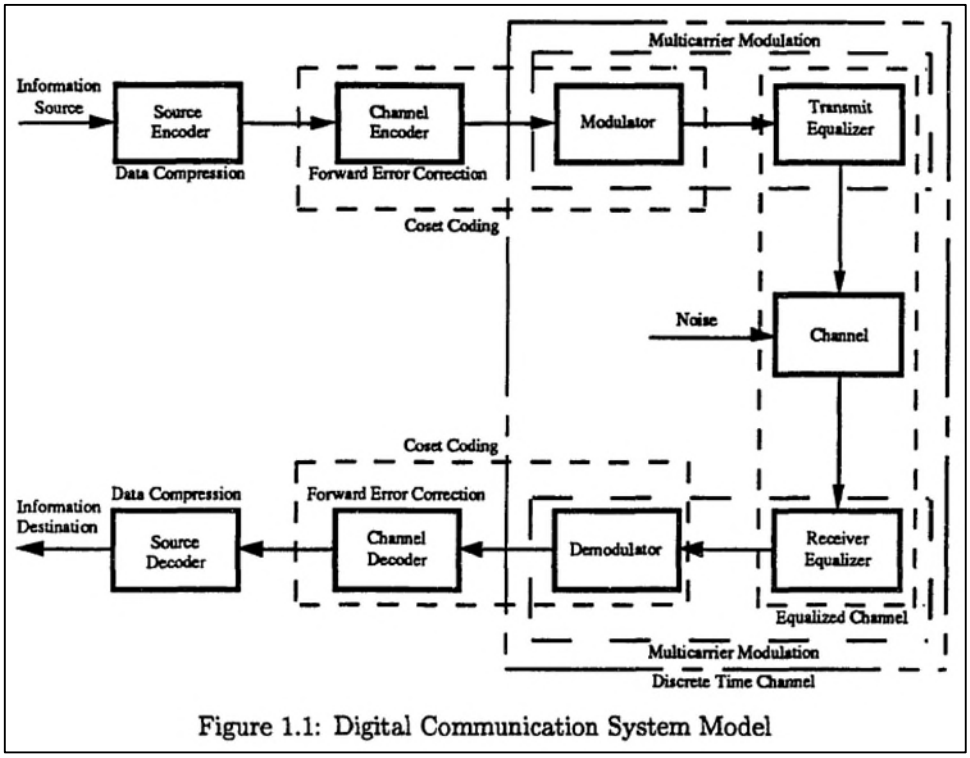

Figure 1.1: Digital Communication System Model

Id. at Fig. 1.1.

332. Figure 3.2 of Chow, copied below, is a block diagram of a DMT receiver.

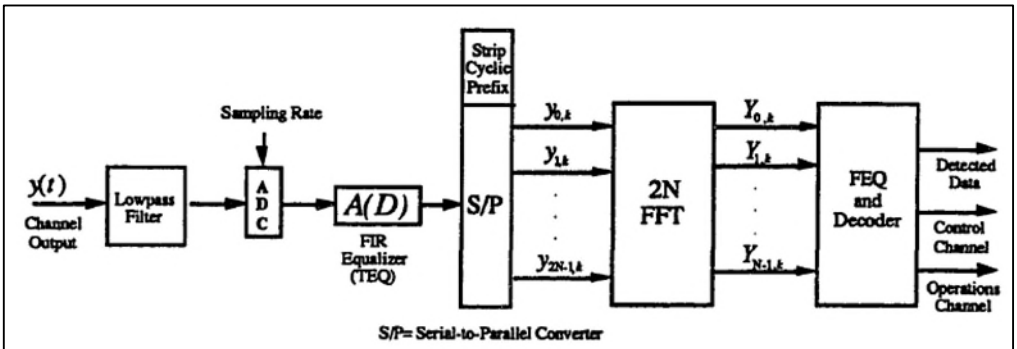

Figure 3.2: The DMT Receiver

Id. at Fig. 3.2

333. Chow discloses that a "DMT modulator divides the data transmission channel into a fixed number of, say *N*, parallel, complex, independent subchannels in the frequency domain as shown in Figure 2.5." *Id.* at 19.

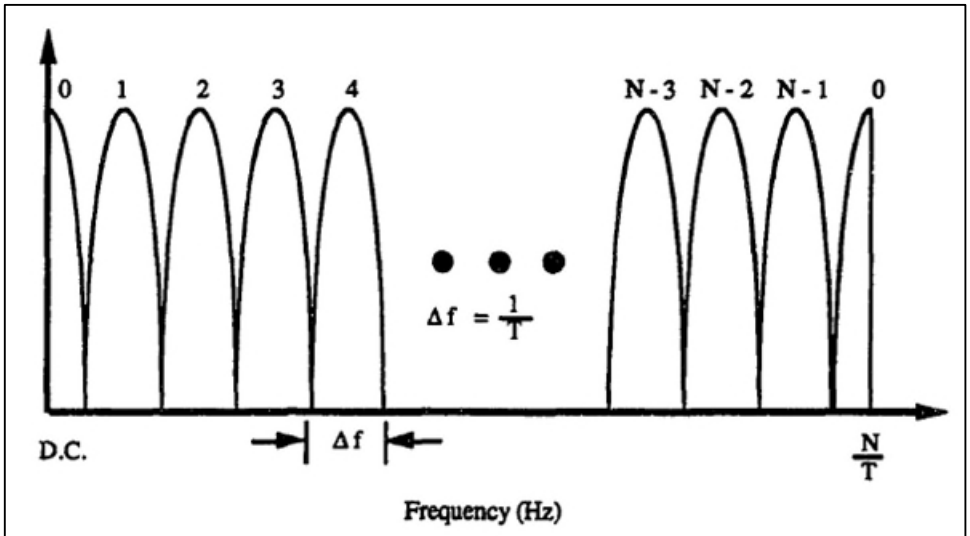

Figure 2.5: Frequency Domain Picture of DMT Modulation

Id. at Fig. 2.5

334. Chow further discloses that:

> Each of the "tones", or subchannels, is $\Delta f = \frac{1}{T}$ wide in the frequency domain, where T is the (block) multicarrier symbol period, and if N is sufficiently large, the channel power spectral density curve will be virtually flat within each of the subchannels.

Id. at 19-20.

335. Accordingly, Chow discloses a multicarrier symbol that includes subchannels, and a receiver, in a transceiver, that is operable to receive the multicarrier symbol.

336. Chow also discloses that each of the subchannels in a multicarrier symbol has its own carrier: "The fundamental goal of all 'multicarrier' modulation techniques is to partition a data transmission channel with ISI into a set of orthogonal, memoryless subchannels, each with its own 'carrier'. (*See* [23] and [24]). Data is transmitted through each subchannel independently of other subchannels, and within each subchannel, the channel response is (ideally) flat, as long as the channel is partitioned sufficiently." *Id.* at 16-17.

337. Chow discloses that the multicarrier symbol comprises a first plurality of carriers because it discloses that each DMT symbol has multiple subchannels, the number of which Chow denotes as *N*. For example, Chow describes a DMT system that is used for simulation of ADSL, and that ADSL system has $N = 256$ subchannels. *Id.* at 86; *see also id.* at 66, 68, 106. As Chow discloses (*see, e.g.*, *id.* at 16-17), and as would have been appreciated by a person having ordinary skill in the art even absent the disclosures of Chow, each of these 256 subchannels is associated with its own carrier. Accordingly, within each DMT symbol are many pluralities of carriers, including a first plurality of carriers.

338. To illustrate, I have copied below an annotated version of Figure 2.5 of Chow, in which I have indicated the subchannels corresponding to one possible first plurality of carriers:

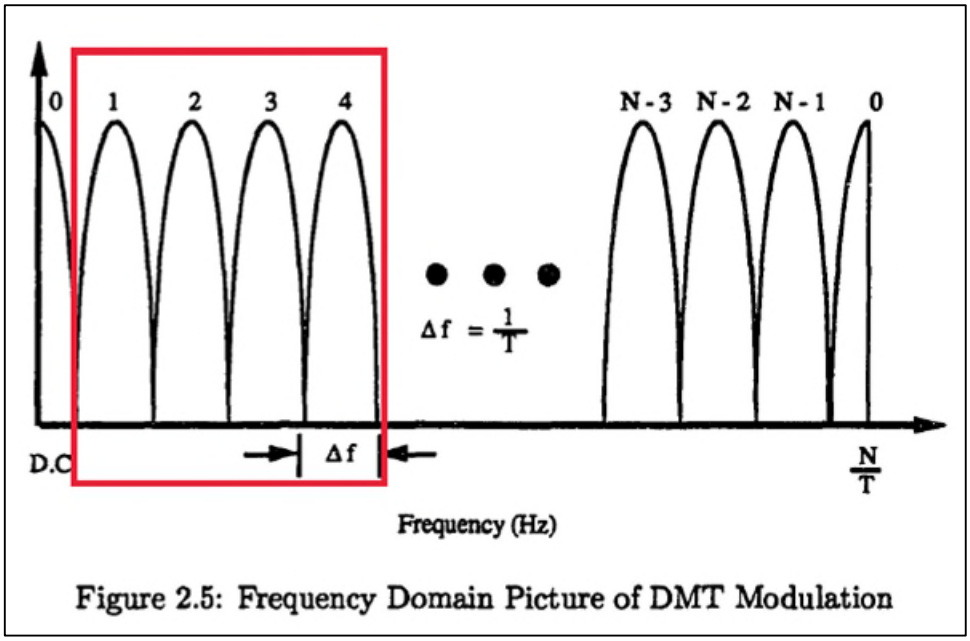

Figure 2.5: Frequency Domain Picture of DMT Modulation

Id. at Fig. 2.5 (annotated).

339. As would have been appreciated by a person having ordinary skill in the art, there are many other pluralities of carriers in the multicarrier symbols disclosed by Chow. Specifically, any two or more carriers make up a first plurality of carriers.

340. As explained further below, Figures 6.20 through 6.27 of Chow also show various pluralities of carriers, including a first plurality of carriers.

341. Thus, it is my opinion that Chow discloses and/or renders obvious claim 10.a.

e. Claim 10.b "and a second plurality of carriers"

342. Chow discloses and/or renders obvious claim 10.b "and a second plurality of carriers."

343. I incorporate by reference my analysis for claim 10.a.

344. As I explained for claim 10.a, Chow describes a DMT system that has 256 subchannels, each of which is associated with its own carrier, and there are many pluralities of carriers within each DMT symbol, including both a first plurality of carriers and a second plurality of carriers. To illustrate, I have copied below a version of Figure 2.5 of Chow in which I have indicated the subchannels corresponding to two possible pluralities of carriers, one plurality in red and the other in blue:

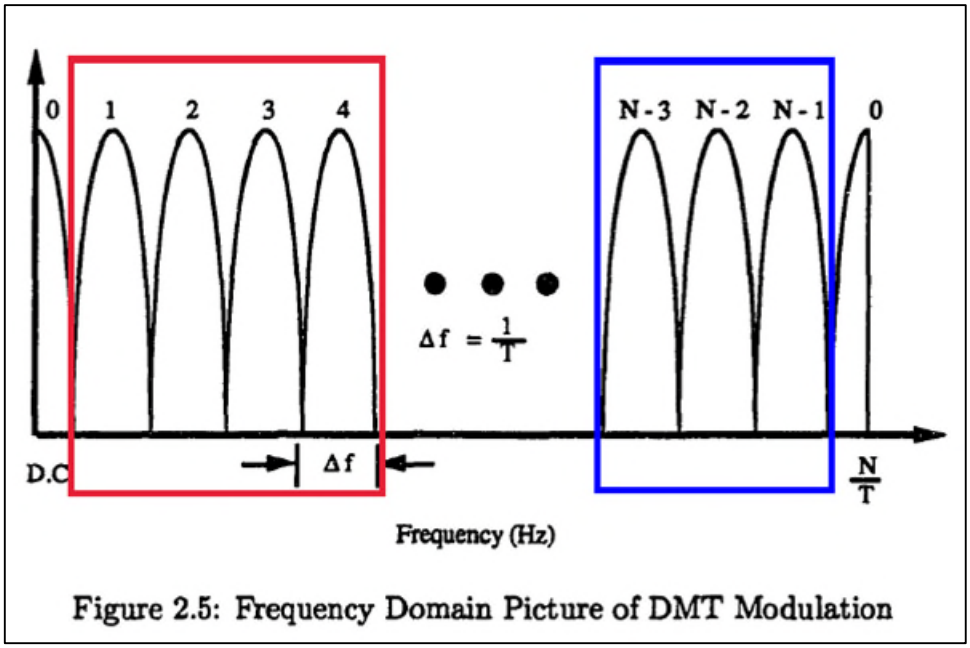

Figure 2.5: Frequency Domain Picture of DMT Modulation

Id. at Fig. 2.5 (annotated).

345. As would have been appreciated by a person having ordinary skill in the art, there are many other first and second pluralities of carriers in the multicarrier symbols disclosed by Chow. Specifically, any two or more carriers make up a first plurality of carriers, and any two or more carriers make up a second plurality of carriers. As shown in the annotated version of Figure 2.5 above, the subsets of two or more carriers can be disjoint so there is no overlap in the carriers of the first plurality and the carriers of the second plurality.

346. I note that the carriers in the first plurality need not be adjacent to each other, nor do the carriers in the second plurality need to be adjacent. As a result, the first plurality of carriers could include, for example, carrier 1 and carrier 3, or carrier 2 and carrier N-3, or any two or more of the carriers available. Likewise, the second plurality of carriers can include any two or more carriers, regardless of whether they are adjacent.

347. As explained further below, Figures 6.20 through 6.27 of Chow also illustrate multiple pluralities of carriers, including a first plurality of carriers and a second plurality of carriers.

348. Thus, it is my opinion that Chow discloses and/or renders obvious claim 10.b.

f. Claim 10.c "receive a first plurality of bits on the first plurality of carriers using a first SNR margin;"

349. Chow discloses and/or renders obvious claim 10.c "receive a first plurality of bits on the first plurality of carriers using a first SNR margin."

350. Chow discloses "2.2 SNR Gap and the Gap Approximation" which includes "System performance, or noise, margin is defined as the additional amount of noise (in dB) that the system can tolerate while still operating under the desired BER requirement." *Id.* at 13.

351. Chow explicitly discloses that SNR margins are used to transport data. "[I]n the case of maximizing total data throughput at a fixed margin lower than the maximum achievable

margin, some of the worst subchannels used may not have the necessary SNR to transport any data at the maximum achievable margin." *Id.* at 59.

352. Moreover, Chow discloses assigning pluralities of bits to carriers, which means pluralities of bits are received on carriers using SNR margins.

353. Chow discloses a DMT system that uses 256 subchannels, each of which always carries a plurality of bits whenever it carries any bits. *See e.g.*, *id.* at 68 (N=256, b_{min}=2). Thus, any plurality of carriers that carries bits always carries a plurality of bits.

> "Here we have also imposed a minimum of 2 bits per used carrier constraint, even though in practice, it is possible to implement 1 bit carriers. We note here that we can always combine two 1 bit carriers into one 2 bit carrier by assigning 2 bits to the original 1 bit carrier with the higher SNR and 0 bit to the original 1 bit carrier with the lower SNR. Then if we place twice the power in the carrier that is now carrying 2 bits and no power in the now 0 bit carrier, we will always do no worse than the original two 1 bit carriers with equal amount of energy in each carrier. The saw-tooth shaped input power distribution is resulting from the fact that the variation in SNR is relatively small between adjacent subchannels (a necessary condition for multicarrier to work well) and that the final power distribution will vary inversely to compensate for the SNR variation in order to maintain a constant bit error rate among all used subchannels. When the input power to a particular subchannel has increased (or decreased) to the level where it is no longer effective to transmit that particular number of bits, the number of bits is decreased (or increased) by one and the amount of input power will be abruptly decreased (or increased) by approximately 3 dB, resulting in a saw-tooth shaped final input power distribution."

Id. at 69-70.

354. Chow provides many plots illustrating pluralities of bits assigned to carriers, and the use of different SNR margins on different pluralities of those carriers.

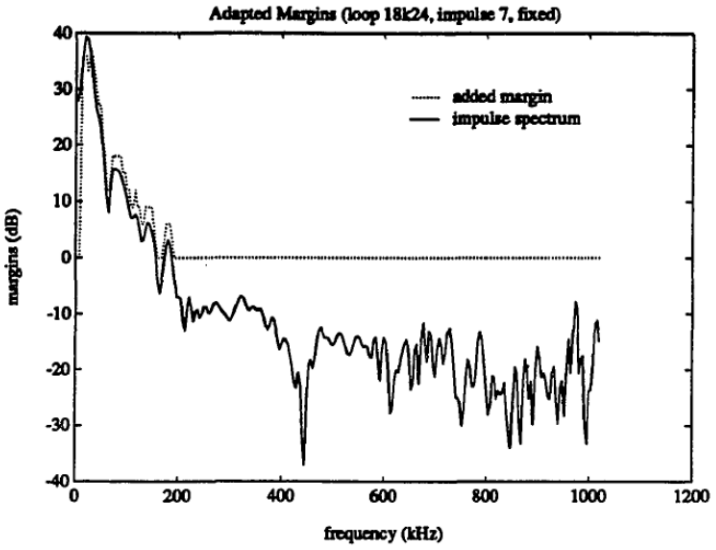

Figure 6.20: Margins for 18 kft, 24 AWG Loop with Impulse 7 and Fixed Updates

Id. at Fig. 6.20.

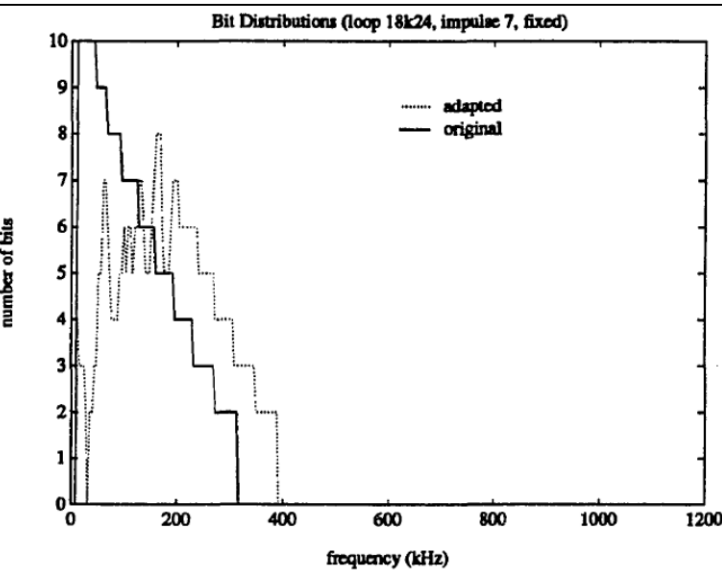

Figure 6.21: Bit Table for 18 kft, 24 AWG Loop, Impulse 7, and Fixed Updates

Id. at 6.21.

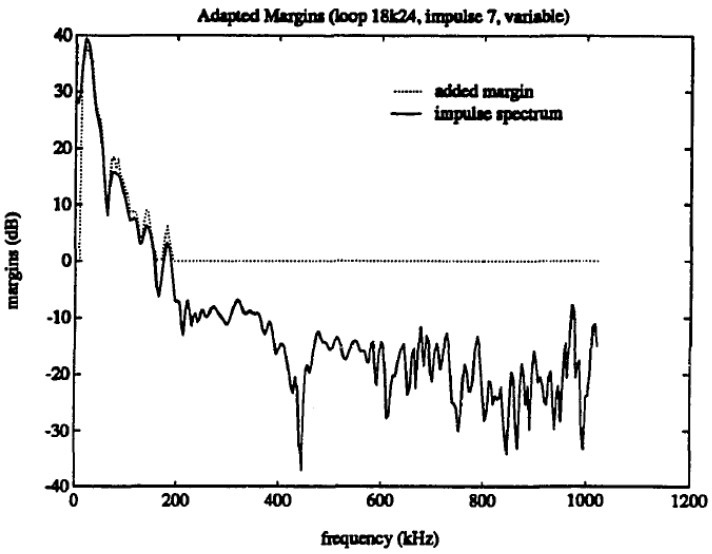

Figure 6.22: Margins for 18 kft, 24 AWG Loop with Impulse 7 and Variable Updates

Id. at Fig. 6.22.

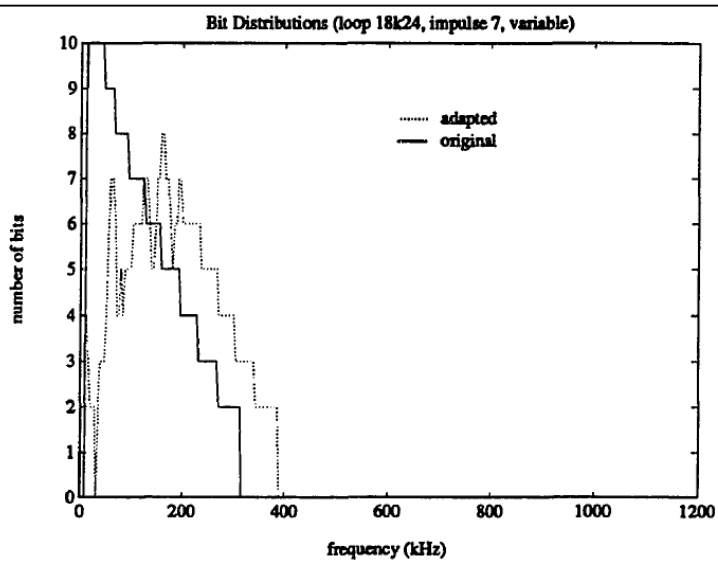

Figure 6.23: Bit Table for 18 kft, 24 AWG Loop, Impulse 7, and Variable Updates

Id. at Fig. 6.23.

"Figures 6.24 to 6.27 present plots of the margin distributions and bit distributions obtained for the two margin update methods, respectively. The plots in Figures 6.24 and 6.26 further confirm that both techniques for adapting the margin distributions will result in increased margin on those tones most affected by impulse noise, and the technique that allows a range of margins to be added per update will provide better performance in terms of matching the distribution of

additional margins to the actual shape of the impulse spectrum. We note that in this test scenario, carriers below 70 kHz are not used due to the lower bandedge of the system. However, there is still significant impulse noise energy in the frequency band available for transmission, and as is evident from the plots, there is not enough margin available to compensate fully for the large degradation in error rate caused by the impulse noise in the lower frequency tones."

Id. at 158-60.

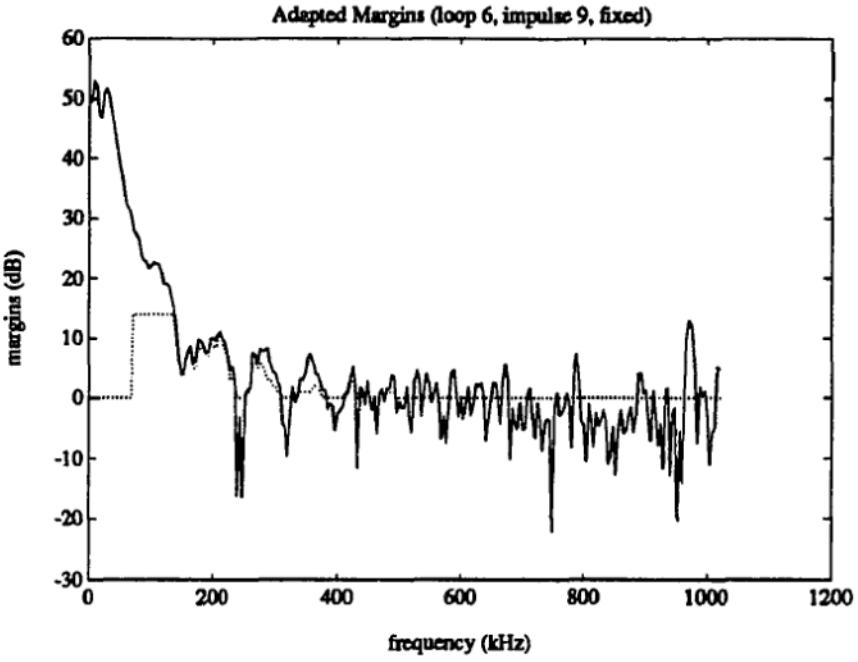

Figure 6.24: Margins for Loop 6 with Impulse 9 and Fixed Updates

Id. at Fig. 6.24.

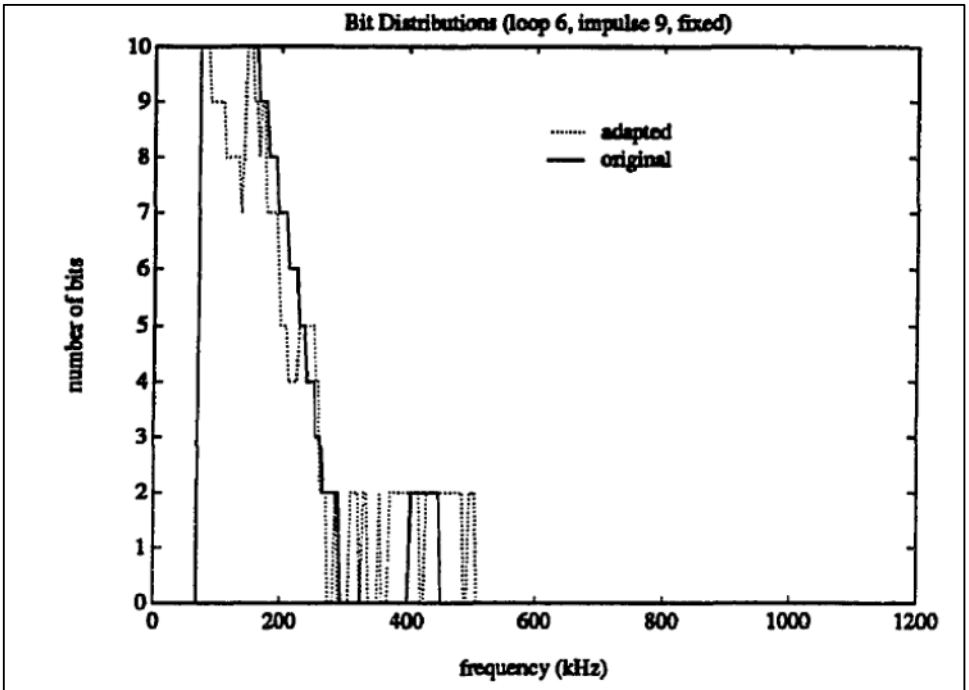

Figure 6.25: Bit Table for Loop 6, Impulse 9, and Fixed Updates

Id. at Fig. 6.25.

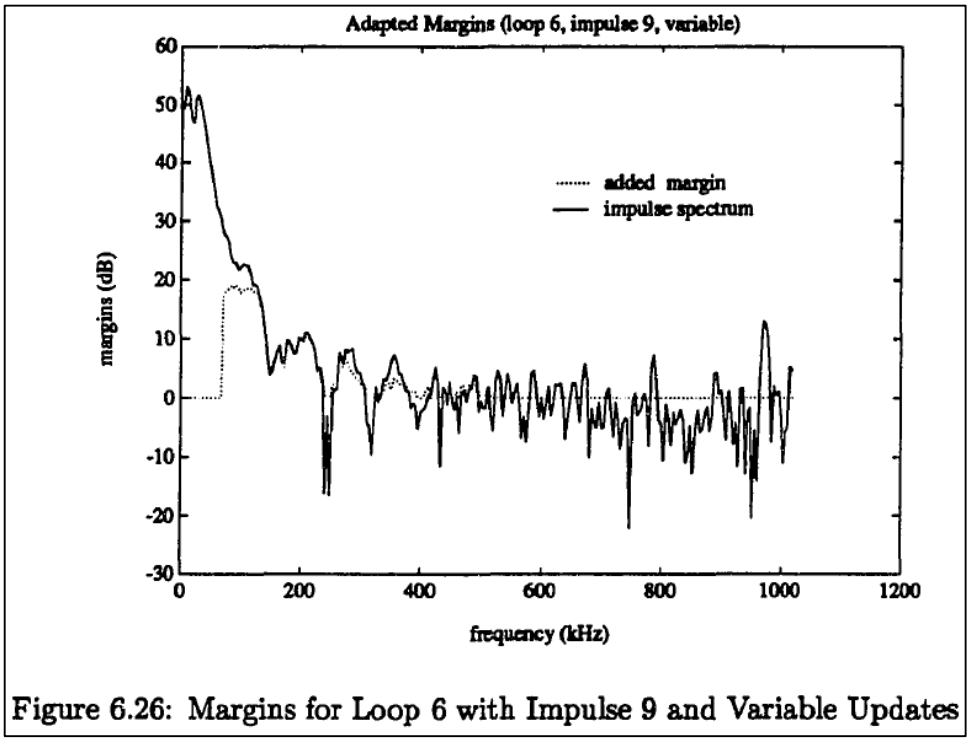

Figure 6.26: Margins for Loop 6 with Impulse 9 and Variable Updates

Id. at Fig. 6.26

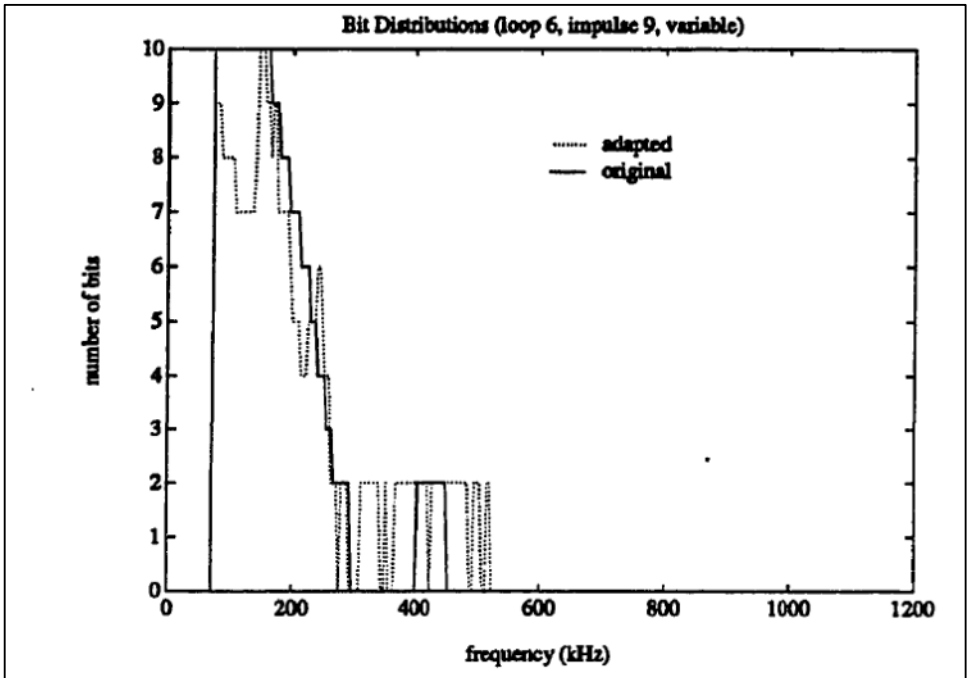

Figure 6.27: Bit Table for Loop 6, Impulse 9, and Variable Updates

Id. at Fig. 6.27.

355. As one of many examples, I have provided below annotated versions of Figures 6.20 (margins) and 6.21 (bit distribution) showing one possible first plurality of bits on the first plurality of carriers using a first SNR margin of approximately 18 dB.

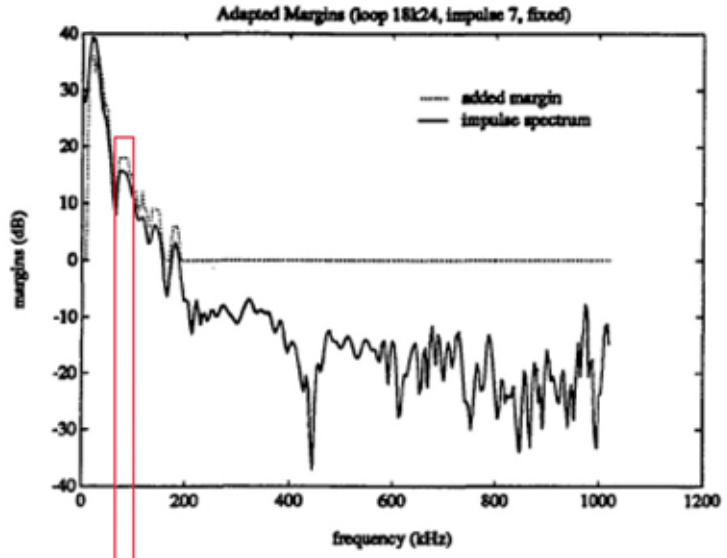

Figure 6.20: Margins for 18 kft, 24 AWG Loop with Impulse 7 and Fixed Updates

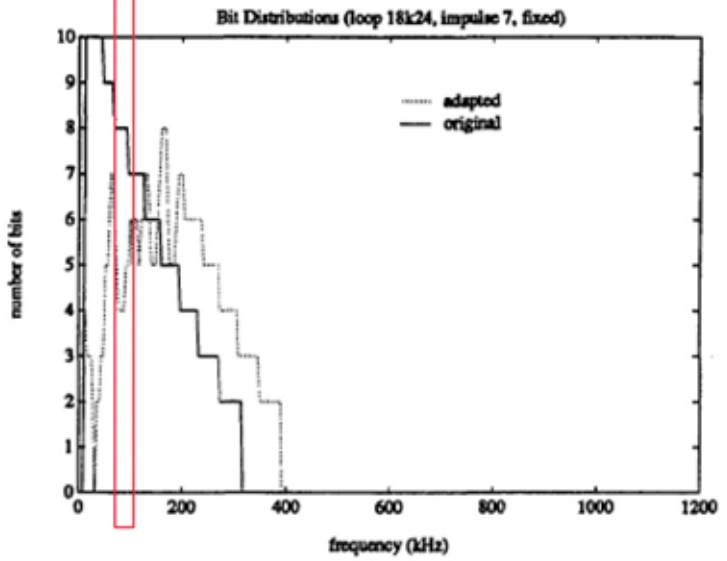

Figure 6.21: Bit Table for 18 kft, 24 AWG Loop, Impulse 7, and Fixed Updates

Id. at Figs. 6.20 and 6.21 (annotated).

356. As another example, I have provided below annotated versions of Figures 6.24 (margins) and 6.25 (bit distribution) showing another possible first plurality of bits on the first plurality of carriers (*i.e.*, those between roughly 50 kHz and 150 kHz) using a first SNR margin of approximately 14 dB.

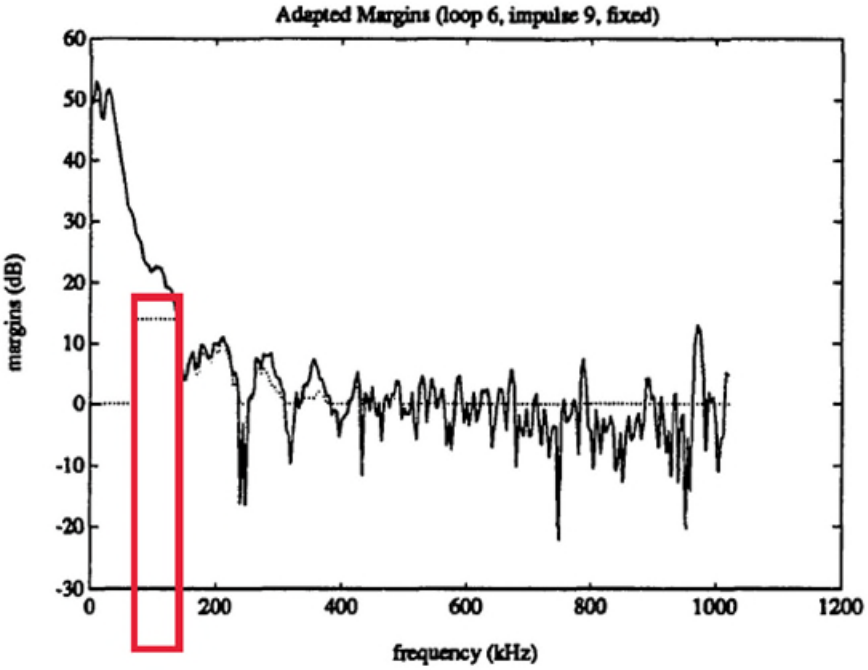

Figure 6.24: Margins for Loop 6 with Impulse 9 and Fixed Updates

Id. at Fig. 6.24 (annotated).

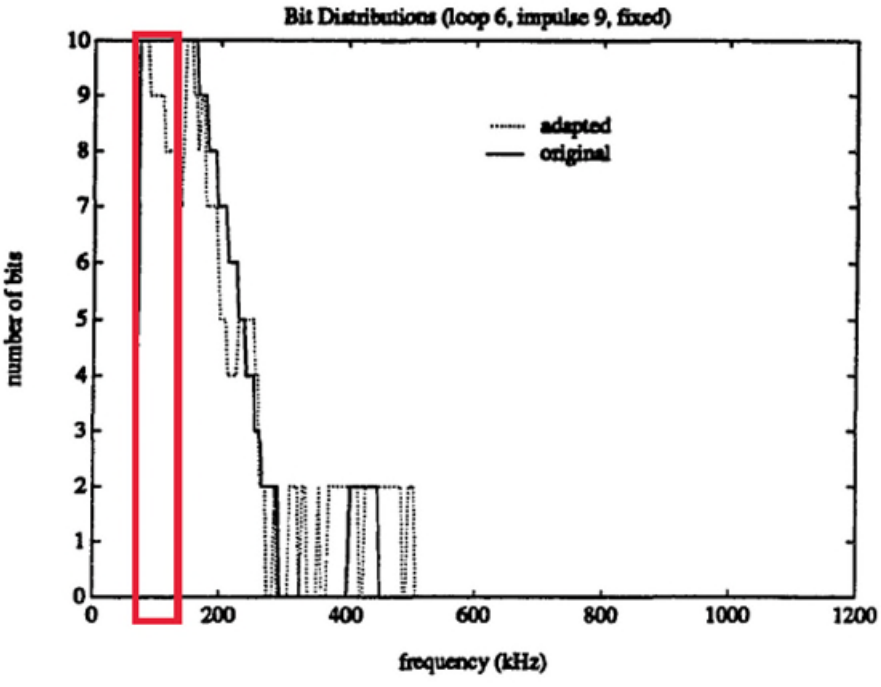

Figure 6.25: Bit Table for Loop 6, Impulse 9, and Fixed Updates

Id. at Fig. 6.25 (annotated).

357. Although I have indicated regions of the plots corresponding to more than two carriers, as few as two carriers can be included to comprise the first plurality of carriers. Again, Chow discloses many possible first pluralities of bits on many possible first pluralities of carriers using a first SNR margin, as illustrated in, for example, Figures 6.20 through 6.27 and described in Chapter 6 of Chow.

358. To the extent it is determined that Chow does not sufficiently disclose that the multicarrier communications transceiver is operable to receive a first plurality of bits on the first plurality of carriers using a first SNR margin, using the same first SNR margin on multiple carriers would have been obvious to a person having ordinary skill in the art. For example, it would have been obvious to a person having ordinary skill in the art to round the added margin amounts to integer numbers of dB or to the nearest tenth of a dB in order to reduce transceiver complexity, given that one goal of Chow's work is to manage and limit complexity. *See, e.g.*, *Id.* at 1 ("The goal of our present work is to facilitate the design of a practical communication system that will approach this theoretically optimal performance with a level of implementational complexity that can be realized with today's technology."). As a result of such rounding, the multicarrier communications transceiver would be operable to receive a first plurality of bits on the first plurality of carriers using a first SNR margin.

359. Thus, it is my opinion that Chow discloses and/or renders obvious claim 10.c.

g. Claim 10.d "receive a second plurality of bits on the second plurality of carriers using a second SNR margin;"

360. Chow discloses and/or renders obvious claim 10.d "receive a second plurality of bits on the second plurality of carriers using a second SNR margin."

361. Among other things, Chow investigates techniques for improving the performance of DMT systems in the presence of impulse noise. *Id.* at 114-15. Chow notes that most practical communication systems are designed "with a built-in performance margin to take the detrimental effects of impulse noise into account." *Id.* at 114. Chow teaches that the use of different margins on different subchannels can improve robustness in the presence of impulse noise. Specifically, Chow discloses that "[i]f the DMT transceiver can adaptively learn the spectral shape of the impulse noise and there is sufficient extra margin available, then the extra margin can be placed intelligently on those tones most susceptible to errors due to impulse noise." *Id.* at 114, 151. Thus, Chow teaches that the performance of a DMT system can be improved by detecting whether a subchannel is suffering from impulse noise and, if it is, allocating excess margin to that subchannel. As would have been recognized by a person having ordinary skill in the art, the result of this allocation would be that different subchannels would have different margins (e.g., some subchannels would have the "base" margin and others would have the base margin plus added margin)..

362. Chow teaches monitoring "the occurrence of a large number of unusually high error signals over the carriers in a DMT symbol" and using a threshold to decide whether "the error signal on a particular subchannel is 'unusually high.'" *Id.* at 151. When more than a threshold number of subchannels have been found to have unusually high error signals, Chow teaches that an impulse is likely to be present. *Id.* In response, "the estimate of the impulse spectrum is updated, using the mean squared error signals on all of the subchannels." *Id.* at 151-52. Chow defines a running sum, α_{ij}, which is the impulse spectral estimate on subchannel *i* at time *j*. *Id.* at 152. Chow also defines another threshold, *impthresh*, and teaches that after some number of suspected impulse occurrences, "additional margin will be given to those subchannels

with mean squared error estimates, α_{ij}," that exceed *impthresh*. *Id.* Chow explains in detail how to determine how much additional margin to allocate to each subchannel whose mean squared error estimate, α_{ij}, exceeds *impthresh*, and Chow presents the results of multiple simulations illustrating the effect of the disclosed techniques. *See id.* at 152-61.

363. Chow discloses a DMT system that uses 256 subchannels, each of which always carries a plurality of bits whenever it carries any bits. *See e.g.*, *id.* at 68 (N=256, b_{min}=2). Thus, any plurality of carriers that carries bits always carries a plurality of bits.

364. Figures 6.20 through 6.27 of Chow illustrate many possible second pluralities of bits on second pluralities of carrier using a second SNR margin. In the annotated versions below, I have indicated in blue the locations of several possible second pluralities of carriers and second pluralities of bits on the second pluralities of carriers. . Although I have indicated regions of the plots corresponding to more than two carriers, as few as two carriers can be included in the second plurality of carriers.

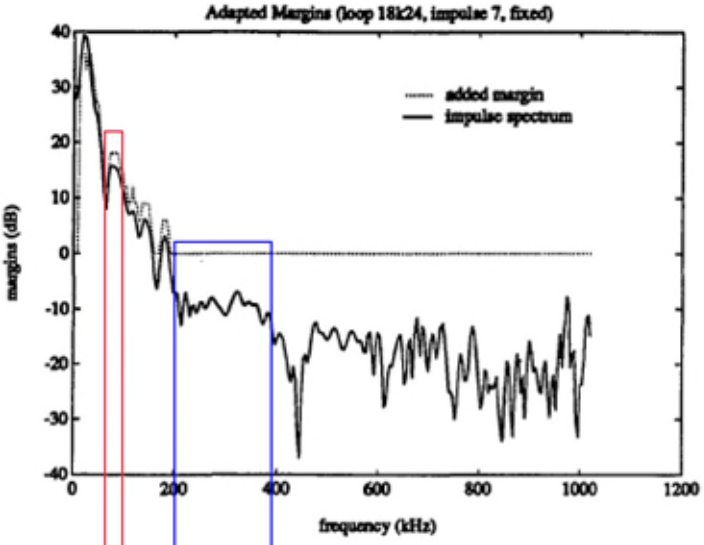

Figure 6.20: Margins for 18 kft, 24 AWG Loop with Impulse 7 and Fixed Updates

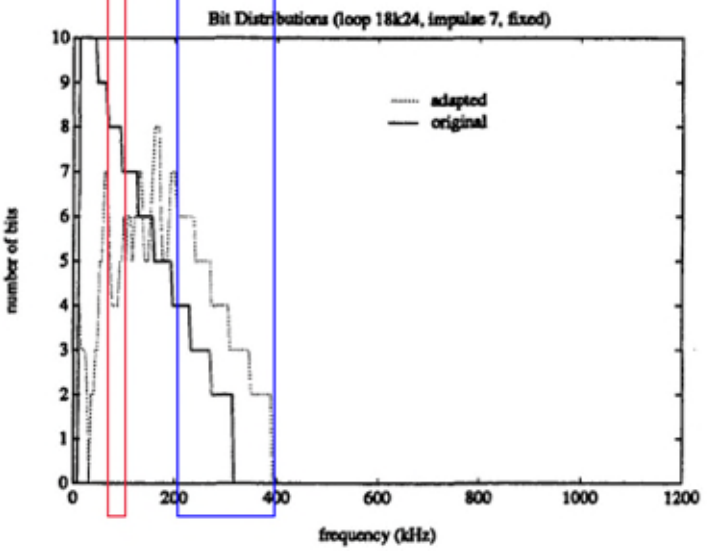

Figure 6.21: Bit Table for 18 kft, 24 AWG Loop, Impulse 7, and Fixed Updates

Id. at Figs. 6.20, 6.21 (annotated).

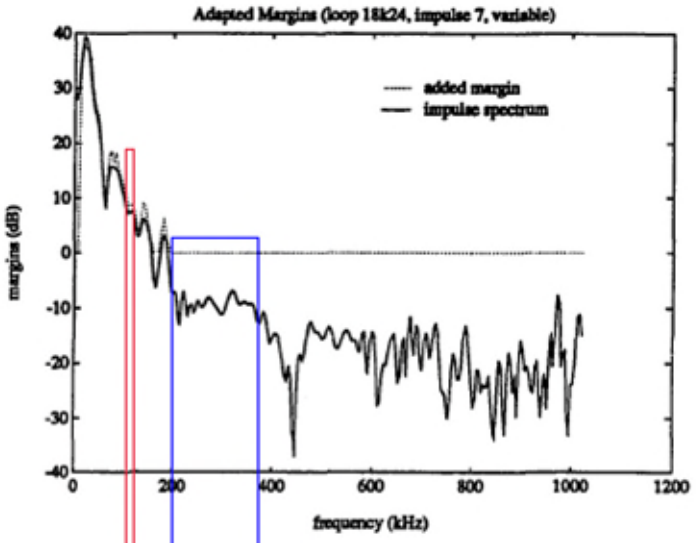

Figure 6.22: Margins for 18 kft, 24 AWG Loop with Impulse 7 and Variable Updates

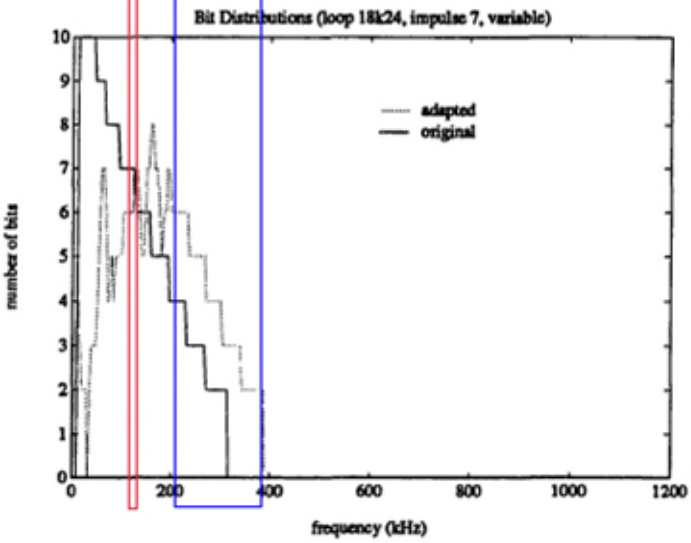

Figure 6.23: Bit Table for 18 kft, 24 AWG Loop, Impulse 7, and Variable Updates

Id. at Figs. 6.22, 6.23 (annotated).

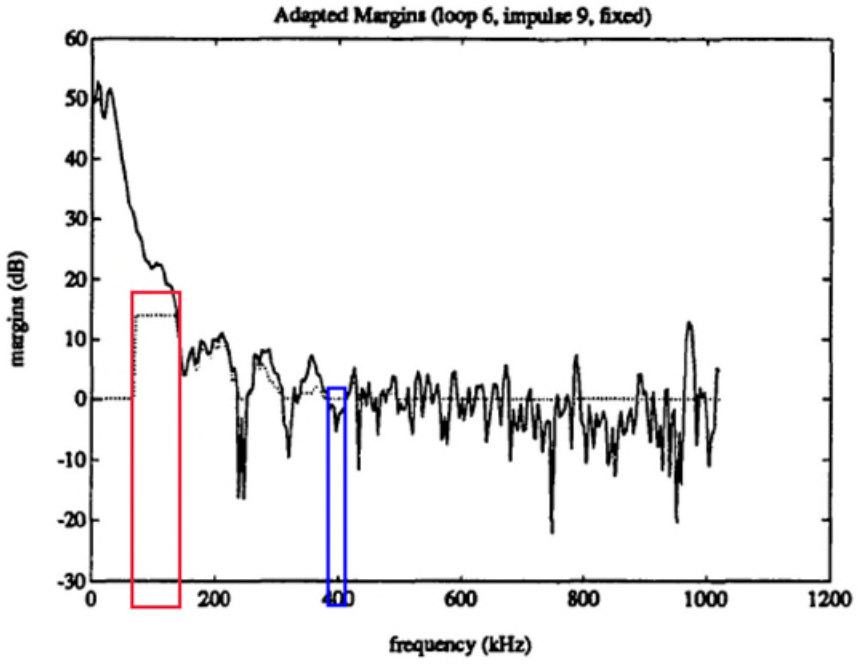

Figure 6.24: Margins for Loop 6 with Impulse 9 and Fixed Updates

Id. at. Fig. 6.24 (annotated).

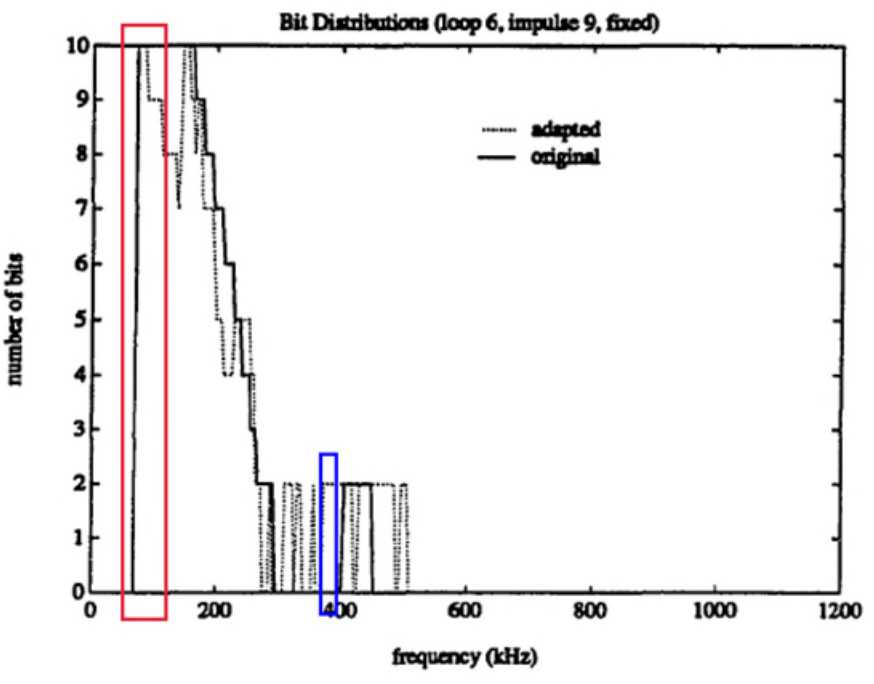

Figure 6.25: Bit Table for Loop 6, Impulse 9, and Fixed Updates

Id. at Fig. 6.25 (annotated).

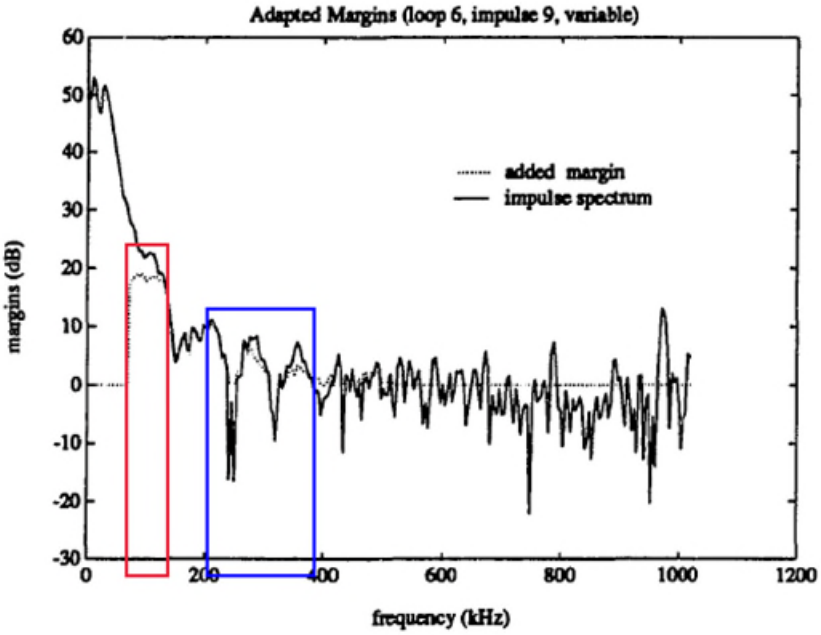

Figure 6.26: Margins for Loop 6 with Impulse 9 and Variable Updates

Id. at Fig. 6.26 (annotated).

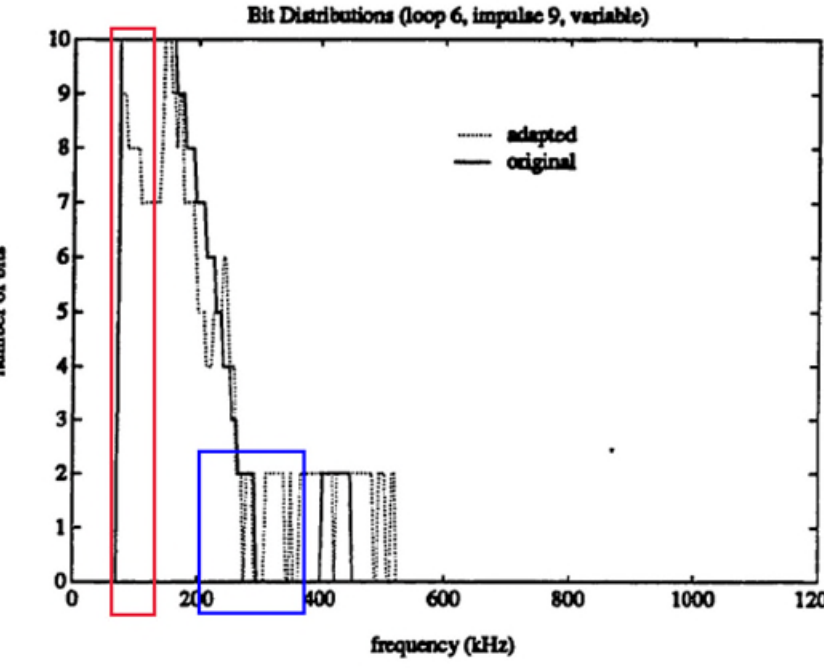

Figure 6.27: Bit Table for Loop 6, Impulse 9, and Variable Updates

Id. at Fig. 6.27 (annotated).

365. Chow details how there can be a delineation of a first carrier and a second carrier such that there can be a second plurality of bits on a second carrier using a second SNR margin. "The performance of this frequency domain clipping technique in general depends on the manner in which power is allocated among the carriers, the channel transfer function, and the actual number of carriers used." *Id.* at 143. In particular "This figure [6.21] clearly demonstrates the ability of a DMT system to move bits from the lower carriers to the higher carriers in order to avoid the large low frequency content of the injected impulse noise. In some instances, the amount of margin required, after adaptation, for a particular carrier that is initially used for data transmission is large enough to force the system to stop using that particular carrier and redistribute those bits among other carriers." *Id.* at 155.

> Here we have also imposed a minimum of 2 bits per used carrier constraint, even though in practice, it is possible to implement 1 bit carriers. We note here that we can always combine two 1 bit carriers into one 2 bit carrier by assigning 2 bits to the original 1 bit carrier with the higher SNR and 0 bit to the original 1 bit carrier with the lower SNR. Then if we place twice the power in the carrier that is now carrying 2 bits and no power in the now 0 bit carrier, we will always do no worse than the original two 1 bit carriers with equal amount of energy in each carrier. The saw-tooth shaped input power distribution is resulting from the fact that the variation in SNR is relatively small between adjacent subchannels (a necessary condition for multicarrier to work well) and that the final power distribution will vary inversely to compensate for the SNR variation in order to maintain a constant bit error rate among all used subchannels. When the input power to a particular subchannel has increased (or decreased) to the level where it is no longer effective to transmit that particular number of bits, the number of bits is decreased (or increased) by one and the amount of input power will be abruptly decreased (or increased) by approximately 3 dB, resulting in a saw-tooth shaped final input power distribution.

Id. at 69-70.

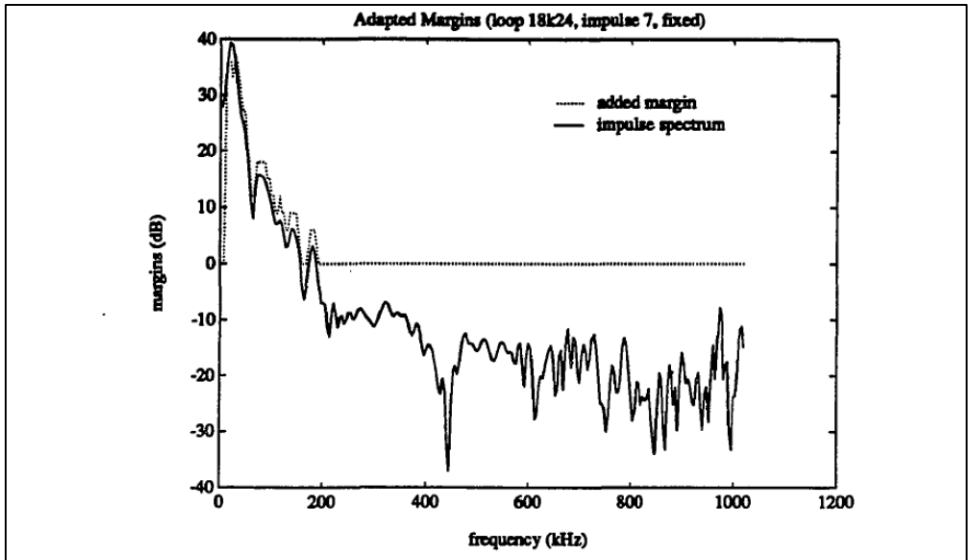

Figure 6.20: Margins for 18 kft, 24 AWG Loop with Impulse 7 and Fixed Updates

Id. at Fig. 6.20.

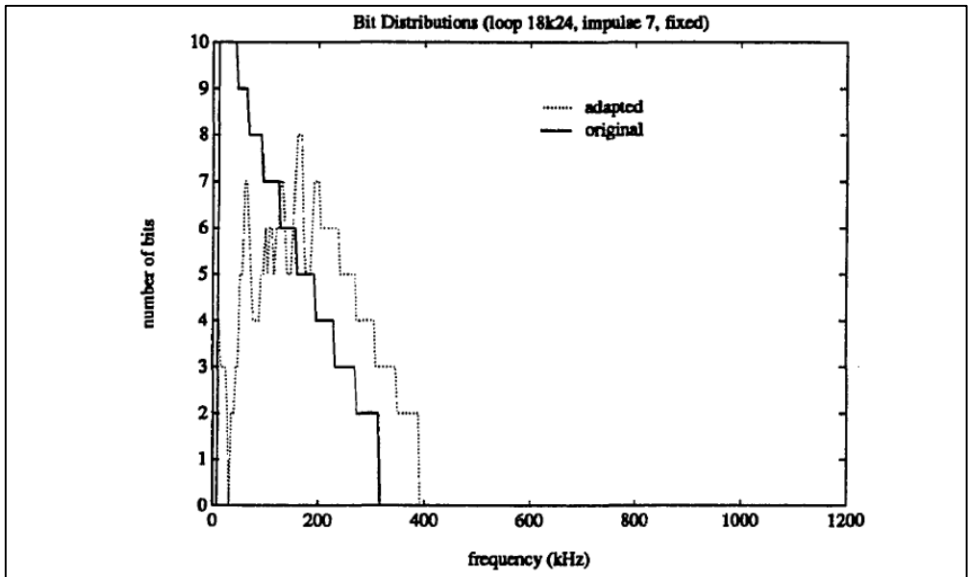

Figure 6.21: Bit Table for 18 kft, 24 AWG Loop, Impulse 7, and Fixed Updates

Id. at Fig. 6.21.

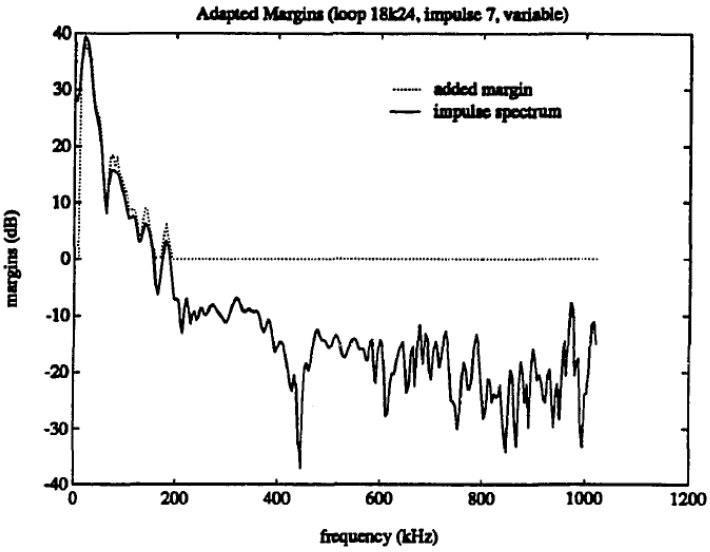

Figure 6.22: Margins for 18 kft, 24 AWG Loop with Impulse 7 and Variable Updates

Id. at Fig. 6.22.

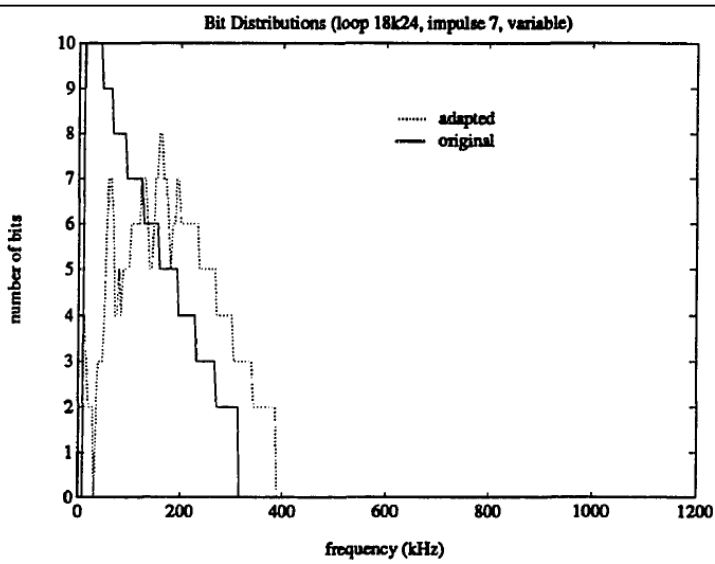

Figure 6.23: Bit Table for 18 kft, 24 AWG Loop, Impulse 7, and Variable Updates

Id. at Fig. 6.23.

366. "Figures 6.24 to 6.27 present plots of the margin distributions and bit distributions obtained for the two margin update methods, respectively. The plots in Figures 6.24 and 6.26 further confirm that both techniques for adapting the margin distributions will result in increased

margin on those tones most affected by impulse noise, and the technique that allows a range of margins to be added per update will provide better performance in terms of matching the distribution of additional margins to the actual shape of the impulse spectrum. We note that in this test scenario, carriers below 70 kHz are not used due to the lower bandedge of the system. However, there is still significant impulse noise energy in the frequency band available for transmission, and as is evident from the plots, there is not enough margin available to compensate fully for the large degradation in error rate caused by the impulse noise in the lower frequency tones." *Id.* at 158-60.

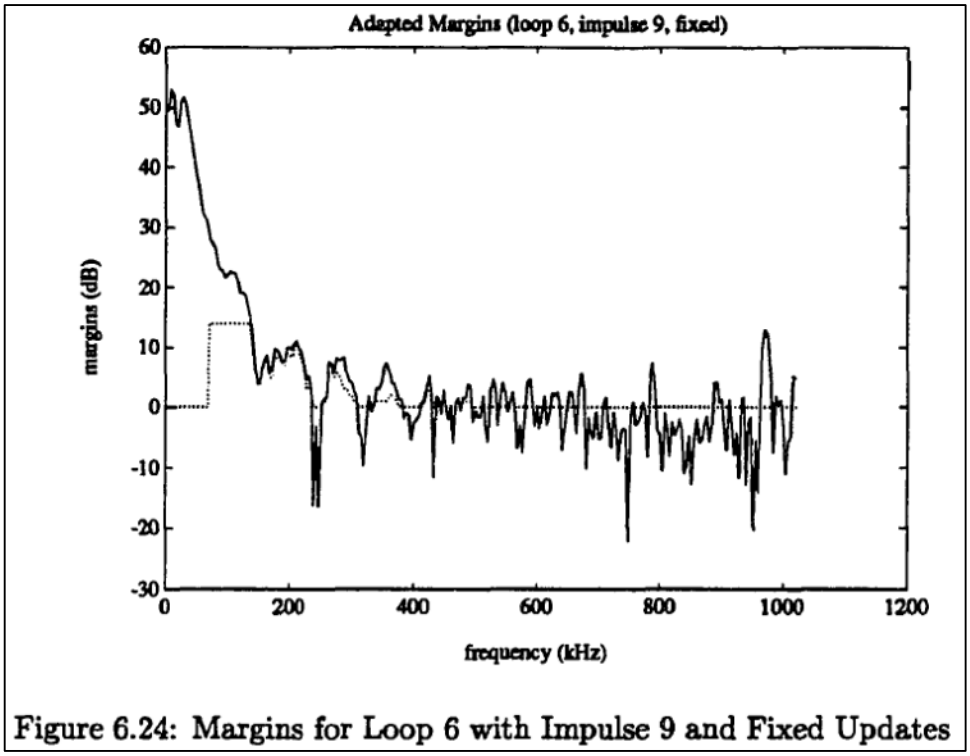

Figure 6.24: Margins for Loop 6 with Impulse 9 and Fixed Updates

Id. at Fig. 6.24.

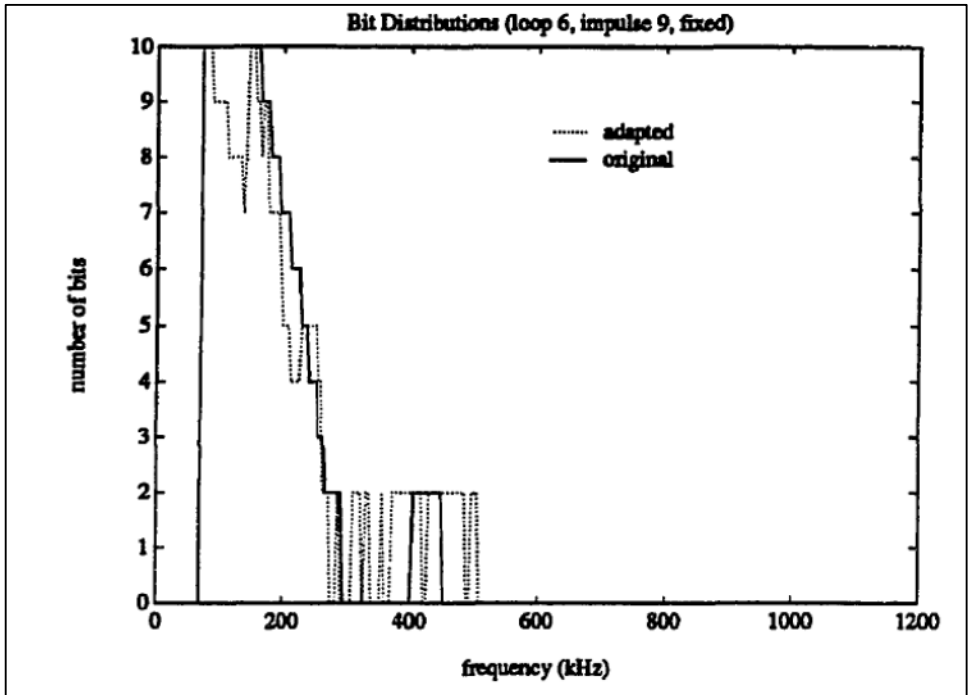

Figure 6.25: Bit Table for Loop 6, Impulse 9, and Fixed Updates

Id. at Fig. 6.25.

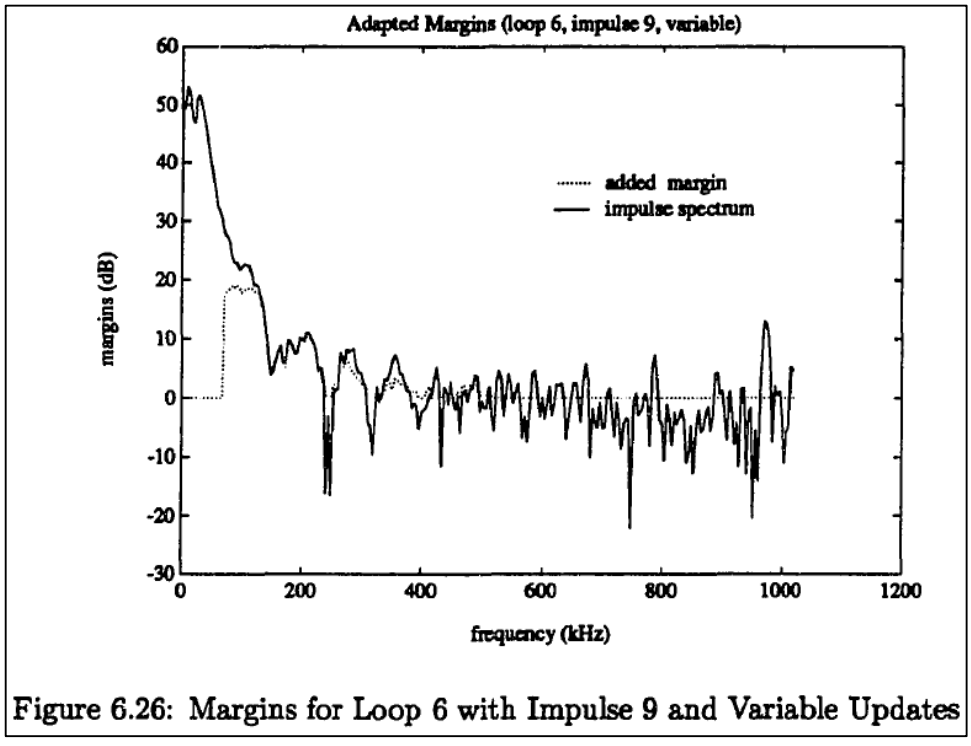

Figure 6.26: Margins for Loop 6 with Impulse 9 and Variable Updates

Id. at Fig. 6.26

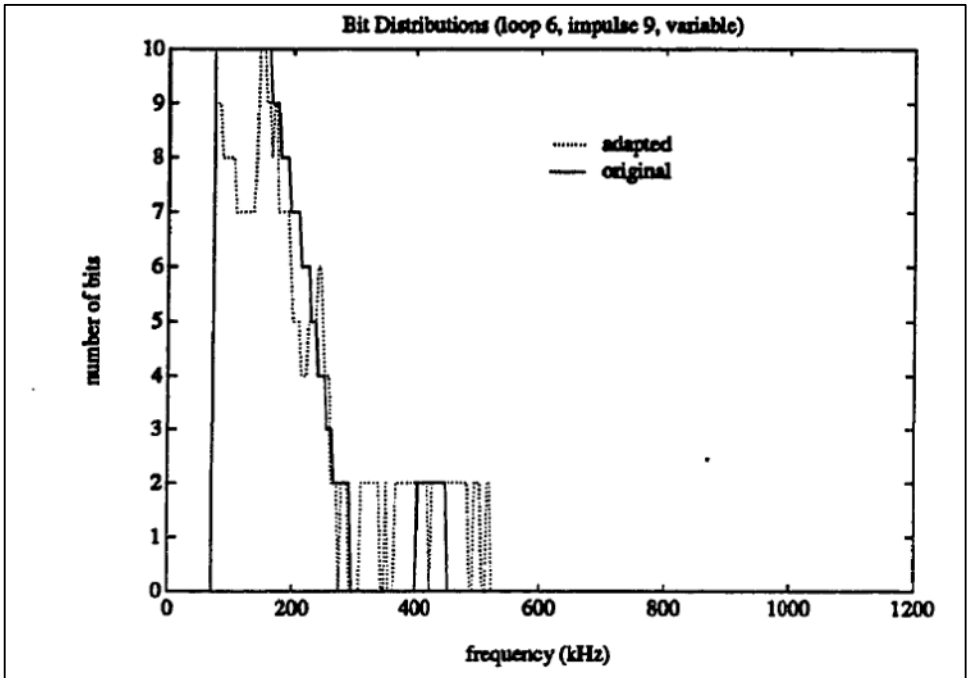

Figure 6.27: Bit Table for Loop 6, Impulse 9, and Variable Updates

Id. at Fig. 6.27.

367. To the extent it is determined that Chow does not sufficiently disclose that the multicarrier communications transceiver is operable to receive a second plurality of bits on the second plurality of carriers using a second SNR margin, using the same second margin on multiple carriers would have been obvious to a person having ordinary skill in the art. For example, it would have been obvious to a person having ordinary skill in the art to round the added margin amounts to integer numbers of dB or to the nearest tenth of a dB in order to reduce transceiver complexity, given that one goal of Chow's work is to manage and limit complexity. *See, e.g., id.* at 1 ("The goal of our present work is to facilitate the design of a practical communication system that will approach this theoretically optimal performance with a level of implementational complexity that can be realized with today's technology."). As a result of such rounding, the multicarrier communications transceiver would operable to receive a second plurality of bits on the second plurality of carriers using a second SNR margin.

368. Thus, it is my opinion that Chow discloses and/or renders obvious claim 10.d.

h. Claim 10.e "wherein the first plurality of carriers is different than the second plurality of carriers,"

369. Chow discloses and/or renders obvious claim 10.e "wherein the first plurality of carriers is different than the second plurality of carriers."

370. As I explained for claim 10.a and claim 10.b, Chow describes a DMT system that has 256 subchannels, each of which is associated with its own carrier, and there are many pluralities of carriers within each DMT symbol, including both a first plurality of carriers and a second plurality of carriers. To illustrate, I have copied below a version of Figure 2.5 of Chow in which I have indicated the subchannels corresponding to two possible pluralities of carriers, one plurality in red and the other in blue, wherein the first plurality of carriers is different than the second plurality of carriers:

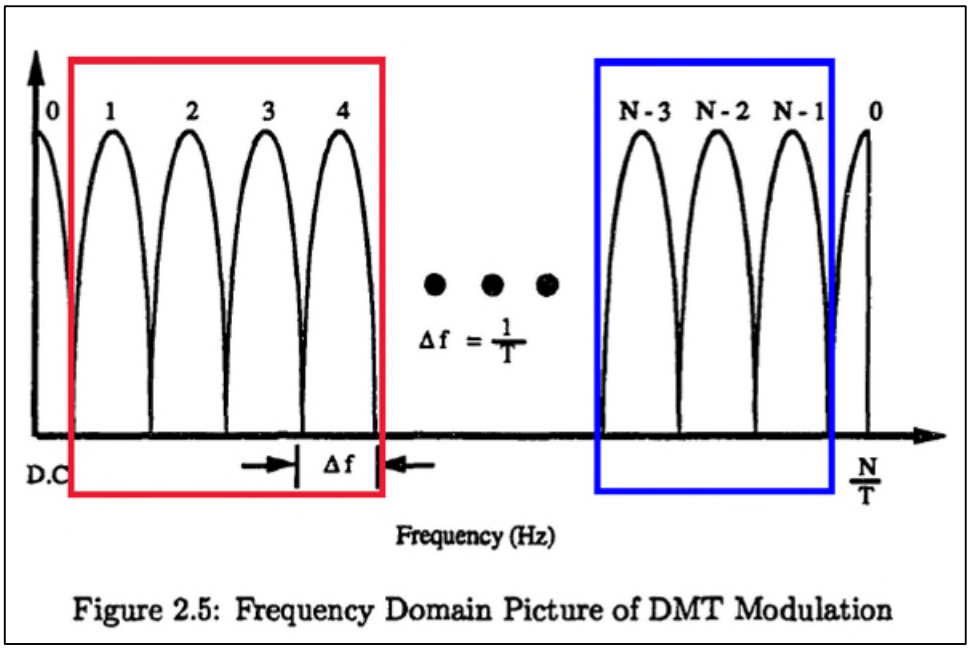

Figure 2.5: Frequency Domain Picture of DMT Modulation

Id. at Fig. 2.5 (annotated).

371. As would have been appreciated by a person having ordinary skill in the art, there are many other first and second pluralities of carriers in the multicarrier symbols disclosed by

Chow. Specifically, any two or more carriers make up a first plurality of carriers, and any two or more carriers make up a second plurality of carriers. Although the carriers in the first plurality I identified above in Figure 2.5 are contiguous, there is no requirement for the carriers in the first plurality to be adjacent to each other, and the carriers in the second plurality need not be adjacent to each other, either. As shown in the annotated version of Figure 2.5 above, the subsets of two or more carriers can be disjoint so there is no overlap in the carriers of the first plurality and the carriers of the second plurality.

372. In addition, Figures 6.20 through 6.27 of Chow illustrate many first and second pluralities of carriers that are different from each other. In the annotated versions below, I have indicated locations for several possible first and second pluralities of carriers that are different from each other, where the different pluralities are indicated by different colors.

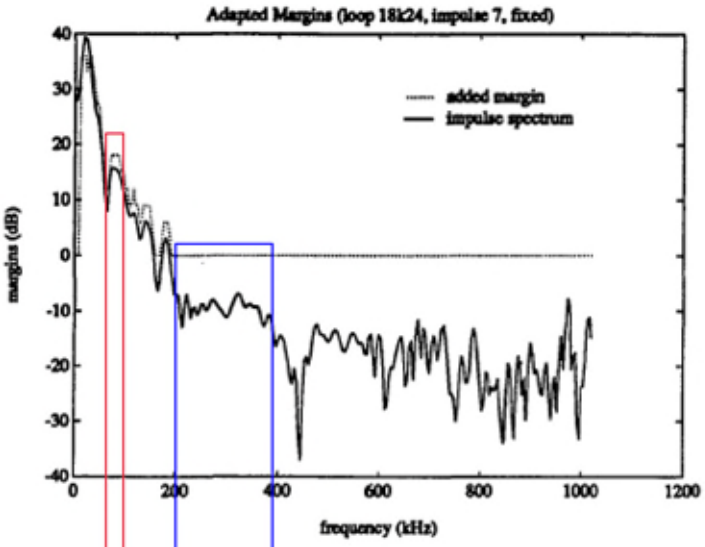

Figure 6.20: Margins for 18 kft, 24 AWG Loop with Impulse 7 and Fixed Updates

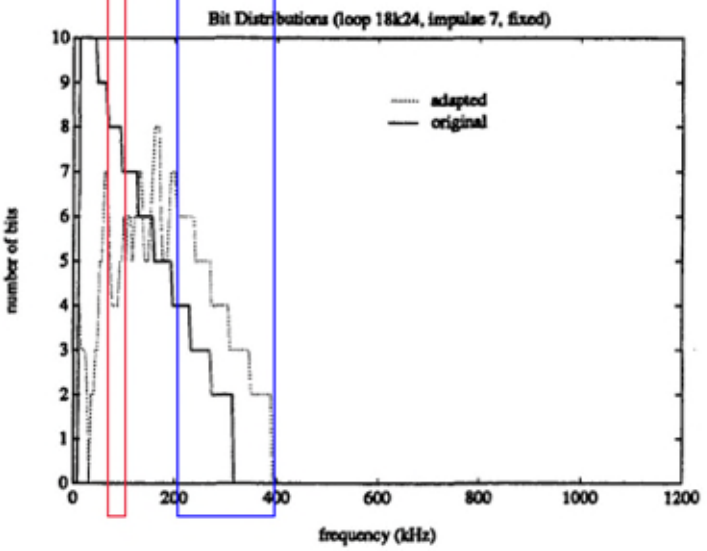

Figure 6.21: Bit Table for 18 kft, 24 AWG Loop, Impulse 7, and Fixed Updates

Id. at Figs. 6.20 and 6.21 (annotated).

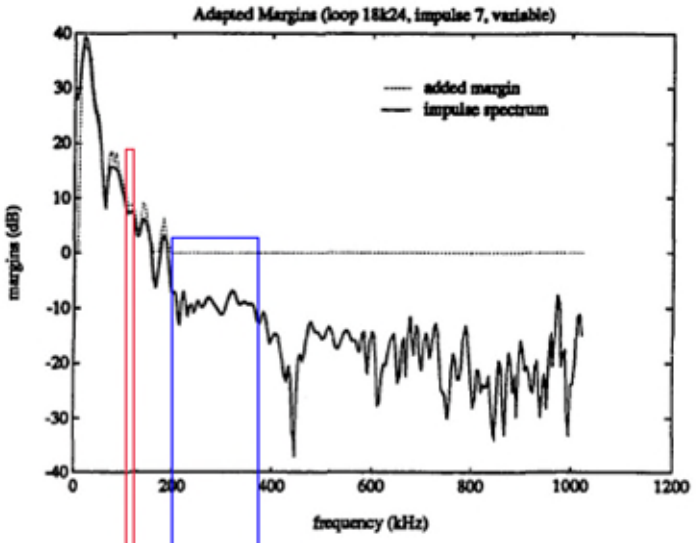

Figure 6.22: Margins for 18 kft, 24 AWG Loop with Impulse 7 and Variable Updates

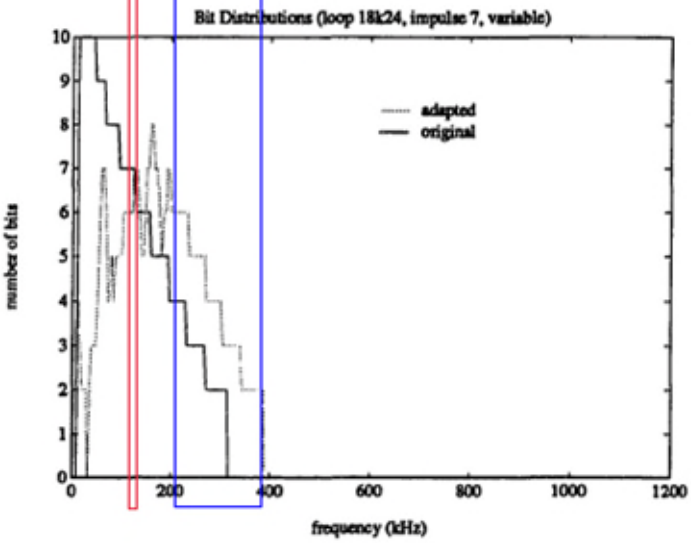

Figure 6.23: Bit Table for 18 kft, 24 AWG Loop, Impulse 7, and Variable Updates

Id. at Figs. 6.22 and 6.23 (annotated).

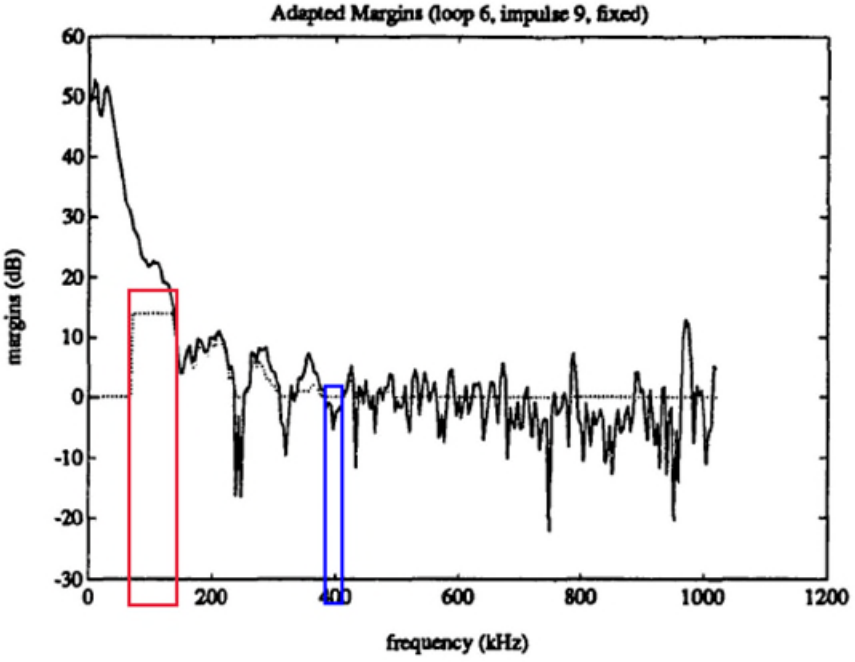

Figure 6.24: Margins for Loop 6 with Impulse 9 and Fixed Updates

Id. at Fig. 6.24 (annotated).

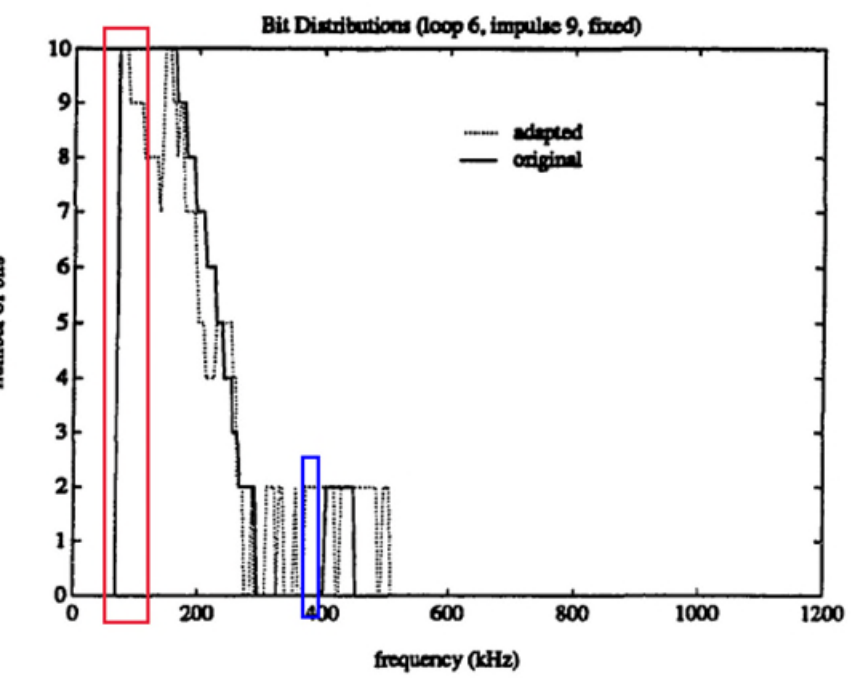

Figure 6.25: Bit Table for Loop 6, Impulse 9, and Fixed Updates

Id. at Fig. 6.25 (annotated).

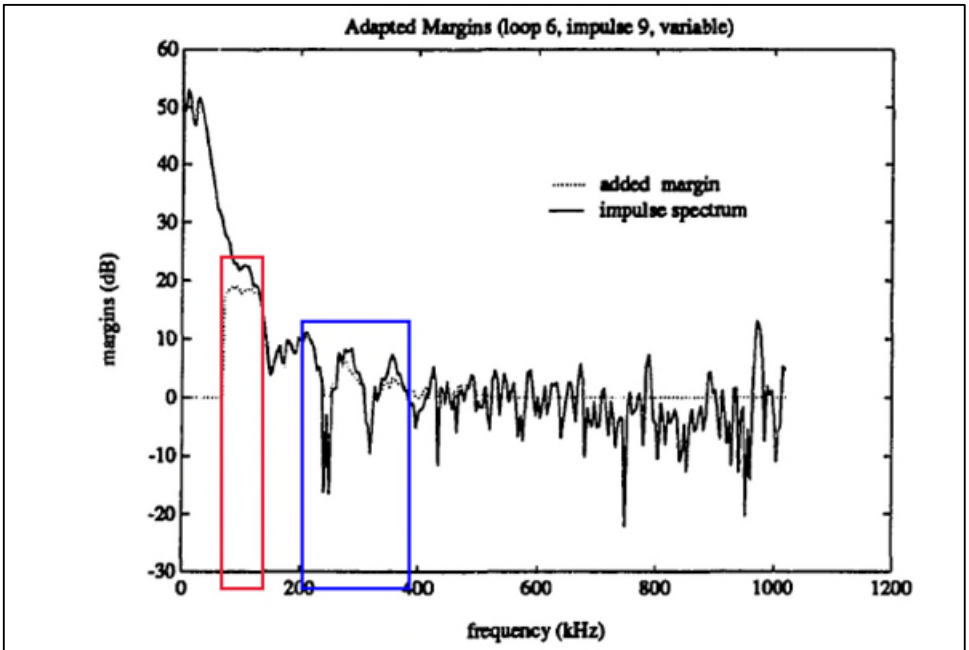

Figure 6.26: Margins for Loop 6 with Impulse 9 and Variable Updates

Id. at Fig. 6.26 (annotated).

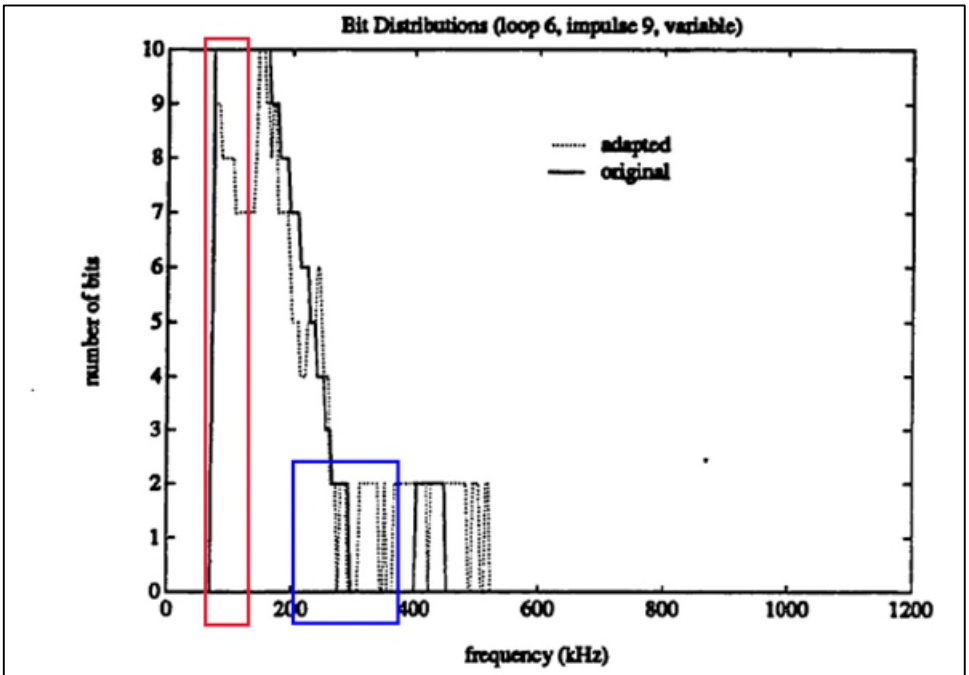

Figure 6.27: Bit Table for Loop 6, Impulse 9, and Variable Updates

Id. at Fig. 6.27 (annotated).

373. Thus, it is my opinion that Chow discloses and/or renders obvious claim 10.e.

i. Claim 10.f "wherein the first SNR margin is different than the second SNR margin,"

374. Chow discloses and/or renders obvious claim 10.f "wherein the first SNR margin is different than the second SNR margin."

375. As shown in the annotated versions of Figures 6.20, 6.22, 6.24, and 6.26, copied below, Chow discloses that the first SNR margin (for the first plurality of carriers) is different from the second SNR margin (for the second plurality of carriers), because the added margin (the amount added to the "base" margin) is different for the two pluralities of carriers:

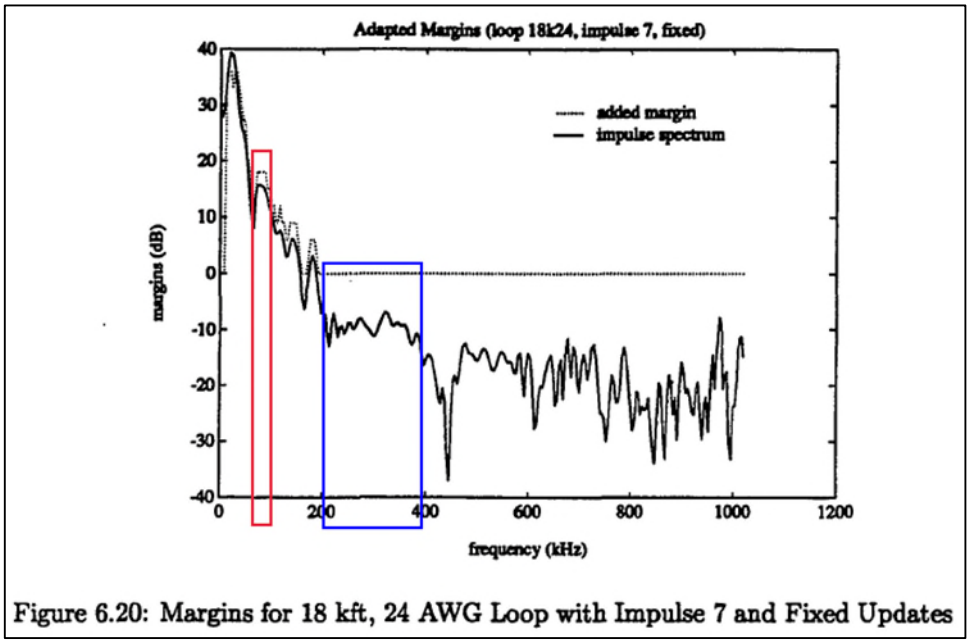

Figure 6.20: Margins for 18 kft, 24 AWG Loop with Impulse 7 and Fixed Updates

Id. at Fig. 6.20 (annotated).

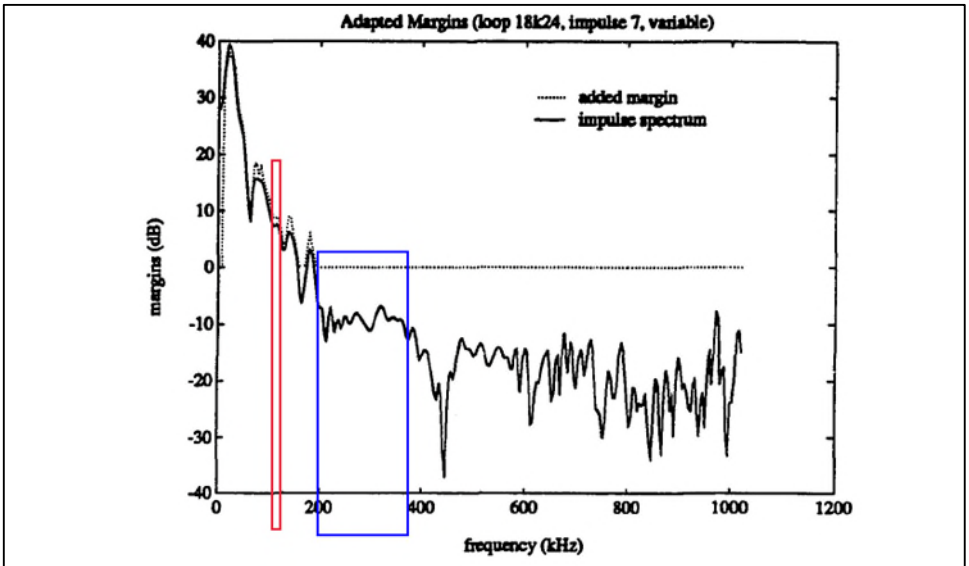

Figure 6.22: Margins for 18 kft, 24 AWG Loop with Impulse 7 and Variable Updates

Id. at Fig. 6.22 (annotated).

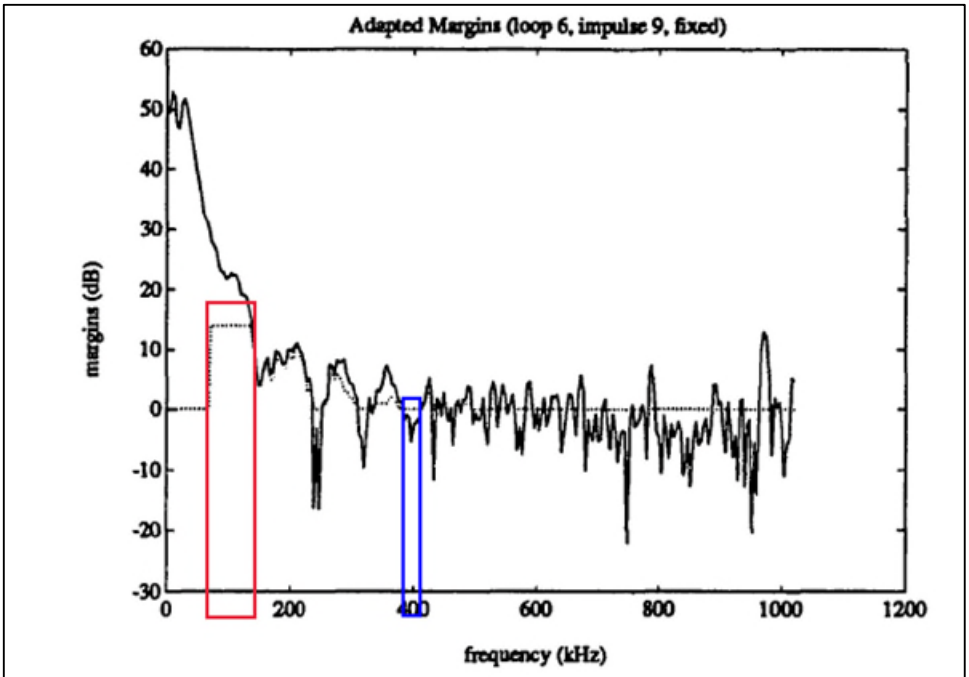

Figure 6.24: Margins for Loop 6 with Impulse 9 and Fixed Updates

Id. at Fig. 6.24 (annotated).

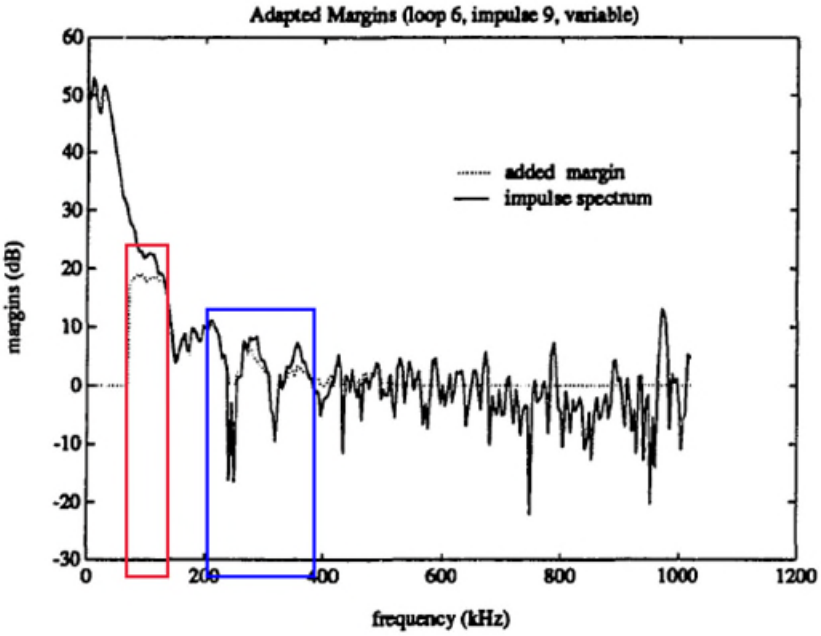

Figure 6.26: Margins for Loop 6 with Impulse 9 and Variable Updates

Id. at Fig. 6.26 (annotated).

376. "As is evident from the figure, this simple adaptation process will give additional margin to those tones most susceptible to the impulsive disturbance. . . . In some instances, the amount of margin required, after adaptation, for a particular carrier that is initially used for data transmission is large enough to force the system to stop using that particular carrier and redistribute those bits among other carriers." *Id.* at 155.

377. Figure 6.22 indicates that updating the margins according to Equation (6.17) provides an improvement over adding fixed additional margin on each update. The resulting distribution of additional margin more closely follows the actual shape of the impulse spectrum than the margin distribution presented in Figure 6.20 for the case of constant updates. Furthermore, by comparing Figures 6.21 and 6.23, we find that the resulting bit distributions are indeed different for the two techniques. Figures 6.20 and 6.22 illustrate that the margin update

process successfully increases the amount of error protection on those tones most susceptible to a particular impulse noise." *Id.*

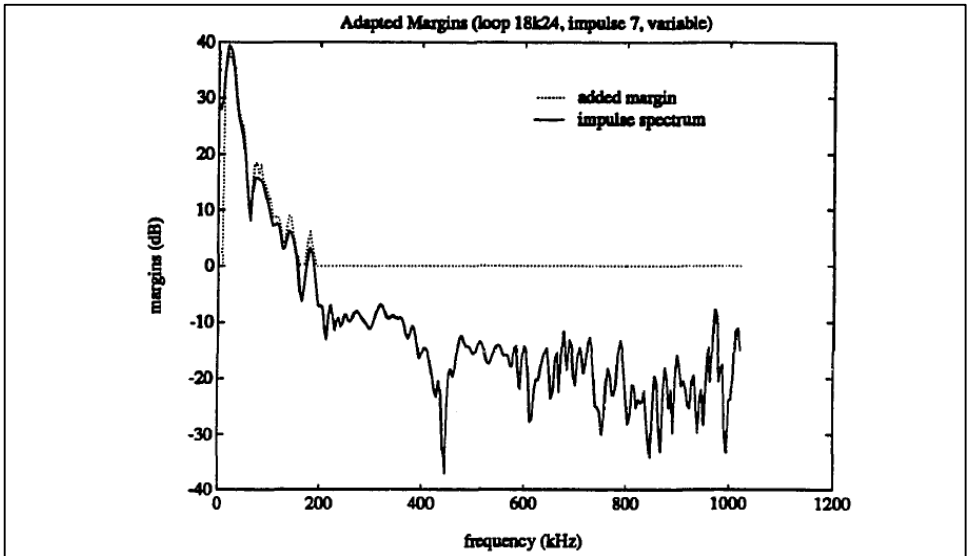

Figure 6.22: Margins for 18 kft, 24 AWG Loop with Impulse 7 and Variable Updates

Id. at Fig. 6.22.

378. "The margins in this table represent the margins on those subchannels to which no additional margin is given and are important in determining the overall BER of the system in the absence of impulse noise." *Id.* at 157.

> Figures 6.24 to 6.27 present plots of the margin distributions and bit distributions obtained for the two margin update methods, respectively. The plots in Figures 6.24 and 6.26 further confirm that both techniques for adapting the margin distributions will result in increased margin on those tones most affected by impulse noise, and the technique that allows a range of margins to be added per update will provide better performance in terms of matching the distribution of additional margins to the actual shape of the impulse spectrum. We note that in this test scenario, carriers below 70 kHz are not used due to the lower bandedge of the system. However, there is still significant impulse noise energy in the frequency band available for transmission, and as is evident from the plots, there is not enough margin available to compensate fully for the large degradation in error rate caused by the impulse noise in the lower frequency tones.

Id. at 158-60.

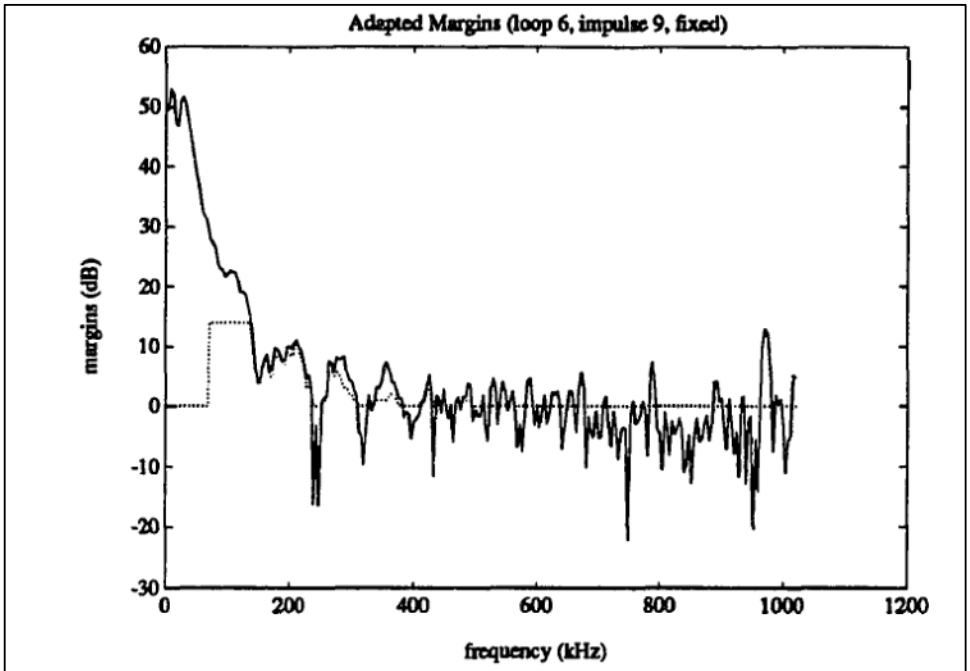

Figure 6.24: Margins for Loop 6 with Impulse 9 and Fixed Updates

Id. at Fig. 6.24.

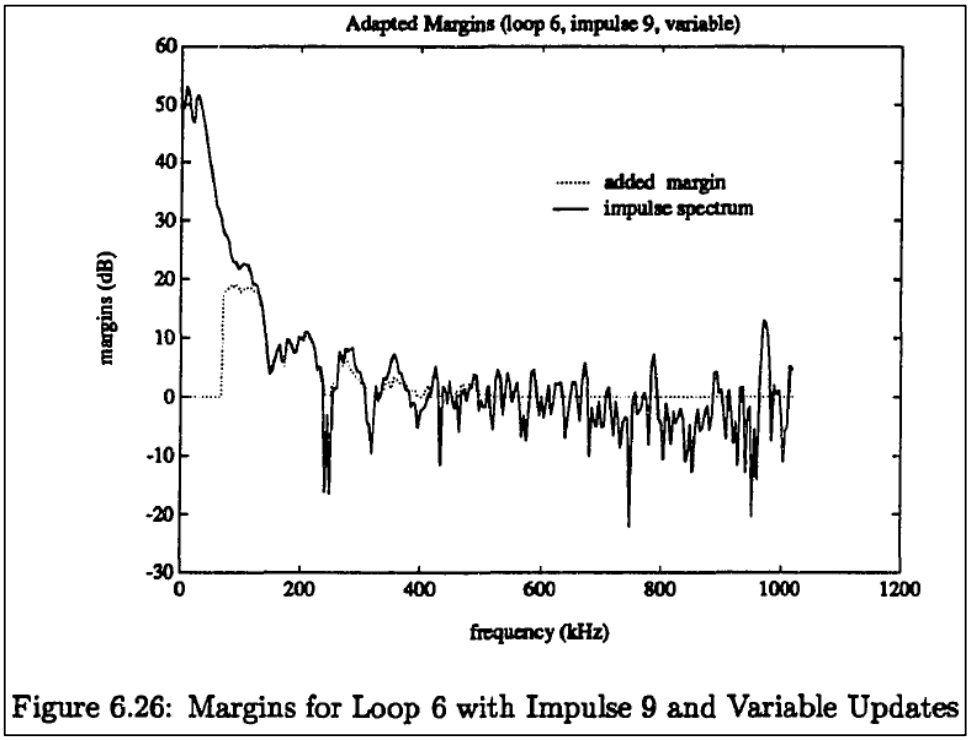

Figure 6.26: Margins for Loop 6 with Impulse 9 and Variable Updates

Id. at Fig. 6.26.

379. Thus, it is my opinion that Chow discloses and/or renders obvious claim 10.f.

j. Claim 10.g "and wherein the first SNR margin provides more robust reception than the second SNR margin."

380. Chow discloses claim 10.g "and wherein the first SNR margin provides more robust reception than the second SNR margin."

381. As would have been understood by a person having ordinary skill in the art as of the priority date, for a given error probability, a higher SNR margin provides more robust reception than a lower SNR margin. Accordingly, by disclosing that, with an error probability of 10^{-7} (Chow, 86), a higher margin is used on one plurality of subchannels and a lower margin is used on a different plurality of subchannels, Chow discloses claim 10.g.

382. As shown in the annotated versions of Figures 6.20, 6.22, 6.24, and 6.26, copied below, Chow discloses that the first SNR margin (the amount of added margin used for the first plurality of carriers), indicated by the red boxes, is higher than the second SNR margin (the amount of added margin for the second plurality of carriers), indicated by the blue boxes.

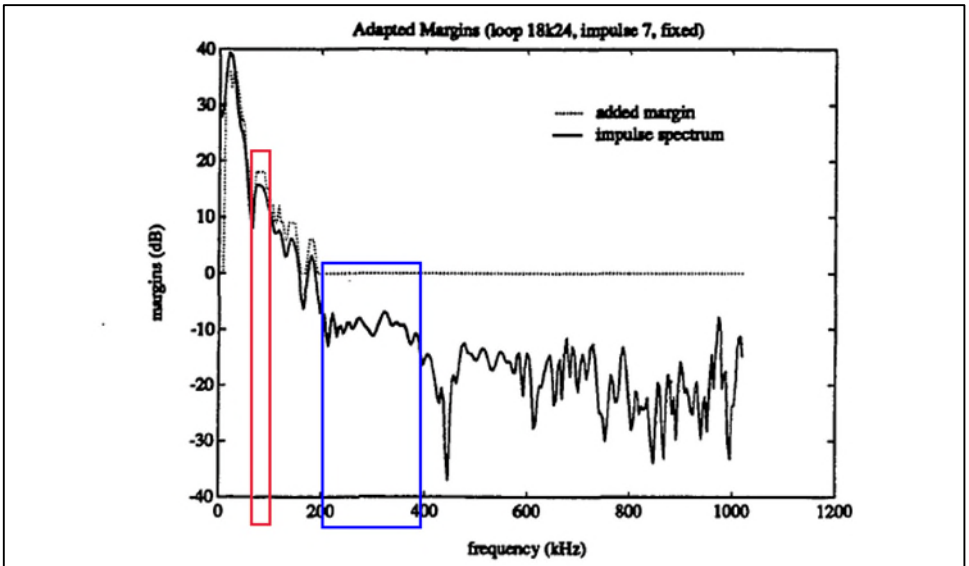

Figure 6.20: Margins for 18 kft, 24 AWG Loop with Impulse 7 and Fixed Updates

Id. at Fig. 6.20 (annotated).

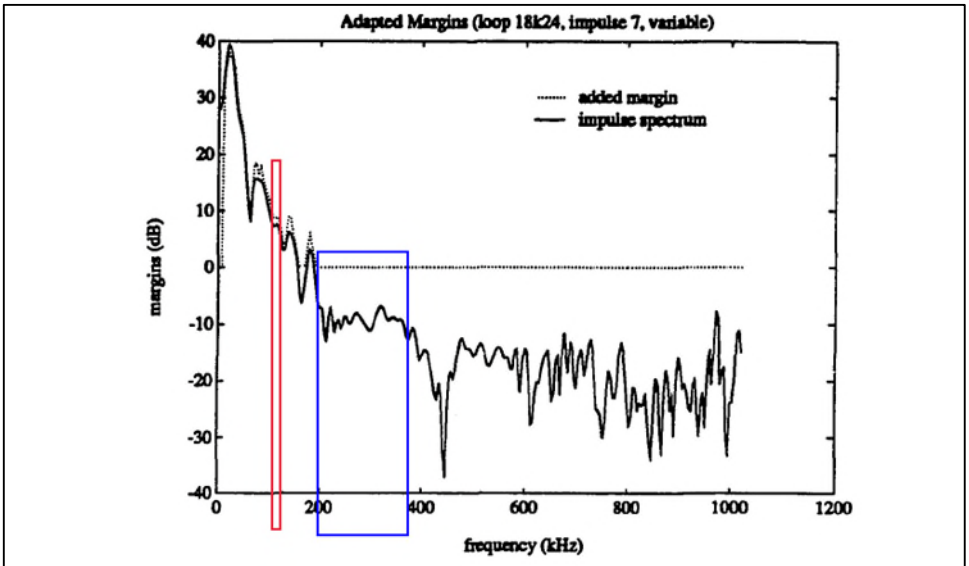

Figure 6.22: Margins for 18 kft, 24 AWG Loop with Impulse 7 and Variable Updates

Id. at Fig. 6.22 (annotated).

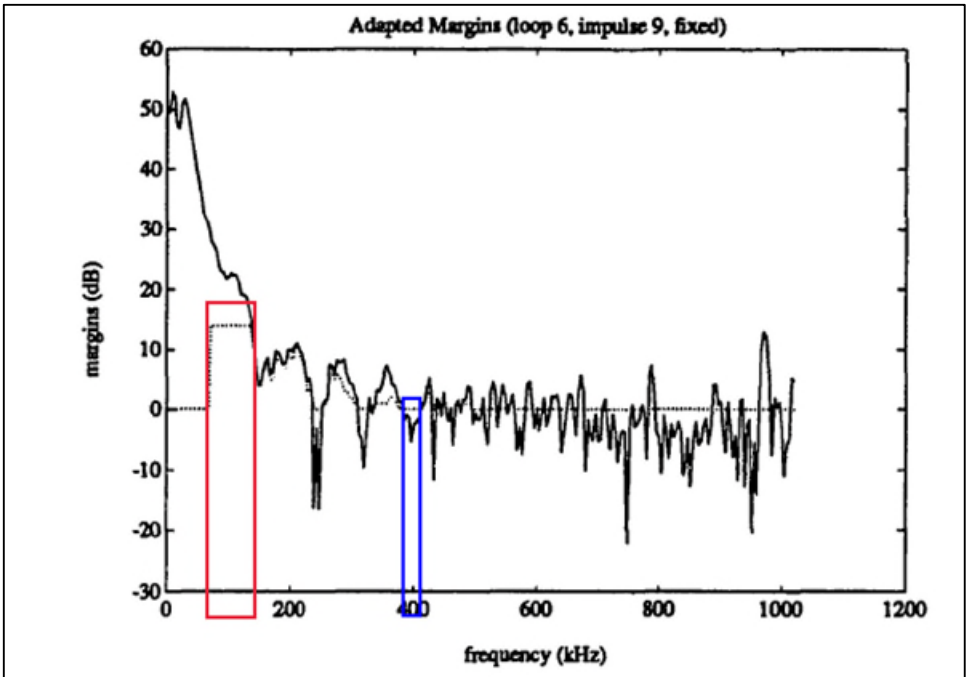

Figure 6.24: Margins for Loop 6 with Impulse 9 and Fixed Updates

Id. at Fig. 6.24 (annotated).

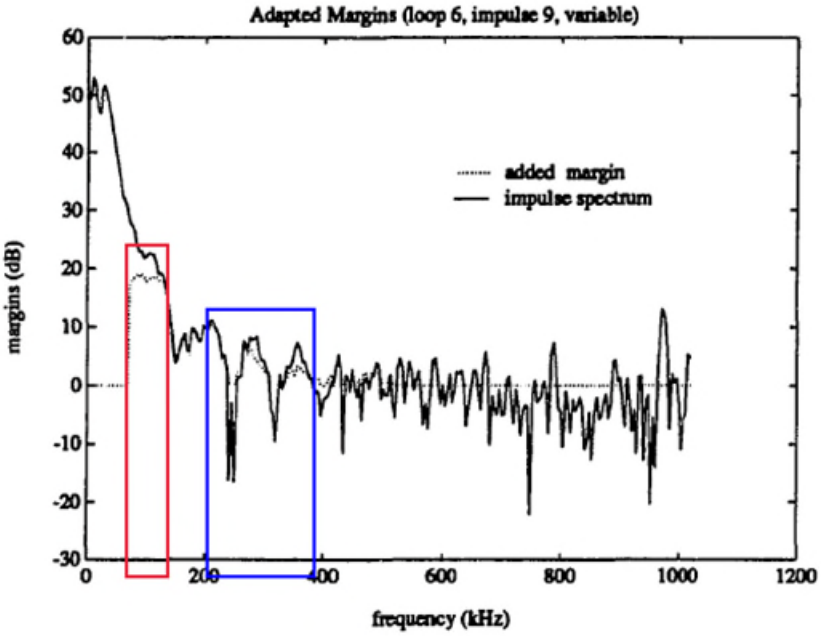

Figure 6.26: Margins for Loop 6 with Impulse 9 and Variable Updates

Id. at Fig. 6.26 (annotated).

383. Thus, the first SNR margin provides more robust reception than the second SNR margin, and Chow discloses claim 10.g.

384. "To aid the analysis of performance for both the DMT and the MMSE-DFE, we make use of a convenient single-parameter characterization of the system, known as the "SNR gap", Γ(Pr(E),C,γmargin) [10], which is a function of the chosen coding scheme C, with a total effective coding gain of γeff(C) the target bit error rate (BER) Pr(E), and the desired system performance (or noise) margin γmargin." *Id.* at 13. In clarifying this, Chow states "System performance, or noise, margin is defined as the additional amount of noise (in dB) that the system can tolerate while still operating under the desired BER requirement." *Id.* at 13 n.1.

385. "Furthermore, different numbers of bits can be conveniently assigned to different subchannels. As a result, more data can be transmitted over those subchannels with larger SNR's and less data can be transmitted over those subchannels with smaller SNR's. In fact, no data will

be transmitted over the worst portion of the frequency band if the received SNR over those subchannels cannot support the minimum number of bits at the required BER. In this manner, either the overall throughput or the system performance margin of the DMT system can be optimized." *Id.* at 20.

386. "As is evident from the figure, this simple adaptation process will give additional margin to those tones most susceptible to the impulsive disturbance. . . . In some instances, the amount of margin required, after adaptation, for a particular carrier that is initially used for data transmission is large enough to force the system to stop using that particular carrier and redistribute those bits among other carriers. *Id.* at 155.

387. Figure 6.22 indicates that updating the margins according to Equation (6.17) provides an improvement over adding fixed additional margin on each update. The resulting distribution of additional margin more closely follows the actual shape of the impulse spectrum than the margin distribution presented in Figure 6.20 for the case of constant updates. Furthermore, by comparing Figures 6.21 and 6.23, we find that the resulting bit distributions are indeed different for the two techniques. Figures 6.20 and 6.22 illustrate that the margin update process successfully increases the amount of error protection on those tones most susceptible to a particular impulse noise. However, as margin is reallocated, the performance of the other carriers will necessarily degrade." *Id.*

388. Thus, it is my opinion that Chow discloses and/or renders obvious claim 10.g.

389. Consequently, it is my opinion that claim 10 is anticipated by Chow and/or rendered obvious to a person having ordinary skill in the art in view of Chow.

Family 10 Patents, whether in its responsive expert reports, or at a later date, I reserve the right to address this evidence in my reply report, or any supplemental reports thereafter.

XIV. CONCLUSION

1068. In my opinion, based on my review of the '354 Patent and '988 Patent, the materials referenced herein, and my knowledge of what a person of ordinary skill in the art would have known at and before April 18, 2000 about the technology at issue, a person of ordinary skill in the art would have understood the Asserted Claims fail to recite patentable subject matter. Moreover the claims are not enabled and lack written description. In addition, one of ordinary skill in the art would have understood all of the claim elements and limitations of the Asserted Claims to be present in Cai, Peeters, Kapoor, Chow, and/or TNETD8000 User Guide whether alone or in combination.

1069. I reserve the right to supplement my opinions in the future to respond to any arguments or positions that TQ Delta or its experts may raise, taking account of new information as it becomes available to me.

Executed in Greenville, Texas.

Date: August 29, 2022

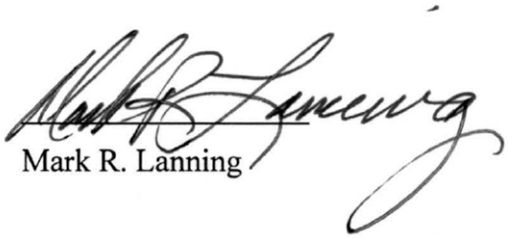

Mark R. Lanning

APPENDIX C

UNITED STATES DISTRICT COURT
FOR THE EASTERN DISTRICT OF TEXAS
MARSHALL DIVISION

TQ DELTA, LLC, *Plaintiff*, v. COMMSCOPE HOLDING COMPANY, INC., COMMSCOPE, INC., ARRIS US HOLDINGS, INC., ARRIS SOLUTIONS, INC., ARRIS TECHNOLOGY, INC., and ARRIS ENTERPRISES, LLC, *Defendants*.	Civil Action No.: 2:21-cv-310

DECLARATION OF SYLVIA D. HALL-ELLIS, PH.D.

I, Sylvia D. Hall-Ellis, Ph.D., declare and state as follows:

1. I have been retained as an expert by CommScope Holding Company, Inc., CommScope Inc., ARRIS US Holdings, Inc., ARRIS Solutions, Inc., ARRIS Technology, Inc., and ARRIS Enterprises, LLC (collectively, "CommScope") and Nokia of America Corporation, Nokia Corporation, and Nokia Solutions and Networks, Oy (collectively "Nokia").

2. I submit this Declaration to provide my expert opinions regarding the date of public availability or accessibility of a publication attached hereto as Exhibit 1: *Bandwidth Optimized Digital Transmission Techniques for Spectrally Shaped Channels with Impulse Noise*, a Ph.D. dissertation written by Peter Sienpin Chow, which was published in May 1993 by Stanford University. My Declaration sets forth my opinions in detail and provides the bases for my opinions.

3. I reserve the right to supplement or amend my opinions, and bases for them, in response to any additional evidence, testimony, discovery, argument, and/or other additional information that may be provided to me after the date of this Declaration.

4. I am being compensated for my time spent working on this matter at my normal consulting rate of $325 per hour, plus reimbursement for any additional reasonable expenses. My compensation does not in any way depend on the content of this Declaration, the substance of my opinions, or the outcome of this litigation. I have no interest in this proceeding or in any of the parties.

5. All of the materials that I considered are discussed explicitly in this Declaration.

I. QUALIFICATIONS & BACKGROUND

6. I am currently an Adjunct Professor in the School of Information at San José State University. I obtained a Master of *Library Science* from the University of North Texas in 1972, a Master of *Professional Studies* from the University of Denver in 2014, and a Ph.D. in *Library Science and Information Science* from the University of Pittsburgh in 1985. Over the last fifty years, I have held various positions in the field of library and information resources. I was first employed as a librarian in 1966 and have been involved in the field of library sciences since, holding numerous positions.

7. I am a member of the American Library Association (ALA) and its Association for Library Collections & Technical Services (ALCTS) Division, and I served on the Committee on Cataloging: Resource and Description (which wrote the new cataloging rules) and as the chair of the Committee for Education and Training of Catalogers and the Competencies and Education for a Career in Cataloging Interest Group. I also served as the founding Chair of the ALCTS Division's Task Force on Competencies and Education for a Career in Cataloging. Additionally,

I have served as the Chair for the ALA Office of Diversity's Committee on Diversity, as a member of the REFORMA National Board of Directors, as a member of the Editorial Board for the ALCTS premier cataloging journal, *Library Resources and Technical Services,* and as a Co-Chair for the Library Research Round Table of the ALA.

8. I have also given over one hundred presentations in the field, including several on library cataloging systems and Machine-Readable Cataloging (MARC) standards. My current research interests include library cataloging systems, metadata, and organization of electronic resources.

9. I have previously served as an expert witness in approximately 600 cases over the course of the last decade. I have extensive experience opining on the publication status of printed references in patent litigations in federal district courts and in proceedings before the Patent Trial and Appeal Board. I have been deposed twenty-one times. I have not testified at trial.

10. During my career I have served as a Dissertation Committee Chair ten times, as a Dissertation Committee member three times, and as a Thesis (Capstone) Chair fourteen times. My personal experiences writing a master's thesis and Ph.D. dissertation and those working with students as a tenured faculty member have provided me with in-depth experience and detailed knowledge of the standardized processes that students follow as part of the culminating process to earn a graduate degree.

11. The steps that a student takes in pursuit of a graduate degree are predictable and include a predefined number.[1] The Dissertation Chair is responsible for guiding the student and overseeing formal coursework; reviewing research activities; the preparation and defense of the proposal; the selection of committee members; drafting the dissertation document; ensuring the

[1] https://study.com/how_to_get_your_phd.html.

completion of requirements for binding; filing in the institutional digital repository and library; and submitting paperwork with the Graduate Office before specified deadlines in anticipation of conferring the degree. While there are materials that one can read about the process, there is no substitute for going through the process personally, serving as a committee member, and chairing the committee for a student. Understanding the intricacies of the process is essential to determine institutional documents, deadlines, and requirements required at institutions other than the one at which someone works.

12. My full curriculum vitae is attached hereto as Exhibit 2.

II. SCOPE OF OPINIONS

13. I am not an attorney and will not offer opinions on the law. I am, however, rendering my expert opinion on the dates of public accessibility of the reference discussed herein, including when and how the reference was disseminated or otherwise made available to persons interested and ordinarily skilled in the subject matter or art, exercising reasonable diligence. In particular, I am rendering opinions on how such persons could have located, before April 18, 2000, the Chow reference discussed below.

III. LEGAL STANDARDS

14. I am informed by counsel and understand that a printed publication is deemed publicly accessible as of the date it was disseminated or otherwise made available such that a person interested in and ordinarily skilled in the relevant subject matter could locate it through the exercise of ordinary diligence.

15. I also understand that public accessibility is a case-by-case determination based on circumstances particular to an individual publication. I further understand, however, that a printed publication is rendered "publicly accessible" if a person of ordinary skill in the art, exercising

reasonable diligence, would have located the publication, or would have known to look for it. I further understand that a printed publication is thus rendered "publicly accessible" if it is filed in an online database, like ProQuest's Dissertations and Theses, that is cataloged and indexed such that a person interested in the relevant subject matter could locate it (*i.e.*, I understand that cataloging and indexing by an online database is sufficient, though there are other ways that a printed publication may qualify as publicly accessible). One manner of sufficient indexing is indexing according to subject matter category. I understand that the cataloging and indexing by a database of a single instance of a particular printed publication is sufficient, even if that database is hosted by a foreign country. I understand that, even if access to a database is restricted, a printed publication that has been cataloged and indexed therein is deemed publicly accessible if the public concerned with the relevant subject matter would know of the printed publication. I also understand that the cataloging and indexing of information that would guide a person interested in the relevant subject matter to the printed publication, such as the cataloging and indexing of an abstract for the printed publication, is sufficient to render the printed publication publicly accessible.

16. I understand that routine business practices, such as general database and library cataloging and indexing practices, can be used to establish an approximate date on which a printed publication became publicly accessible.

IV. PERSONS OF ORDINARY SKILL IN THE ART

17. I am informed by counsel that the subject matter of this proceeding relates to digital subscriber line (DSL) technology.

18. I am informed by counsel that a "person of ordinary skill in the art at the time of the inventions" is a hypothetical person who is presumed to be familiar with the relevant field and

its literature at the time of the inventions. This hypothetical person is also a person of ordinary creativity, capable of understanding the scientific principles applicable to the pertinent field.

19. I am informed by counsel that Petitioners' expert has opined that persons of ordinary skill in this subject matter or art would have had a bachelor's degree in electrical or computer engineering and 5 years of experience in telecommunications or a related field, a Master's degree in electrical engineering and 2-3 years of experience in telecommunications or a related field, or a Ph.D. in electrical engineering with 1-2 years of experience in telecommunications or a related field. I understand that a person with less education, but more relevant practical experience may also meet this standard.

20. It is my opinion that such a person would have been engaged in research, learning, study, and practice in the field, and possibly formal instruction so that bibliographic resources relevant to his or her research would be familiar. Before April 18, 2000, such a person would have had access to an array of long-established print resources in digital communications, DSL technology, or related fields as well as online resources providing indexing information, abstracts, and full text services for digital communications and DSL technology.

V. LIBRARY PROFESSIONAL PRACTICES

21. In preparing this Declaration, I used authoritative databases, including the OCLC bibliographic database, the Library of Congress Online Catalog, the Library of Congress Subject Authorities and ProQuest's *Dissertations and Theses* to confirm citation details of the publication discussed.

22. ***Indexing***. A researcher may discover material relevant to his or her topic in a variety of ways. One common means of discovery is to search for relevant information in an index of periodical and other publications. Having found relevant material, the researcher will then

normally obtain it online, look for it in libraries, or purchase it from the publisher, a bookstore, a document delivery service, or other provider. Sometimes, the date of a document's public accessibility will involve both indexing and library date information. However, date information for indexing entries is often unavailable. This is especially true for online indices.

23. Indexing services use a wide variety of controlled vocabularies to provide subject access and other means of discovering the content of documents. The Library of Congress Subject Authorities includes standard forms of terms and cross references that are included in bibliographic records. Subject headings are terms that an individual seeking a document regardless of format can enter in the search bar of the online catalog. Subjects also connect an authenticated term (one included in the Library of Congress subject headings list) with related, broader, and narrower terms.

24. Online indexing services commonly provide bibliographic information, abstracts, and full-text copies of the indexed publications, along with a list of the documents cited in the indexed publication. These services also often provide lists of publications that cite a given document. A citation of a document is evidence that the document was publicly available and in use by researchers no later than the publication date of the citing document. Prominent indexing services include *Scopus,* the *IEEE Xplore* database, the *ACM Digital Library, Google Scholar,* the *Internet Archive,* and ProQuest databases for dissertations, theses, journals, and digital reference materials.

25. Databases and digital repositories like those mentioned in paragraph 24 provide search capabilities through title, author, subject, keyword, and standard numbers (ISBN and ISSN) that enable information professionals and individuals to locate books, articles, conference papers, and other publications. The databases and digital repositories include retrospective collections of

scanned or digitized materials and are updated regularly. Collegiate and university studies at the undergraduate and graduate level require that students develop familiarity and proficiency using indexing services, databases, and digital repositories.

VI. PUBLICATION

a. *Bandwidth Optimized Digital Transmission Techniques for Spectrally Shaped Channels with Impulse Noise* by Peter Sienpin Chow ("Chow")

26. Attached hereto as Exhibit 1 is a dissertation, *Bandwidth Optimized Digital Transmission Techniques for Spectrally Shaped Channels with Impulse Noise* by Peter Sienpin Chow. Exhibit 1 includes a true and correct copy of the title page, table of contents, and text from the ProQuest[2] database *Dissertations and Theses*.[3] The dissertation title page shows a date of May 1993. I obtained this dissertation from UMI's database *Dissertations and Theses* and made the copy which comprises Exhibit 1. Specifically, the text is complete; no pages are missing, and the text on each page flows seamlessly from one page to the next; further, there are no visible alterations to the document. Exhibit 1 was found within the custody of the custodian to whom the author granted permission to make copies and reproductions. Exhibit 1 is a true and correct copy in a condition that creates no suspicion about its authenticity.

27. A dissertation exhibits the following characteristics: the dissertation is attributed to a single creator or author (in this case Peter S. Chow) who affixes a date of creation (in this case May 1993), recognizes a committee of three or more faculty members with their affiliations (in this case Professors John M. Cioffi, G. David Forney, Jr., and Allen M. Peterson), a list of scholarly

[2] ProQuest is the corporate global information-content and technology company founded as University Microfilms (UMI) in 1939. Over the last 80 years, the firm has grown through corporate acquisitions and product development to be a major supplier globally of databases and digital products (https://www.proquest.com/).

[3] https://about.proquest.com/en/products-services/pqdtglobal.

references (in this case 99 references in the "Bibliography" on pages 177–187), and publishes the document through the higher education institute conferring the doctoral degree (in this case the Department of Electrical Engineering and the Committee on Graduate Studies of Stanford University).

28. Attached hereto as Attachment 1a is a true and correct copy of the online catalog record for this dissertation from the Stanford University Library. The catalog record indicates that copies of the dissertation are located in the Green Library and in the Thesis Special Collection. I personally identified and retrieved the library catalog record which is Attachment 1a.

29. Attached hereto as Attachment 1b is a true and correct copy of the MARC record for the dissertation, *Bandwidth Optimized Digital Transmission Techniques for Spectrally Shaped Channels with Impulse Noise* by Peter Sienpin Chow, obtained from the OCLC bibliographic database. I personally identified and retrieved the MARC record that is Attachment 1b. The library that created the record is recorded in field 040 with a unique library code. For Attachment 1b, that library code is "STF," which means that the MARC record for this dissertation was created at the Stanford University Library. As can be seen in the "Entered" field in the MARC record for this exhibit, a cataloger at the Stanford University Library created OCLC record number 38702667on January 21, 1993, as shown in field 008.

30. Attachment 1b indicates that the Chow dissertation as cataloged at Stanford University is currently available from that institution. In view of above, this dissertation was publicly available no later than May 31, 1993, because by that date it had been received, cataloged, and indexed at the Stanford University Library, placed in the custody of UMI, and made part of the OCLC bibliographic database. For these reasons, it is my opinion that Exhibit 1 was published and accessible to the public no later than May 31, 1993.

VII. SUMMARY OF OPINIONS

31. In view of the foregoing, it is my opinion that the publication described above was publicly available no later than the corresponding date listed in the table below:

Exhibit	Publication	Publicly Available No Later Than
1	*Bandwidth Optimized Digital Transmission Techniques for Spectrally Shaped Channels with Impulse Noise* by Peter Sienpin Chow	May 31, 1993

32. I declare under penalty of perjury that, to the best of my knowledge, the foregoing is true and correct.

Dated: August 29, 2022

Respectfully submitted,

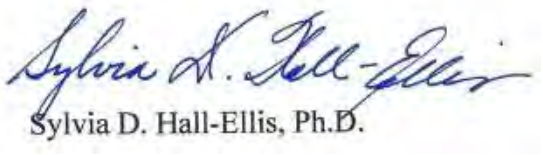

Sylvia D. Hall-Ellis, Ph.D.

EXHIBIT 1

Order Number 9326444

Bandwidth optimized digital transmission techniques for spectrally shaped channels with impulse noise

Chow, Peter Sienpin, Ph.D.

Stanford University, 1993

U·M·I
300 N. Zeeb Rd.
Ann Arbor, MI 48106

BANDWIDTH OPTIMIZED DIGITAL TRANSMISSION TECHNIQUES FOR SPECTRALLY SHAPED CHANNELS WITH IMPULSE NOISE

A DISSERTATION
SUBMITTED TO THE DEPARTMENT OF ELECTRICAL ENGINEERING
AND THE COMMITTEE ON GRADUATE STUDIES
OF STANFORD UNIVERSITY
IN PARTIAL FULFILLMENT OF THE REQUIREMENTS
FOR THE DEGREE OF
DOCTOR OF PHILOSOPHY

By
Peter S. Chow
May 1993

I certify that I have read this thesis and that in my opinion it is fully adequate, in scope and in quality, as a dissertation for the degree of Doctor of Philosophy.

John M. Cioffi
(Principal Advisor)

I certify that I have read this thesis and that in my opinion it is fully adequate, in scope and in quality, as a dissertation for the degree of Doctor of Philosophy.

G. David Forney, Jr.

I certify that I have read this thesis and that in my opinion it is fully adequate, in scope and in quality, as a dissertation for the degree of Doctor of Philosophy.

Allen M. Peterson

Approved for the University Committee on Graduate Studies:

Abstract

Most practical digital transmission channels exhibit intersymbol interference and a number of additive noise impairments, such as thermal noise, residual echo, quantization noise, crosstalk, and impulse noise. In order to reliably transmit and receive the highest data rate possible through such non-ideal channels, every component of the communication system must be optimized. In this dissertation, we focus on one particular element of the overall system optimization; namely, the optimization of the system transmission bandwidth. While the classic water-pouring energy distribution is known to achieve the capacity of a channel, it is typically impractical to implement. By optimizing the system transmission bandwidth, it can be shown that a flat on/off energy distribution will perform virtually as well as the water-pouring energy distribution for most practical applications. Furthermore, by examining and comparing the asymptotic performance levels of a single-carrier system employing Quadrature Amplitude Modulation with a Minimum-Mean-Squared-Error Decision Feedback Equalizer receiver and a multicarrier system using the Discrete Multitone modulation, we show that multicarrier bandwidth optimization techniques can be adapted for single-carrier system use as well. We introduce the concept of adaptive transmitters for quasi-stationary duplex channels in the context of transmission bandwidth optimization. A physical medium on which these proposed techniques can be tested is the copper twisted pairs in the current telephone network; therefore, we will analyze the performance of our proposed bandwidth optimization algorithms when applied to a number of advanced Digital Subscriber Line services. Computer simulation demonstrates that very high data rates (6.4 Mbps or more) can be achieved in the presence of additive white Gaussian noise and crosstalk, on

many Asymmetric Digital Subscriber Line loops utilizing a bandwidth optimized transmission system. In some Digital Subscriber Line services, however, large-amplitude, impulsive disturbances, known collectively as impulse noise, may prove to be a dominant source of impairment. In order to mitigate the effects of impulse noise, we propose several novel error control techniques designed specifically for a Discrete Multitone system that will exploit impulse noise characteristics in both time and frequency domains. Although we concentrate our simulation efforts around Digital Subscriber Line applications, techniques proposed and studied in this dissertation can be applied to a wide range of digital transmission systems over spectrally shaped channels with impulse noise.

Acknowledgements

No usual thanks can sufficiently acknowledge all the people who have affected my work and helped me along the way to the completion of this dissertation. While the doctoral degree represents a significant milestone from a personal perspective, I could not have accomplished it without the support and encouragement from my family, friends, and colleagues.

I wish first to thank my dissertation advisor, Professor John Cioffi, for his continuous and always enthusiastic support over the past four and a half years. John introduced me to the exciting field of digital communications in his class during my first year at Stanford, and consequently, I had the pleasure and privilege to join his "coding" research group. Without question from a technical standpoint, I have benefited tremendously from his research experience and his keen intuition in practical problem solving. Equally important, his insistence for his students to clearly express and present original ideas and results has undoubtedly made me a more effective researcher. Over the years, however, John has also become much more than just a dissertation advisor; he has become a friend whom I respect and whose opinion I value.

I am grateful to Dr. G. David Forney, Jr. for his prompt and careful reading of my dissertation, and I wish to thank Professor Clayton Bates, Professor John Gill, Dr. Dale Harris, and Professor Allen Peterson, for cheerfully agreeing to serve on my orals and reading committees on very short notice.

It is difficult to list all my friends and colleagues in the Information Systems Lab who have aided me in my research and contributed to my intellectual, as well as personal, growth throughout my stay at Stanford. Current and former members

of John's "coding" group have continuously challenged my mind intellectually and provided me with insights to problems not necessarily of a technical nature. To Paul Algoet, Jim Aslanis, Jacky Chow, Glen Dudevoir, Paul Fortier, Minnie Ho, Krista Jacobsen, Sanjay Kasturia, Hui-Ling Lou, Jerry Tu, and Nick Zogakis, I will miss all the interesting discussions that sometimes turned into rather lively debates every Wednesday afternoon during our group meeting. I wish to acknowledge my other officemates in Durand 112 and members of John's other research groups, including Bill Abbott, Naofal Al-Dhahir, Phil Bednarz, Harry Bims, Ivo Dobbelaere, Kevin Fisher, Miki Genossar, Inkyu Lee, Susan Lin, Cory Modlin, Peter Okrah, Nick Sands, Norm Swenson, Paul Voois, Katie Wilson, and Rob Ziegler. Behind the door of Durand 112, hours of stimulating and often educational conversations, ranging from deep philosophical ideas to the latest ISL gossip, have provided a most welcome balance and entertainment. On the softball field, we may not have always won, but we always had fun - ISL Knows Softball! I am also indebted to the entire support staff at ISL and to Joice DeBolt and Charlotte Coe in particular, whose assistance and friendship in the past four years have been invaluable.

Amati Communications Corporation has played an important and unique role in the later phase of my thesis research. In a very rare opportunity for a graduate student, I was able to participate in turning a number of theoretical ideas presented in my dissertation into actual products. I want to thank Professor Cioffi and Kim Maxwell for co-founding the company. I also want to credit the team of world-class software engineers and hardware designers, including two former fellow "coders" (Jim Aslanis and Jacky Chow), Rick Adolf, John Bingham, Mark Flowers, Toni Gooch, Ron Hunt, Steve Macica, Mark Mallory, Po Tong, and Van Whitis, for building the fastest and most ambitious high speed, multicarrier transceiver system to date in the shortest possible time. Furthermore, the financial reward from Amati for my consulting services is gratefully acknowledged, and I wish to thank Jan Lennon for her always cheerful support.

While they may not have contributed directly in the technical sense, I certainly could not have completed my dissertation and enjoyed my years at Stanford as much as I did without some very special friends and roommates. It is no easy task

to put up with someone who regularly works at three in the morning, sleeps in the afternoon, and talks as much as I do. To Alex Clemm, Ken Honer, Yotto Koga, Kent Major, Joe Stevens, and John Suh, thank you for being such understanding and tolerant roommates. I will miss and always cherish the time we spent together. To my other friends at Stanford, both on and off the volleyball court, thank you for five wonderful years. I am also grateful to all my teachers and friends from Princeton, Midland, and Taiwan, for their contributions to my educational development and their continued friendship.

The influence of my parents cannot possibly be expressed in words. They sacrificed everything by moving from Taiwan to the United States to give my brother Sien and me a better opportunity in life. Without their enduring and unconditional love, I would not be where I am today. During my first seven years in this country, I lived with my aunt Grace, who is like a third parent to me. Her love and guidance have made me a better person. Special recognition must also go to my older brother Sien, who has always set an excellent example for me to follow and has been my hero and best friend growing up. While I have only known her for a relatively short period of time, my fiancée's mother Kay has already enriched my life more than she can imagine. Thank you Mama Kay for showing me how to be less judgmental and to see the better side of people. Last but certainly not least, I wish to thank my fiancée Kate. She always sees the best in me, and she brings the best out of me. Her love, understanding, and friendship have made all the difference in the world. Without question, she is the best thing that ever happened to me. To Kate, my parents, and the rest of my family, I dedicate this dissertation.

Contents

List of Tables

List of Figures

Chapter 1

Introduction

With the advent of personal computers in the late twentieth century, our society has entered a new age of information processing, storage, and transmission. Tremendous demands for more information processing ability, larger information storage capacity, and faster information transmission capability have spurred an enormous amount of research interest in these areas. While information processing and storage are of great importance in their own right, it is ultimately the transmission of information that links the individual resources together. The fundamental aim of information transmission, or communication, is to transmit and receive reliably the highest possible rate over the given transmission medium, which, of course, requires the optimization of every component within a communication system. The goal of our present work is to facilitate the design of a practical communication system that will approach this theoretically optimal performance with a level of implementational complexity that can be realized with today's technology. In particular, we will examine the steps of modulation, equalization, and coding involved in a digital communication system for channels with memory and other non-ideal characteristics. The main thrust of this dissertation centers on the optimization of the system transmission bandwidth, which is recognized as a key component in the optimization of the overall system.

1.1 An Overview of Digital Communications

Communication is essentially the reliable transfer of information from one spatial or temporal location to another. Due to its numerous advantages over conventional analog communication, digital communication has rapidly replaced its analog predecessor in many current applications. Figure 1.1 illustrates a block diagram of a typical digital communication system. The information source is assumed to con-

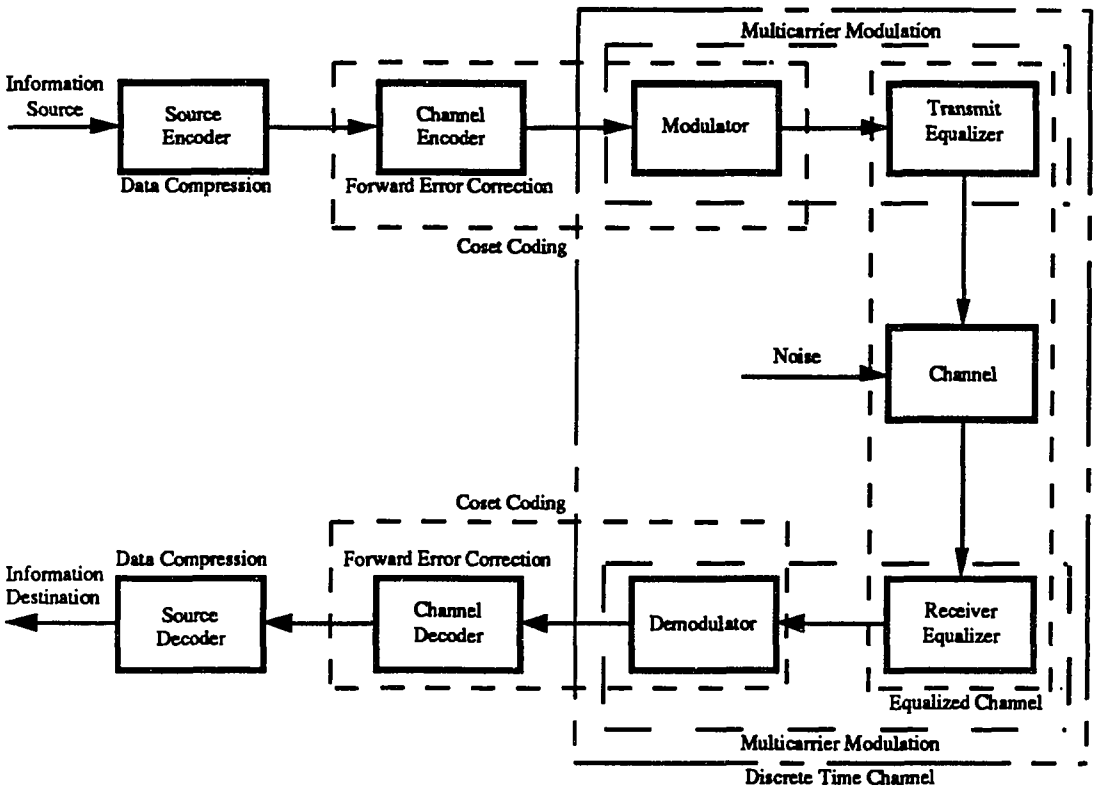

Figure 1.1: Digital Communication System Model

tain data that are already in digital form to be sent over the physical transmission medium to the appropriate information destination. However, all physical channels exhibit non-ideal characteristics that prevent perfectly reliable transmission of data at any desirable rate. As a result, a rich field of theories and techniques have been developed over the years to compensate for these physical imperfections in the

transmission medium with the ultimate goal of transmitting as much information with as good reliability as possible. The source encoder and decoder pair seeks to increase overall data rate by intelligently removing redundancy, through data compression, from the "raw" or the original digital data source, which can consist of text, audio, video, or other forms of data. The channel encoder and decoder pair aims to increase reliability of transmission by efficiently inserting controlled redundancy, through error control coding, back into the transmitted data stream in order to aid in the recovery of data in the presence of noise. Because discrete time symbols cannot be transmitted directly through a physical channel, modulation is necessary to convert a discrete time signal into a continuous time signal, and demodulation performs the inverse operation at the receiver to translate the received continuous time signal back to a digital form. The dispersive nature of the physical medium may introduce memory, or intersymbol interference, into the channel so that the current received data symbol is corrupted by a number of previous data symbols. To mitigate the effects of intersymbol interference, some form of transmit and/or receive equalization is typically used.

In Shannon's original papers [1] and [2], a mathematical foundation of information theory is developed, and the theoretical capacity of a communication channel is derived. Unfortunately, Shannon did not explicitly provide a method of how to achieve this capacity in his landmark work; however, he did show that it is information lossless to completely separate source coding from channel coding, even though the first removes redundancy and the second inserts redundancy. As a result of Shannon's observation, theories for source coding and channel coding have taken parallel paths of development throughout most of the past four and a half decades. We will focus on the channel coding component in our present work. The major breakthrough in the field of channel coding during the past thirty years came with Ungerboeck's trellis codes for memoryless, additive white Gaussian noise channels [3]. Forney further characterized all known good codes for band-limited channels, including trellis codes, as coset codes [4] [5]. Essentially, coset coding combines modulation with channel coding, and in the recent years, a number of researchers have extended this result to channels with memory by combining equalization with

coding [6] [7] [8] [9]. Two main approaches are followed by most combined equalization and coding methods. The first approach performs equalization entirely in the time domain, using a single carrier; while the second approach accomplishes the task in either the frequency domain or the code domain, using multiple carriers.

In our present work, we concentrate on a key component of any combined equalization and coding system; namely, the optimization of the system transmission bandwidth. In particular, we will propose a number of practical bandwidth optimization algorithms that can be implemented with either a single-carrier or a multicarrier system, and we further introduce the idea of using adaptive transmitters for quasi-stationary duplex channels.

1.2 Dissertation Outline

This dissertation addresses a number of problems involved with data transmission at near-capacity rates over band-limited channels with memory, additive Gaussian noise, crosstalk, and impulse noise. We begin with the description of a basic digital communication system model and a brief historical review of data transmission in this chapter.

Chapter 2 examines and compares the two main families of modulation and equalization techniques in use today; namely, the multicarrier and the single-carrier approaches. We start by defining a mathematical model for the discrete-time data transmission channel, and we make use of a well-established analysis tool for digital communication systems, known as the Gap Approximation. For the multicarrier family, the Discrete Multitone modulation is described in detail, and for the corresponding single-carrier family, particular emphasis is given to a Quadrature Amplitude Modulated system implemented with a Minimum-Mean-Squared-Error Decision Feedback Equalizer receiver. These two methods have, in fact, been conjectured to be the canonical forms of modulation and equalization for their respective family of techniques. We analyze the theoretical performance of these two systems in the infinite-length case, and we notice a number of interesting performance similarities between these two fundamentally different techniques.

Chapter 3 extends the infinite-length results from Chapter 2 to the finite-length case. We modify our original mathematical channel model to a vector channel model for this purpose, and we carry out finite-length analysis for both Discrete Multitone modulation and Quadrature Amplitude Modulation with Decision Feedback Equalization. Practical implications due to the finite-length constraint are discussed for both systems in some detail.

Chapter 4 addresses one crucial aspect of data transmission at near-capacity rates that is necessary for any modulation and equalization scheme over band-limited channels with memory: the optimization of system transmission bandwidth. While capacity is known to be achieved with a water-pouring energy distribution, implementational difficulties have prevented a water-pouring energy algorithm from being used in any practical system. In this dissertation, we propose a number of practical algorithms that utilize a (nearly) flat energy distribution and approach the theoretical optimal performance level achieved by the water-pouring distribution. An information theoretic argument is presented to justify the use of a (nearly) flat energy distribution, and simulation results confirm that the loss in performance relative to the optimal water-pouring distribution is negligible for many practical applications, such as a number of advanced Digital Subscriber Line services. These practical bandwidth optimization algorithms can be applied equally well to both multicarrier and single-carrier systems. We further introduce the idea of using adaptive transmitters for quasi-stationary duplex channels.

Chapter 5 applies a band-optimized Discrete Multitone transceiver to a number of specific applications for illustration purposes. Because the copper twisted pairs of the telephone network represent a physical medium that is well modelled as a band-limited channel with memory, we have chosen a number of advanced Digital Subscriber Line services for our simulations. In particular, we present simulation results for the U.S. Asymmetric Digital Subscriber Lines, the European E1-rate High-speed Digital Subscriber Lines, and the contemplated Very High-speed Digital Subscriber Lines services. These services have recently received a tremendous amount of attention from academia and industry alike due to their potential rolls in the current worldwide communication evolution. We find, through simulation, that

Discrete Multitone modulation is an excellent choice for these applications. Our simulation results have been confirmed by numerous prototype system test results from trials conducted by Bell Communications Research and regional telephone companies.

Chapter 6 focuses on the effects of impulsive disturbances, which are known to exist and believed to be highly damaging to many advanced Digital Subscriber Line services studied in Chapter 5. The causes and nature of impulse noise are not well understood at this time. We outline the common physical characteristics of impulse noise and review a number of noise reduction/cancellation techniques proposed in the literature for single-carrier systems. Our primary emphasis, however, is on a number of novel impulse noise mitigation strategies designed specifically for a Discrete Multitone system. We exploit available side information on impulse noise in both the time domain and the frequency domain, and we take advantage of the flexibility of a multicarrier system to adaptively combat impulse noise. Simulation results for these multicarrier impulse noise mitigation schemes are presented.

Lastly, Chapter 7 summarizes the main results of this dissertation and suggests a number of natural extensions for future research in this area based on the conclusions from this work.

1.3 Contributions

Approaching capacity over band-limited channels with memory, through sophisticated modulation, equalization, and coding techniques, has been the primary focus of Professor John Cioffi's research groups at Stanford University, and the "coders" in particular, over the past seven years. As a result of the cooperative nature within our research group, a number of ideas contained in this dissertation appear in several other students' work and vice versa. In this dissertation, Chapter 2 restates previously known results for infinite-length multicarrier (following [9]) and single-carrier (following [10]) modulation systems that provide the necessary background material for the remainder of this dissertation. Striking asymptotic performance similarities between these two fundamentally very different systems are believed to

be first noted by Zervos and Kalet in [11]. The author of this dissertation made the further observation in Section 2.5 that virtually the same flat energy transmission bandwidth is used by both systems to achieve this asymptotic performance level; subsequently, the author came up with the original idea of using multicarrier transmission bandwidth optimization techniques for single-carrier symbol rate optimization as well. Chapter 3 extends the analysis from Chapter 2 with the additional finite-length constraint on the respective systems. Materials in this chapter are previously known, and they are included for the sake of completeness and to provide a starting point for new results contained in the next three chapters. Chapter 4 presents new results and original proofs on transmission bandwidth optimization developed entirely by the author of this dissertation; these results also appear in [12] and [13] by the author. Original flat energy bandwidth optimization algorithms described in Section 4.2 are designed for multicarrier modulation systems; however, they can also be applied to single-carrier systems as first shown by the author in Section 4.2.5. The idea of using adaptive transmitters for quasi-stationary duplex channels in Section 4.3.5 is also new. Original algorithms presented in Sections 4.2.2, 4.2.3, 4.3.4, and 4.3.5 are contained in a recent U.S. patent application filed by the author [14], and the new integer-constellation-size loading algorithm of Section 4.3.2 will be filed in a second U.S. patent application [15], jointly written by the author and John Bingham of Amati Communications Corp. of Palo Alto, CA. The analyses of the various bandwidth optimization algorithms are entirely due to the author as well. Chapter 5 evaluates the feasibility of applying a band-optimized Discrete Multitone transceiver, employing algorithms developed in Chapter 4, to a number of recently proposed Digital Subscriber Line services. Simulation results in Section 5.2.3 represent collaborations between the author and fellow Stanford student Naofal Al-Dhahir, which also appear in [16] by the author, and simulation results in Section 5.3.3 represent collaborations between the author and former Stanford student Jerry Tu, which also appear in [17] and [18] by the author. Other results presented in this chapter are entirely due to the author. Finally, Chapter 6 proposes a number of new impulse noise mitigation strategies designed specifically for a Discrete Multitone system, and it corresponds to joint work done between the

author and fellow Stanford student Nick Zogakis. The original ideas for the various multicarrier impulse noise mitigation techniques are independently conceived by the author and Zogakis. Simulation results presented in Section 6.3.3 and part of Section 6.3.2 are due to Zogakis, while the rest are due to the author. The materials in Chapter 6 are also presented in [19] and [20] by Zogakis and the author.

Chapter 2

Infinite-Length Modulation and Equalization

Any physical communication channel, analog or digital, will be corrupted by non-ideal characteristics that limit the capacity of reliable information transmission. One of the most significant impairments encountered in a discrete-time channel is intersymbol interference (ISI), or channel memory, caused by the dispersive nature of the physical medium, where the current received data symbol is corrupted by previous data symbol(s). To reduce the effects of ISI, some form of equalization is typically employed by a digital transmission system.

In this chapter, we first describe the non-ideal, digital communication channel with memory and outline a mathematical model in Section 2.1, which will serve as the fundamental starting point of this dissertation. Section 2.2 defines a particularly convenient, single-parameter characterization of the digital communication channel, known as the "Signal-to-Noise Ratio (SNR) Gap", which can be applied to the analysis of a number of digital communication systems. We then review the current, state-of-the-art modulation and equalization techniques, which combine equalization with channel coding. These modulation and equalization techniques can be grouped into two main families; namely, the multicarrier and the single-carrier families. Section 2.3 examines infinite-length, multicarrier modulation and equalization. In particular, we focus on Discrete Multitone (DMT) modulation,

which can be implemented very efficiently with fast digital signal processing algorithms and exhibits a number of desirable properties. Section 2.4 considers the corresponding infinite-length, single-carrier modulation and equalization, and particular emphasis is given to Quadrature Amplitude Modulation (QAM) implemented with a Minimum-Mean-Squared-Error Decision Feedback Equalizer (MMSE-DFE) receiver. While fundamentally very different, in the asymptotic case, the DMT and the MMSE-DFE systems can be shown to have virtually the same performance [11], and this performance connection is re-derived in Section 2.5. We further observe that these two systems will also use virtually the same flat energy transmission bandwidth to achieve this asymptotic performance level. Based on this observation, we propose the use of multicarrier techniques to obtain the symbol rate and the carrier frequency, thus the transmission bandwidth, of a single-carrier system as well. This idea will be further developed in Chapter 4.

2.1 Discrete-Time ISI Channel Model

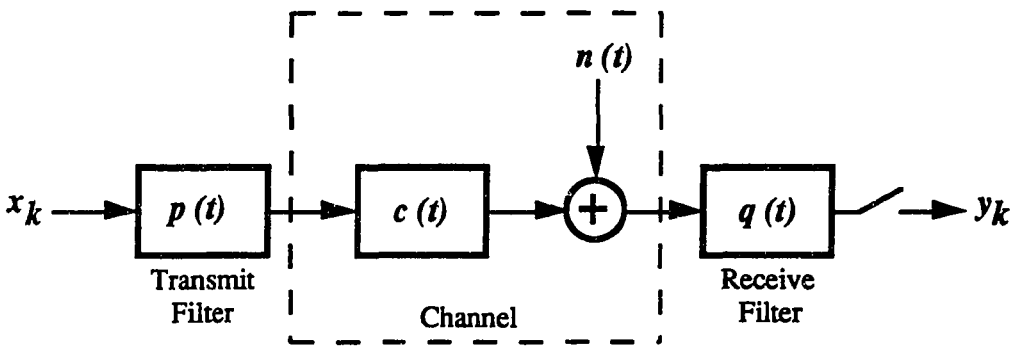

Figure 2.1: Communication Channel Model

We start with a standard linear time-invariant (LTI) communication channel model as shown in Figure 2.1. The physical channel is characterized by a complex channel response $c(t)$ with a Fourier transform $C(f)$ and a complex additive Gaussian noise (AGN) component $n(t)$ with a Fourier transform $N(f)$. Furthermore, the transmit filter is characterized by a complex response $p(t)$ with a Fourier transform $P(f)$, and

the receive filter is characterized by a complex response $q(t)$ with a Fourier transform $Q(f)$. The symbol period is T seconds, and the input sequence is $\{x_k\}$. Therefore, the input waveform to the physical communication channel is $\sum_k x_k\ p(t - kT)$. Assuming a symbol rate sampler, the output sequence is then $\{y_k\}$. We will further denote the composite response of the transmit filter and the channel as $H(f) = P(f)C(f)$ with an inverse Fourier transform $h(t)$. Unless otherwise noted, we will also assume that the receive filter $q(t)$ is just an anti-alias filter with unity gain. The corresponding discrete-time equivalent ISI channel model for this continuous-

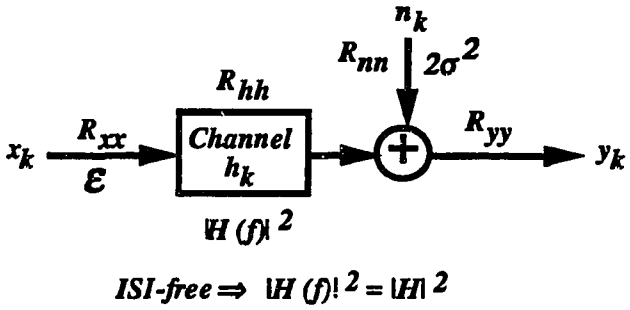

Figure 2.2: Discrete-Time Equivalent (ISI) Channel Model

time communication channel is then illustrated in Figure 2.2. The input-to-output relationship of this discrete-time channel model is given by:

$$y_k = \sum_{i=0}^{\nu} h_i x_{k-i} + n_k\ , \tag{2.1}$$

where ν is the channel constraint length, or channel memory. The input sequence, $\{x_k\}$, is assumed to be a complex, zero-mean (possibly correlated) random variable, the sampled channel pulse response, $\{h_k\}$, represents the aggregate response of the transmit filter, the channel, and the receive (anti-alias) filter, and the noise component, $\{n_k\}$, is assumed to be a complex, zero-mean (possibly colored) Gaussian random variable that is independent of the input sequence. In this dissertation, we will only consider symbol rate systems; however, all results can be generalized to the corresponding fractionally spaced systems.

We now introduce the complex D-transform notation for sequences, which is well known in communication theory. For any complex sequence $\{g_k\}$, its corresponding D-transform $g(D)$ is given by:

$$g(D) = \sum_{k=-\infty}^{\infty} g_k D^k \ . \tag{2.2}$$

Similarly, the sequence $\{g^*_{-k}\}$ has a D-transform of:

$$g^*(D^{-1}) = \sum_{k=-\infty}^{\infty} g^*_k D^{-k} \ , \tag{2.3}$$

where "$*$" denotes the complex conjugate. Therefore "D" is a complex variable representable as $D = |D|e^{-j\theta}$, and if $|D| = 1$ and the sum converges, then the D-transform is equivalent to the discrete-time Fourier Transform of the sequence $\{g_k\}$. The "correlation sequence", $\{R_{gh,i}\}$, of any two stationary complex sequences $\{g_k\}$ and $\{h_k\}$ is defined as:

$$R_{gh,i} = E[g_k \ h^*_{k-i}] \ , \tag{2.4}$$

with a corresponding D-transform of $R_{gh}(D)$. With some abuse of notation, we will refer to $R_{gh}(D)$ as the "correlation function" of the sequences $\{g_k\}$ and $\{h_k\}$ in this dissertation. So the "autocorrelation function" of the stationary sequence $\{g_k\}$ is then denoted as $R_{gg}(D)$, and $R_{gg}(D) = R^*_{gg}(D^{-1})$ due to stationarity. If we let $D = e^{-j\theta}$, then $R_{gg}(D)$ is simply the power spectral density (PSD) of the random sequence, $\{g_k\}$; namely,

$$|S_{gg}(\theta)|^2 = R_{gg}(e^{-j\theta}) \ , \ -\pi < \theta \leq \pi \ , \tag{2.5}$$

which will always be real and non-negative for all values of θ. The average energy (per 2-dimensional symbol) of the sequence is given by:

$$S_g = R_{gg,0} = E[|g_k|^2] = \frac{1}{2\pi} \int_{-\pi}^{\pi} |S_{gg}(\theta)|^2 \ d\theta \ , \tag{2.6}$$

and the average power of the sequence is given by:

$$P_g = \frac{S_g}{T} \ , \tag{2.7}$$

where T is the symbol period (in seconds). We are now in position to rewrite Equation (2.1) in terms of D-transforms, and we get the following:

$$y(D) = x(D)h(D) + n(D) \ . \tag{2.8}$$

In Figure 2.2, the average input signal energy of the system is denoted by $S_x = \mathcal{E}$, and the average noise energy is denoted by $S_n = 2\sigma^2$, respectively, per 2-dimensional symbol.

2.2 SNR Gap and the Gap Approximation

To aid the analysis of performance for both the DMT and the MMSE-DFE, we make use of a convenient single-parameter characterization of the system, known as the "SNR gap", $\Gamma(Pr(E), \mathcal{C}, \gamma_{margin})$ [10], which is a function of the chosen coding scheme $\mathcal{C}$, with a total effective coding gain of $\gamma_{eff}(\mathcal{C})$, the target bit error rate (BER) $Pr(E)$, and the desired system performance (or noise) margin[1] γ_{margin}. Conceptually, SNR gap is a measure of how a particular communication system is performing relative to the channel capacity. Powerful channel coding techniques, such as trellis codes [3] [4] [5] and forward error correcting codes [21], have been developed over the years as methods to narrow the SNR gap of a practical communication system. The total effective coding gain, $\gamma_{eff}(\mathcal{C})$, of a particular coding scheme $\mathcal{C}$ represents the cumulative effects of the code, including possible shaping gain, on an uncoded transmission system.

To define $\Gamma(Pr(E), \mathcal{C}, \gamma_{margin})$ and derive the corresponding "gap approximation", we start with an uncoded, zero-margin, QAM system over an ISI-free, additive white Gaussian noise (AWGN) channel with a power gain of $|H|^2$ (see Figure 2.2). The QAM system is a 2-dimensional system with data symbols, x_k's, chosen from a 2-dimensional signal constellation. Figure 2.3 illustrates the signal constellation of a 16-point QAM (or 16-QAM) system, and the inner 4 signal points in Figure 2.3 form the corresponding 4-QAM signal constellation. The minimum distance between constellation points for both the 16-QAM and the 4-QAM constellations in

[1]System performance, or noise, margin is defined as the additional amount of noise (in dB) that the system can tolerate while still operating under the desired BER requirement.

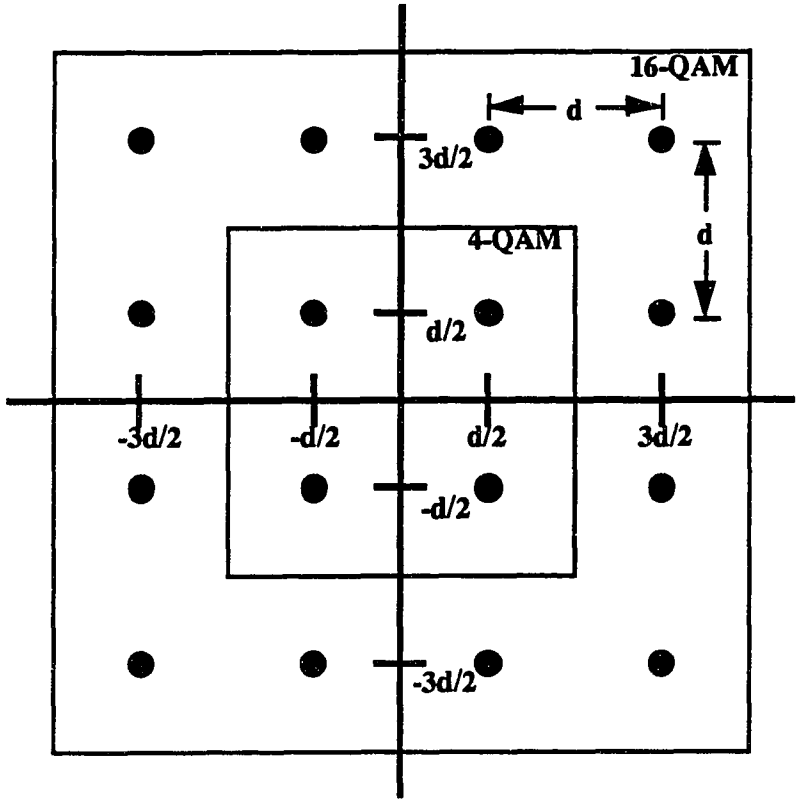

Figure 2.3: 16-QAM and 4-QAM Signal Constellations

Figure 2.3 is d, and both constellations are centered at the origin. For this system, the received SNR (or channel output SNR), $SNR_{rec'd}$, is simply given by:

$$SNR_{rec'd} = \frac{\mathcal{E}|H|^2}{2\sigma^2} , \tag{2.9}$$

where $\mathcal{E}$ is the average input signal energy per 2-dimensional QAM symbol and σ^2 is the received noise variance per dimension. If all points in a square b-bit QAM constellation are equally likely to be transmitted, the average input signal energy is:

$$\mathcal{E} = \frac{d_{min}^2(2^b - 1)}{6} , \tag{2.10}$$

where d_{min} is the minimum distance between constellation points. The probability of symbol error, P_e, for such QAM system is then given by:

$$P_e = N_e\, Q\left[\frac{d_{min}|H|}{2\sigma}\right] , \tag{2.11}$$

$$\leq 4\, Q\left[\frac{d_{min}|H|}{2\sigma}\right] , \tag{2.12}$$

where the Q-function is defined by:

$$Q(x) = \int_x^\infty \frac{1}{\sqrt{2\pi}} e^{\frac{-u^2}{2}} du , \tag{2.13}$$

and N_e is the number of nearest neighbors in the input signal constellation. For QAM systems, $N_e \leq 4$, and for $x \geq 3$, $Q(x)$ is accurately approximated by:

$$Q(x) \approx \frac{1}{\sqrt{2\pi}\, x} e^{\frac{-x^2}{2}} . \tag{2.14}$$

Assuming that the target BER $Pr(E) \approx P_e$ holds, then the "SNR gap", $\Gamma(Pr(E), QAM_{unc})$, for an uncoded, zero-margin, QAM system is defined as:

$$\Gamma(Pr(E), QAM_{unc}) = \frac{d_{min}^2|H|^2}{12\sigma^2} \tag{2.15}$$

$$= \frac{[Q^{-1}(\frac{P_e}{N_e})]^2}{3} . \tag{2.16}$$

Rearrange and combine Equations (2.9), (2.10), and (2.15) we get:

$$b = log_2(1 + \frac{SNR_{rec'd}}{\Gamma(Pr(E), QAM_{unc})}) . \tag{2.17}$$

This is the corresponding "gap approximation" for an uncoded, zero-margin, square QAM system, where the SNR gap accurately estimates the difference between Shannon's channel capacity, C (in bits per 2-dimensional symbol) [1] [2],

$$C = log_2(1 + SNR_{rec'd}) \ , \tag{2.18}$$

and the actual achievable rate, $R = b$ (in bits per 2-dimensional symbol). For an uncoded, zero-margin QAM system with a target BER of $Pr(E) = 10^{-7}$ per dimension, the SNR gap, $\Gamma(10^{-7}, QAM_{unc})$, is approximately 9.8 (dB). For a general QAM system with a target BER of $Pr(E)$, a desired system performance margin of γ_{margin}, and a total effective coding gain of γ_{eff} that includes the effects of shaping, the SNR gap, $\Gamma(Pr(E), \gamma_{margin}, \gamma_{eff})$, is given (in dB) by:

$$\Gamma(Pr(E), \gamma_{margin}, \gamma_{eff}) = [Q^{-1}(\frac{P_e}{N_e})]^2 + \gamma_{margin} - \gamma_{eff} - 4.77 \ (dB) \ , \tag{2.19}$$

because

$$P_e = N_e \ Q\left[\frac{d_{min}|H|}{2\sigma} \sqrt{\frac{\gamma_{eff}}{\gamma_{margin}}}\right] . \tag{2.20}$$

The corresponding gap approximation for this general QAM system is then:

$$R = log_2(1 + \frac{SNR_{rec'd}}{\Gamma(Pr(E), \gamma_{margin}, \gamma_{eff})}) \ , \tag{2.21}$$

where R is again in bits per 2-dimensional symbol. For brevity of notation, we will use Γ for $\Gamma(Pr(E), \gamma_{margin}, \gamma_{eff})$ from now on, whenever the system parameters are either implicit from context or inconsequential to the current development. We note here that in order for the gap approximation to hold, the noise component is assumed to have a Gaussian distribution, though it need not necessarily be white. This assumption is valid for many practical applications, including those with crosstalk noise, such as in Digital Subscriber Line (DSL) services discussed in Chapter 5. (It has been shown in [22] that the Gaussian model for crosstalk is actually somewhat pessimistic.)

2.3 Multicarrier Modulation and Equalization

The fundamental goal of all "multicarrier" modulation techniques is to partition a data transmission channel with ISI into a set of orthogonal, memoryless subchannels,

each with its own "carrier". (See [23] and [24].) Data is transmitted through each subchannel independently of other subchannels, and within each subchannel, the channel response is (ideally) flat, as long as the channel is partitioned sufficiently. A number of channel partitioning techniques have been proposed in the literature, including using the channel eigenvectors, or eigenfunctions, in Vector Coding (VC) [8] and in Structured Channel Signalling (SCS) [25], using the Inverse Discrete Fourier Transform (IDFT) and the Discrete Fourier Transform (DFT) vectors in DMT modulation [9] [26], using the discrete Hartley transform in a variation of the DMT modulation [27], and using the M-band wavelet transforms in Discrete Wavelet Multitone (DWMT) modulation [28].

In general, the optimal channel partitioning scheme depends on the particular representation of the channel and the noise. It can be shown that Vector Coding and Discrete Multitone are special cases of optimal multicarrier modulation in the code domain and the frequency domain, respectively, under certain sets of conditions and assumptions [29]. From a performance perspective, Vector Coding is preferred because of the redundant transmit power used by the DMT for cyclic extension, or cyclic prefix, (see Section 3.2.1 for more detail); however, in practice, DMT modulation is the preferred methodology because of its advantage in computational complexity. Furthermore, DMT modulation enjoys a number of "canonical" properties that will become clear in this and the next two chapters. For these reasons, we will focus on DMT modulation in this dissertation as the representative method in the multicarrier family of modulation and equalization techniques. In this section, we will review the basics of DMT modulation and derive the ideal performance level of an infinite-length DMT system. Similar performance analysis for a DMT system with a finite-length constraint, as well as practical DMT implementational issues, will be addressed in Section 3.2. We note here that for infinite-length multicarrier modulation, Discrete Multitone is equivalent to Vector Coding, because the complex exponentials are eigenfunctions of any LTI system.

2.3.1 Discrete Multitone Modulation

The general structure of a DMT system is illustrated in Figure 2.4, where $\{X_0, X_1, \ldots, X_{N-1}\}$ are the original, complex, input data symbols, $\{x_k\}$ is the modulated data sequence (before cyclic prefix), $\{y_k\}$ is the received sequence (after the removal of cyclic prefix), and $\{\tilde{X}_0, \tilde{X}_1, \ldots, \tilde{X}_{N-1}\}$ are the decoded, complex data symbols. The $\mathbf{p}_i$'s and $\mathbf{p}_i^*$'s in Figure 2.4 are known as the modulating and the demodulating

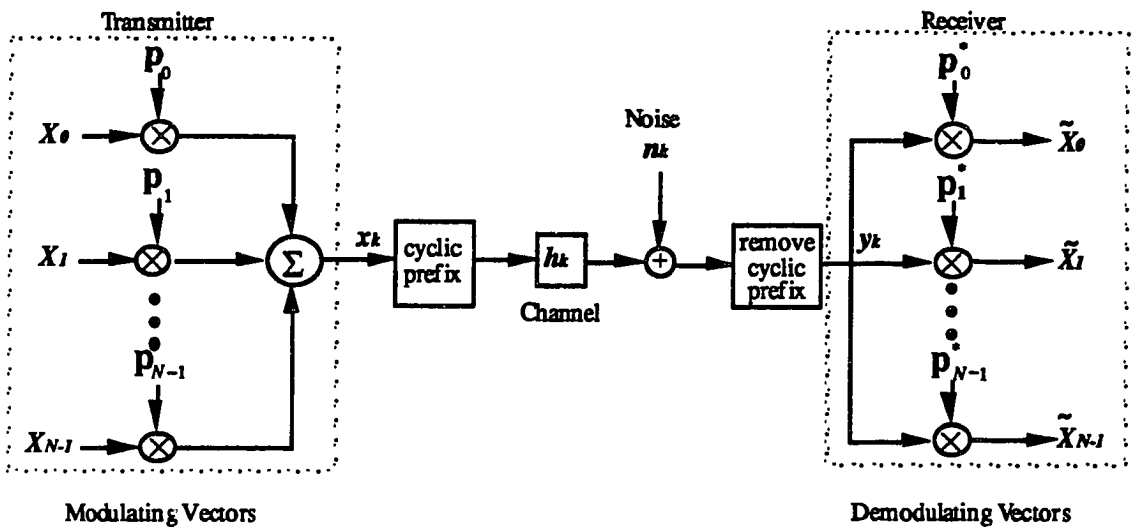

Figure 2.4: Basic Structure of Discrete Multitone Modulation

vectors for discrete-time systems, or basis functions for continuous-time systems, and in general, they are chosen to be orthonormal. Therefore, for a discrete-time system, we must satisfy the following condition:

$$\mathbf{p}_i \odot \mathbf{p}_j^* = \delta_{ij} \ , \tag{2.22}$$

where $\odot$ denotes the dot product of two vectors and the "δ-function" is defined as

$$\delta_{ij} = \begin{cases} 1 & i = j \\ 0 & i \neq j \end{cases} \ . \tag{2.23}$$

Similarly, for a continuous-time system, we need:

$$\int_{-\infty}^{\infty} p_i(t)\, p_j^*(t)\, dt = \delta_{ij} \ . \tag{2.24}$$

For the DMT system, the independent modulating and demodulating vectors in Figure 2.4 are the IDFT and the DFT vectors, given by the following pair of relationships:

$$X_m = \frac{1}{\sqrt{2N}} \sum_{n=0}^{2N-1} x_n e^{\frac{-j2\pi mn}{2N}} \tag{2.25}$$

$$x_n = \frac{1}{\sqrt{2N}} \sum_{m=0}^{2N-1} X_m e^{\frac{j2\pi mn}{2N}} . \tag{2.26}$$

A DMT system with N complex subchannels in the frequency domain requires a DFT size of $2N$, and the forced conjugate symmetry in the frequency domain will result in the desired real-valued time domain samples. The cyclic prefix is a discrete-time technique used to eliminate interblock interference (IBI), and it will be discussed in more detail in Section 3.2.

Conceptually, the DMT modulator divides the data transmission channel into a fixed number of, say N, parallel, complex, independent subchannels in the frequency domain as shown in Figure 2.5. Each of the "tones", or subchannels, is

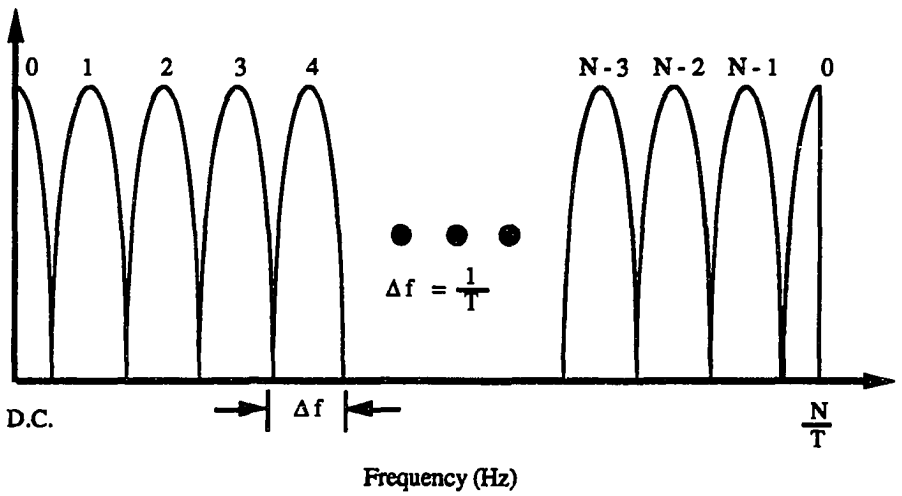

Figure 2.5: Frequency Domain Picture of DMT Modulation

$\Delta f = \frac{1}{T}$ wide in the frequency domain, where T is the (block) multicarrier symbol period, and if N is sufficiently large, the channel power spectral density curve will be

virtually flat within each of the subchannels. This assumption becomes valid in the infinite-length case, where we let $N \rightarrow \infty$, or equivalently let $\Delta f \rightarrow 0$. Furthermore, different numbers of bits can be conveniently assigned to different subchannels. As a result, more data can be transmitted over those subchannels with larger SNR's and less data can be transmitted over those subchannels with smaller SNR's. In fact, no data will be transmitted over the worst portion of the frequency band if the received SNR over those subchannels cannot support the minimum number of bits at the required BER. In this manner, either the overall throughput or the system performance margin of the DMT system can be optimized. To illustrate this concept, we plotted an arbitrary channel power spectral density curve in Figure 2.6. Each of the vertical bins in this figure corresponds to a subchannel with its own

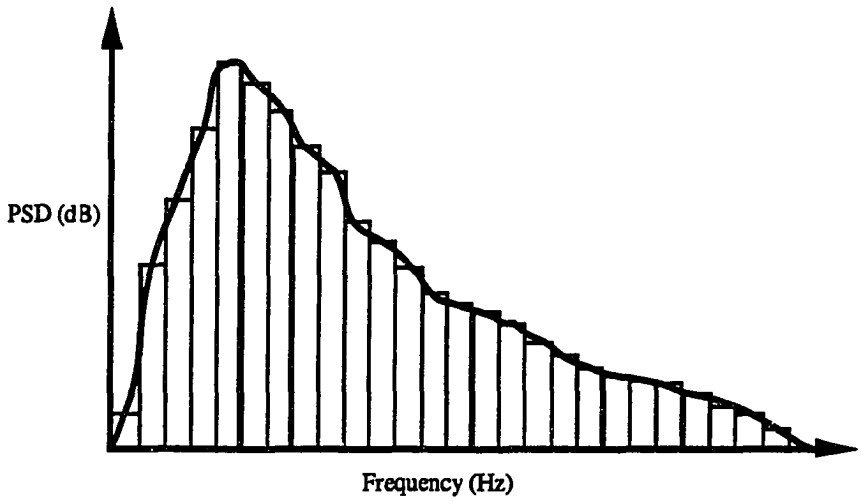

Figure 2.6: DMT Bit Allocation in the Frequency Domain

carrier, and within each subchannel, the PSD is approximately flat. The height of each vertical bin represents the approximate amount of data[2], or information, transmitted over that particular subchannel. Thus, for the channel shown in Figure 2.6, very little information is allocated and transmitted over the DC and high

[2]Here we have ignored the effects of noise and the transmit power spectrum. In reality, of course, it is the SNR, not the channel PSD, curve that ultimately determines the optimal bit, or information, allocation.

frequency subchannels, where channel attenuation is most severe.

One attractive feature of DMT modulation is that powerful channel coding techniques, such as trellis codes and/or forward error correcting codes, can be readily applied to the modulation structure, and the total effective coding gain of these outer error control codes, varying from 3 to 6 dB, can be realized by the system. This is the direct consequence of the fact that the independent subchannels are essentially memoryless. We will take advantage of this property when we apply DMT modulation to various DSL applications in Chapter 5, where powerful channel coding is needed to insure reliable data transmission, and when we design coding strategies for impulse noise mitigation in Chapter 6. A number of outer code concatenation techniques developed specifically for DMT modulation can be found in [30].

2.3.2 Infinite-Length DMT Analysis

To analyze the performance of an infinite-length DMT system, we first note that in the finite-length case, each of the N parallel, complex subchannels is effectively ISI-free, as long as N is chosen sufficiently large. As noted in Section 2.3.1, this ISI-free assumption becomes exact as $N \rightarrow \infty$. Therefore, we can simply analyze the DMT performance as an aggregate of N ISI-free QAM subchannels and then let $N \rightarrow \infty$. The received SNR for each of the subchannels is given by:

$$SNR(i) = \frac{\mathcal{E}(i)|H(i)|^2}{2\sigma(i)^2}, \tag{2.27}$$

where $\mathcal{E}(i)$ is the average signal energy per 2-dimensional input symbol, $|H(i)|^2$ is the channel power spectral density, and $\sigma(i)^2$ is the noise variance per dimension, respectively, for the i^{th} subchannel. Using the gap approximation from Section 2.2, the number of bits transported in the i^{th} subchannel is given by:

$$b(i) = log_2(1 + \frac{SNR(i)}{\Gamma}) . \tag{2.28}$$

Now if we let $N \rightarrow \infty$, then Equations (2.27) and (2.28) become:

$$SNR(f) = \frac{\mathcal{E}(f)|H(f)|^2}{2\sigma(f)^2}, \tag{2.29}$$

and

$$b(f) = log_2(1 + \frac{SNR(f)}{\Gamma}) \ , \tag{2.30}$$

respectively, where $SNR(f)$ is just the instantaneous signal-to-noise ratio at frequency f and $b(f)\Delta f$ is the amount of data in bits per second transmitted at frequency f in the limit as $\Delta f \to 0$. The total amount of data, $\tilde{R}_{DMT}$, (in bits per second), transmitted by an infinite-length DMT system is then given by:

$$\tilde{R}_{DMT} = \int_{W_{DMT}} log_2 \left(1 + \frac{SNR(f)}{\Gamma}\right) df \ , \tag{2.31}$$

where W_{DMT} is the range of frequencies that is actually used for data transport. If we are allowed to assume the ideal case of infinite granularity in constellation size, then the optimal W_{DMT} is the frequency band within which the integrand in Equation (2.31) is positive. However, if we employ strictly QAM constellations, then the optimal W_{DMT} is the frequency band within which the integrand in Equation (2.31) is greater than or equal to two, because there must be two or more bits per transmitted QAM symbol. Recall that the Shannon capacity, in bits per second, for ISI channels is given by:

$$\tilde{C} = \int_{W_{\tilde{C}}} log_2 \ (1 + SNR(f)) \ df \ , \tag{2.32}$$

where $W_{\tilde{C}}$ is the range of frequencies where the integrand in Equation (2.32) is positive. Therefore, if the gap approximation in Section 2.2 is strictly valid, then the maximum achievable data rate $\tilde{R}_{DMT}$ of an infinite-length DMT system over any ISI, AGN channel with input power P is the capacity of the same channel with input power $\frac{P}{\Gamma}$. Furthermore, the transmit spectrum W_{DMT} used to achieve $\tilde{R}_{DMT}$ is the same as the capacity achieving spectrum $W_{\tilde{C}}$ for the channel with input power $\frac{P}{\Gamma}$, which strongly suggests that the DMT modulation is a "canonical" structure for multicarrier modulation and equalization.

2.4 Single-Carrier Modulation and Equalization

Conventional methods of mitigating ISI in a digital communication system use either an equalizer, such as a linear equalizer (LE) [31], or a decision feedback equalizer

(DFE) [32] [33] [34] [35], a precoder, such as the Tomlinson-Harashima precoder [36] [37], or a sequence estimator, such as the Maximum Likelihood Sequence Estimator (MLSE) [38]. These transceiver structures can be applied to the family of modulation techniques that includes baseband Pulse Amplitude Modulation (PAM), passband QAM, and passband Phase Shift Keying (PSK), to name a few. Because they are inherently time domain systems, we will denote this family of modulation and equalization methods as the "single-carrier" approach in this dissertation.

While the MLSE receiver has been shown to achieve optimum performance over ISI, AWGN channels [38], it is typically, however, impractical to implement from a complexity standpoint. As a result, we will focus on a particular receiver structure known as the Minimum-Mean-Squared-Error Decision Feedback Equalizer in this dissertation, and we will apply the MMSE-DFE to a basic QAM system. Unlike the zero-forcing DFE, MMSE-DFE does not suffer from excess noise enhancement, and it is well known that a decision feedback equalizer will always outperform the corresponding linear equalizer because past decisions are used to aid the current decision. In this dissertation we will also make the assumption that the MMSE-DFE is ideal; in other words, there is no error propagation. In practice, error propagation can be eliminated by moving the feedback section of the DFE to the transmitter, thus forming the Tomlinson-Harashima precoder. All analyses, however, remain valid. A particular variant of the QAM system implemented with a MMSE-DFE receiver that has been shown to be well suited for DSL applications from an implementational perspective is the so-called Carrierless Amplitude Modulation/Phase Modulation (Carrierless AM/PM or CAP) [39]. The theoretical performance of the CAP system, however, is identical to that of the basic QAM implemented with a MMSE-DFE receiver. Lastly, as DMT is to multicarrier modulation, the MMSE-DFE receiver has been conjectured to be the canonical receiver structure for the single-carrier family of modulation and equalization techniques [10], and the reasons for this conjecture will become clear in the following two subsections.

2.4.1 Decision Feedback Equalization for QAM Modulation

The block diagram of a single-carrier system implemented with a MMSE-DFE receiver is shown in Figure 2.7, where $\{x_k\}$ is the modulated transmit data sequence,

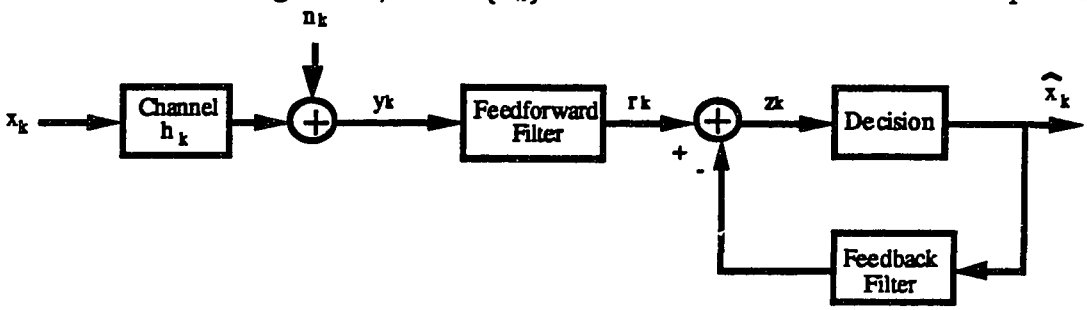

Figure 2.7: Basic Structure of the MMSE-DFE

$\{y_k\}$ is the received sequence, $\{r_k\}$ is the output sequence of the feedforward (FF) filter, $\{z_k\}$ is the sum of $\{r_k\}$ and the negated output sequence of the feedback (FB) filter, and $\{\hat{x}_k\}$ is the output of the decision element. Ideally, the condition:

$$x_k = \hat{x}_k \tag{2.33}$$

holds, which implies that all past decisions are correct and no error propagation will occur through the FB filter. This condition is not achieved in practice when decision, or decoding, errors do occur with non-zero probability; nevertheless, we will make the ideal feedback assumption in order to simplify our analysis.

Conceptually, the feedforward section of the MMSE-DFE is a mean-square whitened matched filter (MS-WMF) [10], which effectively minimum-phase-filters[3] the received data sequence and whitens the distortion sequence consisting of an additive Gaussian noise sequence and an ISI sequence. The feedback section then subtracts out the whitened distortion sequence using the knowledge of past decisions. In other words, the feedforward filter acts on pre-cursor ISI components, while the feedback filter subtracts off post-cursor ISI components. Furthermore, for an infinite-length MMSE-DFE, the FF filter with response $a(D)$ needs not necessarily be causal[4], but the FB filter with response $b(D) - 1$ must be strictly causal,

[3]By minimum-phase-filtering, we mean that the output of the filter, not the filter itself, is a minimum-phase sequence.

[4]Non-causal filters can be implemented with delay in a real system.

or equivalently, $b(D)$ is causal and monic.

We will now re-derive the optimal settings for the FF and the FB filters of an infinite-length MMSE-DFE over an ISI, AWGN channel, following the development given in [10], and we will make heavy use of the well known Spectral Factorization (SF) given by the following lemma:

Lemma 2.1 (Spectral Factorization) *If $|S(\theta)|^2$ is any power spectral density, as defined by Equation (2.5), such that both $|S(\theta)|^2$ and log $|S(\theta)|^2$ are integrable over $-\pi < \theta \leq \pi$, and $R(D)$ is the corresponding autocorrelation function, then $R(D)$ is said to be factorizable, and there is a unique canonical discrete-time response, $g(D)$, that yields the following factorization of $R(D)$:*

$$R(D) = S_0 \, g(D) \, g^*(D^{-1}) \, , \tag{2.34}$$

where S_0 is given by:

$$log \; S_0 = \frac{1}{2\pi} \int_{-\pi}^{\pi} log \; |S(\theta)|^2 d\theta \, , \tag{2.35}$$

and the logarithms in Equation (2.35) may have any common base. Furthermore, S_0 is a positive real number, $g(D)$ is a canonical filter response[5], and $g^*(D^{-1})$ is a anticanonical filter response; that is, anticausal, monic, and maximum phase. Since $g(D)$ is monic, we observe that $||g||^2 = \sum_{i=-\infty}^{\infty} |g_i|^2 \geq 1$, and equality holds if and only if $g(D) = 1$.

For a discrete-time, ISI, AWGN channel, as given in Figure 2.1, we define the "system autocorrelation function", $R_{ss}(D)$, as:

$$R_{ss}(D) = \mathcal{E} R_{hh}(D) + 2\sigma^2 \, , \tag{2.36}$$

with $R_{hh}(D)$ being the discrete-time channel autocorrelation function. Whenever $\sigma^2 > 0$, $R_{ss}(D)$ will be factorizable. In particular, $R_{ss}(D)$ will admit the following spectral factorization:

$$S_0 g_\lambda(D) g_\lambda^*(D^{-1}) = \mathcal{E} R_{hh}(D) + 2\sigma^2 \, , \tag{2.37}$$

[5]A filter response $g(D)$ is said to be canonical if it is causal; that is, $g_k = 0 \; \forall \; k < 0$, monic; that is, $g_0 = 1$, and minimum phase; that is, all of its poles are outside of the unit circle, and all of its zeros are on or outside of the unit circle in the D-plane.

where S_0 is the "system average energy", and $g_\lambda(D)$ is the "system canonical response". Under the ideal MMSE-DFE assumption, where $\hat{x}(D) = x(D)$, the error sequence, $e(D)$, of the system can be written as:

$$\begin{aligned} e(D) &= z(D) - \hat{x}(D) && (2.38)\\ &= a(D)y(D) - [b(D) - 1]x(D) - x(D) && (2.39)\\ &= a(D)y(D) - b(D)x(D)\ . && (2.40) \end{aligned}$$

Now we wish to minimize $e(D)$ by choosing the appropriate $a(D)$ and $b(D)$, and we note that for any fixed $b(D)$, the optimal $a(D)$ is the same filter that forms the optimal linear estimator for the sequence $b(D)x(D)$, based on the known sequence $y(D)$. Applying the well known orthogonality principle of linear estimation, the best estimator $a(D)$ will result in zero cross-correlation between the error sequence, $e(D)$, and the known sequence $y(D)$. Therefore, using the correlation function notation defined in Section 2.1, we have the following:

$$\begin{aligned} 0 &= R_{ey}(D) && (2.41)\\ &= E[(a(D)y(D) - b(D)x(D))\ y^*(D^{-1})] && (2.42)\\ &= a(D)R_{yy}(D) - b(D)R_{xy}(D)\ . && (2.43) \end{aligned}$$

So the optimal $a(D)$ for a given $b(D)$ must be:

$$a(D) = b(D)R_{xy}(D)R_{yy}^{-1}(D)\ . \qquad (2.44)$$

It has been shown in [40] and [38] that, without loss of optimality, the front-end of the receiver may always consists of a continuous-time, matched filter (MF) and a symbol rate sampler, followed by further discrete-time processing. Making use of this fact, we replace our original channel input/output relationship, given by Equation (2.8), with a new, equivalent channel input/output relationship, which includes a front-end MF at the receiver, and it is given by:

$$y(D) = x(D)R_{hh}(D) + n(D)h^*(D^{-1})\ . \qquad (2.45)$$

Therefore, $R_{xy}(D)$ and $R_{yy}(D)$ are now given by:

$$R_{xy}(D) = E[x(D)\ y^*(D^{-1})] \qquad (2.46)$$

$$= E[x(D)\ (x^*(D^{-1})R_{hh}(D) + n^*(D^{-1})h(D))] \quad (2.47)$$

$$= \mathcal{E}R_{hh}(D)\ , \quad (2.48)$$

and

$$R_{yy}(D) = E[y(D)\ y^*(D^{-1})] \quad (2.49)$$

$$= E[(x(D)R_{hh}(D) + n(D)h^*(D^{-1}))\ (x^*(D^{-1})R_{hh}(D) \quad (2.50)$$

$$+ n^*(D^{-1})h(D))] \quad (2.51)$$

$$= \mathcal{E}[R_{hh}(D)]^2 + 2\sigma^2 R_{hh}(D)\ . \quad (2.52)$$

Combining Equations (2.37), (2.44), (2.48), and (2.52) we get:

$$a(D) = b(D)\frac{\mathcal{E}}{\mathcal{E}R_{hh}(D) + 2\sigma^2} \quad (2.53)$$

$$= b(D)\frac{\mathcal{E}}{S_0 g_\lambda(D)g_\lambda^*(D^{-1})}\ . \quad (2.54)$$

Combining Equations (2.40) and (2.54) we get the following:

$$e(D) = b(D)\left[\frac{\mathcal{E}}{S_0 g_\lambda(D)g_\lambda^*(D^{-1})}y(D) - x(D)\right] \quad (2.55)$$

$$= b(D)e'(D)\ , \quad (2.56)$$

and the autocorrelation function of the sequence $e'(D)$ can simply be written as:

$$R_{e'e'}(D) = \left[\frac{\mathcal{E}}{S_0 g_\lambda(D)g_\lambda^*(D^{-1})}\right]^2 R_{yy}(D) - 2\frac{\mathcal{E}R_{xy}(D)}{S_0 g_\lambda(D)g_\lambda^*(D^{-1})} + \mathcal{E} \quad (2.57)$$

$$= \frac{\mathcal{E}}{S_0 g_\lambda(D)g_\lambda^*(D^{-1})}[S_0 g_\lambda(D)g_\lambda^*(D^{-1}) - \mathcal{E}R_{hh}(D)] \quad (2.58)$$

$$= \frac{\frac{\mathcal{E}2\sigma^2}{S_0}}{g_\lambda(D)g_\lambda^*(D^{-1})}\ . \quad (2.59)$$

However, since $b(D)$ is necessarily causal and monic and Equation (2.59) defines the unique spectral factorization of $R_{e'e'}(D)$, the optimum $b(D)$ that minimizes $e(D)$ must then just be the whitening filter $g_\lambda(D)$ for the sequence $e'(D)$. Therefore, the optimal settings for the MMSE-DFE feedforward filter, $a(D)$, and the MMSE-DFE feedback filter, $b(D) - 1$, are finally given by:

$$a(D) = \frac{\mathcal{E}}{S_0}\frac{1}{g_\lambda^*(D^{-1})}\ , \quad (2.60)$$

and

$$b(D) - 1 = g_\lambda(D) - 1 \,, \tag{2.61}$$

respectively.

2.4.2 Infinite-Length MMSE-DFE Analysis

We are now in position to analyze the theoretic performance of an ideal, infinite-length MMSE-DFE. From Equations (2.56), (2.59), and (2.61), the Mean-Squared-Error (MSE), R_{ee}, of the infinite-length MMSE-DFE is given by:

$$MSE_{MMSE-DFE} = R_{ee} = \frac{\mathcal{E}2\sigma^2}{S_0} \,, \tag{2.62}$$

and the MMSE-DFE output SNR, $SNR_{MMSE-DFE}$, is then:

$$SNR_{MMSE-DFE} = \frac{S_0}{2\sigma^2} \,, \tag{2.63}$$

where S_0 is again the system average energy defined by:

$$log\left(\frac{S_0}{2\sigma^2}\right) = \frac{1}{2\pi}\int_{-\pi}^{\pi} log\left[\frac{\mathcal{E}}{2\sigma^2}|S_{hh}(\theta)|^2 + 1\right] d\theta \,. \tag{2.64}$$

This MMSE-DFE output SNR expression, however, is biased with respect to the decision rule. Therefore, performance can be further enhanced by removing the bias, which will actually lead to a worse output SNR but an improved probability of error. It was shown in [10] that this bias can be removed by simply scaling the output sequence $r(D)$ from the feedforward filter by a factor of $\frac{S_0}{S_0 - 2\sigma^2}$, while keeping the remaining MMSE-DFE settings unchanged. The unbiased output SNR of the MMSE-DFE is then given by:

$$SNR_{MMSE-DFE,U} = \frac{S_0 - 2\sigma^2}{2\sigma^2} \tag{2.65}$$

$$= SNR_{MMSE-DFE} - 1 \,. \tag{2.66}$$

The MMSE-DFE capacity, $C(T)$, in bits per two-dimensional symbol, of an ISI channel with a symbol period of T is then found in [10] to be:

$$C(T) = log_2(1 + SNR_{MMSE-DFE,U}) \,. \tag{2.67}$$

Utilizing the gap approximation from Section 2.2, the achievable data rate, $R(T)$ (in bits per two-dimensional symbol), using a MMSE-DFE receiver with a fixed target BER of $Pr(E)$ and coding scheme $\mathcal{C}$ is now given by:

$$R(T) = log_2(1 + \frac{SNR_{MMSE-DFE,U}(T)}{\Gamma(Pr(E),\mathcal{C})}) \ . \tag{2.68}$$

Remarkably, the channel capacity $C(T)$ and the achievable data rate $R(T)$ for any ISI-channel using an ideal MMSE-DFE receiver have exactly the same forms as those for the memoryless channel, with only the received channel SNR, $SNR_{rec'd}$, replaced by the unbiased equalizer output SNR, $SNR_{MMSE-DFE,U}$, which strongly suggests that the unbiased MMSE-DFE receiver is a "canonical" structure for single-carrier modulation and equalization.

2.5 The Connection

Although the two methodologies discussed in Sections 2.3.1 and 2.4.1 are fundamentally very different, there exist some interesting performance similarities [11]. As the size of the IDFT and DFT vectors in the DMT system approaches infinity, the ISI-free assumption within each subchannel becomes valid. In the limit, the total aggregate data rate, in bits per second, of an infinite-length DMT system is given by Equation (2.31), which is:

$$\tilde{R}_{DMT} = \int_{W_{DMT}} log_2 \left(1 + \frac{SNR(f)}{\Gamma}\right) df \ , \tag{2.69}$$

where W_{DMT} is the range of frequencies, or subchannels, that is actually used for data transport. If we employ strictly QAM constellations within each subchannel, then the optimal W_{DMT} is the frequency band within which the integrand in Equation (2.69) is greater than or equal to two, because there must be two or more bits per transmitted QAM signal. As for the infinite-length MMSE-DFE, it is easy to see, by combining Equations (2.64), (2.66), and (2.68), that for the moderate to high SNR case, the total data rate in bits per second is given approximately by:

$$\tilde{R}_{MMSE-DFE} \approx \int_{W_{MMSE-DFE}} log_2 \left(\frac{1 + SNR(f)}{\Gamma}\right) df \ , \tag{2.70}$$

where the optimal $W_{MMSE-DFE}$ is the range of frequencies where the integrand in (2.70) is positive. Therefore, if $SNR(f) >> 1$ for most of the frequency band of interest, or $f : f \in W$, and the frequency range where $SNR(f) \geq 3\Gamma$ is much larger than the range where $(\Gamma - 1) < SNR(f) < 3\Gamma$, as in the case of many DSL applications discussed in Chapter 5, then the two equalization approaches will achieve virtually the same performance in the infinite-length case, using virtually the same transmission bandwidth. Thus we have shown:

Theorem 2.1 (Relation of Infinite-Length DMT to Infinite-Length MMSE-DFE) *For an infinite-length DMT system and an ideal (no error propagation), infinite length MMSE-DFE system under the conditions of:*

1. $SNR(f) >> 1$ *for most* $f \in W$ *and*
2. $\{f : SNR(f) \geq 3\Gamma\} >> \{f : (\Gamma - 1) < SNR(f) < 3\Gamma\}$ *if the DMT system is restricted to using integer bit QAM constellations,*

the asymptotic behaviors of the two systems approach one another, such that:

$$\tilde{R}_{MMSE-DFE,\infty} \approx \tilde{R}_{DMT,\infty} , \tag{2.71}$$

and

$$W_{MMSE-DFE,\infty} \approx W_{DMT,\infty} . \tag{2.72}$$

We note here that condition 2 above can be removed if the DMT system is allowed to use constellations with infinite granularity in size, which unfortunately is not realizable in an actual system. We also note here that the resulting bandwidths $W_{MMSE-DFE,\infty}$ and $W_{DMT,\infty}$ may not necessarily be continuous, in the sense that they may contain disjoint regions of frequency. This will happen when the channel contains frequency notches (or dips) in its power spectral density curve and/or when the additive noise component consists of colored noise spectral densities. For example, unterminated bridged taps in copper twisted pairs will result in significant "ripples" in the channel frequency response, and crosstalk due to a number of different services within the same wire bundle may result in significant variation of

the noise spectrum along the frequency band. While discontinuity in the optimal transmission bandwidth does not pose any real difficulties in analysis, it does have a number of practical implications. In the case of the DMT, discontinuous bandwidth can be implemented just as easily as continuous bandwidth with digital signal processing, by assigning no energy to those carriers falling outside of the optimal transmission bandwidth. However, in the case of QAM implemented with a MMSE-DFE receiver, discontinuous bandwidth can lead to very serious implementational difficulties, because effectively the transmit filter will consist of a number of bandpass filters. The complexity of this transmit filter can be staggering, if implemented in a straightforward manner with a finite impulse response (FIR) filter, depending on the number of discontinuities and the required sharpness of the bandedges. Furthermore, this transmit filter has to be real-time trainable, and preferably real-time adaptive, because the optimal transmission bandwidth may vary significantly from line to line. This type of flexibility requires complicated initialization procedure in addition to elaborate multirate digital signal processing. One possible solution is to use Fast Fourier Transform (FFT) and Inverse Fast Fourier Transform (IFFT) interpolators and decimators; however, that implies frequency domain processing. Another possibility is to use multiple MMSE-DFE's, but then the resulting system is no longer a "single"-carrier system. Moreover, the complexity of such system is not likely to be practical for implementation with current technology, because the symbol rates and carrier frequencies of the different MMSE-DFE's will have to be made adaptive. Therefore, from a complexity/performance tradeoff standpoint, the DMT appears to be more suitable for applications where discontinuities within the optimal transmission band are common. The single-carrier MMSE-DFE system, on the other hand, appears to have an edge for applications where the channel constraint length is short, because the DMT transceiver requires certain minimum overhead to implement.

Chapter 3

Finite-length Modulation and Equalization

Because all practical communication systems are implemented under finite-length constraints, we will now extend our results from Chapter 2 to the finite-length case. We will start by redefining, in Section 3.1, the discrete-time channel model from the previous chapter to a form suitable for finite-length analysis. The resulting channel model will be in vector form, with the transmission channel described by a channel matrix instead of a channel pulse response. Section 3.2 considers finite-length multicarrier modulation, including the various implications and implementational issues due to the finite block length constraint. The performance analysis of a finite-length DMT system is presented, which is based closely on its infinite-length counterpart given in Section 2.3.2. Section 3.3 examines the corresponding issues for the single-carrier modulation system, implemented with a MMSE-DFE using finite-length feedforward and feedback filters. In particular, Cholesky Factorization is used in place of Spectral Factorization when analyzing the performance of a finite-length MMSE-DFE.

3.1 Vector Channel Model

As all practical modulation and equalization methods act on block data in some sense (as long as the channel constraint length $\nu < \infty$), it is often convenient to represent Equation (2.1) in its vector form as follows:

$$\begin{bmatrix} y_k \\ y_{k-1} \\ \vdots \\ y_{k-2N+2} \\ y_{k-2N+1} \end{bmatrix} = \begin{bmatrix} h_0 & h_1 & \dots & h_\nu & 0 & \dots & 0 & 0 \\ 0 & h_0 & h_1 & \dots & h_\nu & 0 & \dots & 0 \\ \vdots & \ddots & \ddots & \ddots & & \ddots & \ddots & \vdots \\ 0 & \dots & 0 & h_0 & h_1 & \dots & h_\nu & 0 \\ 0 & 0 & \dots & 0 & h_0 & h_1 & \dots & h_\nu \end{bmatrix} \begin{bmatrix} x_k \\ x_{k-1} \\ \vdots \\ x_{k-2N-\nu+2} \\ x_{k-2N-\nu+1} \end{bmatrix} + \begin{bmatrix} n_k \\ n_{k-1} \\ \vdots \\ n_{k-2N+2} \\ n_{k-2N+1} \end{bmatrix} . \tag{3.1}$$

Equation (3.1) can be written more compactly as:

$$\mathbf{y}_{k:k-2N+1} = \mathbf{H}\mathbf{x}_{k:k-2N-\nu+1} + \mathbf{n}_{k:k-2N+1} , \tag{3.2}$$

where $\mathbf{H}$ is the $(2N) \times (2N + \nu)$ fully-windowed Toeplitz matrix in Equation (3.1), and $\mathbf{x}$, $\mathbf{y}$, and $\mathbf{n}$ are the corresponding column vectors of the appropriately indexed size. Our choice of the received data block to be size $2N$ is for convenience in the analysis of the DMT system only, as it will become clear in later sections. However, we can just as easily use N as the size of our received data block. For infinite-length systems, we simply take the limit of $2N$ as $2N \to \infty$. The input and noise autocorrelation matrices for our vector channel model are then given by:

$$\mathbf{R}_{xx} = E\left[\mathbf{x}_{k:k-2N-\nu+1}\mathbf{x}^*_{k:k-2N-\nu+1}\right] , \tag{3.3}$$

and

$$\mathbf{R}_{nn} = E\left[\mathbf{n}_{k:k-2N+1}\mathbf{n}^*_{k:k-2N+1}\right] . \tag{3.4}$$

We will further assume that both $\mathbf{R}_{xx}$ and $\mathbf{R}_{nn}$ are positive-definite matrices. So in the special case of AWGN with noise spectral density σ^2 per complex dimension, the noise autocorrelation matrix reduces to $\mathbf{R}_{nn} = \sigma^2\mathbf{I}_{2N}$. Similarly, if the input sequence is independent and identically distributed with an average power (or energy) of $\mathcal{E}$ (per 2-dimensional symbol), then the input autocorrelation matrix is given by $\mathbf{R}_{xx} = \frac{\mathcal{E}}{2}\mathbf{I}_{2N+\nu}$. Lastly, in the special case of a memoryless (or ISI-free) channel,

$\nu = 0$ and $\mathbf{H} = h_0\mathbf{I}_{2N}$, which is just a constant factor of attenuation. We will make use of the vector channel model defined in this section for the remainder of this dissertation, when analyzing practical, finite-length modulation and equalization systems.

3.2 Finite-length Discrete Multitone Modulation

The detailed block diagrams of a finite-length DMT transmitter and receiver pair are illustrated in Figures 3.1 and 3.2, respectively. Serial input data, along with

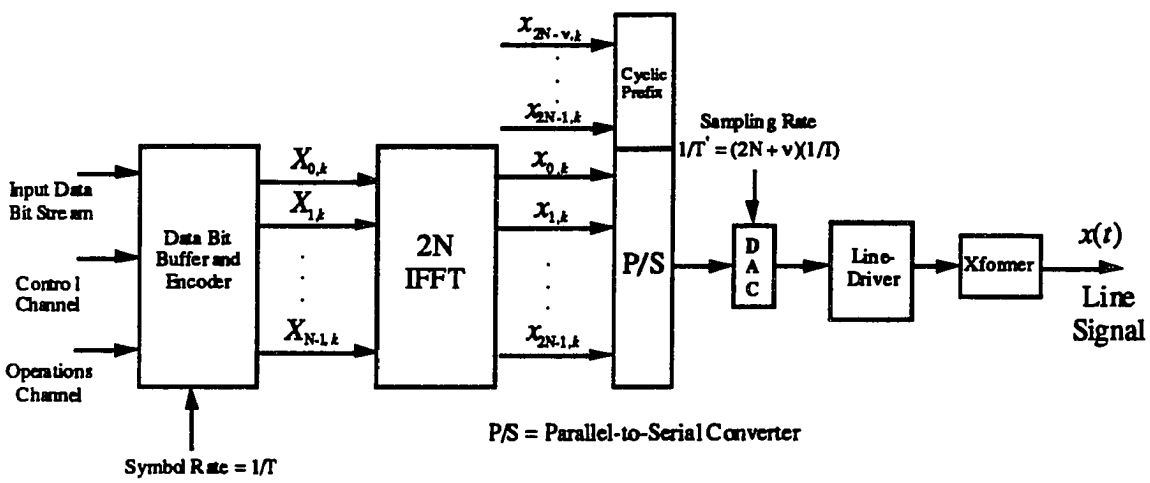

Figure 3.1: The DMT Transmitter

any additional control and operations information, at a rate of $\frac{b_{total}}{T}$ bits per second are first buffered and grouped into b_{total} bits for each block multicarrier symbol, with a block symbol period of T. The b_{total} bits are appropriately encoded, converted to a parallel form, and modulated by N separate carriers, with b_i bits modulated by the i^{th} carrier. The modulation process is accomplished by a $2N$-point IFFT operation. The parallel outputs of the IFFT are converted back to serial form with the appropriate cyclic prefix attached before passing through a Digital-to-Analog Converter (DAC) that operates at a sampling rate of $\frac{1}{T'} = \frac{2N+\nu}{T}$. The resulting

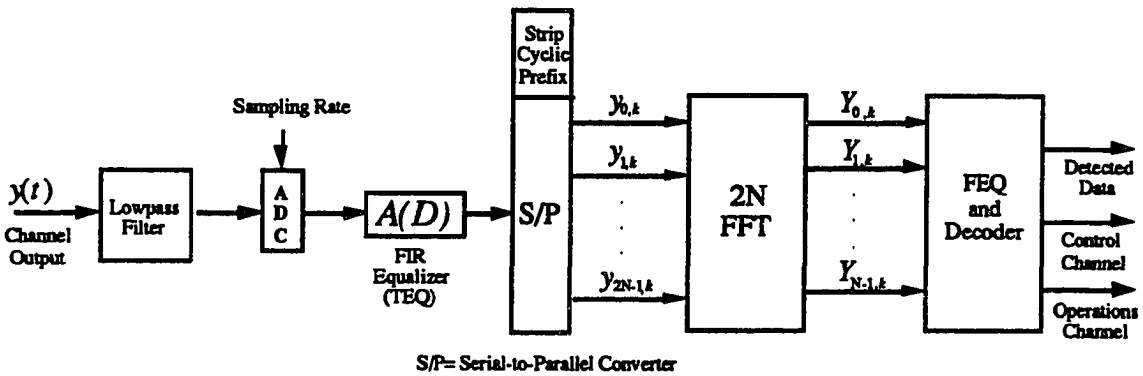

Figure 3.2: The DMT Receiver

analog waveform is lowpass filtered and sent through a D.C. isolating transformer to produce an analog transmit line signal. At the receiver end, the received analog signal is passed through a D.C. isolating transformer, low-pass filtered, and converted back to digital form by an Analog-to-Digital Converter (ADC) operating at the same sampling rate of $\frac{1}{T}$. The resulting digital received sequence is passed through a FIR time domain filter to limit the effective memory of the channel, and the cyclic prefix is stripped before the time domain filtered, received sequence is passed to the FFT demodulator, which converts the sequence back to parallel frequency domain signals. A bank of 1-tap, complex, frequency domain filters are used on these signals to scale them for a common decision element, which decodes the frequency domain signals and serially outputs the resulting data stream. A major advantage of finite-length Discrete Multitone modulation, in addition to its canonical properties, is that the modulating/demodulating vectors can be computed very efficiently using the well known IFFT and FFT algorithms. As mentioned before, a DMT system with N complex subchannels in the frequency domain requires a FFT size of $2N$, and by forcing conjugate symmetry in the frequency domain, a real valued time domain signal can be sent over the transmission line.

3.2.1 Implications of Finite-length DMT

As a direct consequence of the finite-length constraint, a number of practical, implementational issues for the DMT system need to be addressed. In particular, we will briefly describe three important features of a practical DMT system: the cyclic prefix or the cyclic extension, the pre-demodulate time domain equalizer (TEQ), and the post-demodulate frequency domain equalizer (FEQ). For more in-depth discussions of these and other implementational issues and tradeoffs of a finite length DMT system, the interested reader is referred to [41] and [42].

Cyclic Prefix

In a finite-length DMT system, the effective length of the channel impulse response, or the channel constraint length ν, will cause interblock interference, as the tail of the previous block multicarrier symbol will corrupt the beginning of the current block multicarrier symbol. As a result, the subchannels are not strictly independent of each other in the frequency domain. To mitigate the effect of IBI, a technique known as cyclic prefix, or cyclic extension (see [9] and [26]) is applied to the modulated block multicarrier symbol. The length of such cyclic prefix will be the same as ν. The cyclic prefix procedure is a simple wrapping around of the current block symbol so that to the discrete-time equivalent channel the input data sequence appears periodic, and it is illustrated in Figure 3.3. The cyclic nature of the DFT and IDFT vectors is the reason for making the input data sequence to appear periodic to the channel. In particular, if the input data sequence is periodic, then multiplication in the frequency domain due to linear filtering corresponds to time domain circular convolution [43], and all of our analysis will remain valid. Conversely, the effect of cyclic prefix can be absorbed into the channel matrix, and Equation (3.2) can now be written as:

$$\mathbf{y}_{k:k-2N+1} = \tilde{\mathbf{H}}\mathbf{x}_{k:k-2N+1} + \mathbf{n}_{k:k-2N+1} \,, \tag{3.5}$$

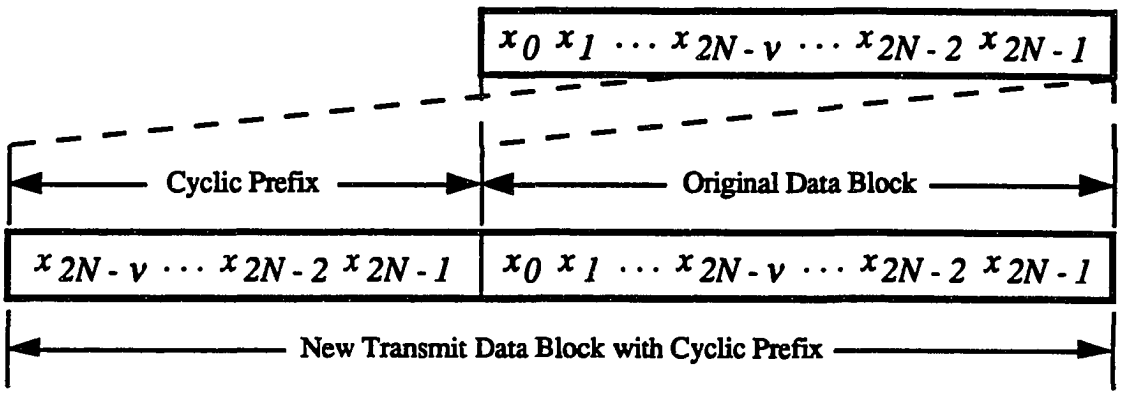

Figure 3.3: Cyclic Prefix

where $\tilde{\mathbf{H}}$ is a $(2N) \times (2N)$ square, circulant channel matrix given by:

$$\tilde{\mathbf{H}} = \begin{bmatrix} h_0 & h_1 & \dots & h_\nu & 0 & \dots & 0 \\ 0 & h_0 & h_1 & \dots & h_\nu & 0 & \vdots \\ \vdots & 0 & h_0 & h_1 & \dots & h_\nu & 0 \\ 0 & \dots & 0 & h_0 & h_1 & \dots & h_\nu \\ h_\nu & 0 & \dots & 0 & h_0 & h_1 & \vdots \\ \vdots & h_\nu & 0 & \dots & 0 & h_0 & h_1 \\ h_1 & \dots & h_\nu & 0 & \dots & 0 & h_0 \end{bmatrix}. \tag{3.6}$$

It has been shown in [29] that the capacity achieving set of modulating/demodulating vectors for the channel representation given by Equation (3.5) is precisely the IDFT and the DFT vectors. The use of a cyclic prefix, however, does result in a reduction of data rate by a factor of $\frac{\nu}{2N+\nu}$, because ν redundant time domain symbols are added to each block of $2N$ information-containing time domain symbols. Equivalently, we can view this reduction in data rate as a form of excess bandwidth in the system. Ideally, if $\nu << 2N$, then this loss is negligible, and in fact, as $2N$ approaches infinity, this penalty approaches zero.

Pre-Demodulate Time Domain Equalizer

Unfortunately, in many practical applications, such as DSL services, the channel constraint length, ν, may not be negligible when compared to the block size, $2N$, of the modulated block multicarrier symbol. Typically, the FFT/IFFT block size, $2N$, is chosen to be somewhere between 128 and 1024 for the best computational complexity/performance tradeoff, and in the case of DSL applications, ν may be a significant fraction of the chosen block size at the desired high sampling rate. To reduce the length of cyclic prefix, a technique involving a short, adaptive time domain equalizer concatenated to the channel after the ADC and before the FFT block, as shown in Figure 3.2, is proposed in [26]. The purpose of this time domain equalizer is not to flatten the channel completely as in a traditional linear or decision feedback equalizer, but rather it is to reduce the length of cyclic prefix to a more manageable number, without sacrificing performance significantly. In other words, this time domain equalizer, when concatenated with the channel, will produce a new target channel with a much smaller effective constraint length. This idea of using a linear equalizer to shorten the channel response is borrowed from single-carrier systems employing sequence detection (see [38]). The relationship between the size of cyclic prefix and the length of the TEQ is that of a compromise, from an implementational point of view, between a very long symbol and a very long equalizer. In the case of DSL services, empirical studies indicate that a 16-tap FIR filter is usually adequate for implementing this time domain equalizer, and the resulting effective channel constraint length, or equivalently the cyclic prefix size, that is necessary to bring the system performance to within 1 to 2 dB of the ideal theoretical performance is approximately ten to twenty taps [44]. The algorithm for determining the optimal settings of the TEQ involves an iterative process, making use of a known cyclic, pseudo-random training sequence and a variable step size, and it is detailed in [45] and in a recent U.S. patent application filed by J.S. Chow and J.M. Cioffi [46].

Post-Demodulate Frequency Domain Equalizer

The phases of the received FFT outputs, $Y_{i,k}$'s in Figure 3.2, are unlikely to be exactly the same as the phases of the transmitted 2-dimensional symbols at the input to the IFFT at the transmitter, or $X_{i,k}$'s in Figure 3.1. This phase distortion is the result of a (possibly varying) phase offset between the sampling clocks in the transmitter and the receiver of a practical transceiver system. Furthermore, even if the receiver sampling time can be adjusted perfectly, one still has to cope with the phase responses of the channel and the concatenated time domain equalizer. Typically, this phase distortion may increase linearly with frequency due to the cyclic prefix, which rotates the original FFT coefficients by a factor that is linearly proportional to the frequency. To compensate for this phase distortion, a set of "frequency domain equalizers" that consists of N 1-tap complex Least-Mean-Square (LMS) adaptive filters is used following the FFT block before the received signal is decoded. These 1-tap equalizers offer the additional benefit of received signal scaling before decoding. From a practical standpoint, it is convenient to use these 1-tap equalizers to adjust the gain of each FFT output so that a single decision element can be used for all subchannels regardless of the different subchannel attenuations. Furthermore, these adaptive 1-tap frequency domain equalizers can partially compensate for minor errors in channel estimation during DMT initialization, as well as slow drift between the sampling clocks at the transmitter and the receiver.

3.2.2 Finite-length DMT Analysis

The performance analysis of an ideal, finite-length DMT system[1] follows identically to that of the infinite-length analysis given in Section 2.3.2. We will first make the simplifying assumption that each of the N parallel, complex subchannels is effectively ISI-free, which becomes more valid as N increases in size. Therefore, we can again simply analyze the DMT performance as an aggregate of N ISI-free QAM

[1]By an ideal, finite-length DMT system, we mean one that absorbs the effects of the TEQ into the channel response and one that does not require a FEQ after demodulation.

subchannels, and the number of bits that can be supported by the i^{th} subchannel is given by Equation (2.28) from Section 2.3.2. The total number of bits transmitted in one block multicarrier symbol is then the sum of the numbers of bits supported by each of the used subchannels, and it is given by:

$$b_{total} = \sum_{i=1}^{\bar{N}} log_2(1 + \frac{SNR(i)}{\Gamma}) , \tag{3.7}$$

where $\bar{N} \leq N$ is the total number of subchannels used, and the total aggregated data throughput (in bits per second) is then $b_{total}\frac{1}{T}$, where T is the block multicarrier symbol period of the DMT system. To compute the system performance margin given a fixed target data rate, we define "average SNR", $\overline{SNR}$, as:

$$1 + \frac{\overline{SNR}}{\Gamma} = \left[\prod_{i=1}^{\bar{N}}(1 + \frac{SNR(i)}{\Gamma})\right]^{\frac{1}{\bar{N}}} \tag{3.8}$$

or

$$\overline{SNR} = \Gamma\left\{\left[\prod_{i=1}^{\bar{N}}(1 + \frac{SNR(i)}{\Gamma})\right]^{\frac{1}{\bar{N}}} - 1\right\} . \tag{3.9}$$

We can now rewrite Equation (3.7) as:

$$b_{total} = \bar{N}\ log_2(1 + \frac{\overline{SNR}}{\Gamma}) . \tag{3.10}$$

In the moderate to high SNR case, we may ignore the ± 1 terms in Equation (3.9), and our "average SNR" becomes the geometric average of $SNR(i)$'s:

$$\overline{SNR} \approx \left[\prod_{i=1}^{\bar{N}} SNR(i)\right]^{\frac{1}{\bar{N}}} . \tag{3.11}$$

Now $\overline{SNR}$ is expressed in terms independent of Γ, which is unknown if we are trying to compute the margin. By combining Equations (2.19) and (3.10), the system margin, γ_{margin}, for a BER of 10^{-7} and a target bit rate (per block symbol) of b_{target} may now be computed as:

$$\gamma_{margin} = 10\ log_{10}(\frac{\overline{SNR}}{2^{\frac{b_{target}}{\bar{N}}} - 1}) + \gamma_{eff} - 9.8\ (dB) . \tag{3.12}$$

A more precise and detailed analysis that takes the effects of the TEQ and the FEQ into account is given in [42].

3.3 Finite-length Decision Feedback Equalization

We now turn our attention to the corresponding finite-length decision feedback equalization, where FIR filters are used in place of Infinite Impulse Response (IIR) filters to implement the feedforward and feedback sections of the MMSE-DFE. In particular, the IIR filters $a(D)$ and $b(D)-1$ in Section 2.4.1 are now replaced with FIR filters $\mathbf{a}$ and $\mathbf{b}-1$, respectively, in their finite vector representations, which are given by:

$$\mathbf{a} = [w^*_{N_a-1-\Delta}\ w^*_{N_a-2-\Delta}\ \cdots\ w^*_{-\Delta}]\ , \tag{3.13}$$

and

$$\mathbf{b} = [\mathbf{0}_{1\times\Delta}\ 1\ b^*_1\ \cdots\ b^*_{N_b}\ \mathbf{0}_{1\times s}]\ , \tag{3.14}$$

where Δ is the delay of the feedforward filter, $s = N_a + \nu - \Delta - N_b - 1$, and N_a and N_b are the lengths of the feedforward and the feedback sections, respectively. Again, we note that the results given in this chapter on finite-length MMSE-DFE can be generalized directly from a symbol rate system to a fractional-spaced feedforward system.

3.3.1 Derivation of Finite-length MMSE-DFE

Before re-deriving the closed-form expressions for the optimal feedforward and feedback filter settings of the MMSE-DFE, we will first introduce the so-called Cholesky Factorization, which is the finite dimensional analog of the Spectral Factorization introduced in Section 2.4.1, in the following lemma:

Lemma 3.1 (Cholesky Factorization) *Any positive-definite, autocorrelation (therefore Hermitian), $M \times M$ matrix $\mathbf{R}_{xx}$ will admit a unique factorization of the following form:*

$$\mathbf{R}_{xx} = \mathbf{G}\mathbf{S}\mathbf{G}^* \ , \tag{3.15}$$

where $\mathbf{G}$ is a monic[2], $M \times M$, lower triangular matrix, and $\mathbf{S}$ is a $M \times M$, diagonal matrix with positive real entries. Furthermore, the columns in $\mathbf{G}$ are orthonormal to the rows in $\mathbf{G}^{-1}$. This particular factorization is known as the Cholesky

[2]A monic matrix $\mathbf{G}$ has ones along the main diagonal; therefore, if $\mathbf{G}$ is also triangular, then $|\mathbf{G}| = 1$.

compensate for the integer rounding operation.

4.3.4 An Extension of the Flat Energy Throughput Optimization Algorithm

The two integer bit bandwidth optimization algorithms presented in Sections 4.3.1 and 4.3.2 are designed to determine the near-optimal bandwidth in terms of maximizing the system performance margin at a given target data rate. In this section, we seek to extend the flat energy, total throughput optimization algorithm given in Section 4.2.2, subject to an integer bit constellation constraint; furthermore, we will allow for an arbitrary input power mask, as well as variable target bit-error-rates, across the subchannels. Of course, a similar extension can be made to the flat energy, margin optimization algorithm given in Section 4.2.3 as well.

Here we start with the same idea as the one in Section 4.2.2, but we round the resulting number of bits that can be supported by each carrier to the nearest integer value. At the end, we adjust the energy allocation accordingly, so that the overall power constraint, the arbitrary power mask, and the variable target bit-error-rates are all satisfied. Algorithmically, this procedure can be summarized in the following steps:

1. Compute $SNR(i)\ \ \forall i$, when all carriers are used and $\mathcal{E}(i) = 1\ \ \forall i$.
2. Calculate $\frac{SNR(i)}{\Gamma(i)}$, where $\Gamma(i)$ is the "SNR gap" for the i^{th} carrier and it is determined by the desired bit-error-rate and other chosen system parameters for the i^{th} carrier.
3. Sort resulting $\frac{SNR(i)}{\Gamma(i)}$'s into descending order and label so that $\frac{SNR(j)}{\Gamma(j)} \geq \frac{SNR(j+1)}{\Gamma(j+1)}$ $\forall j < N$. The mapping from the original carrier labels to the sorted carrier labels is stored and is invertible.
4. Let $k = 1$, $b_{max} = 0$, and initialize $\{\hat{b}_j\}$ to all zeros, where b_{max} is the current maximum number of bits achievable in a multicarrier symbol and $\{\hat{b}_j\}$ is the current bit allocation table that achieves b_{max}.

5. Compute $b_{target}(k)$ according to:

$$b_{target}(k) = \sum_{j=1}^{k} b_j \tag{4.58}$$

and

$$b_j = min \left\{ \begin{array}{c} round\{log_2(1 + \frac{\frac{\mathcal{E}_{target}}{k} SNR(j)}{\Gamma(j)})\} \\ floor\{log_2(1 + \frac{\mathcal{E}_{max,j} SNR(j)}{\Gamma(j)})\} \end{array} \right\} . \tag{4.59}$$

In Equation (4.59), $round\{x\}$ is the integer rounding operation, $floor\{x\}$ is the floor operation, $\mathcal{E}_{target}$ is the total input energy, or power, constraint at the transmitter, k is the number of used carriers, and $\mathcal{E}_{max,j}$ is the maximum energy, or power, allowable in the j^{th} carrier due to the transmit power mask. So for each of the k used carriers, equal amount of transmit energy $\frac{\mathcal{E}_{target}}{k}$ is used, but in no event greater than the allowable amount of individual carrier transmit energy due to the power mask, to calculate the achievable number of bits per multicarrier symbol.

6. If $b_{target}(k) > b_{max}$, then set $b_{max} = b_{target}(k)$ and keep track of the current bit allocation table, $\{\hat{b}_j\} = \{b_j\}$, that achieves b_{max}.

7. If $k \neq N$, then set $k = k + 1$ and go to step 5, else go to step 8. At this point b_{max} will indicate the maximum achievable data rate, and the currently stored bit allocation table that achieves b_{max}, $\{\hat{b}_j\}$, can be used to obtain the initial system bit allocation table, $\{\tilde{b}_i\}$, since the mapping in step 3 is invertible.

8. Allocate input energies, $\{\tilde{\mathcal{E}}_i\}$, accordingly so that $P_e(i)$ is achieved $\forall i$ given the bit allocation table $\{\tilde{b}_i\}$, where $P_e(i)$ is the target probability of error for the i^{th} used carrier. Typically, we want equal probabilities of error for all subchannels, or $P_e(i) = P_{e,target}$ $\forall i$, where $P_{e,target}$ is the target overall probability of error.

9. Calculate the current total transmit energy, $\mathcal{E}_{total}$, according to:

$$\mathcal{E}_{total} = \sum_{i=0}^{N-1} \tilde{\mathcal{E}}_i \ , \tag{4.60}$$

where $\tilde{\mathcal{E}}_i$ is the current transmit energy used by the i^{th} carrier.

10. Scale final energy distribution, $\{\tilde{\mathcal{E}}_i\}$, according to:

$$\tilde{\mathcal{E}}_i = min \left\{ \begin{array}{c} \frac{\mathcal{E}_{target}}{\mathcal{E}_{total}} \tilde{\mathcal{E}}_i \\ \mathcal{E}_{max,i} \end{array} \right\}, \tag{4.61}$$

where $\mathcal{E}_{target}$ is the target input power constraint.

The initial bit and energy allocation tables of this algorithm are now given by $\{\tilde{b}_i\}$ and $\{\tilde{\mathcal{E}}_i\}$, respectively.

4.3.5 An Adaptive Bit Swap Algorithm

In many practical systems, the channel characteristics may be slowly time varying in nature. For example, the frequency response of an ADSL loop may vary in time with temperature variations, and the noise characteristics may also change with different number of active crosstalkers. In situations like this, we can no longer model our transmission channel as stationary and time invariant; instead, we are faced with a quasi-stationary, slowing time varying system. As a result, the optimal transmission bandwidth and bit distribution identified during multicarrier system initialization may become suboptimal in time. Therefore, some adaptive algorithm that can modify the system bit distribution and/or transmission bandwidth in real time during normal system operations would be highly desirable. In this section, we propose a simple, but relatively slow, adaptive bit swap procedure[9], which will be adequate in tracking channel variations for DSL applications. This procedure, however, will not be sufficient in a fast time varying environment, such as those encountered in mobile radio communications. The key idea here is to make the transmitter adaptive, in addition to the receiver, in a quasi-stationary duplex transmission environment.

The first step in our adaptive bit swap procedure is to keep track of the steady-state MSE's of all subchannels in the receiver of a multicarrier system in the background during normal operation. When the MSE of one subchannel is over certain predetermined threshold value, say over 3 dB worse than another subchannel, a

[9]This algorithm is currently implemented in Amati's prototype ADSL and E1-HDSL systems.

bit is swapped from the worse subchannel to the better subchannel, so that the overall BER will be reduced. The bit swap information is then communicated back to the transmitter through a simple hand-shaking procedure. Algorithmically, this procedure can be summarized in the following steps:

1. Monitor steady-state MSE's of all used subchannels in the background according to:

$$|E_{i,j}|^2 = \mathcal{R}\{E_{i,j}^2\} + \mathcal{I}\{E_{i,j}^2\} \ , \tag{4.62}$$

$$\varepsilon_{i,j} = (\lambda)\varepsilon_{i,j-1} + (1-\lambda)|E_{i,j}|^2 \ , \tag{4.63}$$

   where $E_{i,j}$ is the error, or difference between the input and the output of the hard decision slicer at time j, and it is computed independently for the real ($\mathcal{R}\{E_{i,j}\}$) and the imaginary ($\mathcal{I}\{E_{i,j}\}$) dimensions of each subchannel i. The noise energy estimate for the i^{th} subchannel at time j, $\varepsilon_{i,j}$, is then computed by averaging successive squared error magnitudes, where λ is a positive fraction slightly less than 1.

2. Search through all used subchannels for $\varepsilon_{j,max}$ and $\varepsilon_{j,min}$ in the background, where $\varepsilon_{j,max}$ and $\varepsilon_{j,min}$ are the maximum and the minimum steady-state MSE estimates, respectively, among the used subchannels.

3. If $\varepsilon_{j,max} > \varepsilon_{j,min} + \varepsilon_{threshold}$ then go to step 4, else go to step 1. Here, $\varepsilon_{threshold} = 3\ (dB)$ is the predetermined threshold value.

4. Let $b(min) = b(min) + 1$ and $b(max) = b(max) - 1$, where $b(max)$ and $b(min)$ are the bit allocation table entries for the carriers corresponding to $\varepsilon_{j,max}$ and $\varepsilon_{j,min}$, respectively.

5. Let $\varepsilon_{j,min} = 2\varepsilon_{j,min}$ and $\varepsilon_{j,max} = 0.5\varepsilon_{j,max}$.

6. Adjust slicer settings for the two subchannels accordingly.

7. Send bit swap information back to transmitter via control channel and synchronize change through a simple handshake procedure.

This particular bit swap algorithm can work with either the Hughes-Hartogs algorithm or the alternative loading algorithms presented in Sections 4.3.2 and 4.3.4 for a multicarrier transceiver system.

Chapter 5

Applications of Band-Optimized DMT

In recent years, various Digital Subscriber Line [58] [59] applications, such as the High-speed Digital Subscriber Line (HDSL) and the Asymmetric Digital Subscriber Line services, have been proposed as bridges to the eventual full deployment of fiber. As a result, these DSL applications have generated a tremendous amount of research interest in designing ultra-high performance, yet cost effective, digital data transmission systems. Efficient modulation and equalization techniques are necessary in these transmission environments because of severe channel attenuation, intersymbol interference, and a host of other line impairments, including crosstalk, additive white Gaussian noise, and impulse noise. These highly challenging data transmission environments offer the ideal testing grounds for those digital communication techniques presented in the previous three chapters of this dissertation, and we will now focus on three particularly promising DSL applications; namely, the U.S. ADSL service, the European E1-rate HDSL (E1-HDSL) service, and the closely related Very High-speed Digital Subscriber Line (VHDSL) service.

In this chapter, we will apply a Discrete Multitone transceiver, with optimized transmission bandwidth, to these three potential DSL applications. Section 5.1 focuses on the U.S. ADSL service, which seeks to deliver high-speed data (1.6 Mbps

or more) in one direction only (from the telephone company central office to customer premises). A detailed description of the ADSL transmission environment is presented, and results of computer simulation on the performance of a DMT transceiver for ADSL are given. Furthermore, we compare the performance of a bandwidth optimized DMT system to a fixed symbol rate single-carrier QAM system with a MMSE-DFE receiver over various ADSL canonical loop configurations. Section 5.2 considers the European E1-HDSL service, which has a target data rate of 2.048 Mbps. In particular, we outline the transmission characteristics encountered in E1-HDSL and present performance projections of a DMT transceiver operating over both British and German loop plants. Lastly, Section 5.3 investigates the feasibility of the VHDSL service, using a multicarrier transceiver, to transport data at rates in excess of 10 or even 100 Mbps over very short copper twisted pairs. The simulation results presented in Section 5.2 and Section 5.3 are joint work done with fellow graduate students Naofal Al-Dhahir [16] and Jerry Tu [17], respectively, and their contributions are gratefully acknowledged here.

5.1 Asymmetric Digital Subscriber Lines

In this section we apply the transmission bandwidth optimization techniques presented in Chapter 4 to the provisioning of ADSL service over copper twisted pairs. ADSL was first proposed by Lechleider of Bell Communications Research in 1990 (see [58] and [59]) as an interim solution, using the existing copper loop plant, to the eventual full scale deployment of Broadband Integrated Services Digital Network (B-ISDN) on optical fiber. In particular, ADSL calls for a (possibly variable) downstream (from the telephone company central office to customer premises) data rate targeted at 1.6 to 6.4+ Mbps and an (possibly variable) upstream (return) data rate targeted at 16 to 384+ kbps. This "asymmetry" or difference in data rate between the two directions of transmission gave rise to the term ADSL. Furthermore, ADSL is proposed to coexist with current baseband services, including Basic-rate Access Integrated Services Digital Network (BA-ISDN) and the plain old telephone service (POTS). The required BER for ADSL is 10^{-7}, and some of

the intended applications of ADSL include video on demand, multimedia services, telecommuting, distance learning, and information distribution/exchange. In this dissertation, we will focus our simulation efforts on the downstream, or the high speed, direction of transmission, as it is by far the more difficult scenario. Moreover, we will concentrate primarily on the multicarrier approach because the DMT modulation has recently been adopted as the standard line code for ADSL by the American National Standards Institute (ANSI) Subcommittee T1E1.4 [60]. However, we will compare the performance of a DMT ADSL transceiver with a QAM ADSL transceiver in Section 5.1.3.

5.1.1 ADSL Transmission Environment

Lines encountered in the ADSL transmission environment are of a large variety of configurations, including wire gauge changes as well as unterminated bridged taps. All loops are nonloaded and consist of 26 gauge or coarser cables, and they are used either alone or in combination with other gauge cables. The range of ADSL coverage is not determined precisely at this point in time; however, it has been proposed to span up to 18 kft in length including bridged taps. The set of canonical

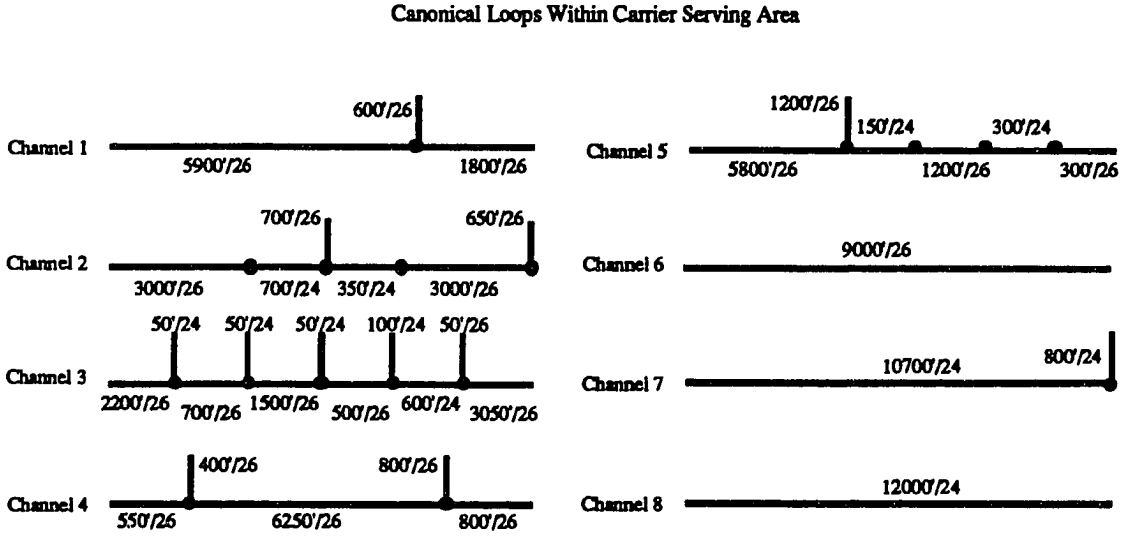

Figure 5.1: Canonical DSL Loops within the Carrier Serving Area

loops under study in this section are shown in Figure 5.1, where the first number in each wire segment denotes the length of the wire and the second number denotes the size, or gauge, of the wire. They are representative of "lossy" loops within the Carrier Serving Area (CSA) [61], which covers approximately 85 % of the currently installed copper loop plant, and this set of test loops is first proposed by Bellcore [62] for HDSL and ADSL system evaluation purposes.

The impulse response and power spectral density[1] characteristics for these channels have been determined with data in [63], using a modified version of the LINEMOD program.[2] A brief review of two-port transmission line theory used in the LINEMOD program is given in Appendix B. A pole-zero model is added to the response of each loop to eliminate the DC component and to simulate the effects of the transformer couplings that exist at both ends of the twisted pair. This pole-zero model consists of a double-zero at DC and a double-pole that makes the power gain of the transformer equals to -6 dB at 300 Hz. We will also assume a termination load resistance of 110 Ω for these loops.

Line attenuation characteristics of various channels in the frequency domain are illustrated in Figures 5.2 and 5.3, which compare the power spectral densities of the canonical CSA loops. Clearly from these plots, any ADSL transmission system will suffer from significant channel attenuation and intersymbol interference, as the channel transfer function may fluctuate over 50 dB between near baseband to 1 MHz. Furthermore, we can see that unterminated bridged taps will cause significant "ripples" in the channel power spectral density. This is due to the reflection of the transmitted signal from the mismatched termination. System performance can be reduced significantly as a result of such ripples in the transfer function. We note here that these power spectral densities are calculated based on source-to-load loss; therefore, power spectral densities of the same loops calculated based on insertion loss should be scaled 6 dB higher uniformly across the entire frequency band, assuming that the source and load impedances are matched.

[1] We define the "power spectral density" of a channel as the magnitude squared of the Fourier transform of the channel impulse response.

[2] We thank Professor. D. G. Messerschmitt of University of California at Berkeley for making the source code of this program available to us.

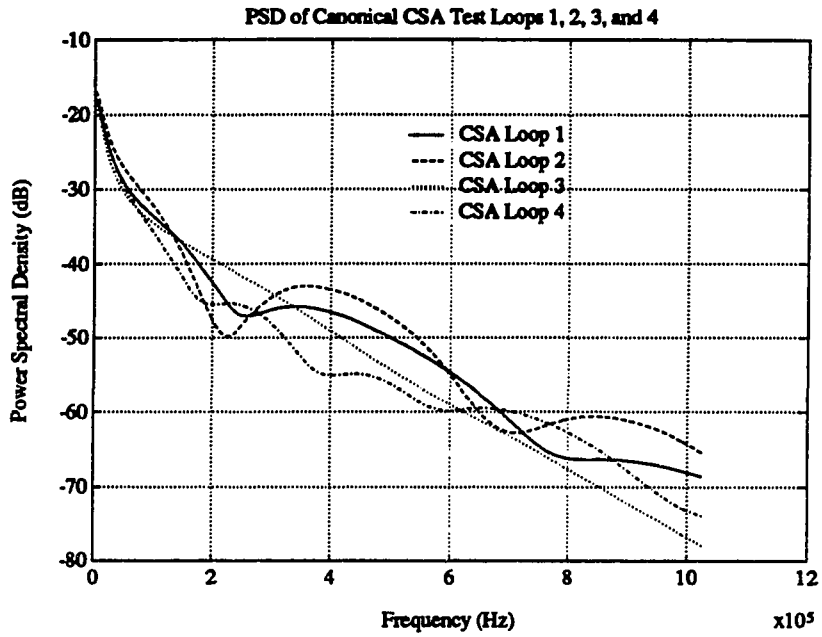

Figure 5.2: Power Spectral Densities of Canonical CSA Loops 1, 2, 3, and 4

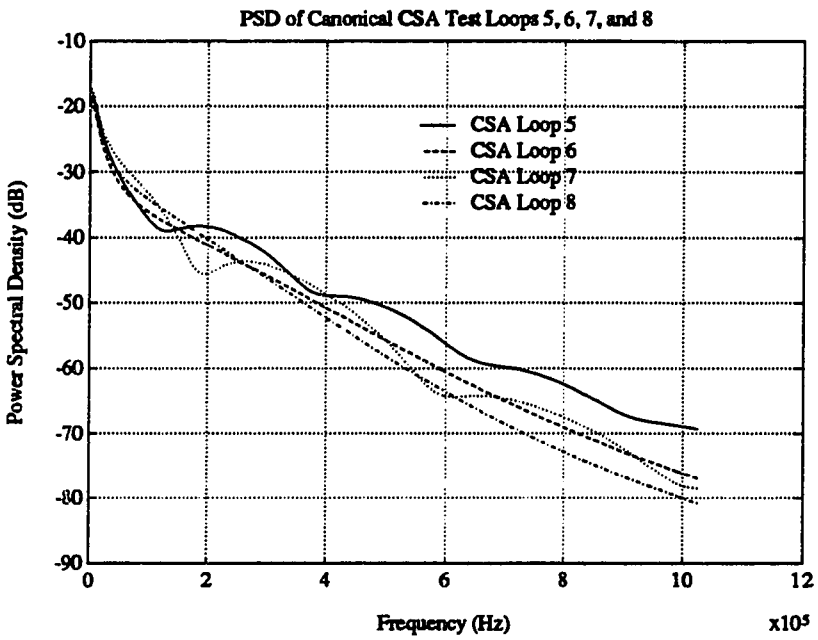

Figure 5.3: Power Spectral Densities of Canonical CSA Loops 5, 6, 7 and 8

In addition to severe channel attenuation and intersymbol interference, the ADSL transmission environment introduces a variety of additive impairments that serve to degrade the performance of any applied modulation scheme. These impairments include additive white Gaussian noise from a number of possible sources, both near-end and far-end crosstalk from adjacent twisted pairs within the same 50-pair wire bundle, and impulse noise [64]. For our computer simulations, we will assume an AWGN floor of -143 dBm/Hz (two-sided), a conservative estimate representing noise in the receiver front end, quantization noise in the analog-to-digital converter, and thermal noise. Due to the asymmetric nature of ADSL transmission, we have assumed that echo will not be present (or at least will not be severe), and an echo canceler is not necessary. However, if an echo canceler does become necessary, the background AWGN level needs to also include residual echo. For the interested reader, a full-duplex multicarrier echo canceler is presented in [65], and a number of traditional single-carrier full-duplex echo canceler structures are given in [31].

Crosstalk noise due to a number of possible sources, such as BA-ISDN transceivers, HDSL transceivers, and other ADSL transceivers, transmitting over adjacent twisted pairs within the same wire bundle will also be included in our simulations. It has been shown that the crosstalk phenomenon can be accurately modeled using only two terms, namely the near-end crosstalk (NEXT) and the far-end crosstalk (FEXT) [66]. The NEXT and FEXT terms are identified in Figure 5.4. In the ADSL environment, high-speed data is transmitted unidirectionally; thus, there will be no NEXT term in the frequencies of interest due to other ADSL services in the same wire bundle. However, there will be a significant amount of spill-over NEXT from bidirectional baseband services in the same wire bundle due to non-ideal filtering. The particular crosstalk scenario, which depends on the exact wire bundle configuration, may vary for different ADSL loops, and we will use a number of possible scenarios for our simulations. Furthermore, both NEXT and FEXT may be considered as colored Gaussian noise for our purposes [17]. The FEXT coupling function is modeled by the following equation [67]:

$$|H(f)|^2_{FEXT} = K_{FEXT} d |H(f)|^2 f^2 \,, \tag{5.1}$$

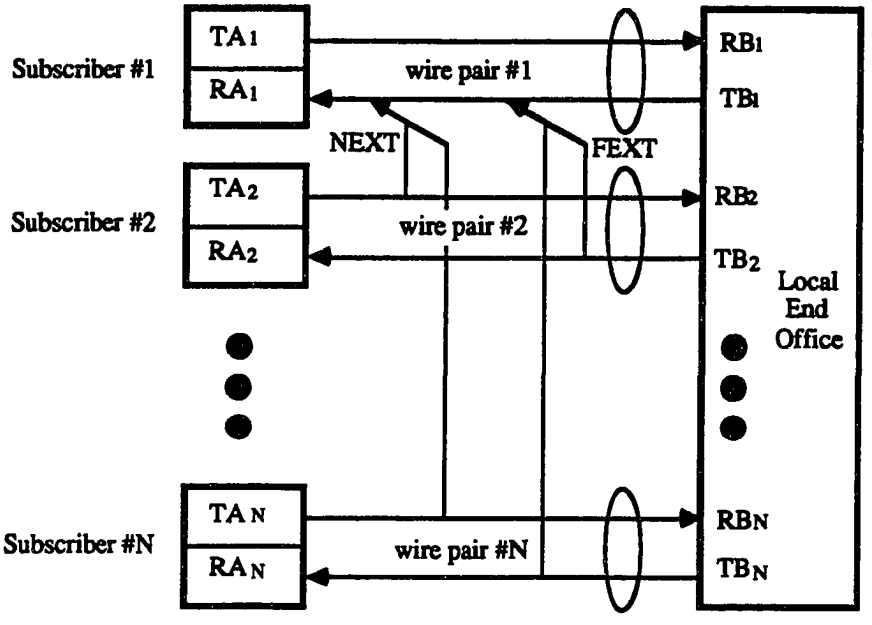

Figure 5.4: Near-end and Far-end Crosstalk

where f is frequency in Hz, $K_{FEXT} = 8 \times 10^{-20}$ for a worst case scenario of 49 disturbers [68] [69] [70], d is the loop length in ft, and $|H(f)|^2$ is the magnitude squared of the transfer function of the loop. The input power spectrum to this coupling function is the transmit spectrum of the interfering service. In a similar manner, the NEXT coupling function is modeled as [66]:

$$|H(f)|^2_{NEXT} = K_{NEXT} f^{1.5} , \tag{5.2}$$

where f is again frequency in Hz and $K_{NEXT} = 10^{-13}$ for a worst case scenario of 49 disturbers [71] [72]. Again, the transmit spectrum of the interfering service will be the input power spectrum to this coupling function. We will assume that each BA-ISDN transmitter uses 25 mW of power and occupies mostly the lower 40 kHz of the transmission band, while each HDSL transmitter uses 25 mW of power and occupies mostly the lower 200 kHz of the transmission band.

In addition to the AWGN component and crosstalk noise, there are several other impairments that will degrade the performance of any ADSL system operating over twisted copper pairs, including spill-over baseband signal, impulse noise, non-linear

distortion, inductive noise, and single frequency metallic noise. Because we have assumed that ADSL service is superimposed on the same wire that delivers baseband BA-ISDN, the spill-over far-end signal from BA-ISDN on the same wire will be received along with the ADSL signal, and this spill-over baseband "signal" must be treated as noise by the ADSL receiver[3]. Impulse noise is potentially one of the limiting impairments for ADSL, because when it hits, it could be more damaging than either crosstalk or additive Gaussian noise. Fortunately, impulse noise only occurs at infrequent intervals; as a result, impulse noise is not included in our simulations in this chapter. A detailed treatment of impulse noise and corresponding mitigation strategies are the subjects of Chapter 6. One fact worth stating now is that the block-processing nature of a multicarrier system is inherently more immune to short-duration, high-amplitude disturbances such as impulse noise, since the energy contained in the impulse is effectively distributed over the entire symbol block of a multicarrier symbol in the frequency domain. Non-linear distortion (NLD) in a subscriber loop is caused mainly by the transformer at the transmitter side of the loop, which carries a large D.C. in its primary winding.

Because a multicarrier signal has a higher peak-to-average power ratio than a single-carrier signal, it is more susceptible to NLD of this type; however, the signal-to-distortion ratio (SDR) due to NLD is typically in the order of 50 dB or higher. This is much more than the SNR resulting from AWGN and crosstalk noise; therefore, we can simply ignore NLD in our simulations. Power line inductive noise at 60 Hz and its harmonics do not seem to cause a serious problem in Digital Subscriber Lines at ADSL frequency range of interest (see [61]); therefore, it will also be ignored in our simulations. Lastly, certain single-frequency metallic noise may exist in some ADSL loops. However, the multicarrier adaptive bandwidth optimization update technique proposed in Section 4.3.5 can be used to accommodate such sinusoidal disturbances in a graceful and transparent manner, so that the degradation in performance is essentially negligible.

[3]If the BA-ISDN signal content is available to the ADSL receiver, this spill-over noise may be adaptively canceled out to some extent.

5.1.2 ADSL System Description

The ideal[4] DMT system that is used for simulation of ADSL service consists of the following parameters:

1. FFT size = $2N = 512$.
2. Number of subchannels = $N = 256$.
3. Sampling rate = 2.048 MHz.
4. Multicarrier symbol rate = $\frac{1}{T} = \frac{2.048MHz}{512} = 4000$ Hz.
5. Multicarrier symbol period = $T = 250$ μs.
6. Target data rate = $R = \frac{b}{T}$ = as specified.
7. Bits per multicarrier symbol = b = as specified.
8. Insertion point transmit power level = 20 dBm or as specified.
9. Integer bit assignment within bins varying from 0 bit to 10 bits per 2D carrier or as specified.
10. Target bit error rate = BER = 10^{-7}.
11. Wei's 4D 16-state code with an effective coding gain of 4.2 dB when trellis coding is used.

The exact noise scenario and certain system parameters will vary between individual simulations, and they will be given later as needed.

[4]By ideal, we mean a system that neglects the effects of cyclic prefix and the time domain equalizer.

5.1.3 ADSL Performance

In this section, we first compare the performance of a band-optimized DMT system (equivalently, a symbol rate optimized single-carrier system) to that of a single-carrier QAM system with a fixed symbol rate of 400 kHz. The reason for limiting the single-carrier QAM system to a fixed symbol rate is to further emphasize the importance of bandwidth optimization on a line-by-line basis for applications like ADSL. We will compare the two systems over the set of 8 canonical CSA loops from Section 5.1.1. In addition to the basic parameters given in Section 5.1.2, the DMT system considered here has a lower bandedge of 70 kHz and uses the practical bit allocation scheme described in Section 4.3.2 with half-bit granularity, 2 bit minimum, and 10 bit maximum constellation sizes. The single-carrier QAM system assumes a infinite-length, ideal MMSE-DFE receiver with a fixed symbol rate of 400 kHz (variable constellation sizes for variable target data rates) and the same transmit power level and lower bandedge as the DMT system. Both systems assume 0 dB margin and no additional coding. We have chosen three different data rates; namely, 1.544 Mbps (T1 rate), 3.1 Mbps (2 $\times$ T1 rate), and 6.312 Mbps (DS-2 rate), and two different noise scenarios; namely, AWGN plus 49 BA-ISDN NEXT disturbers and AWGN plus 24 HDSL NEXT disturbers.

The purpose of these simulations is to see exactly how well can a band-optimized system perform over these canonical CSA loops and to show the advantage of a band-optimized system, either multicarrier or single-carrier, over a fixed symbol rate single-carrier system, when a particular application (such as ADSL) encounters a wide variety of channel characteristics as well as data rates. In Figures 5.5, 5.6, and 5.7, we show the performance of a band-optimized (DMT) system with a target data rate of 1.544 Mbps, 3.1 Mbps, and 6.312 Mbps, respectively. In all three figures, the higher bar graph levels correspond to the achievable margins of the system under the noise scenario of AWGN plus 49 BA-ISDN NEXT disturbers, and the lower bar graph levels correspond to the achievable margins of the system under the noise scenario of AWGN plus 24 HDSL NEXT disturbers. In all cases, even the most difficult case of DS-2 rate data transmission, a band-optimized system can reliably meet the BER requirement of ADSL with a significant margin.

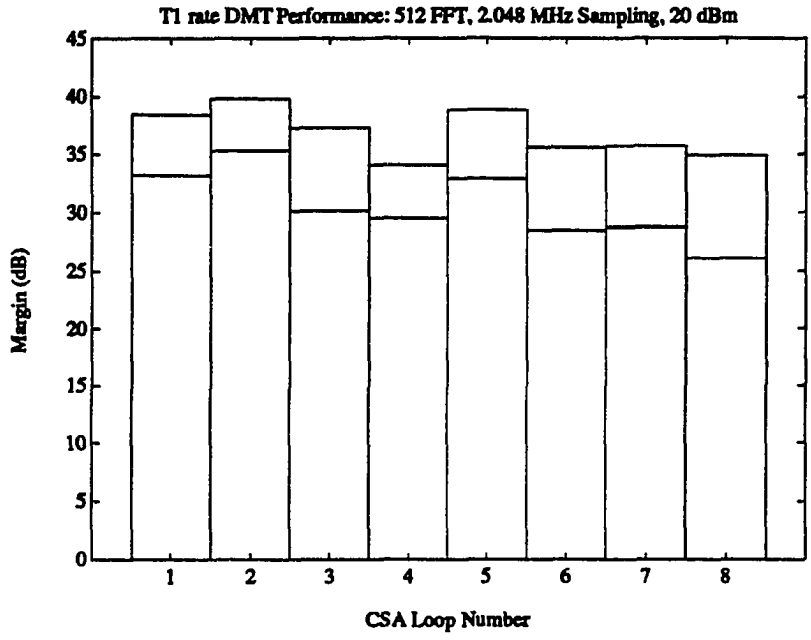

Figure 5.5: T1-Rate DMT Performance over Canonical CSA Loops

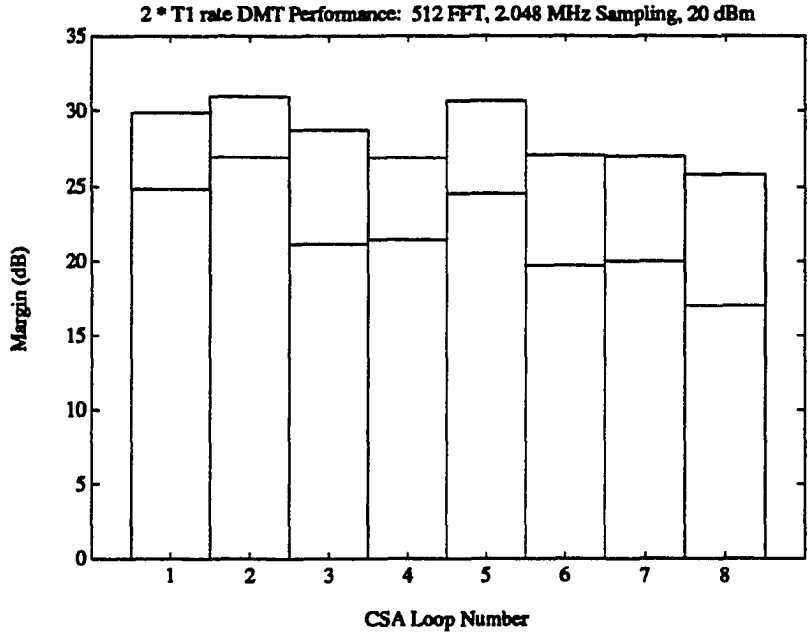

Figure 5.6: 2 × T1-Rate DMT Performance over Canonical CSA Loops

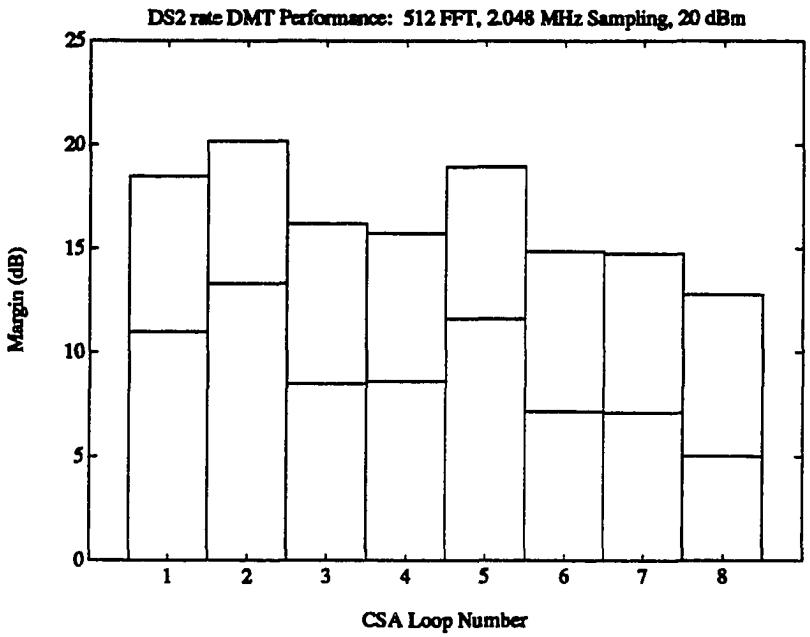

Figure 5.7: DS2-Rate DMT Performance over Canonical CSA Loops

In Figures 5.8 and 5.9, we show the loss in terms of system performance margin (in dB) of the fixed symbol rate, single-carrier QAM system with an ideal MMSE-DFE receiver relative to a band-optimized (DMT) system, for the two different noise scenarios. In both figures, the highest bar graph levels correspond to the margin advantage of a band-optimized system over the fixed symbol rate (400 kHz) QAM system transmitting at a rate of 6.312 Mbps, the middle bar graph levels correspond to transmitting at a rate of 3.1 Mbps, and the lowest bar graph levels correspond to transmitting at a rate of 1.544 Mbps. From these figures, we conclude that the loss due to restricting a single-carrier system to a fixed symbol rate can be unacceptably large for different channel, noise, and transmission rate characteristics.

Now, we will turn our attention to ADSL range of coverage using a band-optimized DMT transmission system over typical copper twisted pairs. In addition to the basic system parameters, we have also varied the input power level (10, 14, 20, or 30 dBm), chosen a 70 kHz lower bandedge, added a 6 dB system margin, and included a 4.2 dB trellis code. The noise scenario now includes AWGN, 49 ADSL

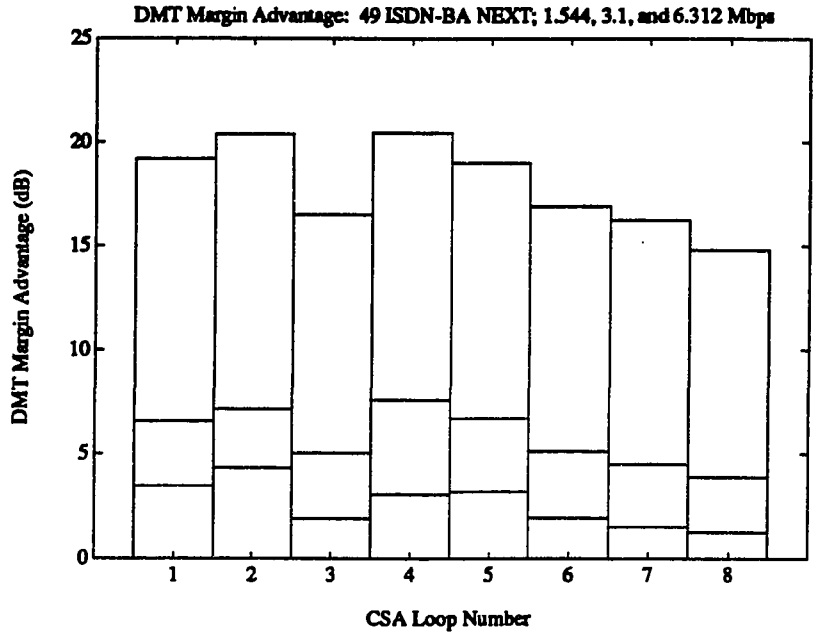

Figure 5.8: DMT vs. MMSE-DFE over Canonical CSA Loops with 49 BA-ISDN Interferers

FEXT disturbers, and 49 BA-ISDN NEXT disturbers. Figures 5.10 and 5.11 show the performance of the band-optimized DMT system over 26 gauge and 24 gauge wires, respectively. In both figures, the X-axis is the length of the line in kft, and the Y-axis is the total achievable data rate in Mbps. In each figure, the four curves correspond to transmit power levels of 10, 14, 20, and 30 dBm, where the higher the transmit power level, the higher the performance curve. From Figure 5.10, we note that the ideal DMT system can cover up to approximately 9 kft of 26 gauge wire at a rate of 6.4 Mbps with reasonable transmit power levels, and it can cover close to 18 kft at the T1 rate. For the 24 gauge wire, Figure 5.11 shows that the ideal DMT system can now achieve twice the T1 rate out to 18 kft with reasonable transmit power levels, and it can transmit at 6.4 Mbps with 20 dBm of power out to approximately 13 kft. In both figures, we notice that the achievable data rates due to the different input power levels will be approximately the same when the line is relatively short. This is because shorter lines have relatively small amount of

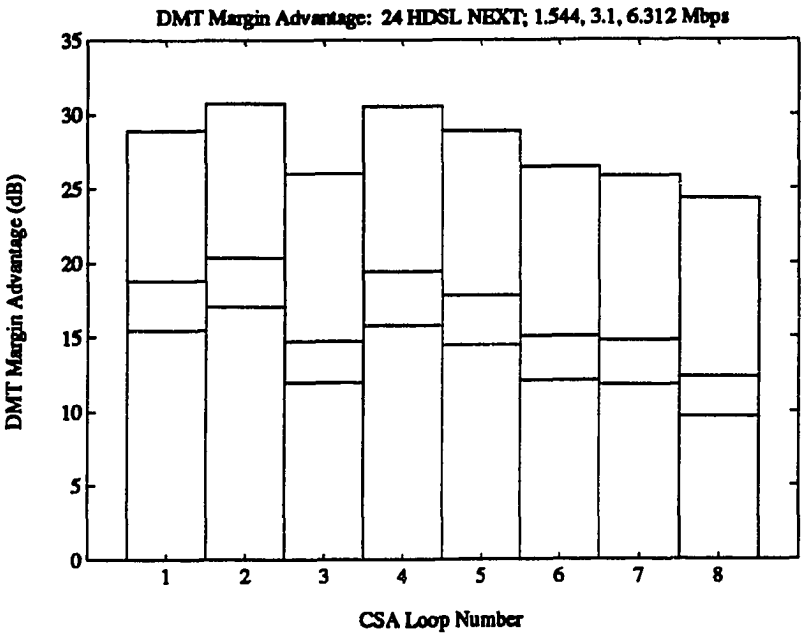

Figure 5.9: DMT vs. MMSE-DFE over Canonical CSA Loops with 24 HDSL Interferers

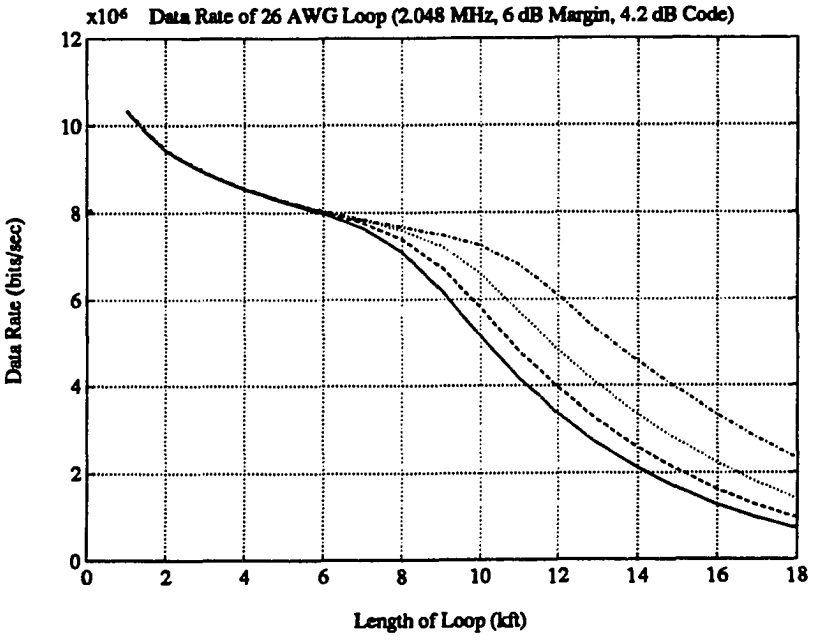

Figure 5.10: DMT Range of ADSL Coverage for 26 Gauge Wires

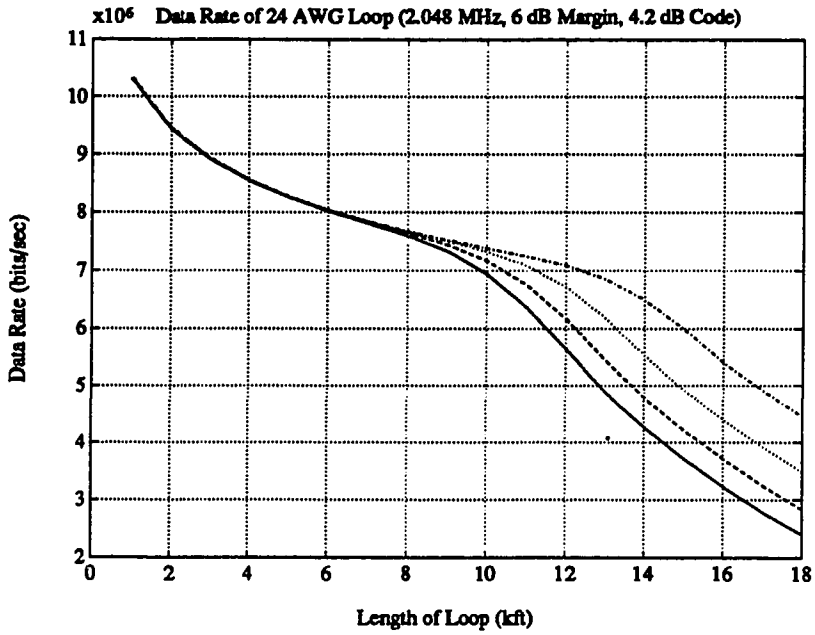

Figure 5.11: DMT Range of ADSL Coverage for 24 Gauge Wires

channel attenuation, which implies the corresponding FEXT from other ADSL users will be more significant. Therefore, the noise component due to ADSL FEXT will dominate other noise components, and because FEXT is both channel and input transmit power dependent, no matter how much power we use at the transmitter, we can no longer improve our received SNR or system performance.

5.1.4 Discussion of ADSL Performance

From simulation results in Section 5.1.3, we conclude that a bandwidth-optimized DMT transceiver can reliably deliver even the DS-2 rate of 6.312 Mbps over all CSA loops, which represents approximately 85% of the currently installed loop plant. This would allow live broadcast of a compressed, studio quality video signal, or several compressed, VCR-quality video signals, over the copper phone line to the home. A fixed symbol rate, single-carrier system would not be able to offer the same performance level for all possible data rate and line combinations without major hardware changes because it lacks the flexibility of the multicarrier system.

As pointed out in the previous section, the achievable data rate of any system will eventually saturate for all ADSL loops, due to the presence of far-end crosstalk, regardless of the total transmit power level. We can explain this saturation level from the following saturation capacity approximation, assuming that FEXT is the only dominant source of line impairment:

$$\tilde{C} = \frac{1}{T}\sum_{i=1}^{N} log_2(1+SNR(i)) \tag{5.3}$$

$$\cong \int_{W_{\tilde{C}}} log_2(1+SNR(f))df \tag{5.4}$$

$$= \int_{W_{\tilde{C}}} log_2(1+\frac{\mathcal{E}(f)|H(f)|^2}{\mathcal{E}(f)K_{FEXT}d|H(f)|^2f^2})df \tag{5.5}$$

$$= \int_{W_{\tilde{C}}} log_2(1+\frac{1}{(K_{FEXT}d)f^2})df\ . \tag{5.6}$$

We note here that this saturation level is independent of channel characteristics other than the channel length. Therefore, we can characterize the saturation level of any FEXT dominated channel as a function of $K_{FEXT} \times d$. In Figure 5.12, we have plotted the achievable data rates as a function of $K_{FEXT} \times d$ for the coded and the uncoded cases as well as the theoretical channel capacity calculated using Equation (5.6) above. For this particular plot, we have chosen a sampling rate of 640 kHz and a lower bandedge of 50 kHz; however, these numbers are selected for illustration purposes only. Note that the uncoded saturation data rates differ from the coded saturation data rates, and this phenomenon is due to the fact that trellis codes effectively increase the minimum distance between signal points while not affecting the noise variance.

5.2 E1-Rate High-Speed Digital Subscriber Lines

In this section, we turn our attention to the European E1-HDSL service, which is currently being studied by the European Telecommunications Standards Institute (ETSI) Subcommittee TM3 for near future deployment in Europe. The target duplex, data rate of the E1-HDSL service is 2.048 Mbps plus control information over repeaterless twisted-pair telephone lines, and the BER requirement is at 10^{-7}. Like

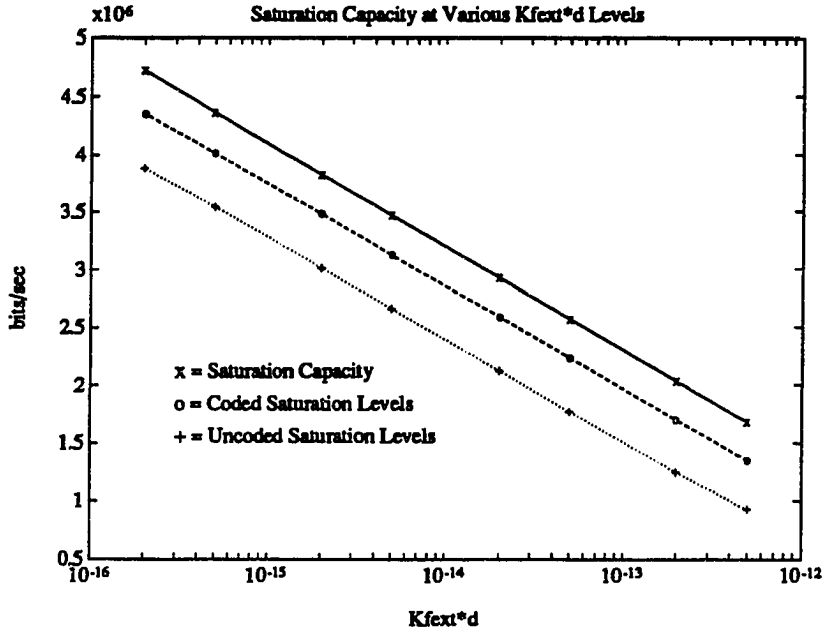

Figure 5.12: Data Rates at Saturation Power Level

U.S. ADSL loops, European E1-HDSL loops are of a large variety of configurations, including wire gauge changes as well as unterminated bridged taps. Furthermore, different European nations have different standards for their respective loop plants, which may be significantly different from those found in other countries. As a result, we will consider both the British and the German[5] loop plants in this dissertation. The precise range of E1-HDSL coverage is not standardized at this point in time; however, it has been proposed to span four or more kilometers, depending on the configuration, employing either a dual-duplex or a dual-simplex transmission scheme.

5.2.1 E1-HDSL Transmission Environment

The set of loops under study in this dissertation is shown in Figure 5.13. They are representative of some worst-case loops being considered for E1-HDSL coverage.

[5]The German loops studied in this chapter are generated from primary loop characteristics of twisted-pairs currently installed in the former East Germany.

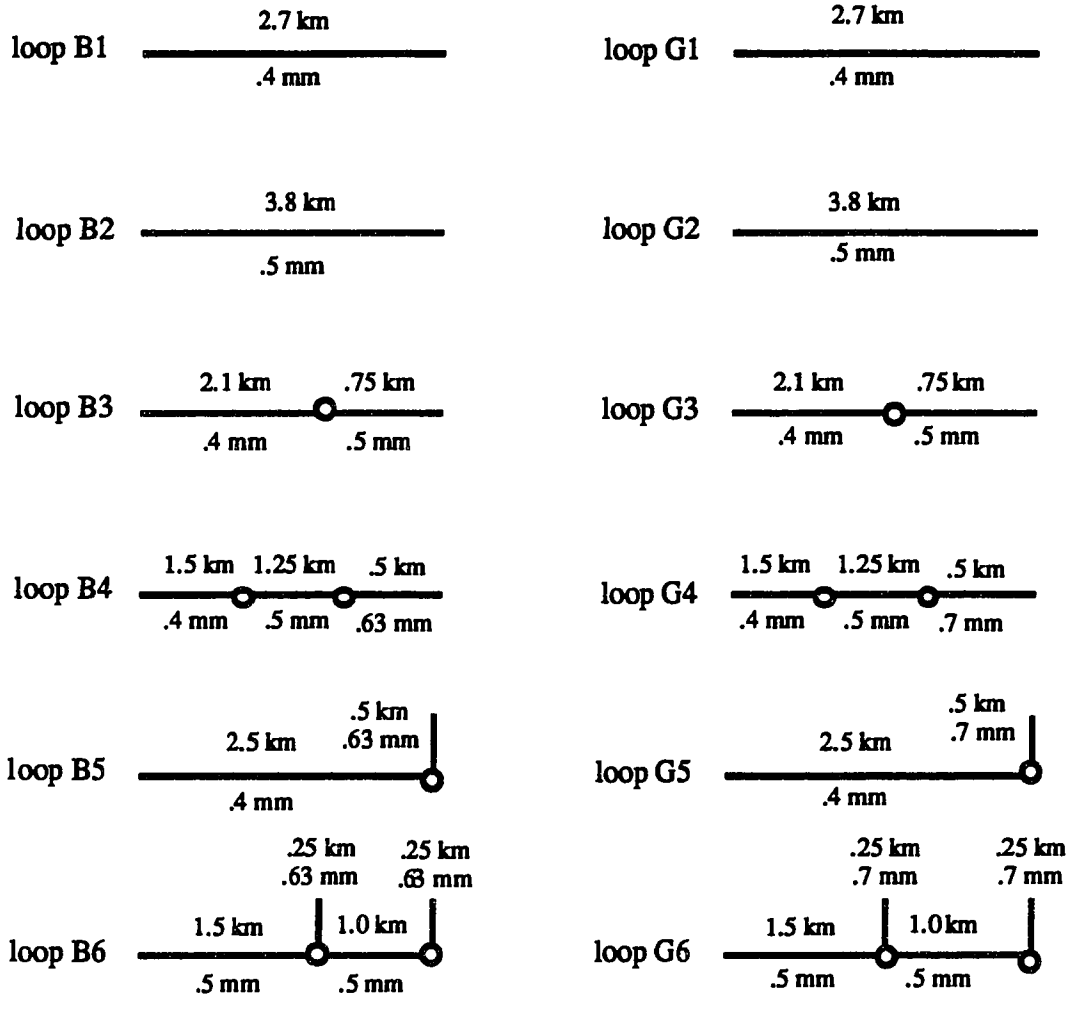

British Test Loops **German Test Loops**

Figure 5.13: British and German Test Loop Sets

The first four loops from both sets correspond to test loops 1, 2, 3, and 6 proposed in the British Telecommunications Specification RC 9006. The last two loops from both sets are examples of loops containing bridged tap(s). The impulse responses and power spectral densities of these loops have been determined from primary and secondary transmission parameters obtained from British Telecommunications Ltd. and Deutsche Bundespost for the British and the German loops, respectively. Two 1:1 transformer couplings are added to these loops to eliminate the DC component. In Figures 5.14 and 5.15, we have plotted the power spectral densities of channel insertion loss in dB vs. frequency for the British and the German test loops, respectively. These curves have already taken the transformers into account. In the case of the British loops, we have assumed a termination load resistance of 135 Ω, and for the German loops, the load consists of a 130 Ω resistor. Clearly from these

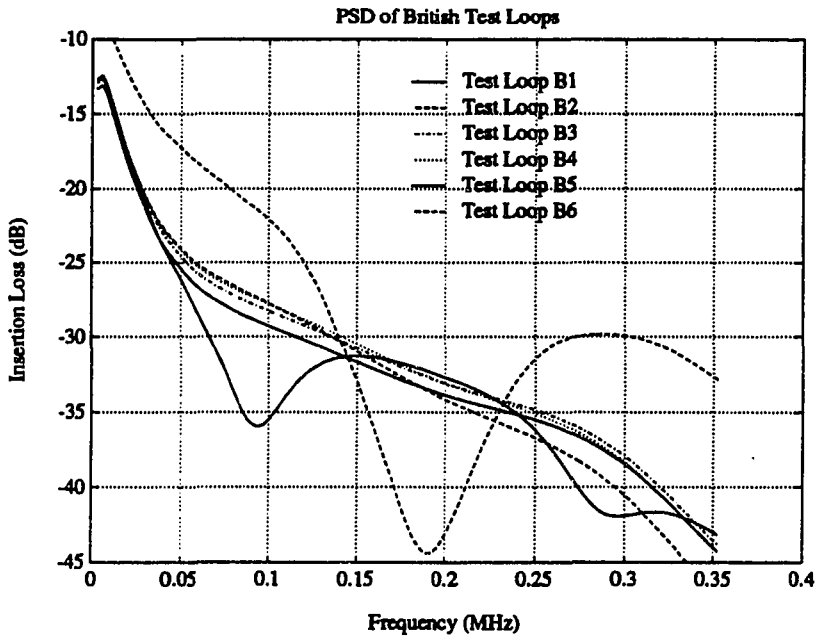

Figure 5.14: Power Spectral Densities of British Test Loops

plots, E1-HDSL transmission systems suffer from significant channel attenuation and intersymbol interference, similar to those encountered in the U.S. ADSL loops. Furthermore, unterminated bridged taps will again cause significant "ripples" in

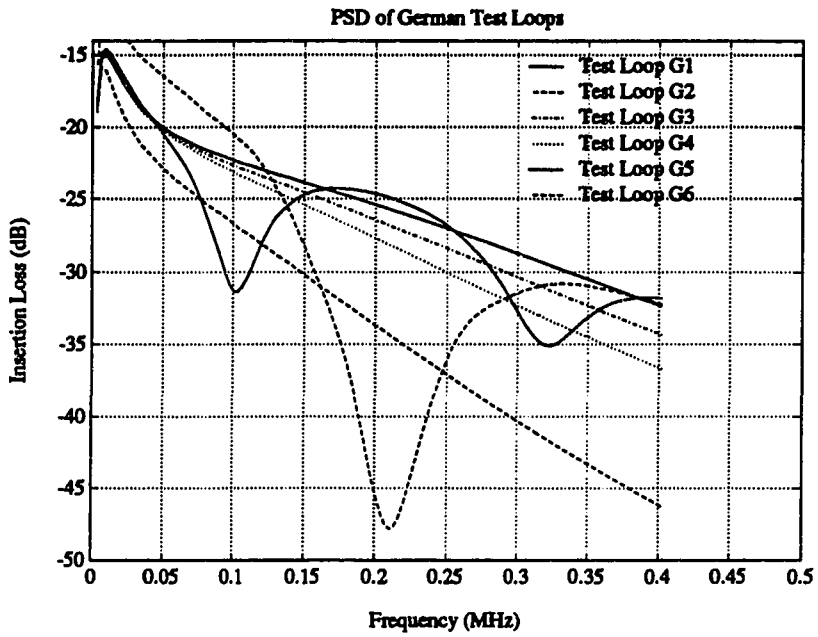

Figure 5.15: Power Spectral Densities of German Test Loops

the channel power spectral density, and system performance can be reduced significantly due to the presence of such ripples in the transfer function. We will, however, show later in this chapter that the DMT system will perform well even in the presence of these in-band frequency dips/nulls.

In addition to severe channel attenuation and intersymbol interference at the sampling rate required for the E1-HDSL service, we must also contend with an array of additional impairments in E1-HDSL, similar to those encountered in the ADSL environment. From empirical studies, it can be shown that crosstalk noise, which depends on input power, is likely to be one of the limiting impairments for full-duplex transmission at the E1-HDSL frequencies of interest. Unlike ADSL, where high-speed data are only transmitted in one direction and little or no self-NEXT is present, both self-NEXT and self-FEXT are encountered in E1-HDSL. When both NEXT and FEXT exist, it is well known that NEXT will dominate, as FEXT is attenuated by the channel. For this dissertation, we will considering two E1-HDSL scenarios. In the British system, it is assumed that every pair within the

same wire binder group will be transmitting E1-HDSL signal, and NEXT can be modeled by:

$$|H(f)|^2_{NEXT-B} = K_{NEXT-B} f^{\frac{3}{2}} , \tag{5.7}$$

where f is frequency in Hz and K_{NEXT-B} is determined through empirical measurements. This equation has exactly the same form as that of the near-end crosstalk equation for U.S. ADSL loops, given in Section 5.1.1. In our simulations, we will assume $K_{NEXT-B} \approx 10^{-13}$, thus achieving a crosstalk transfer function of -52.9 dB at 150 kHz as given in the British Telecommunications Specification RC 9006. In the case of German cables, however, the Deutsche Bundespost has specified a preliminary dual-simplex version of E1-HDSL, where different directions of data transmission are assigned to different binder groups. This requirement significantly lowers the crosstalk level for the German system, and the measured crosstalk level can be modeled by:

$$|H(f)|^2_{NEXT-EG} = K_{NEXT-EG} f^{1.725} , \tag{5.8}$$

where f is again frequency in Hz and $K_{NEXT-EG}$ is set at a value of $K_{NEXT-EG} \approx 10^{-15.6}$, which along with the exponent of 1.725 are obtained through empirical measurements conducted by the Deutsche Bundespost.

A second impairment that will degrade the performance of any E1-HDSL system is AWGN due to electronics noise, such as quantization noise from the analog-to-digital converter and thermal noise from the analog section of system hardware, and residual echo in full duplex transmission with echo cancellation. In our simulations, we will assume an AWGN level of $1.7\mu V/\sqrt{Hz}$ for both the British and the German systems. This results in approximately 2×10^{-11} mW/Hz of AWGN (1-sided) power. Other sources of line impairments that may be encountered in E1-HDSL but are not modeled explicitly in our simulations include impulse noise, non-linear distortion, inductive noise, and single frequency metallic noise. The reasons for not including these impairments in our simulation model are the same as those given in Section 5.1.1 for ADSL.

5.2.2 E1-HDSL System Description

Due to the differences in line and crosstalk noise characteristics between the British and the German cables, as well as the different target data rate requirements per twisted-pair, different system parameters have been chosen for our simulation. For the British system, we follow the requirements given by British Telecommunications Specification RC 9006, and for the German system, we follow the requirements specified by the Deutsche Bundespost.

System Parameters for British Loops

For British loops, We use a DMT system with the following parameters:

1. FFT size = $2N = 128$.
2. Number of subchannels = $N = 64$.
3. Size of cyclic prefix = $\nu = 6$ samples.
4. Sampling rate = $\frac{1}{T'} = 703.5$ kHz.
5. Multicarrier symbol rate = $\frac{1}{T} = \frac{703.5\ kHz}{128+6} = 5250$ Hz.
6. Multicarrier symbol period = $T = 190\ \mu$s.
7. Target data rate = $R = \frac{b}{T} = 1.024$ Mbps (0.5 × E1) + 24 kbps (operations and control channels) = 1.048 Mbps.
8. Bits per multicarrier symbol = $b = 200$ bits.
9. Insertion point transmit power level = 17 dBm.
10. TEQ size = 16 taps.
11. Integer bit assignment within bins varying from 0 bit to 10 bits per 2D carrier.
12. Target bit error rate = BER = 10^{-7}.

13. Wei's 4D 16-state code with effective coding gain of 4.2 dB included as specified.

Noise parameters used in our simulation for the British test loops are as follows:

1. AWGN = 1.7×10^{-6} V/$\sqrt{Hz}$ across 135 Ω load resistor (1-sided), totalling 7.5×10^{-6} mW of power.
2. NEXT constant = $K_{NEXT-B} = 10^{-13}$, achieving -52.9 dB of NEXT at 150 kHz.

These system parameters represent a dual-duplex mode of operation, where two sets of twisted-pairs, each carrying 1.048 Mbps (1.024 Mbps of data plus 24 kbps of operations and control information), are used to transmit the required E1 data rate. As the two sets of twisted-pairs will transmit data independently of one another, in the event when one of the two sets goes down, it is still possible for data transmission at half of the E1 rate, provided that the units are coordinated at both the central office and the customer premises via the operations and control channels.

System Parameters for German Loops

For German loops, we use a DMT system with the following parameters:

1. FFT size = $2N = 128$.
2. Number of subchannels = $N = 64$.
3. Size of cyclic prefix = $\nu = 6$ samples.
4. Sampling rate = $\frac{1}{T'} = 804$ kHz.
5. Multicarrier symbol rate = $\frac{1}{T} = \frac{804\ kHz}{128+6} = 6000$ Hz.
6. Multicarrier symbol period = $T = 167\ \mu s$.
7. Target data rate = $R = \frac{b}{T} = 2.048$ Mbps (E1) + 16 kbps (operations and control channels) = 2.064 Mbps.

8. Bits per multicarrier symbol = $b = 344$ bits.
9. Insertion point transmit power level = 17 dBm.
10. TEQ size = 16 taps.
11. Integer bit assignment within bins varying from 0 bit to 10 bits per 2D carrier.
12. Target bit error rate = BER = 10^{-7}.
13. Wei's 4D 16-state code with effective coding gain of 4.2 dB included as specified.

Noise parameters used in our simulation for the German test loops are as follows:

1. AWGN = 1.7×10^{-6} V/$\sqrt{Hz}$ across 130 Ω load resistor (1-sided), totalling 8.9×10^{-6} mW of power.
2. NEXT constant = $K_{NEXT-EG} = 10^{-15.6}$.

These system parameters represent a dual-simplex mode of operation, where one set of twisted-pairs, carrying 2.064 Mbps (2.048 Mbps of data plus 16 kbps of operations and control information), is used to transmit the required E1 data rate in each direction.

5.2.3 E1-HDSL Performance

The results of our computer simulation for the British and the German loop sets are summarized in Tables 5.1 and 5.2 respectively. By "ideal", we mean a system that requires no time domain equalizer; or equivalently, if we assume that an infinite-length TEQ is feasible.

5.2.4 Discussion of E1-HDSL Performance

From Table 5.1 above, we see that it is indeed possible to achieve the required target data rate of 1.048 Mbps over all 6 British test loops even without an additional trellis code, if we assume the ideal situation where no time domain equalizer is

Loop	ideal w/o code	ideal w/ code	w/ TEQ w/o code	w/ TEQ /w code
1	2.83	7.12	0.85	5.05
2	3.25	7.54	1.06	5.26
3	3.71	7.91	1.62	5.82
4	3.86	8.14	1.72	5.92
5	1.66	5.86	-2.00	2.26
6	6.82	11.07	3.67	7.87

Table 5.1: Margins for the British test loops

Loop	ideal w/o code	ideal w/ code	w/ TEQ w/o code	w/ TEQ /w code
1	12.48	16.68	10.47	14.67
2	4.38	8.58	2.82	7.04
3	11.54	15.74	9.51	13.73
4	10.32	14.52	8.30	12.50
5	10.67	14.87	5.51	9.71
6	8.57	12.77	5.33	9.53

Table 5.2: Margins for the German test loops

necessary. In a real system implementation, however, such an idealistic scenario is not realizable from a practical standpoint, and with the inclusion of a finite length (16-tap) TEQ, we will lose somewhere from 2 to about 3.5 dB for the worst-case channels. We note that this TEQ loss is more severe for channels with unterminated bridged taps. This is expected because the TEQ needs to work harder in order to equalize the power spectral density "ripples" in the frequency domain of a channel with unterminated bridged taps. To achieve the same level of equalization, we need a longer TEQ for such a channel than for one that is monotonically decreasing; equivalently, if we fix the size of the TEQ, we would expect a bigger SNR loss due to the TEQ over loops with significant PSD ripples within the used transmission band. In the case of test loop BT-5, we can no longer achieve the required data rate with a positive margin; in other words, we can no longer maintain the desired bit error rate of 10^{-7}, without an additional trellis code after we include a 16-tap TEQ. With Wei's 4D 16-state trellis code, however, we will obtain a positive margin between 2 to 8 dB for all 6 British test loops with the presence of the TEQ. This strongly suggests that a powerful trellis code is necessary if we intend to offer

E1-HDSL service to the currently defined coverage area of British loops.

In the case of the German E1-HDSL scenario, our proposed DMT system will be able to achieve the required 2.064 Mbps transmission rate with a positive margin over all 6 test loops, as shown in Table 5.2, with the inclusion of a TEQ and without an additional trellis code. When we concatenate Wei's code to this system, we achieve at least a 7 dB margin in the set of test loops. This suggests that with the addition of a powerful trellis code, we will be able to extend the currently proposed coverage area of East German loops, or perhaps we can increase the data rate beyond E1.

5.3 Very High-Speed Digital Subscriber Lines

The proposed VHDSL service is an enhancement of the HDSL service, and it seeks to provide reliable, bidirectional data transmission at rates of 10 Mbps or higher over only relatively short distances. Loops intended for use with VHDSL service are those that are located between the pedestal and the customer premises. These are generally no more than 150 feet in length and no smaller than 26 gauge in size. As in the case of ADSL and E1-HDSL, VHDSL is a new transport concept with no established design rules yet. Some of the target data rates that may be desirable for VHDSL applications include:

- Current Ethernet standard rate = 10 Mbps.
- DS-3 (Digital Signal, Level 3) rate = T3 rate = 44.736 Mbps.
- OC-1 (Optical Carrier, Level 1) rate = 51.84 Mbps.
- FDDI (Fiber Distributed Data Interface) rate = 100 Mbps.
- OC-3 (Optical Carrier, Level 3) rate = 155.52 Mbps.

5.3.1 VHDSL Transmission Environment

In this dissertation, we will only consider the worst case VHDSL loop, which is 150 feet of 26 gauge wire. Furthermore, we assume that PIC cables operating at 70° F

with matched source and load resistances of 110 Ω are used and that within this short 150 feet line there are no bridged taps or wire gauge changes. As in ADSL and E1-HDSL loops, a transformer is added to both ends of the cable to eliminate the DC component in the frequency response. Again, the effects of the transformer coupling is simulated by a pole-zero model that consists of a double-zero at DC and a double-pole that makes the power gain of the transformer equals to -6 dB at 300 Hz. Using the modified version of LINEMOD with data in [63], we can determine the impulse response and power spectral density characteristics for this channel. We found that the maximum useful bandwidth of this worst case loop is around 12

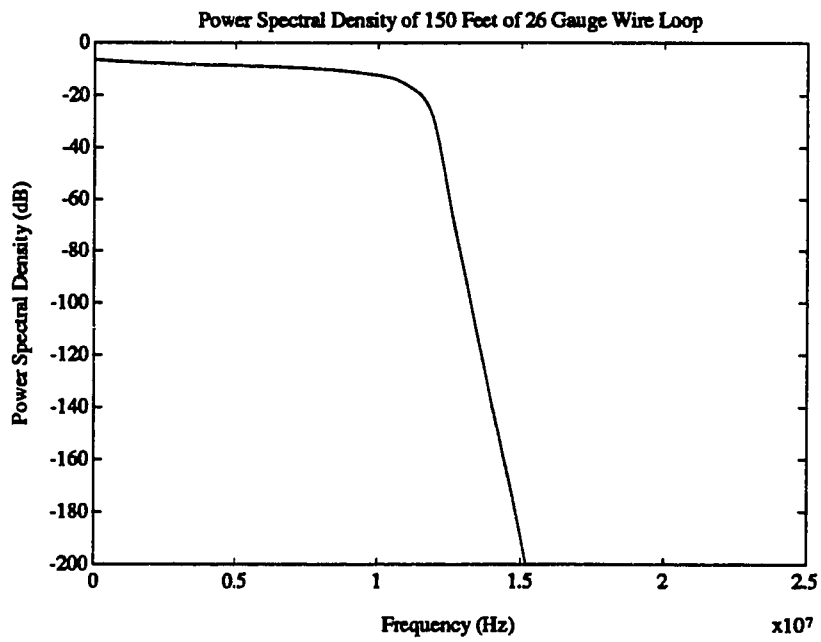

Figure 5.16: Power Spectral Density for 150 Feet of 26 Gauge Copper Twisted Pair

MHz (see Figure 5.16); thus, a maximum signaling rate of 24 MHz will be used in this study.

As in the case of all other DSL applications, NEXT and FEXT are two of the most serious line impairments encountered in VHDSL. The coupling function for NEXT is given by Equation (5.2) in Section 5.1.1. In [71], Lin estimated that

$K_{NEXT} \approx 10^{-13}$ for the 49-crosstalker case from data in a Bellcore Technical Reference [72]. In the case of VHDSL, however, the twisted pairs are most likely unbundled; therefore, instead of 49-crosstalkers, there will usually be a maximum of only one crosstalker, as existing customer lines often contain two twisted pairs into each customer premises. We will assume that $K_{NEXT} \approx \frac{1}{50} \times 10^{-13} = 2 \times 10^{-15}$ for our test loop. Note that if we assume there are normally only 6 dominant crosstalkers in a 50-pair bundle, then the VHDSL K_{NEXT} with one crosstalker should be closer to $\frac{1}{6} \times 10^{-13}$. We will investigate the effect of varying the level of K_{NEXT} in Section 5.3.3. The coupling function for FEXT is given by Equation (5.1) in Section 5.1.1. As in the case of K_{NEXT}, K_{FEXT} is determined through empirical measurement [68] [69] [70]. In this study, we will assume that $K_{FEXT} \times d \approx \frac{1}{50} \times 150 \times 8 \times 10^{-20} = 2.4 \times 10^{-19}$ for the test loop, because there will only be one far-end crosstalker instead of 49 and $d = 150$ ft. The performance of DMT for K_{FEXT} varying over several orders of magnitude are discussed in Section 5.1.4. Besides NEXT and FEXT, the transmitted data may also be corrupted by interaction crosstalk and apparatus crosstalk at VHDSL frequencies. However, the specific effects of interaction crosstalk, which is the coupling between two pairs involving other pairs, and apparatus crosstalk, which takes place at terminals, splices, and cross-connects, are not well understood [59]; thus, they will not be included here.

In addition to various forms of crosstalk, there are several other potential impairments that will degrade the performance of a VHDSL system. Residual echo noise does exist in VHDSL loops, and it is typically modeled as additive white Gaussian noise. Assuming an input signal power of around 20 mW, a typical VHDSL loop will attenuate the signal by approximately 10 dB, resulting in a total received signal power of 3 dBm. With an excellent echo canceler that can reduce the echo to a level of 40 dB below the received signal, we expect a total noise power of around -37 dBm across a two-sided bandwidth of 24 MHz, yielding a noise power spectral density of approximately -110 dBm/Hz. Therefore, we will fix the level of AWGN due to residual echo at a constant level of -110 dBm/Hz throughout our simulations. Other sources of AWGN noise, such as electronic noise and thermal noise are less damaging. We will assume a fixed level of electronic noise at -140 dBm/Hz

[73], which represents a fairly conservative estimate and can be ignored because it is much lower than the AWGN level of the residual echo noise. Lastly, the effects of inductive noise and impulse noise in VHDSL are similar to those in ADSL.

5.3.2 VHDSL System Description

The ideal DMT system that is used for simulation of VHDSL service consists of the following default parameters:

1. FFT size = $2N = 512$ or as specified.
2. Number of subchannels = $N = 256$ or as specified.
3. Sampling rate = 24 MHz or as specified.
4. Multicarrier symbol rate = $\frac{1}{T} = \frac{24MHz}{512} = 46{,}875$ Hz or as specified.
5. Multicarrier symbol period = $T = 21.3$ μs or as specified.
6. Target data rate = $R = \frac{b}{T}$ = as specified.
7. Bits per multicarrier symbol = b = as specified.
8. Insertion point transmit power level = 10 dBm or 23 dBm or as specified.
9. Target bit error rate = BER = 10^{-7}.
10. Wei's 4D 16-state code with an effective coding gain of 4.2 dB when trellis coding is used.
11. System performance margin = 6 dB or as specified.

Throughout our evaluation of VHDSL, however, we study the effect of different system parameters on the achievable data rate. We will vary the sampling rate from 640 kHz to 24 MHz, transmit power from 0 dBm to 30 dBm, and system blocklength from 128 to 1024. In addition, we examine the relative importance of near-end and far-end crosstalk in the VHDSL environment by varying these crosstalk effects over

three orders of magnitude. The exact noise scenario and system parameters will, therefore, vary significantly between individual simulations, and they will be given later as needed.

5.3.3 VHDSL Performance

Now we will analyze the performance of the DMT transceiver for VHDSL in a similar manner as was performed for ADSL and E1-HDSL service in previous sections.

Signaling Rate

It is important to choose the best signaling rate to fully utilize the available bandwidth of VHDSL loops. In Section 5.3.1 we showed that the worst case VHDSL loop has a usable bandwidth of 12 MHz (24 MHz signaling rate), so we investigate here the effect of varying signaling rate up to 24 MHz. Figure 5.17 shows the achievable throughputs for signaling rates of 640 kHz to 24 MHz. The DMT system configuration is blocklength 512 with 10 dBm transmit power. Crosstalk coupling constants are $K_{NEXT} = 2 \times 10^{-15}$ and $K_{FEXT} \times d = 2.4 \times 10^{-19}$. The achievable throughput ranges from about 4 Mbps at 640 kHz signaling rate to 90 Mbps at 24 MHz signaling rate. It is clear that, with all other system parameters constant, the choice of signaling rate is crucial to achieve the highest possible throughput. We conclude that, when feasible, 24 MHz signaling rate, or some convenient number close to 24 MHz, should be used to fully utilize all the available VHDSL loop bandwidth.

Transmit Power

We studied the effect of increasing the transmit power of the DMT transceiver, holding constant the system blocklength at 512 and VHDSL crosstalk coupling at $K_{NEXT} = 2 \times 10^{-15}$ and $K_{FEXT} \times d = 2.4 \times 10^{-19}$. Figure 5.18 shows the achievable throughputs as a function of transmit power for various signaling rates. We see that the data rate improves with increasing power at low power levels and that the increase is negligible at levels above 20 dBm. The data rate "saturates" above this level because of crosstalk noise that depends on transmit power. Assuming

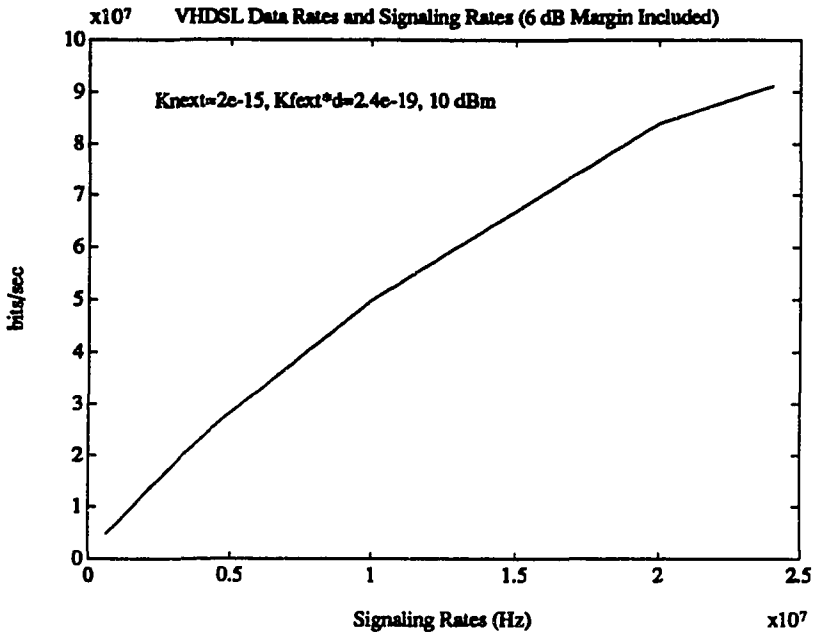

Figure 5.17: DMT Performance at Different Signaling Rates

that the crosstalker uses the same signaling strategy and power level as the DMT transceiver, as the transmit power increases the crosstalk noise level increases by the same proportion, and the overall SNR remains constant. The achievable data rate therefore saturates as the crosstalk noise level dominates over background AWGN. We see from Figure 5.18 that 10 to 15 dBm of transmit power is sufficient to achieve the best throughputs at most signaling rates.

Blocklength

We studied the effect of system blocklength on achievable throughput. We found that varying the blocklength from 128 to 1024 (not including cyclic prefix) had minimal effect on the data rate. Using 24 MHz signaling rate, 10 dBm transmit power, $K_{NEXT} = 2 \times 10^{-15}$ and $K_{FEXT} \times d = 2.4 \times 10^{-19}$, we found that the DMT can transmit approximately 90 Mbps for all blocklengths from 128 to 1024. There is negligible performance improvement in going from blocklength 512 to blocklength 1024 (see Figure 5.19). Using a longer blocklength incurs longer decoding delay, but it

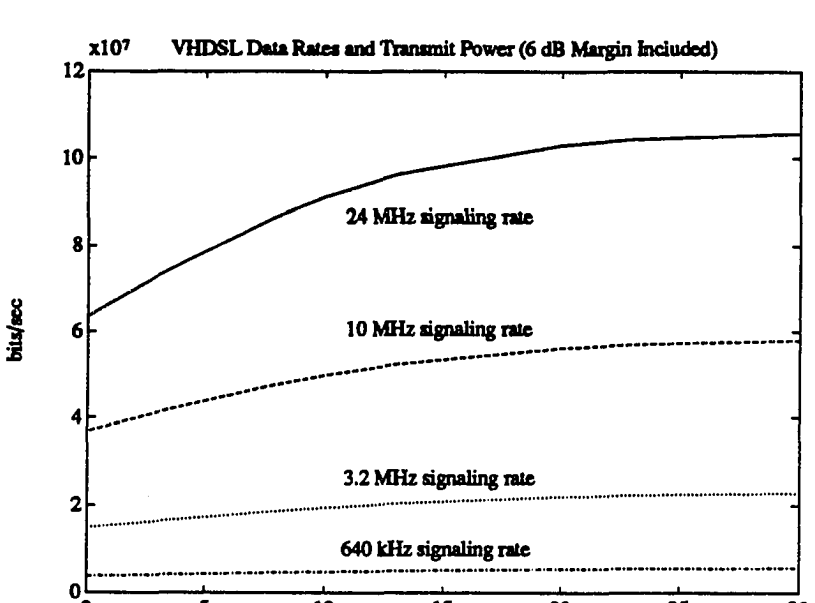

Figure 5.18: DMT Performance with Different Transmit Power Levels

results in easier implementation as computations are distributed over a longer block interval. Also, a longer block allows the DMT system to have additional immunity to short impulsive noise spikes. Considering all of these issues, we conclude that a blocklength of 512 offers the best balance between implementation ease, immunity to impulse noise, and decoding delay.

NEXT Noise

In Section 5.3.1, we suggested that crosstalk interference limits the system performance at high power levels. Now we will examine the relative importance of NEXT and FEXT for VHDSL applications. We varied the NEXT coupling coefficient over four orders of magnitude to investigate whether NEXT is the dominant noise source. Using 24 MHz signaling rate and blocklength of 512, we evaluated DMT performance as a function of K_{NEXT} for two different transmit powers. We maintained $K_{FEXT} \times d$ at 2.4×10^{-19}. The results are shown in Figure 5.20. Our results show that the achievable data rates depend significantly on the value of K_{NEXT}.

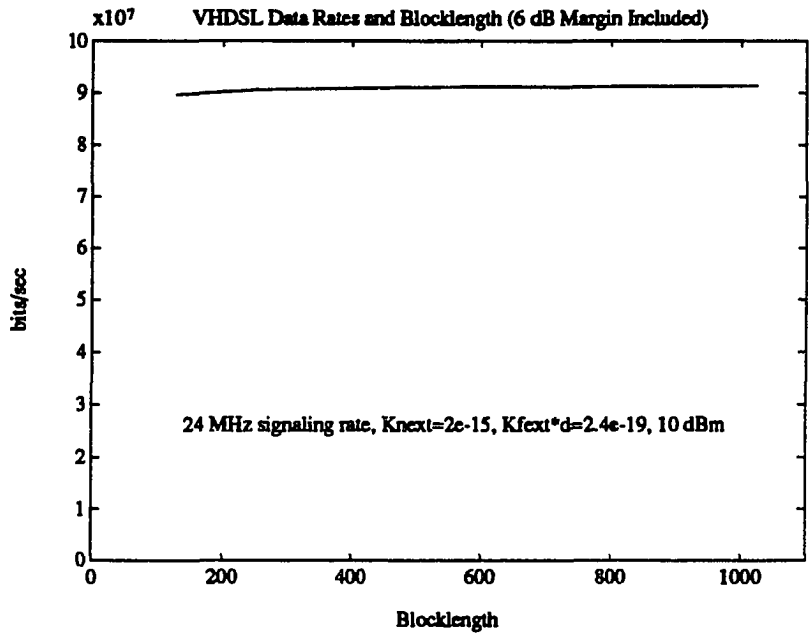

Figure 5.19: DMT Performance as a Function of System Blocklength

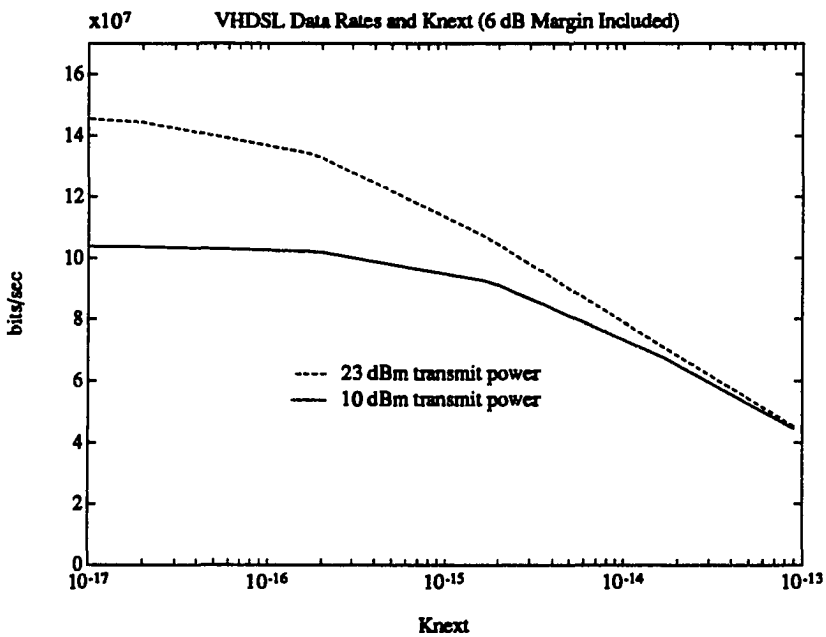

Figure 5.20: Effect of K_{NEXT} on DMT Performance

With 23 dBm of transmit power, as K_{NEXT} is increased over three orders of magnitude, the achievable VHDSL data rate dropped from 140 Mbps to 50 Mbps. This suggests that NEXT is a significant, if not dominant, noise impairment in VHDSL at 24 MHz signaling rate.

FEXT Noise

We varied the factor $K_{FEXT} \times d$ over four orders of magnitude, keeping K_{NEXT} constant at 2×10^{-15}. We used a DMT transceiver with 24 MHz signaling rate and blocklength 512. We studied two different transmit powers, and the results are shown in Figure 5.21. We see that the achievable data rate does not decrease

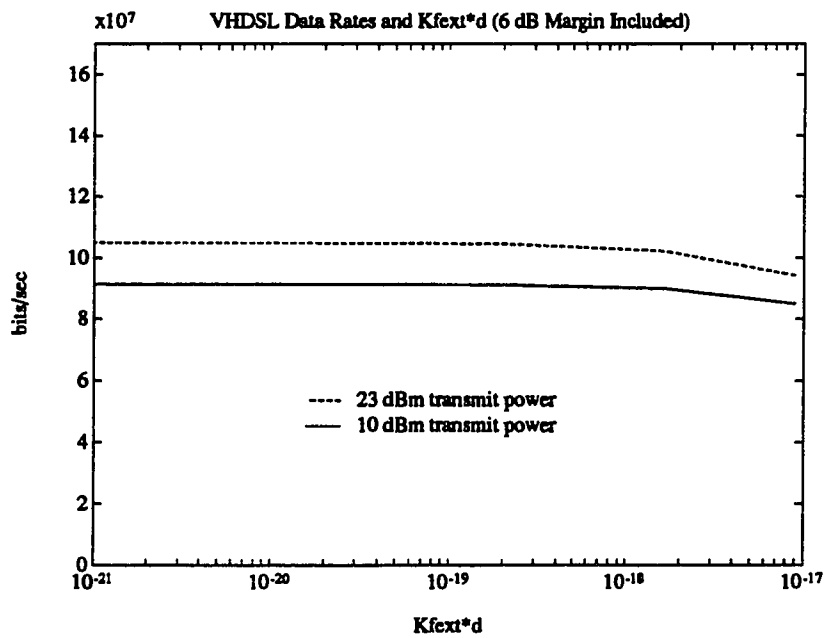

Figure 5.21: Effect of K_{FEXT} on DMT Performance

appreciably with increasing K_{FEXT}. The insensitivity of VHDSL performance as a function of $K_{FEXT} \times d$ indicates that FEXT is not the dominating noise impairment in VHDSL applications with high signaling rate.

No Crosstalk

A final evaluation assumed the absence of all crosstalk noise and considered only AWGN at -110 dBm/Hz. This scenario is present if we silence one of the two twisted pairs in the VHDSL loop, or if we use coordinated transmission on the two pairs with crosstalk cancellation/equalization across the two pairs in the loop. If there is no crosstalk present, then the achievable data rates for VHDSL does not saturate with increasing transmit power, as shown in Figure 5.22. Very high data rates are achievable in the complete absence of crosstalk noise (> 100 Mbps). However, physical limitations on transmit power, including power dissipation within the twisted pairs, will prevent implementing very high power transmitters.

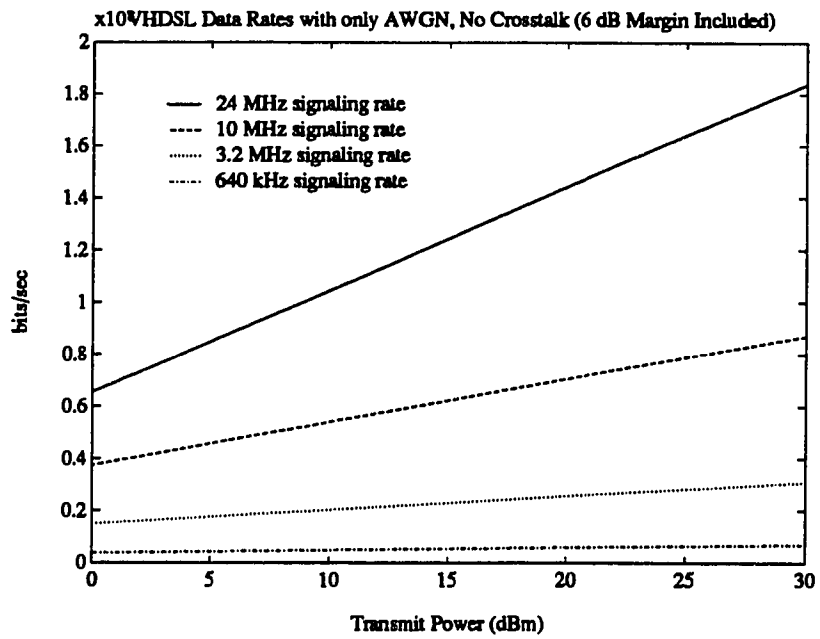

Figure 5.22: DMT Performance in the Absence of Crosstalk

5.3.4 Discussion of VHDSL Performance

Our performance evaluation showed that high data rates (> 50 Mbps) are possible for the DMT transceiver in the VHDSL application, provided that the system

parameters are properly chosen. The analysis identified the most crucial design parameter to be the signaling rate; the parameters of blocklength and transmit power level have less significant impact on achievable throughput. Our evaluation also showed that NEXT is the dominant noise impairment when high signaling rates are used. NEXT depends on transmit power level and causes the achievable throughput to saturate when transmit power exceeds 20 dBm. FEXT is of secondary importance in VHDSL since the cable lengths are very short in VHDSL.

When neither NEXT or FEXT is present, our analysis predicts that very high data rates may be achieved provided that a sufficiently powerful transmitter is used. However, other noise impairments may limit system performance at these high transmit powers. We note in Figure 5.22 that we can achieve over 100 Mbps data rates while signaling at 24 MHz with 10 dBm of transmit power in the absence of crosstalk. This zero-crosstalk scenario may be achieved in two ways: silencing one pair and transmit solely on the other twisted pair (single-duplex), or using coordinated transmission on two pairs (dual-duplex) along with crosstalk cancellation and/or equalization. We currently believe that the single-duplex option is the more desirable alternative. Silencing one of the two pairs in a bundle eliminates the interference posed by NEXT and FEXT and allows much higher throughputs that do not saturate with increasing transmit power. Achieving over 100 Mbps in single-duplex mode rather than dual-duplex is desirable for hardware complexity/cost issues as well, because only one transceiver is required. Crosstalk cancellation or equalization across two coordinated pairs is a less desirable option. It requires crosstalk equalization that is analogous to complex multi-dimensional equalization for adjacent channel interference. Finally, the VHDSL environment may not always have two pairs of twisted pair available from the pedestal to the customer for dedicated VHDSL service, making dual-duplex operation less flexible and less applicable.

Chapter 6

Error Control Techniques for Impulse Noise

A class of highly irregular, short-duration, and large-amplitude disturbances has long been observed in the telephone network. This type of disturbance is collectively known as impulse noise, and it is potentially one of the limiting impairments for many advanced DSL applications, including ADSL and E1-HDSL, because when an impulse hits, it often dwarfs the received signal in terms of instantaneous power. Unfortunately, the origin and the exact nature of impulse noise are not well understood at this time. Furthermore, impulse noise occurrences are highly unpredictable and vary significantly from loop to loop. As a result, there does not exist a universally satisfactory model for impulse noise, and because impulse noise only occurs at infrequent intervals, it is difficult to capture the precise effects of impulse noise in analysis as well as in computer simulation. Most practical communication systems are therefore designed with a built-in performance margin to take the detrimental effects of impulse noise into account. In this chapter, we propose a number of novel impulse noise mitigation strategies designed specifically for a multicarrier system, which is inherently more immune to wideband impairments such as impulse noise than a single-carrier system in the first place.

We will outline the common characteristics of impulse noise and present a number of representative impulse noise samples to be used in simulation throughout the

remainder of this chapter in Section 6.1. While we focus mainly on impulse noise mitigation strategies designed specifically for the DMT system in this dissertation, Section 6.2 briefly reviews a number of single-carrier mitigation strategies that have been proposed in the literature. Section 6.3 considers the corresponding multicarrier impulse noise mitigation strategies that take advantage of side information in both the time as well as the frequency domain, including simple forward error correction techniques, hard decision erasure declaration schemes, and soft decision adaptive margin algorithms. Simulation results will be presented in conjunction with each of the proposed multicarrier error control techniques when applied to the ADSL transmission environment. Some of the ideas and simulation results presented in this chapter are joint work done with fellow graduate student Nick Zogakis of Stanford University under the supervision of Professor. John Cioffi [19] [20], and his contribution is gratefully acknowledged here.

6.1 Nature of Impulse Noise

The phenomenon of impulse noise in copper twisted pairs has been recognized and studied for many years by communication engineers, and some of the early attempts to model and characterize impulse noise are published in [74], [75], and [76]. The origin of impulse noise, while not exactly known, has been attributed to a variety of sources, such as lightning surges, electrostatic discharges, and switching transients caused by analog relays [64]. For the various DSL applications studied in Chapter 5, where the data rates are high and the received signal power is typically low, the effects of impulse noise may indeed be the limiting impairment in satisfying the desired bit error rate requirement. As a result, a number of recent impulse noise measurement surveys have been conducted, over Digital Subscriber Lines, in an attempt to better understand the causes and effects of impulse noise. From the impulse noise measurement survey performed by NYNEX at customer locations in New York City in 1986 [77] and a separate measurement survey conducted in the Dutch loop plant [78], it turns out that the "typical" impulse noise has most of its energy concentrated below 200 kHz, which is more narrowband than what many

people had originally believed. The peak amplitude of a measured impulse noise sample is usually less than 30 mV in magnitude, and the typical time duration of impulse noise is no more than 250 μs. Furthermore, the average time between arrivals is found to be 67 ms [79], which is significantly longer than the average duration of an impulse noise hit. Thus, while it is highly damaging to the severely attenuated ADSL and/or E1-HDSL signals when an impulse noise hits, impulse noise fortunately only occurs at infrequent intervals.

For our simulations in this chapter, we will make heavy use of 10 representative impulses recorded at customer locations in the NYNEX measurement survey. These impulses are recorded at the output of a 500 kHz lowpass filter, across a 120 Ω load, and with a sampling rate of 2 MHz. The time domain plots of these 10 representative impulses are shown in Figures 6.1, 6.2, and 6.3. The corresponding power spectral

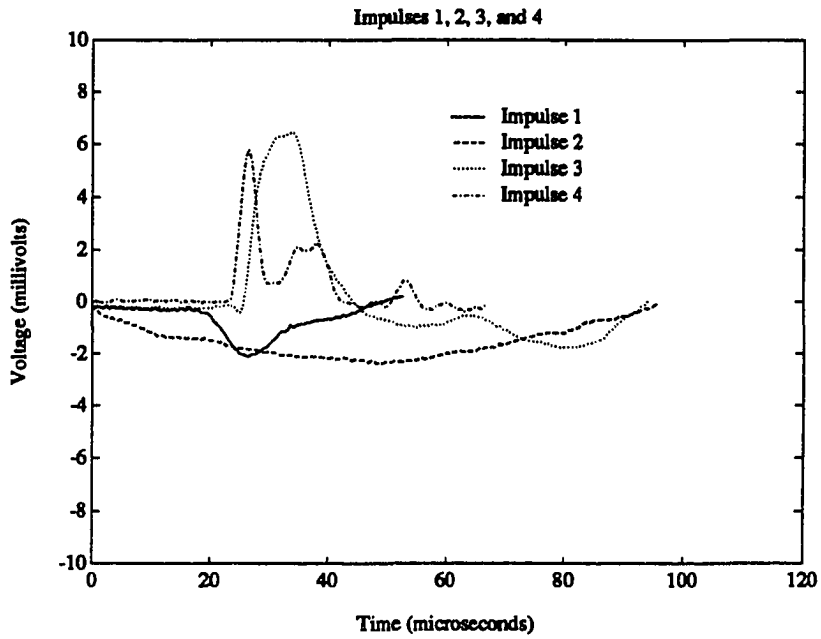

Figure 6.1: NYNEX Impulses 1, 2, 3, and 4

densities of these 10 representative impulses are given in Figures 6.4 to 6.13.

In addition to these NYNEX impulses, we will also make use of a pulse shape known as the "Cook pulse", which is derived from the analysis of approximately

Factorization of $\mathbf{R}_{xx}$.

We are now in position to derive the optimal settings for the finite-length MMSE-DFE for the general correlated input and noise scenario, following the development given in [47] and [48], which closely parallels the derivation for the infinite-length case given in Section 2.4.1. The error sequence, under the assumption of correct past decisions, of this finite-length MMSE-DFE can be expressed in its vector form as:

$$\mathbf{e} = \mathbf{a}^*\mathbf{y} - \mathbf{b}^*\mathbf{x} \; . \tag{3.16}$$

To minimize the mean squared error, or the determinant of the autocorrelation matrix, $\mathbf{R}_{ee}$, of the error sequence, we again make use of the orthogonality principle from linear estimation theory, which states that the minimal error sequence, $\mathbf{e}$, is completely uncorrelated with the observed output sequence, $\mathbf{y}$. Therefore, we get the following condition:

$$\begin{aligned} 0 &= \mathbf{R}_{ey} && (3.17)\\ &= \mathbf{a}^*\mathbf{R}_{yy} - \mathbf{b}^*\mathbf{R}_{xy} && (3.18)\\ &\Rightarrow \mathbf{a}^*\mathbf{R}_{yy} = \mathbf{b}^*\mathbf{R}_{xy} \; , && (3.19) \end{aligned}$$

where $\mathbf{R}_{xy}$ and $\mathbf{R}_{yy}$ are given by:

$$\mathbf{R}_{xy} = \mathbf{R}_{xx}\mathbf{H}^* \; , \tag{3.20}$$

and

$$\mathbf{R}_{yy} = \mathbf{H}\mathbf{R}_{xx}\mathbf{H}^* + \mathbf{R}_{nn} \; , \tag{3.21}$$

respectively. Therefore, we get:

$$\mathbf{a}^* = \mathbf{b}^*\mathbf{R}_{xy}\mathbf{R}_{yy}^{-1} \; , \tag{3.22}$$

and

$$\begin{aligned} \mathbf{R}_{ee} &= \mathbf{a}^*\mathbf{R}_{yy}\mathbf{a} - \mathbf{a}^*\mathbf{R}_{yx}\mathbf{b} - \mathbf{b}^*\mathbf{R}_{xy}\mathbf{a} + \mathbf{b}^*\mathbf{R}_{xx}\mathbf{b} && (3.23)\\ &= \mathbf{b}^*(\mathbf{R}_{xx} - \mathbf{R}_{xy}\mathbf{R}_{yy}^{-1}\mathbf{R}_{yx})\mathbf{b} && (3.24)\\ &= \mathbf{b}^*\mathbf{R}_{x|y}\mathbf{b} \; , && (3.25) \end{aligned}$$

where $\mathbf{R}_{x|y}$, the Schur complement of $\mathbf{R}_{yy}$, is a very useful term that will come up again in Section 4.1. Expand the Schur complement, we get the following convenient form:

$$\begin{aligned} \mathbf{R}_{x|y} &= \mathbf{R}_{xx} - \mathbf{R}_{xy}\mathbf{R}_{yy}^{-1}\mathbf{R}_{yx} && (3.26)\\ &= \mathbf{R}_{xx} - (\mathbf{R}_{xx}\mathbf{H}^*)(\mathbf{H}\mathbf{R}_{xx}\mathbf{H}^* + \mathbf{R}_{nn})^{-1}(\mathbf{H}\mathbf{R}_{xx}) && (3.27)\\ &= [\mathbf{R}_{xx}^{-1} + \mathbf{H}^*\mathbf{R}_{nn}^{-1}\mathbf{H}]^{-1}\,, && (3.28) \end{aligned}$$

where we have made use of the well known matrix inversion identity [49]:

$$(A + BCD)^{-1} = A^{-1} - A^{-1}B(DA^{-1}B + C^{-1})^{-1}DA^{-1}\,, \qquad (3.29)$$

by letting $A = \mathbf{R}_{xx}^{-1}$, $B = \mathbf{H}^*$, $C = \mathbf{R}_{nn}^{-1}$, $D = \mathbf{H}$, and assuming $\mathbf{R}_{xx}$ and $\mathbf{R}_{nn}$ are invertible. Now we take the Cholesky factorization of the inverse of the Schur complement, and we get the following unique factorization:

$$(\mathbf{R}_{x|y})^{-1} = \mathbf{R}_{xx}^{-1} + \mathbf{H}^*\mathbf{R}_{nn}^{-1}\mathbf{H} = \mathbf{G}\mathbf{S}\mathbf{G}^*\,, \qquad (3.30)$$

where

$$\mathbf{S} = \begin{bmatrix} s_0 & 0 & \dots & 0 \\ 0 & s_1 & \ddots & \vdots \\ \vdots & \ddots & \ddots & 0 \\ 0 & \dots & 0 & s_{2N+\nu-1} \end{bmatrix}. \qquad (3.31)$$

Now we can rewrite the MSE term as:

$$\mathbf{R}_{ee} = \mathbf{b}^*\mathbf{G}^{-*}\mathbf{S}^{-1}\mathbf{G}^{-1}\mathbf{b}\,, \qquad (3.32)$$

To simplify our analysis, we will assume that the number of feedback taps is optimal, or equal to the channel constraint length[3]; that is, $N_b = \nu$. Furthermore, we assume that the delay of the feedforward filter is set to the maximum; that is, $\Delta = N_a - 1$. Under these assumptions, the MSE given by Equation (3.32) is clearly minimized when $\mathbf{b}$ matches the N_a^{th} column of $\mathbf{G}$. In general, the MSE given by Equation

[3]Having the number of feedback taps greater than the channel constraint length will only lead to additional complexity without any improvement in system performance, while having the number of feedback taps less than the channel constraint length will degrade performance.

(3.32) is minimized when $\mathbf{b}$ matches the appropriate column of $\mathbf{G}$, depending on the value chosen for N_b and Δ. We can now determine the optimal settings for the feedforward filter, using Equations (3.22), (3.20), (3.21), and (3.30), and we get the following:

$$\begin{aligned}
\mathbf{a}^* &= \mathbf{b}^*(\mathbf{R}_{xx}\mathbf{H}^*)[\mathbf{H}\mathbf{R}_{xx}\mathbf{H}^* + \mathbf{R}_{nn}]^{-1} && (3.33)\\
&= \mathbf{b}^*[\mathbf{R}_{xx}^{-1} + \mathbf{H}^*\mathbf{R}_{nn}^{-1}\mathbf{H}]^{-1}\mathbf{H}^*\mathbf{R}_{nn}^{-1} && (3.34)\\
&= \mathbf{b}^*[\mathbf{G}^{-*}\mathbf{S}^{-1}\mathbf{G}^{-1}]\mathbf{H}^*\mathbf{R}_{nn}^{-1} && (3.35)\\
&= s_{N_a-1}^{-1}\mathbf{e}_{N_a}^*\mathbf{G}^{-1}\mathbf{H}^*\mathbf{R}_{nn}^{-1}\,, && (3.36)
\end{aligned}$$

where

$$\mathbf{e}_{N_a}^* = [\mathbf{0}_{1\times(N_a-1)}\ 1\ \mathbf{0}_{1\times(2N+\nu-N_a)}]\,. \qquad (3.37)$$

Therefore, the optimal settings for the finite-length MMSE-DFE feedforward FIR filter, $\mathbf{a}$, and feedback FIR filter $\mathbf{b}-1$, are succinctly given by:

$$\mathbf{a}^* = s_{N_a-1}^{-1}\mathbf{e}_{N_a}^*\mathbf{G}^{-1}\mathbf{H}^*\mathbf{R}_{nn}^{-1}\,, \qquad (3.38)$$

and

$$\mathbf{b} = \mathbf{G}\mathbf{e}_{N_a}\,, \qquad (3.39)$$

respectively.

3.3.2 Finite-length MMSE-DFE Analysis

Utilizing the optimal feedforward and feedback filter tap settings derived from the previous section, we can now calculate the optimal performance of a finite-length MMSE-DFE. Combining Equations (3.32) and (3.39), we get the following optimal MSE expression:

$$MSE_{MMSE\text{-}DFE,\ finite} = \mathbf{R}_{ee} = s_{N_a-1}^{-1}\,. \qquad (3.40)$$

The corresponding optimal output SNR of the finite-length MMSE-DFE is given by:

$$\begin{aligned}
SNR_{MMSE\text{-}DFE,\ finite} &= \frac{\mathcal{E}}{MSE_{MMSE\text{-}DFE,\ finite}} && (3.41)\\
&= \mathcal{E}s_{N_a-1}\,. && (3.42)
\end{aligned}$$

As in the infinite-length case, this output SNR is biased; therefore, we can further improve the probability of error performance of the system by removing this bias. The unbiased output SNR for a finite-length MMSE-DFE receiver is then given by:

$$SNR_{MMSE-DFE,U,\ finite} = SNR_{MMSE-DFE,\ finite} - 1 \tag{3.43}$$

$$= \mathcal{E}_{s_{N_e-1}} - 1\ . \tag{3.44}$$

Finally, we note here that for both the infinite-length case and the finite-length case, the feedforward and feedback filters of the MMSE-DFE are the backward and forward linear prediction filters. The optimal feedforward filter in both cases is a form of the mean-square whitened matched filter; but in the finite-length case, the feedback and feedforward filters are not necessarily minimum phase and maximum phase filters. Furthermore, in both cases, the receiver is biased with respect to the decision rule, and the bias term has exactly the same form. However, in the finite-length case, the error sequence is no longer exactly white. More detailed discussions of these and other properties of finite-length MMSE-DFE can be found in [50] and [48].

Chapter 4

Transmission Bandwidth Optimization

It has long been known that the theoretical optimal or capacity achieving energy distribution for a spectrally shaped channel corresponds to a "water-pouring" distribution [51]. In [10] and [30], similar water-pouring arguments have been applied to the MMSE-DFE and the DMT, respectively, in optimizing the transmitter. However, while the water-pouring energy allocation will indeed yield the optimal solution, it is typically difficult to compute. Furthermore, for the single-carrier system, a (typically complicated) transmit filter is required to implement the water-pouring energy allocation, which may not be practical in an actual system, especially when the resulting water-pouring allocation consists of disjoint sets of frequency bands. In the multicarrier case, water-pouring allocation tacitly assumes infinite granularity in constellation size, which is strictly speaking never realizable. Fortunately, a flat on/off energy distribution has been observed to achieve near-optimal performance (see [10]) for channel and noise characteristics encountered in many practical situations. As a result, in this dissertation, we will focus our attention primarily on flat (or nearly flat) energy allocation algorithms. An optimal water-pouring-based energy allocation algorithm for a DMT system operating over channels with far-end crosstalk (FEXT) and AWGN only is given in Appendix A.

We will present an information theoretic argument in Section 4.1 and demonstrate through simulation in Section 4.2.4 that the loss in performance of a flat energy solution with respect to the optimal water-pouring solution is indeed negligible, for practical applications such as the Asymmetric Digital Subscriber Lines (ADSL) service. Section 4.2 considers flat energy, DMT bit allocation strategies, as well as the consequences of a perfectly flat energy allocation on the parameters of optimization. We propose multicarrier algorithms that will maximize either the total data rate at a given target performance margin or the system performance margin at a fixed data rate. While concentrating on multicarrier techniques, we will illustrate how the introduced flat energy DMT algorithms can be applied directly to single-carrier systems based on the theoretical performance parallels derived in Section 2.5, and computer simulation results in Section 4.2.5 confirm this connection. Section 4.3 extends our flat energy algorithms to practically realizable algorithms that use only constellations with integer number of bits per 2-dimensional symbol. We show through simulation that the performance loss due to the integer bit constraint will be minimal in DSL applications, and we propose a simple adaptive scheme that will maintain near-optimal system performance during run-time, in terms of optimal transmission bandwidth, in the event that the channel characteristics are slowly time varying.

4.1 Capacity of a Multicarrier Channel

From basic information theory (see [52]), the differential entropy, $h(\mathbf{x})$ of the random vector $\mathbf{x}$ with a probability density function $p(\mathbf{x})$ is given by:

$$h(\mathbf{x}) = E[-log\ p(\mathbf{x})] \tag{4.1}$$

$$= -\int p(\mathbf{x})\ log\ p(\mathbf{x})\ d\mathbf{x}\ . \tag{4.2}$$

The mutual information between the input data block, $\mathbf{x}_{k:k-2N-\nu+1}$, and the output data block, $\mathbf{y}_{k:k-2N+1}$, defined in Section 3.1 on a per input symbol basis is then given by:

$$I(\mathbf{x};\mathbf{y}) = \frac{1}{2N+\nu}\left(h(\mathbf{x}) - h(\mathbf{x}|\mathbf{y})\right)\ . \tag{4.3}$$

Assuming that $\mathbf{x}$ is a complex Gaussian vector[1], then we have:

$$p(\mathbf{x}) = \frac{1}{(\pi)^{2N+\nu}\,|\mathbf{R}_{xx}|}\, e^{-\mathbf{x}^*\,\mathbf{R}_{xx}^{-1}\,\mathbf{x}}\,, \tag{4.4}$$

$$\begin{aligned} h(\mathbf{x}) &= (2N+\nu)\;log\;(\pi) + log\;|\mathbf{R}_{xx}| + E[\mathbf{x}^*\,\mathbf{R}_{xx}^{-1}\,\mathbf{x}] && (4.5)\\ &= (2N+\nu)\;log\;(\pi e) + log\;|\mathbf{R}_{xx}|\,, && (4.6)\end{aligned}$$

and, because the channel is LTI,

$$h(\mathbf{y}) = 2N\;log\;(\pi e) + log\;|\mathbf{R}_{yy}|\,. \tag{4.7}$$

The conditional differential entropy, $h(\mathbf{x}|\mathbf{y})$, of our system is defined as:

$$h(\mathbf{x}|\mathbf{y}) = h(\mathbf{x},\mathbf{y}) - h(\mathbf{y})\,, \tag{4.8}$$

where $h(\mathbf{x},\mathbf{y})$ is the joint differential entropy of $\mathbf{x}$ and $\mathbf{y}$, and for a multivariate Gaussian distribution, $h(\mathbf{x},\mathbf{y})$ is given by:

$$h(\mathbf{x},\mathbf{y}) = (4N+\nu)\;log\;(\pi e) + log \begin{vmatrix} \mathbf{R}_{xx} & \mathbf{R}_{xy} \\ \mathbf{R}_{yx} & \mathbf{R}_{yy} \end{vmatrix}. \tag{4.9}$$

Combining Equations (4.7), (4.8), and (4.9), we get the following:

$$\begin{aligned} h(\mathbf{x}|\mathbf{y}) &= (2N+\nu)\;log\;(\pi e) + log \left(\frac{\begin{vmatrix} \mathbf{R}_{xx} & \mathbf{R}_{xy} \\ \mathbf{R}_{yx} & \mathbf{R}_{yy} \end{vmatrix}}{|\mathbf{R}_{yy}|} \right). && (4.10)\\ &= (2N+\nu)\;log\;(\pi e) + log\;|\mathbf{R}_{x|y}|\,, && (4.11)\end{aligned}$$

where $\mathbf{R}_{x|y}$ is again the Schur complement of $\mathbf{R}_{yy}$ given by:

$$\mathbf{R}_{x|y} = \mathbf{R}_{xx} - \mathbf{R}_{xy}\mathbf{R}_{yy}^{-1}\mathbf{R}_{yx}\,. \tag{4.12}$$

Equivalently, $\mathbf{R}_{x|y}$ can be interpreted as the residual correlation matrix of the input $\mathbf{x}$ after subtracting the best linear predictor given the output $\mathbf{y}$ [53]. Expanding

[1]It is well known that $I(\mathbf{x};\mathbf{y})$ will be maximized when $\mathbf{x}$ has a Gaussian distribution.

Equation (4.12) we get the following alternative form:

$$\mathbf{R}_{x|y} = \mathbf{R}_{xx} - (\mathbf{R}_{xx}\mathbf{H}^*)(\mathbf{H}\mathbf{R}_{xx}\mathbf{H}^* + \mathbf{R}_{nn})^{-1}(\mathbf{H}\mathbf{R}_{xx}) \quad (4.13)$$

$$= \mathbf{R}_{xx}[I_{2N+\nu} - \mathbf{H}^*(\mathbf{H}\mathbf{R}_{xx}\mathbf{H}^* + \mathbf{R}_{nn})^{-1}\mathbf{H}\mathbf{R}_{xx}] \quad (4.14)$$

$$= \mathbf{R}_{xx}(I_{2N+\nu} + \mathbf{H}^*\mathbf{R}_{nn}^{-1}\mathbf{H}\mathbf{R}_{xx})^{-1}\,, \quad (4.15)$$

where we have again made use of the well known matrix inversion identity given by Equation (3.29) in Section 3.3.1, by letting $A = I_{2N+\nu}$, $B = \mathbf{H}^*$, $C = \mathbf{R}_{nn}^{-1}$, $D = \mathbf{H}\mathbf{R}_{xx}$, and assuming $\mathbf{R}_{nn}$ is invertible. Combining Equations (4.3), (4.6), (4.11), and (4.15), the mutual information of our system can be compactly expressed as:

$$I(\mathbf{x};\mathbf{y}) = \frac{1}{2N+\nu}\, log\, \frac{|\mathbf{R}_{xx}|}{|\mathbf{R}_{x|y}|} \quad (4.16)$$

$$= \frac{1}{2N+\nu}\, log\, |\mathbf{R}_{x|y}^{-1}\mathbf{R}_{xx}| \quad (4.17)$$

$$= \frac{1}{2N+\nu}\, log\, |I_{2N+\nu} + \mathbf{H}^*\mathbf{R}_{nn}^{-1}\mathbf{H}\mathbf{R}_{xx}|\,, \quad (4.18)$$

where for any singular $\mathbf{R}$, $\mathbf{R}^{-1}$ should be taken as the pseudo-inverse of $\mathbf{R}$. Because $\mathbf{H}^*\mathbf{H}$ has a rank of $2N$, it will admit the following eigen-decomposition:

$$\mathbf{H}^*\mathbf{H} = \mathbf{U}\begin{bmatrix} \gamma_1 & & & & & \\ & \ddots & & & & \\ & & \gamma_{2N} & & & \\ & & & 0 & & \\ & & & & \ddots & \\ & & & & & 0 \end{bmatrix}\mathbf{U}^*\,. \quad (4.19)$$

It has been shown in detail (see [50]) that the capacity achieving $\mathbf{R}_{xx} = \mathbf{R}_{opt}$ will have the following eigen-decomposition:

$$\mathbf{R}_{opt} = \mathbf{U}\begin{bmatrix} \delta_1 & & & & & \\ & \ddots & & & & \\ & & \delta_{2N} & & & \\ & & & 0 & & \\ & & & & \ddots & \\ & & & & & 0 \end{bmatrix}\mathbf{U}^*\,, \quad (4.20)$$

where the eigenvectors of $\mathbf{R}_{opt}$ are matched to the eigenvectors of the channel, or $\mathbf{H}^*\mathbf{H}$, and the eigenvalues of $\mathbf{R}_{opt}$ in the special case of a AWGN channel with a noise variance of σ^2 per dimension are simply given by:

$$\delta_i = max\ \{c - \frac{\sigma^2}{\gamma_i}\ ,\ 0\}\ , \tag{4.21}$$

where δ_i is always non-negative. The "c" in Equation (4.21) is just the water-pouring level, and it is given by:

$$c = \frac{1}{\tilde{N}}(\mathcal{E}_{total} + \sum_{i=1}^{\tilde{N}} \frac{\sigma^2}{\gamma_i})\ , \tag{4.22}$$

where $\mathcal{E}_{total} = \sum_{i=1}^{2N} \delta_i$ is the total transmit energy constraint, $\tilde{N} \leq 2N$ is the number of usable "dimensions", and we have also implicitly ordered the "SNR's" of the $2N$ possible "dimensions". If we make the simplifying assumption that all "dimensions" are usable, or $\tilde{N} = 2N$, then the optimum $I(\mathbf{x};\mathbf{y})$, or the "capacity", is given by:

$$C = I(\mathbf{x};\mathbf{y})_{opt} = \frac{1}{2N+\nu} \sum_{i=1}^{2N} log[\frac{\gamma_i}{2N}(\frac{\mathcal{E}_{total}}{\sigma^2} + \sum_{j=1}^{2N} \frac{1}{\gamma_j})]\ . \tag{4.23}$$

Now let us assume that a flat energy distribution is used for all $2N + \nu$ "dimensions", so the corresponding input autocorrelation matrix is given by:

$$\mathbf{R}_{flat} = \mathbf{U} \begin{bmatrix} \frac{\mathcal{E}_{total}}{2N+\nu} & & \\ & \ddots & \\ & & \frac{\mathcal{E}_{total}}{2N+\nu} \end{bmatrix} \mathbf{U}^*\ . \tag{4.24}$$

We note here that in the limit of $N \rightarrow \infty$, the eigenvectors of the channel matrix become the IDFT vectors, and we have the DMT modulation. The mutual information using the autocorrelation $\mathbf{R}_{flat}$ given in Equation (4.24) is then:

$$I(\mathbf{x};\mathbf{y})_{flat} = \frac{1}{2N+\nu} \sum_{i=1}^{2N} log[1 + \frac{\gamma_i \mathcal{E}_{total}}{(2N+\nu)\sigma^2}]\ . \tag{4.25}$$

Comparing Equations (4.23) and (4.25), we see that $I(\mathbf{x};\mathbf{y})_{opt} \approx I(\mathbf{x};\mathbf{y})_{flat}$ as long as $2N >> \nu$ and the eigenvalue spread of the original channel matrix is not too large; that is, $\gamma_i \approx \gamma_j\ \ \forall\ i,j$, which unfortunately may not necessarily be the case for practical channels. However, if not all $2N$ dimensions are used in the capacity

achieving energy allocation, or if the eigenvalue spread of the original channel matrix is large, then not all $2N$ dimensions should be used in the flat energy scheme either. In particular, no energy should be assigned to those dimensions that are not used in the capacity achieving energy distribution, and dimensions with very small eigenvalues; that is, those δ_i's such that $\delta_i << \frac{1}{\tilde{N}} \sum_{i=1}^{\tilde{N}} \delta_i$ where $\tilde{N}$ is the number of usable dimensions, should also be discarded. The new input autocorrelation matrix with a "bandwidth optimized" flat energy distribution is then given by:

$$\mathbf{R}_{flat,opt} = \mathbf{U} \begin{bmatrix} \frac{\mathcal{E}_{total}}{\hat{N}+\nu} & & & & & & \\ & \ddots & & & & & \\ & & \frac{\mathcal{E}_{total}}{\hat{N}+\nu} & & & & \\ & & & 0 & & & \\ & & & & \ddots & & \\ & & & & & 0 & \\ & & & & & & \frac{\mathcal{E}_{total}}{\hat{N}+\nu} \end{bmatrix} \mathbf{U}^* , \qquad (4.26)$$

where the $\hat{N}$ actually used dimensions, or the first $\hat{N}$ diagonal elements in $\mathbf{R}_{flat,opt}$, employ a flat energy, $\frac{\mathcal{E}_{total}}{\hat{N}+\nu}$, distribution, and the same flat energy is also placed, therefore wasted, on the last ν diagonal elements in $\mathbf{R}_{flat,opt}$, which corresponds to the cyclic prefix. The resulting mutual information of the system, using $\mathbf{R}_{flat,opt}$, is then:

$$I(\mathbf{x};\mathbf{y})_{flat,opt} = \frac{1}{2N+\nu} \sum_{i=1}^{\hat{N}} log[1 + \frac{\gamma_i \mathcal{E}_{total}}{(\hat{N}+\nu)\sigma^2}] , \qquad (4.27)$$

and the corresponding capacity of this channel is given by:

$$C = I(\mathbf{x};\mathbf{y})_{opt} = \frac{1}{2N+\nu} \sum_{i=1}^{\tilde{N}} log[\frac{\gamma_i}{\tilde{N}}(\frac{\mathcal{E}_{total}}{\sigma^2} + \sum_{j=1}^{\tilde{N}} \frac{1}{\gamma_j})] . \qquad (4.28)$$

We note here that typically $\tilde{N} \geq \hat{N}$, since some of the dimensions usable by the capacity achieving energy distribution will be wasteful to use in a flat energy scheme. However, now the eigenvalue spread for those $\hat{N}$ channel eigenvalues corresponding to the used dimensions in the bandwidth optimized flat energy scheme will be

relatively small. So if $\tilde{N} \approx \hat{N}$, as in the case of most practical applications, then $I(\mathbf{x};\mathbf{y})_{opt} \approx I(\mathbf{x};\mathbf{y})_{flat,opt}$. Based on this observation, we conjecture that a bandwidth optimized, flat energy distribution will perform virtually as well as a water-pouring energy distribution, and we will verify this conjecture for the application of ADSL in Section 4.2.4.

4.2 Flat Energy Algorithms

Our objective for this section is to find ways of determining the optimal transmission bandwidth(s), under the flat energy constraint, for a number of optimization parameters, including maximizing total data rate as well as maximizing the system performance margin, such that:

1. they should perform very near the theoretical optimum given by the water-pouring distribution,
2. they should be of comparatively low implementational complexity, and
3. they should be applicable to both multicarrier and single-carrier systems.

We will develop these algorithms primarily from a multicarrier perspective; however, we will show that multicarrier techniques can be applied to determine the optimal symbol rate, thus the optimal transmission bandwidth, of single-carrier systems based on the connection between the two approaches. Furthermore, for all of our proposed multicarrier algorithms in this dissertation, we will design for equal probability of error across all used subchannels; in other words, $P_e(i) = P_e(j) \ \forall \ used \ i,j's$ unless otherwise noted.

4.2.1 Parameters of Optimization

Four obvious parameters for transmission bandwidth optimization are:

1. the data rate,
2. the average input power,

3. the system performance margin, and

4. the probability of error.

Clearly, by fixing three of these four parameters for optimization, we can determine the transmission bandwidth that will optimize the remaining parameter. However, it is easy to see that maximizing the achievable system performance margin is equivalent to minimizing the overall probability of error, because in both cases, we optimize the SNR gap, $\Gamma(Pr(E), \gamma_{margin}, \gamma_{eff})$. In other words, assuming a fixed coding scheme and consistent signal constellations; that is, fixed γ_{eff}, the bandwidth that minimizes P_e for a fixed γ_{margin} also maximizes γ_{margin} for a fixed P_e, because in both instances, Γ is maximized. This observation is summarized by the following lemma.

Lemma 4.1 (Margin vs. Probability of Error Optimization) For specified target data rate and input power constraint, the optimal bandwidth for a single-carrier (or a multicarrier) system over a fixed AGN channel in terms of minimizing P_e for a fixed γ_{margin} will also maximize γ_{margin} for a fixed P_e.

Proof: We start by considering an uncoded QAM system employing a square b-bit constellation, where all points within the constellation are equally likely to be transmitted. The probability of symbol error, P_e, for such QAM system is simply given by:

$$P_e = N_e\, Q\left[\sqrt{\frac{3SNR_{decision}}{2^b-1}}\right] \tag{4.29}$$

$$\leq 4\, Q\left[\sqrt{\frac{3SNR_{decision}}{2^b-1}}\right], \tag{4.30}$$

where the Q-function is again defined by:

$$Q(x) = \int_x^\infty \frac{1}{\sqrt{2\pi}} e^{\frac{-u^2}{2}}\, du\,. \tag{4.31}$$

N_e is the number of nearest neighbors in the input constellation, and $SNR_{decision}$ is the decision point signal-to-noise ratio. In the case of a MMSE-DFE receiver, $SNR_{decision} = SNR_{MMSE\text{-}DFE,U}$, and for QAM systems, $N_e \leq 4$. Assuming that

the target BER $Pr(E) \approx P_e$ holds, then the SNR gap, $\Gamma(Pr(E), QAM_{unc})$, for this uncoded QAM system is given by:

$$\Gamma(Pr(E), QAM_{unc}) = \frac{[Q^{-1}(\frac{P_e}{N_e})]^2}{3}, \tag{4.32}$$

as shown in Section 2.2. Extending this result to a general system with a total effective coding gain of γ_{eff} and system performance margin of γ_{margin}, we have the following:

$$\Gamma(Pr(E), \gamma_{margin}, \gamma_{eff}) = \frac{\gamma_{margin}}{3\gamma_{eff}}[Q^{-1}(\frac{P_e}{N_e})]^2 . \tag{4.33}$$

Rearranging Equation (4.33) and solving for P_e, we get:

$$P_e = N_e\, Q\left[\sqrt{\frac{3\Gamma\gamma_{eff}}{\gamma_{margin}}}\right] . \tag{4.34}$$

It is clear that for fixed γ_{margin} and γ_{eff}, P_e is minimized when Γ is maximized. Conversely, rearranging Equation (4.33) and solving for γ_{margin}, we get:

$$\gamma_{margin} = \frac{3\Gamma\gamma_{eff}}{[Q^{-1}(\frac{P_e}{N_e})]^2} . \tag{4.35}$$

Therefore, for fixed P_e and γ_{eff}, γ_{margin} is also maximized when Γ is maximized. However, from Equations (2.69) and (2.70), we see that Γ is related to the target data rate, the channel SNR, and the transmission bandwidth only, for both the DMT and the MMSE-DFE. Thus, once the target data rate and the input power constraint are fixed, there will be an optimal transmission bandwidth, $W_{opt\ \Gamma}$, with certain energy distribution, such that Γ is maximized, independent of P_e and γ_{margin}. This particular bandwidth $W_{opt\ \Gamma}$ will then minimize P_e for a fixed γ_{margin} as well as maximize γ_{margin} for a fixed P_e.

Q.E.D.

Furthermore, once we restrict ourselves to use a flat energy distribution over the entire used portion of the transmission band, the number of free optimization parameters reduces to just two: the total data rate and the system performance margin. In other words, there will be a unique transmission bandwidth, W_{opt}, which will maximize the system performance margin with a fixed data rate and a baseline

BER for any input power level, and this same bandwidth, W_{opt}, will also minimize the total input power for any chosen margin. This observation is summarized by the following lemma.

Lemma 4.2 (Margin vs. Power Optimization for Flat Energy Distribution) For a specified target data rate and a nominal bit error rate, the optimal bandwidth for a DMT system over a fixed AGN channel in terms of maximum margin is independent of the total power constraint, under the following two assumptions:

1. Equal energy allocation among all used subchannels, and
2. ideal, infinite precision, 2D constellations[2].

Proof: Start with the design of a fictitious system over a fixed channel operating at the specified target data rate and the nominal bit error rate with a 0 dB margin. Determine the bandwidth that will satisfy those performance criteria with the minimum amount of total power. Call this bandwidth W_{opt} and the level of power (in mW/Hz) A_{min}. (See Figure 4.1) Thus, the minimum amount of total

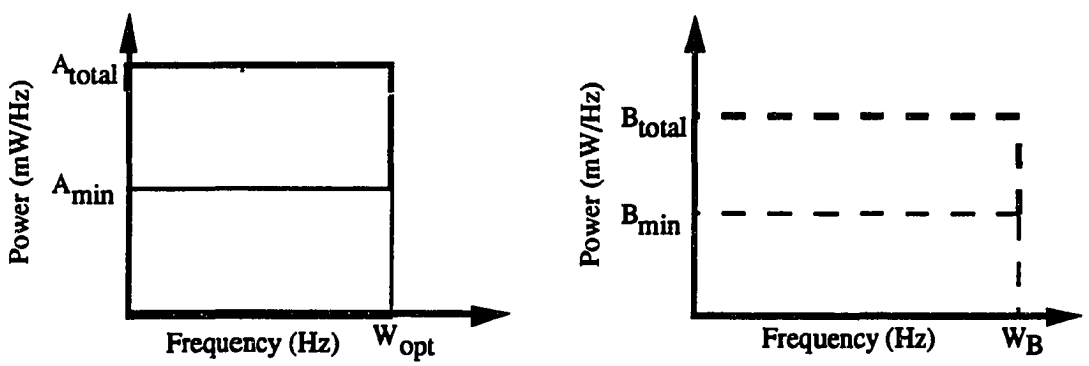

Figure 4.1: System Margin with Flat Energy Allocation

[2]This assumption is not strictly necessary as long as assumption (1) is observed and the system employs a consistent bit allocation algorithm. However, (1) implies (2) if we use gap approximation for bit allocation; that is, $b(i) = log_2(1 + \frac{SNR(i)}{\Gamma})$.

power, P_{min}, for this fictitious system is given by:

$$P_{min} = W_{opt} A_{min} \ . \tag{4.36}$$

Now let us assume that the same system will employ a different bandwidth, say W_B, such that $W_B = W_{opt} + \Delta W$ and the power level necessary (in mW/Hz) to meet those same specified criteria at this bandwidth is B_{min}. (See Figure 4.1) Because this is not the optimal bandwidth for this 0 dB system in terms of total power, we know that:

$$P_B = W_B B_{min} > P_{min} \qquad (if \quad \Delta W \neq 0) \ . \tag{4.37}$$

Now let us impose a total power constraint of P_{total} on our actual system, which has the same target data rate and nominal bit error rate as our fictitious system above. Our objective is now to determine the bandwidth that will maximize the system margin under our two original assumptions. If we use a bandwidth of W_{opt} from above, our system margin will be given by: (See Figure 4.1)

$$\Gamma_A = \frac{P_{total}}{P_{min}} \tag{4.38}$$

$$= \frac{W_{opt} A_{total}}{W_{opt} A_{min}} \tag{4.39}$$

$$= \frac{A_{total}}{A_{min}} \ . \tag{4.40}$$

Now let us consider the same power constraint P_{total} and performance criteria, but this time we use a system bandwidth of $W_B = W_{opt} + \Delta W$. For this particular choice of bandwidth, our system margin will be given by: (See Figure 4.1)

$$\Gamma_B = \frac{P_{total}}{P_B} \tag{4.41}$$

$$= \frac{W_B B_{total}}{W_B B_{min}} \tag{4.42}$$

$$= \frac{B_{total}}{B_{min}} \ . \tag{4.43}$$

However, from Equation (4.37), we know that:

$$P_B > P_{min} \ \Rightarrow \ \frac{1}{P_B} < \frac{1}{P_{min}} \tag{4.44}$$

$$\Rightarrow \frac{P_{total}}{P_B} < \frac{P_{total}}{P_{min}} \tag{4.45}$$

$$\Rightarrow \Gamma_B < \Gamma_A \,. \tag{4.46}$$

That indicates W_{opt} will yield better performance than W_B in terms of margin. However, recall that $W_B = W_{opt} + \Delta W$, and ΔW can be any non-zero value. Thus we can conclude that W_{opt} is also the optimal bandwidth at the given power constraint P_{total}, and for that matter, at any power constraint, once we specify the target data rate and the nominal bit error rate of the system.

Q.E.D.

4.2.2 DMT Throughput Optimization

We propose the following algorithm for the optimization of system bandwidth in terms of maximizing data rate with fixed input power level, desired system performance margin, and target BER for a DMT system, under the additional constraint of a perfectly flat on/off energy allocation:

1. Compute $SNR(i) \;\; \forall i$, according to Equation (2.27), assuming that all subchannels are used and $\mathcal{E}(i) = 1 \;\; \forall i$.

2. Sort resulting $SNR(i)$'s into descending order and label so that $SNR(j) \geq SNR(j+1) \;\; \forall j < N$.[3]

3. Let $k = 1$, $b_{max} = 0$, and $count = 0$, where k is the current iteration counter, b_{max} is the current maximum number of bits achievable per multicarrier symbol, and $count$ is the current number of carriers used to achieve b_{max}, respectively.

4. Compute $b_{target}(k)$ according to[4]:

$$b_{target}(k) = \sum_{j=1}^{k} log_2(1 + \frac{\frac{\mathcal{E}_{total}}{k} SNR(j)}{\Gamma}) \,. \tag{4.47}$$

[3] We will need to keep track of the mapping from the original subchannel labels to the sorted subchannel labels here.

[4] $\mathcal{E}_{total}$ is the total input energy, or power, constraint at the transmitter.

5. If $b_{target}(k) > b_{max}$, then set $b_{max} = b_{target}(k)$ and $count = k$.

6. If $k \neq N$, then set $k = k+1$ and go to step 4, else stop and *count* will indicate the optimal number of subchannels to use, thus the optimal transmission bandwidth, since our labeling scheme in step 2 is invertible.

The basic idea behind this algorithm is to determine the optimal number of DMT subchannels to use over sorted subchannel $SNR(i)$'s, which will in turn yield the optimal transmission bandwidth for maximizing data rate. In fact, $b_{target}(k)$ above is generally a convex function of k, which allows us to stop once $b_{target}(k) < b_{max}$. Furthermore, we can modify our bandwidth optimization algorithm above to perform a binary-like search in finding b_{max}, which will converge after at most $\mathcal{O}\left(log_2 \frac{N}{2}\right)$ iterations.

Given the flat energy constraint, this algorithm will indeed yield the optimal system bandwidth for maximizing overall DMT throughput. To see this, we note that once the optimal "number" of usable subchannels is determined, we must have chosen the best set of subchannels for such given number, because we have ordered all available subchannels in descending order of $SNR(j)$'s. Recall that the amount of transmit energy placed into each used subchannel is the same, and $log_2\ (x)$ is a strictly non-decreasing function with non-decreasing x. Furthermore, our algorithm will also yield the optimal number of subchannels to use, as we are effectively performing an exhaustive search over all N possibilities. Lastly, it is clear from the looping structure in steps (4) to (6), where the counter, k, is monotonically increasing, that this algorithm will converge in finite time, which is N iterations for the brute force implementation.

4.2.3 DMT Margin Optimization

A modified version of the above algorithm with the same basic idea can be used to obtain the optimal bandwidth under the same flat energy constraint but with the objective of maximizing performance margin given a fixed target data rate, desired BER, and total input power. We modify steps 3, 4, and 5 of the above algorithm to the following:

3. Let $k = 1$, $\gamma_{max} = 0$, and $count = 0$, where k is again the current iteration counter, γ_{max} is the current maximum achievable margin, and $count$ is the current number of carriers used to achieve γ_{max}, respectively.

4. Compute $\gamma(k)$ according to:

$$\gamma(k) = 10\ log_{10}\ (\frac{\overline{SNR(k)}}{2^{\frac{b_{target}}{k}} - 1}) + \gamma_{eff} - 9.8\ (dB)\ , \tag{4.48}$$

where b_{target} is the target number of bits to be supported by each multicarrier symbol and $\overline{SNR(k)}$ is calculated as:

$$\overline{SNR(k)} = \left[\prod_{j=1}^{k} \frac{\mathcal{E}_{total}}{k} SNR(j)\right]^{\frac{1}{k}}\ . \tag{4.49}$$

5. If $\gamma(k) > \gamma_{max}$, then set $\gamma_{max} = \gamma(k)$ and $count = k$.

As in the case of optimizing over total data rate, our modified algorithm given in this section will indeed yield the optimal system bandwidth that results in maximum DMT performance margin at a fixed data rate, as long as Equation (4.49) is accurate, which is indeed the case in the moderate to high SNR region. The proof follows along the same line as that given in Section 4.2.2. The resulting bandwidth may be different from the one for maximizing total data throughput, depending on our fixed target data rate. In general, the optimal bandwidth for maximizing total data throughput will be equal to or wider than the optimal bandwidth for maximizing margin, as long as the maximum achievable throughput is greater than or equal to our fixed target data rate when maximizing the margin. This is because when we find the maximum margin for a particular target data rate, the margin is applied unilaterally across all used subchannels. On the other hand, in the case of maximizing total data throughput at a fixed margin lower than the maximum achievable margin, some of the worst subchannels used may not have the necessary SNR to transport any data at the maximum achievable margin.

4.2.4 Performance Degradation from Ideal Energy Distribution

In this section, the performance of a system implemented with an ideal water-pouring energy allocation is compared to that of a band-optimized DMT system implemented with a perfectly flat energy allocation through computer simulation over the ADSL transmission environment. We have chosen two representative ADSL loops, namely the 9 kft, 26 gauge wire and the 18 kft, 24 gauge wire, and two lower bandedges, namely 50 kHz and 100 kHz, to guard against possible baseband service spillovers. We will use a DMT system with a FFT size of 512, a sampling rate of 2.048 MHz, and a transmit power level of 17 dBm, or 50 mW, at the insertion point, and the noise component will consist of the AWGN floor plus 49 ADSL FEXT disturbers only. A more detailed description of the ADSL transmission environment will be given in Chapter 5. The maximum data rates (in Mbps) of the two systems (both with 0 dB margin and no coding) are summarized in Table 4.1. Clearly, the performances are almost identical in all four test scenarios, which suggests that flat energy allocation is virtually as good as water-pouring for applications like ADSL, as long as we use the correct transmission bandwidth.

Exclude	Length	Gauge	Water-Pour	Flat Energy
100 kHz	9 kft	26 AWG	8.24 Mbps	8.23 Mbps
50 kHz	9 kft	26 AWG	8.88 Mbps	8.87 Mbps
100 kHz	18 kft	24 AWG	3.92 Mbps	3.90 Mbps
50 kHz	18 kft	24 AWG	4.54 Mbps	4.52 Mbps

Table 4.1: Water-Pouring DMT vs. Flat Energy DMT

4.2.5 Connection to MMSE-DFE

Bandwidth optimization in the single-carrier approach corresponds to finding the optimal symbol rate (or symbol rates for discontinuous transmission bands) for the MMSE-DFE. In [10], a water-pouring energy distribution method of symbol rate optimization is presented, and the given method will always yield the optimal symbol rate (or rates) in principle. However, the computational complexity of such

technique is formidable for many practical applications, including ADSL. Hence, a more efficient algorithm is needed for the implementation of real-time systems. Based on the performance parallels shown in Section 2.5, we propose that the optimal bandwidth found for the DMT system with algorithms described in previous sections to be used for real-time MMSE-DFE systems as well, because our proposed algorithms are more efficient than any existing single-carrier symbol rate optimization algorithms of which we presently know. In fact, these two algorithms can be applied directly to a MMSE-DFE system, under a set of rather mild conditions, namely:

1. $SNR(f) >> 1$ for most $f \in W_{DMT}$ and
2. there are not too many spectral nulls within W_{DMT}.

Fortunately, many practical applications, including many ADSL loops as we will show later through simulation, do satisfy these conditions. For single-carrier passband systems, such as a QAM system implemented with a MMSE-DFE receiver, we need to modify our algorithms so that they will first artificially zero out $SNR(i)$'s from DC to the lower bandedge of the desired QAM system. In the case when there are a number of spectral nulls within W_{DMT}, or equivalently within $W_{MMSE-DFE}$, the optimal single-carrier system cannot be implemented in a straightforward manner as noted previously in Section 2.5. In that case, the single-carrier system has to be implemented with either multiple DFE's (thus, strictly speaking it is no longer a "single"-carrier system) or a suboptimal, single DFE with a multiple bandpass transmit filter. In both cases, the complexity of the single-carrier system will most likely be much greater than the corresponding multicarrier DMT system. The optimal structures for such single-carrier systems, however, are likely to be application-dependent and beyond the scope of this dissertation. A more detailed treatment of symbol rate optimization for finite-length MMSE-DFE in particular can be found in [54].

Now we will compare a multicarrier DMT system employing our proposed flat energy bandwidth optimization algorithms versus several fixed bandwidth single-carrier passband QAM systems with a MMSE-DFE receiver. We will use the same

test scenarios as in Section 4.2.4, but instead of data rate, we will compare the systems in terms of achievable performance margin based on two target data rates (1.6 Mbps and 4.0 Mbps). The passband QAM systems with MMSE-DFE are assumed to be ideal with infinite length filters, and we consider three different fixed line codes (16-QAM, 32-QAM, and 64-QAM)[5] with their corresponding nominal center frequencies. We use 17 dBm of power at the insertion point for all systems. Tables 4.2 and 4.3 give the performance projections, in terms of margin in dB, for the four systems under the various scenarios. The loss in dB of a fixed symbol rate

Rate	Exclude	DMT	16-QAM	32-QAM	64-QAM
1.6 Mbps	50 kHz	27.2 dB	26.7 dB	26.1 dB	25.0 dB
1.6 Mbps	100 kHz	25.4 dB	24.8 dB	23.9 dB	22.6 dB
4.0 Mbps	50 kHz	15.6 dB	15.1 dB	15.4 dB	14.8 dB
4.0 Mbps	100 kHz	14.1 dB	13.8 dB	13.9 dB	13.2 dB

Table 4.2: Performance of the 9 kft, 26 AWG Loop

Rate	Exclude	DMT	16-QAM	32-QAM	64-QAM
1.6 Mbps	50 kHz	20.6 dB	19.6 dB	20.4 dB	20.0 dB
1.6 Mbps	100 kHz	17.1 dB	16.1 dB	17.0 dB	16.7 dB
4.0 Mbps	50 kHz	2.9 dB	-5.4 dB	-1.4 dB	1.2 dB
4.0 Mbps	100 kHz	-0.7 dB	-7.6 dB	-4.9 dB	-2.4 dB

Table 4.3: Performance of the 18 kft, 24 AWG Loop

QAM system relative to the bandwidth optimized DMT system and the amount of transmission bandwidth actually used by the different systems for various scenarios with a lower bandedge of 50 kHz are summarized in Tables 4.4 and 4.5, respectively. From these tables we see that the optimal single-carrier line code, thus the transmission bandwidth, is highly dependent on the channel and the target data rate, and if the symbol rate is chosen incorrectly (but certainly within practical limits), it is possible to lose more than 8 dB in performance with respect to the

[5]In this dissertation we will only consider integer-bit QAM constellations. Fractional-bit QAM constellations can be realized with multidimensional mapping techniques and will result in better performance for the single-carrier approach in some of the test scenarios in this section. However, the emphasis here is not merely a comparison of the two systems, but to demonstrate that bandwidth optimization on a line-by-line basis is necessary for applications like ADSL.

Rate	Length	Gauge	16-QAM	32-QAM	64-QAM
4.0 Mbps	18 kft	24 AWG	8.3 dB	4.3 dB	1.7 dB
1.6 Mbps	18 kft	24 AWG	1.0 dB	0.2 dB	0.6 dB
4.0 Mbps	9 kft	26 AWG	0.5 dB	0.2 dB	0.8 dB
1.6 Mbps	9 kft	26 AWG	0.5 dB	1.1 dB	2.2 dB

Table 4.4: Optimized Flat Energy DMT Advantage over Fixed Line Code QAM with MMSE-DFE

Rate	Length	Gauge	DMT	16-QAM	32-QAM	64-QAM
4.0 Mbps	18 kft	24 AWG	508 kHz	1000 kHz	800 kHz	667 kHz
1.6 Mbps	18 kft	24 AWG	324 kHz	400 kHz	320 kHz	267 kHz
4.0 Mbps	9 kft	26 AWG	848 kHz	1000 kHz	800 kHz	667 kHz
1.6 Mbps	9 kft	26 AWG	476 kHz	400 kHz	320 kHz	267 kHz

Table 4.5: Transmission Bandwidth Usage Comparison

optimal achievable multicarrier (or single-carrier) system. In particular, the loss in performance becomes large as the symbol rate of the single-carrier system extends beyond the optimum bandwidth. Based on these results, we conclude that bandwidth optimization is indeed critical for ADSL, and one cannot choose a single fixed transmission bandwidth for all possible ADSL loops and data rates and expect to perform well. Also apparent from these tables is the fact that the bandwidth determined by the multicarrier algorithm will accurately predict the best single-carrier line code. For example, the DMT system uses 476 kHz of bandwidth for the 9 kft, 26 gauge wire transmitting at 1.6 Mbps, and as expected, the single-carrier system that performs the best is the 16-QAM system, which uses 400 kHz of bandwidth, as opposed to 320 kHz and 267 kHz used by the 32-QAM and the 64-QAM systems, respectively.

4.3 Integer Bit Constellation Algorithms

While the algorithms presented in Sections 4.2.2 and 4.2.3 can be applied directly to both multicarrier and single-carrier systems and will indeed yield the optimal

transmission bandwidth under a flat energy constraint for total data rate and system performance margin, respectively, both of these algorithms implicitly assume infinite granularity in constellation size, which is not realizable in practice[6]. This assumption is the direct result of a perfectly flat energy distribution over all used carriers, or over the entire used portion of the transmission band, if we insist on equal probability of error for all used carriers. Because the Q-function (see Equation (2.13)) is not a linear function, the relationship between the input energy $\mathcal{E}$ and the resulting probability of error P_e will not be linear either, and in the moderate to high SNR region; that is, $SNR \geq 10\ dB$, where most practical systems operate, the optimal solution for a multicarrier system can be shown to have virtually equal probability of error for all used subchannels. In other words, for two subchannels with moderate to high SNR's, the aggregate probability of error between them will be minimized if we force the two carriers to have the same P_e. From Equations (2.9), (2.10), and (2.11), we see that in order to maintain equal probability of error, or equivalently to keep the argument of the Q-function constant, we can either vary the input energy to each of the used carriers or vary the number of bits supported by each of the carriers. In the case of a perfectly flat energy constraint, we then need to vary the number of bits per carrier and have infinite granularity in constellation size. However, as infinite granularity in constellation size is not practically realizable, we will now investigate multicarrier algorithms that have a finite granularity in constellation size constraint, and for these bit loading algorithms, we will need to adjust the input energy accordingly on a subchannel-by-subchannel basis to compensate for the effect of rounding.

4.3.1 The Hughes-Hartogs Algorithm

The first multicarrier, finite granularity loading algorithm that we will consider is due to Hughes-Hartogs (see [55]). In this particular algorithm, we only support integer number of bits per subchannel. The key idea is to acquire accurate estimates of subchannel SNR's during initialization and then set up an "incremental power"

[6]It is clearly not practical to design a 2D constellation with, for instance, 5.18 bits per 2D symbol.

matrix, ΔP, where:

$$\Delta P_{i,j} = P_{i,j} - P_{i-1,j} \; . \tag{4.50}$$

Here $P_{i,j}$ is defined to be the amount of transmit power that is necessary in the j^{th} subchannel to support i bits per 2D symbol at the desired bit error rate, and $P_{0,j} = 0 \; \forall \; j$. The algorithm then incrementally assigns, one bit at a time, the total number of bits to be transmitted in a multicarrier symbol, and each time it will choose the carrier that requires the least amount of incremental power to support an additional bit, until the desired data rate or power constraint is satisfied. Algorithmically, it can be summarized in the following steps:

1. Let $B_{total} = 0$ and $P_{total} = 0$, where B_{total} is the current number of bits supported by a multicarrier symbol and P_{total} is the corresponding amount of power necessary.

2. Search the first row of the matrix ΔP for the smallest $\Delta P_{i,j}$.

3. Assign one more bit to the resulting j^{th} subchannel; in other words, $b(j) = b(j) + 1$.

4. Let $B_{total} = B_{total} + 1$ and $P_{total} = P_{total} + \Delta P_{i,j}$.

5. Shift the j^{th} column of ΔP up one place; in other words, $\Delta P_{i,j} = \Delta P_{i+1,j} \; \forall \; i$.

6. If $B_{total} < B_{target}$ for margin optimization or if $P_{total} < P_{target}$ for data rate maximization, go to step 2, else stop.

For margin optimization, the resulting P_{total} may of course be greater than or less than the desired P_{target}, which corresponds to a negative or a positive margin, respective. In that case, we need to scale all subchannel powers accordingly so that $P_{target} = P_{total}$ is satisfied during run time. The resulting energy allocation of the Hughes-Hartogs algorithm will no longer be perfectly flat. However, the differences in energy between subchannels should be no more than approximately 3 dB, because asymptotically it takes about 3 dB of extra energy to support an additional bit. This particular bit loading algorithm with a nearly flat energy allocation is optimal under the integer bit constellation constraint because it will always place the

incremental energy into the currently most efficient subchannel, and it will always converge in finite time, because eventually either $B_{total} = B_{target}$ or $P_{total} \geq P_{target}$ will be satisfied as we continue to increase them in each iteration by 1 bit and approximately 3 dB, respectively. Unfortunately, the Hughes-Hartogs algorithm is typically very slow for applications like ADSL, where a typical B_{total} is in the range of 400 to 1600+ bits and N may be 256 or more QAM subchannels. This implies that the margin optimization algorithm will only converge after B_{total} (or 400 to 1600+) iterations, and for each iteration, approximately N (or 256 or more) compares are necessary. Therefore, the average running time for the Hughes-Hartogs algorithm is proportional to $\mathcal{O}(B_{total}\, N)$

4.3.2 An Alternative Loading Algorithm

As an alternative to the Hughes-Hartogs algorithm, we propose the following algorithm[7], which finds the near optimal transmission bandwidth for maximizing system performance margin through an iterative process. This algorithm consists of three main sections. It first finds the (approximately) optimal margin, then it guarantees convergence with a suboptimal loop, and lastly it adjusts the energy distribution accordingly on a subchannel-by-subchannel basis. Algorithmically, this procedure can be summarized in the following steps:

1. Compute $SNR(i)$ $\forall i$, assuming that all subchannels are used and $\mathcal{E}(i) = 1$ $\forall i$. (Unlike algorithms of Sections 4.2.2 and 4.2.3, we do not need to sort the subchannel SNR's here.)

2. Let $\gamma_{margin} = 0$ (dB) and $IterateCount = 0$, where γ_{margin} is the current margin of the system.

3. Let $B_{total} = 0$ and $UsedCarriers = N$, where B_{total} is the total number of bits that can be supported by a multicarrier symbol with the current margin.

[7]This algorithm is developed by the author while working in conjunction with John A.C. Bingham of Amati Communications Corp. of Palo Alto, CA. It is programmed by the author in Motorola DSP 56002 assembly language and is currently in use by Amati's prototype ADSL and E1-HDSL systems.

4. For $i = 1$ to N, calculate $b(i)$, $\hat{b}(i)$, $diff(i)$, and $UsedCarriers$ according to:

$$b(i) = log_2(1 + \frac{SNR(i)}{9.8 + \gamma_{margin}\ (dB)}) , \quad (4.51)$$

$$\hat{b}(i) = round[b(i)] , \quad (4.52)$$

$$diff(i) = b(i) - \hat{b}(i) , \quad (4.53)$$

$$If\ \hat{b}(i) = 0,\ UsedCarriers = UsedCarriers - 1 , \quad (4.54)$$

where "*round*" is the integer rounding operation.

5. Let $B_{total} = \sum_{i=1}^{N} \hat{b}(i)$. Stop and declare bad channel if $B_{total} = 0$.

6. Compute new γ_{margin} according to:

$$\gamma_{margin} = \gamma_{margin} + 10\ log_{10}(2^{\frac{B_{total} - B_{target}}{UsedCarriers}}) , \quad (4.55)$$

where B_{target} is the target number of bits to be supported by a multicarrier symbol.

7. Let $IterateCount = IterateCount + 1$.

8. If $B_{total} \neq B_{target}$ and $IterateCount < MaxCount$, go to step 3, else go to step 9. $MaxCount$ is set to the maximum number of iterations to be executed in this portion of the algorithm.

9. If $B_{total} > B_{target}$, then subtract one bit at a time from the current bit table, $\hat{b}(i)$, on the carrier that presently has the smallest value of $diff(i)$, adjust $diff(i)$ accordingly, and repeat until $B_{total} = B_{target}$.

10. If $B_{total} < B_{target}$, then add one bit at a time to the current bit table, $\hat{b}(i)$, on the carrier that presently has the largest value of $diff(i)$, adjust $diff(i)$ accordingly, and repeat until $B_{total} = B_{target}$.

11. Adjust input energy distribution accordingly so that $P_e(i) = P_{e,target}\ \forall i$ given the bit allocation $\hat{b}(i)$.

12. Scale final energy distribution so that $\mathcal{E}_{total} = \mathcal{E}_{target}$ is satisfied.

In steps 1 to 8, we try to iteratively find the appropriate margin. If this section does not converge after a predetermined number of iterations; that is, after $MaxCount$ iterations, we will force convergence with steps 9 to 10, which will always work as long as we are within some reasonable range; that is, if $|B_{total} - B_{target}| \leq UsedCarriers$. Lastly, steps 11 and 12 fine tune the energy distribution on a subchannel-by-subchannel basis to assure equal probabilities of error across all used subchannels.

While it may be slightly suboptimal relative to the Hughes-Hartogs algorithm, the above algorithm will typically converge much faster than Hughes-Hartogs for applications like ADSL. The worst case running time for this alternative loading algorithm is proportional to $\mathcal{O}\ (MaxCount \times N + N + N)$. Based on actual system implementation with Digital Signal Processing (DSP) chips, it has been found that the number of iterations, $IterateCount$, necessary to bring this algorithm to convergence over real ADSL loops is no more than ten [56]; in other words, $MaxCount = 10$ will be sufficient. Generally speaking, this algorithm will converge if the true optimal margin of the system is within the following upper and lower bounds:

$$\gamma_{margin} - [(MaxCount - 1)(b_{target} - b_{min})(10\ log_{10}\ 2)] \leq \gamma_{margin} \tag{4.56}$$

$$\leq \gamma_{margin} + [(MaxCount - 1)(b_{max} - \frac{b_{target}}{N})(10\ log_{10}\ 2)]\ , \tag{4.57}$$

where b_{max} and b_{min} are the maximum and minimum non-zero numbers of bits per 2D symbol that an used carrier may support. Typically, $b_{min} = 2$ (or 1) for QAM (or PAM) constellations, and b_{max} is a function of current technology of the ADC. Some realistic numbers for an ADSL DMT system are: $\gamma_{margin,initial} = 0(dB)$, $MaxCount = 10$, $b_{target} = 432$, $N = 256$, $b_{min} = 2$, and $b_{max} = 10$. For this system, our proposed algorithm converges if the true optimal margin of the system is between -11650 dB and +225 dB. The lower bound of this system is somewhat deceiving, because when $SNR(i) < SNR_{min}\ \forall i$, the channel will be declared bad, and no data transmission will be attempted. Here SNR_{min} is the minimum SNR that will allow us to assign b_{min} bits to any subchannel at the required probability of error $Pr(E)$. For $b_{min} = 2$, $\gamma_{margin,initial} = 0\ (dB)$, and $Pr(E) = 10^{-7}$, a $SNR_{min} \approx 12.4\ dB$ is necessary for at least one subchannel; otherwise, the entire channel will

be declared bad.

Furthermore, this algorithm offers the added advantage of no additional penalty in terms of execution time when we reduce the granularity of constellation size from integer number of bits to fractional number of bits, say half integer increments, where as the running time for Hughes-Hartogs will be doubled with half integer constellation sizes. To illustrate the operation of this algorithm, in Figure 4.2 we plot the received SNR curve for ADSL canonical test loop 9 [57] with 100 mW of input power in the presence of 49 ADSL far-end crosstalkers and AWGN. We have assumed a sampling rate of 2.048 MHz, a lower bandedge of 40 kHz, and a FFT size of 512. The frequency domain "ripples" are due to unterminated bridged taps[8]. This type of frequency domain dips can also be present in wireless data transmission with frequency-selective fading. In Figures 4.3 and 4.4, we show the resulting bit and input power distributions, respectively. The data rate for this particular simulation is 1.728 Mbps, which corresponds to a (216,200) Reed-Solomon coded transmission at a raw data rate of 1.6 Mbps. Here we have also imposed a minimum of 2 bits per used carrier constraint, even though in practice, it is possible to implement 1 bit carriers. We note here that we can always combine two 1 bit carriers into one 2 bit carrier by assigning 2 bits to the original 1 bit carrier with the higher SNR and 0 bit to the original 1 bit carrier with the lower SNR. Then if we place twice the power in the carrier that is now carrying 2 bits and no power in the now 0 bit carrier, we will always do no worse than the original two 1 bit carriers with equal amount of energy in each carrier. The saw-tooth shaped input power distribution is resulting from the fact that the variation in SNR is relatively small between adjacent subchannels (a necessary condition for multicarrier to work well) and that the final power distribution will vary inversely to compensate for the SNR variation in order to maintain a constant bit error rate among all used subchannels. When the input power to a particular subchannel has increased (or decreased) to the level where it is no longer effective to transmit that particular number of bits, the number of bits

[8]ADSL canonical test loop 9 consists of a segment of (3000 ft/26 AWG) wire, followed by a (1500 ft/26 AWG) bridged tap, followed by a segment of (6000 ft/26 AWG) wire, followed by another (1500 ft/26 AWG) bridged tap, followed by a segment of (1500 ft/26 AWG) wire, and followed by a last (1500 ft/26 AWG) bridged tap.

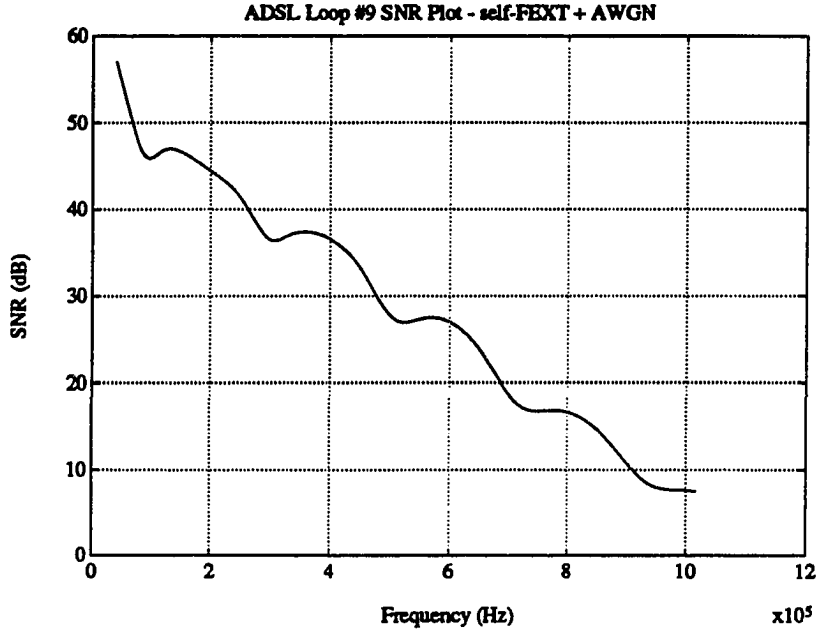

Figure 4.2: ADSL Loop 9 Received SNR Curve with 49 ADSL FEXT Disturbers + AWGN

is decreased (or increased) by one and the amount of input power will be abruptly decreased (or increased) by approximately 3 dB, resulting in a saw-tooth shaped final input power distribution. We will show later, through simulation, that the net loss of using this algorithm over the perfectly flat energy algorithm described in Section 4.2.3 is quite small for the ADSL examples we tried.

4.3.3 Performance Degradation from Infinite Precision Case

Now we turn our attention to the performance of multicarrier algorithms with the additional constraint of integer number of bits per 2D constellation. We compare the performance of a DMT system using the algorithm presented in Section 4.3.2 with that of an optimized, flat energy DMT system. In fact, we will further restrict our integer bit constellation algorithm to have at least 2 bits and at most 10 bits per used carrier, which reflects what is practical to implement with existing technology. Again, we will use the same set of system parameters with a 50 kHz lower bandedge

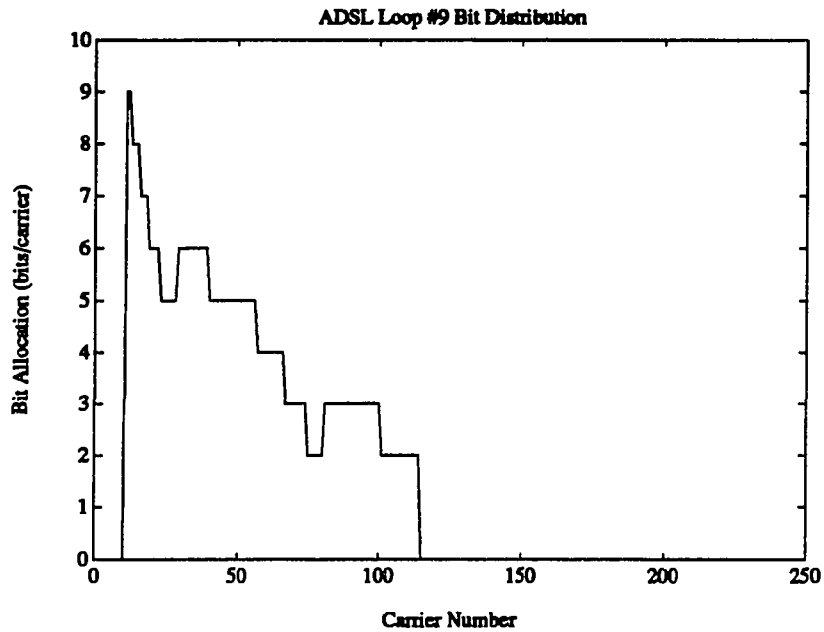

Figure 4.3: ADSL Loop 9 Bit Distribution with 49 ADSL FEXT Disturbers + AWGN

and the same two test loops as in the two previous sections. Table 4.6 summarizes our results. Basically, the performances of the two systems are virtually identical,

Rate	Length	Gauge	∞Granularity	Integer Bit	Difference
4.0 Mbps	9 kft	26 AWG	15.8 dB	15.7 dB	0.1 dB
1.6 Mbps	9 kft	26 AWG	27.4 dB	27.3 dB	0.1 dB
4.0 Mbps	18 kft	24 AWG	2.9 dB	1.7 dB	1.2 dB
1.6 Mbps	18 kft	24 AWG	20.8 dB	20.7 dB	0.1 dB

Table 4.6: Infinite Granularity DMT vs. Integer Bit Granularity DMT

except for the worst case scenario, where we are trying to transmit 4.0 Mbps over the 18 kft, 24 gauge loop, and in that case, we lose 1.2 dB. This degradation in performance turns out to be caused mainly by the 2 bit minimum/10 bit maximum constraint that we imposed on our system. Based on these results, we conclude that the integer bit constellation size constraint will not seriously degrade the DMT system performance, as long as the energy distribution is modified appropriately to

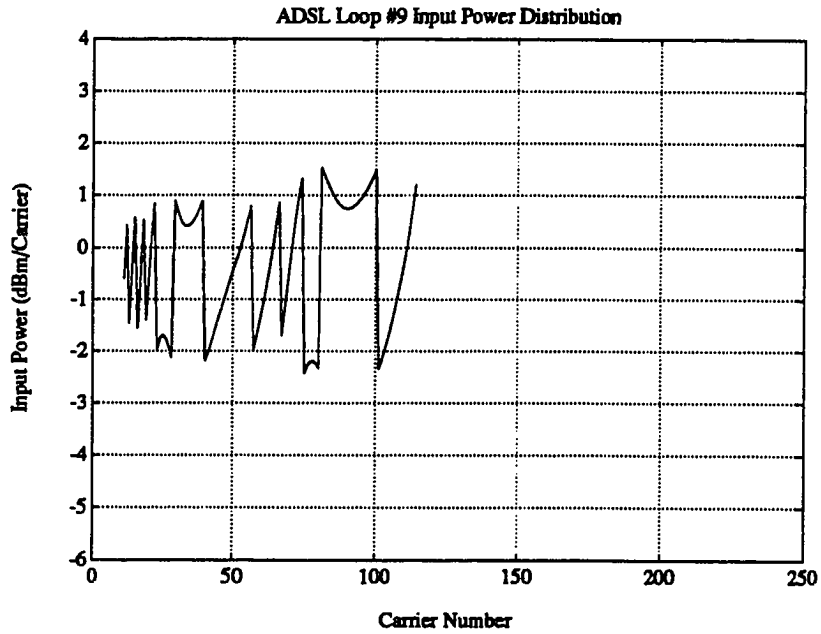

Figure 4.4: ADSL Loop 9 Input Power Distribution with 49 ADSL FEXT Disturbers + AWGN

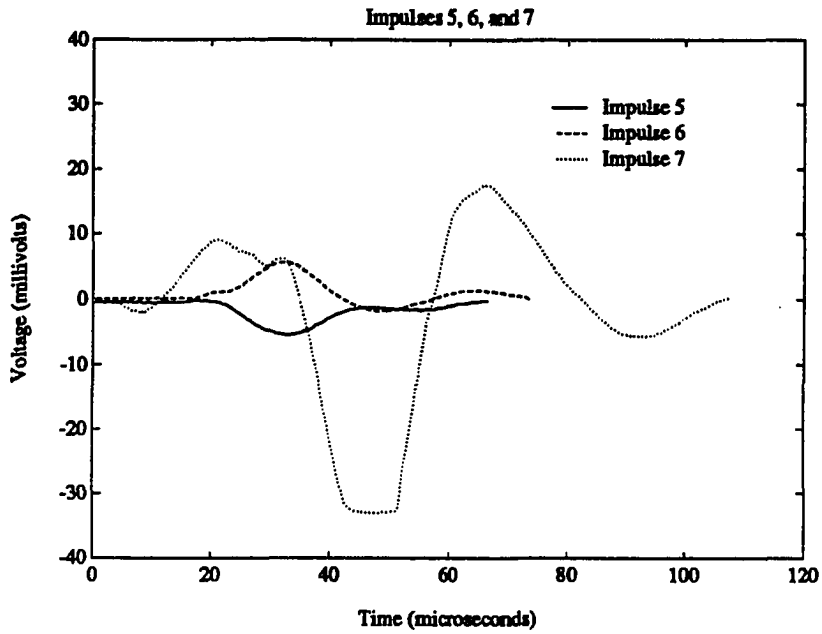

Figure 6.2: NYNEX Impulses 5, 6, and 7

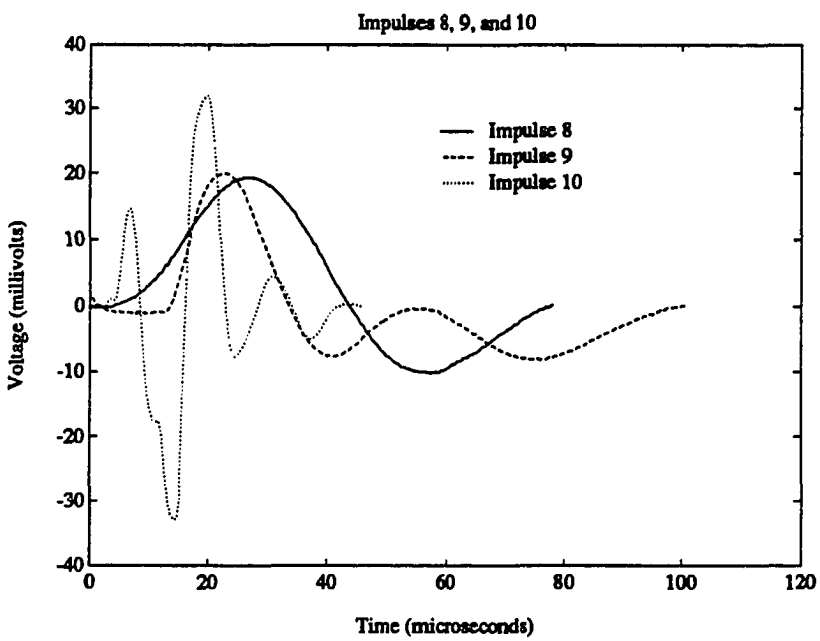

Figure 6.3: NYNEX Impulses 8, 9, and 10

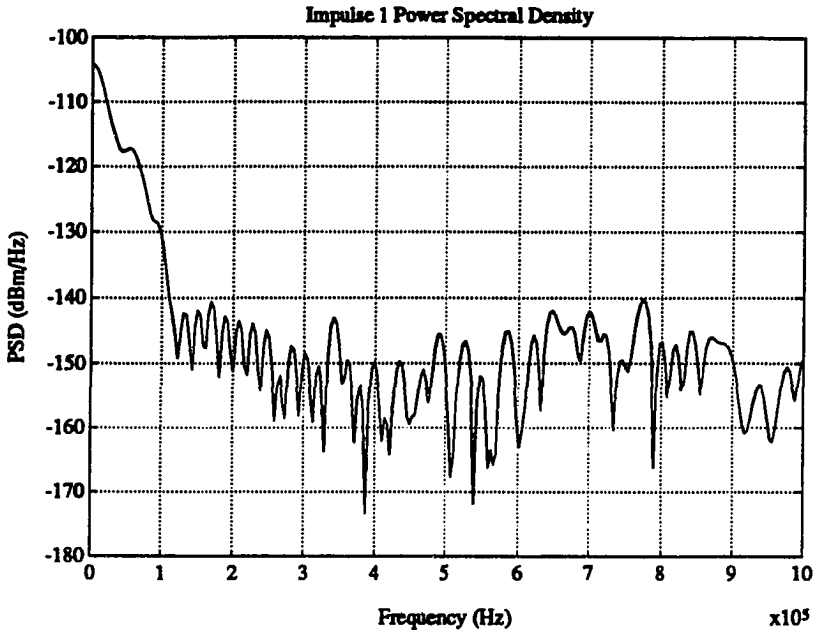

Figure 6.4: NYNEX Impulse 1 Power Spectral Density

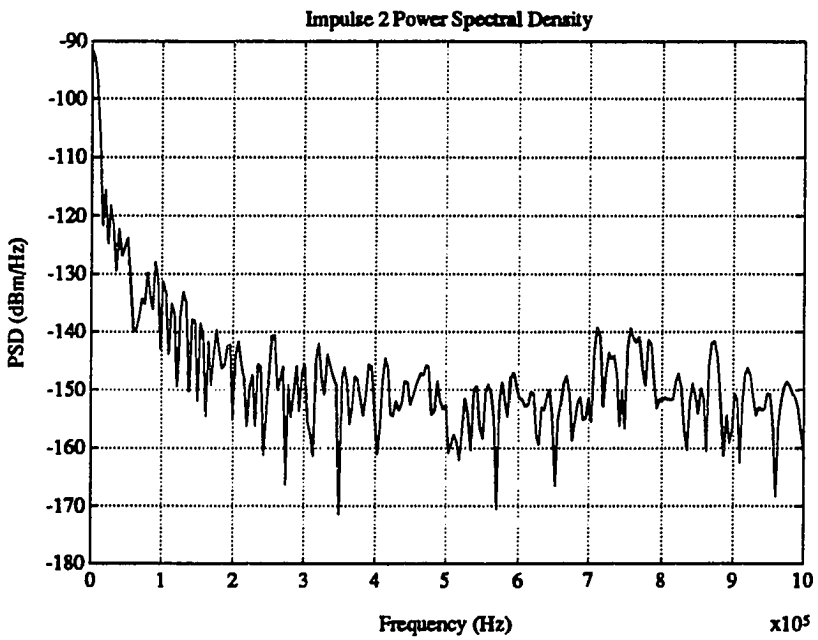

Figure 6.5: NYNEX Impulse 2 Power Spectral Density

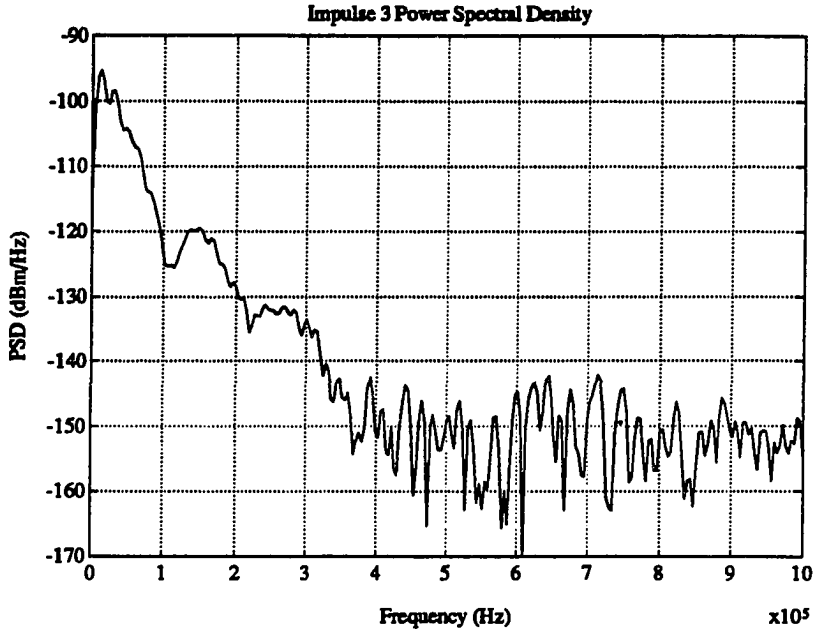

Figure 6.6: NYNEX Impulse 3 Power Spectral Density

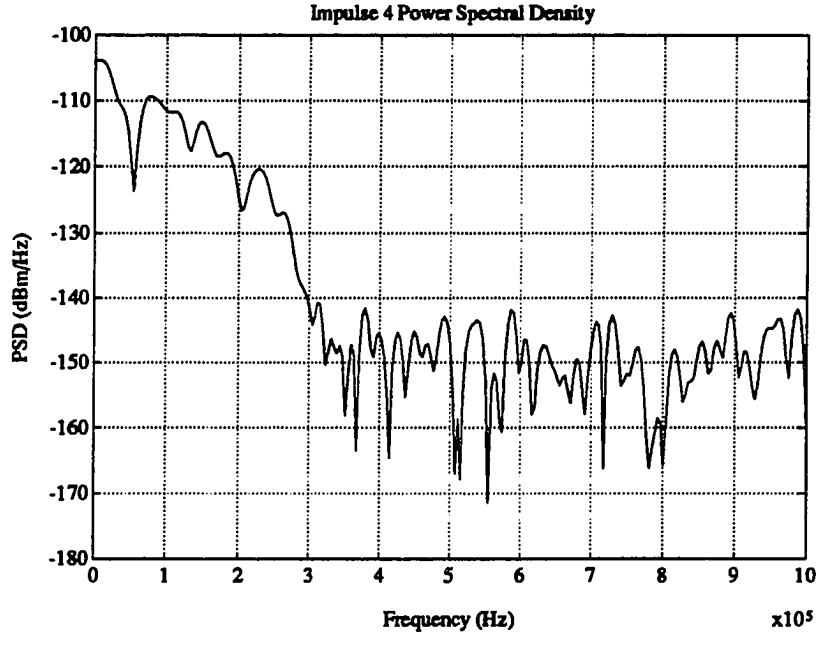

Figure 6.7: NYNEX Impulse 4 Power Spectral Density

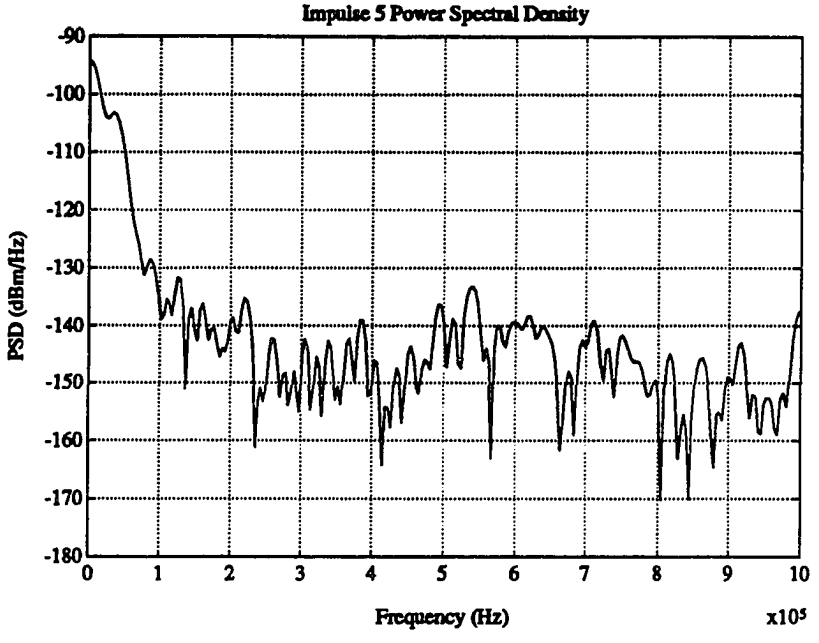

Figure 6.8: NYNEX Impulse 5 Power Spectral Density

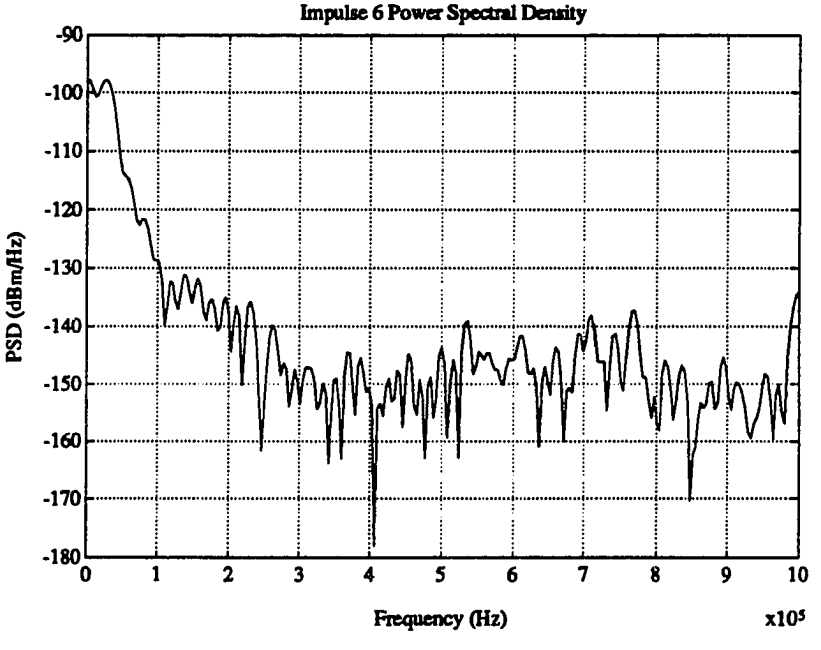

Figure 6.9: NYNEX Impulse 6 Power Spectral Density

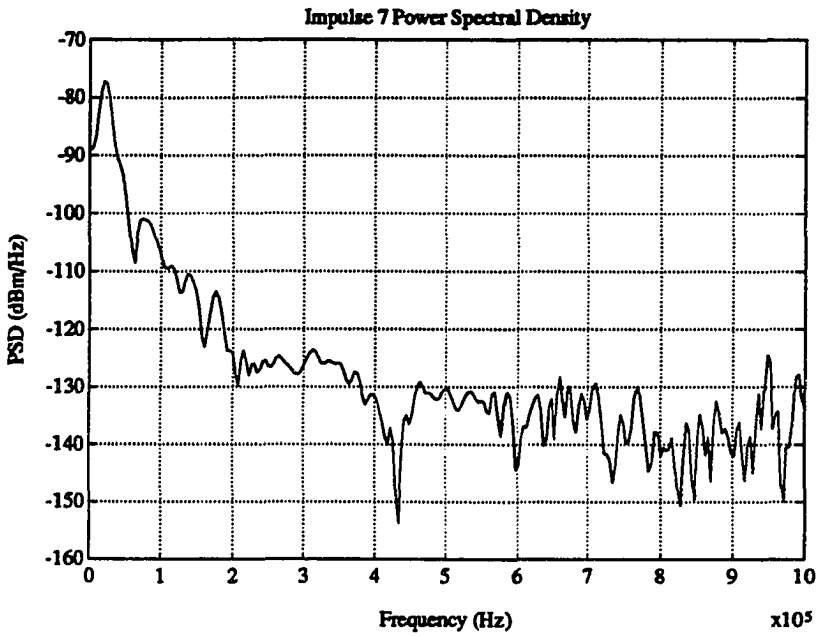

Figure 6.10: NYNEX Impulse 7 Power Spectral Density

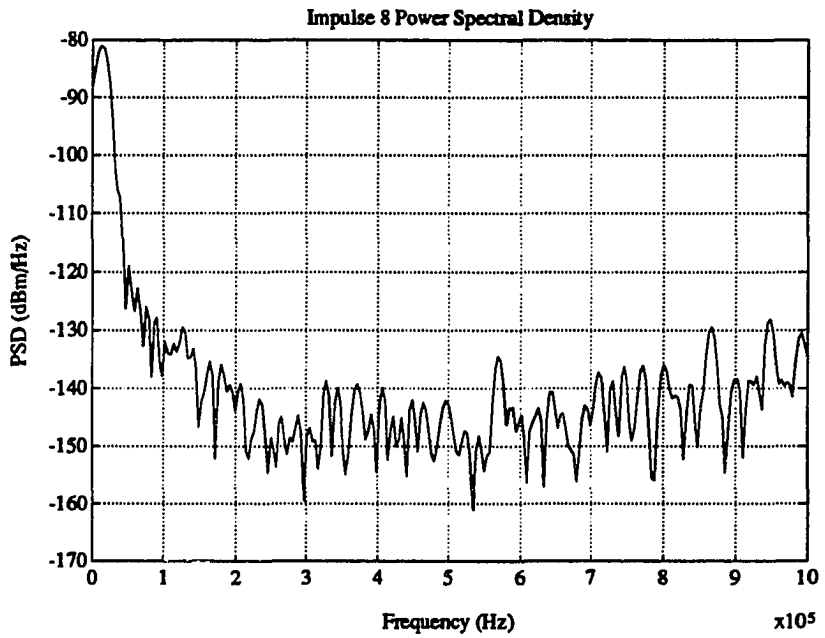

Figure 6.11: NYNEX Impulse 8 Power Spectral Density

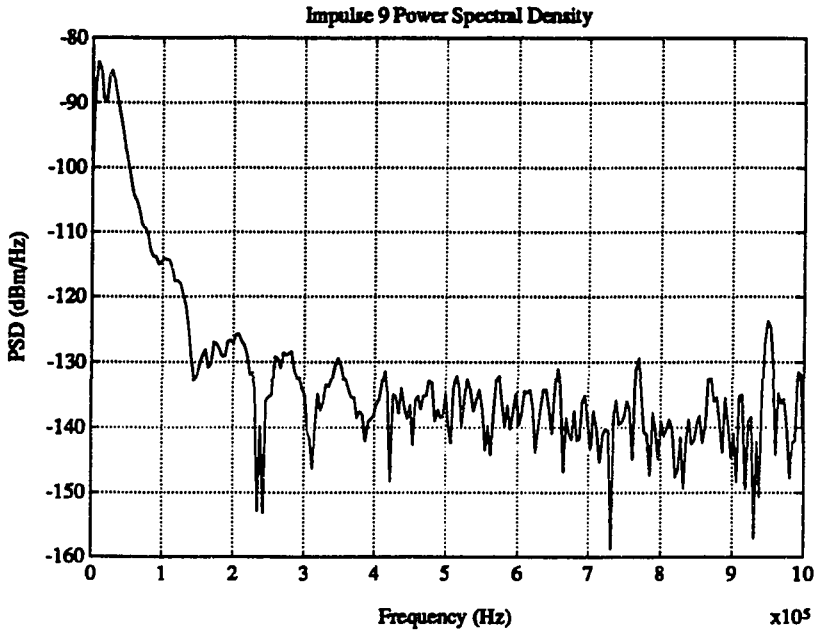

Figure 6.12: NYNEX Impulse 9 Power Spectral Density

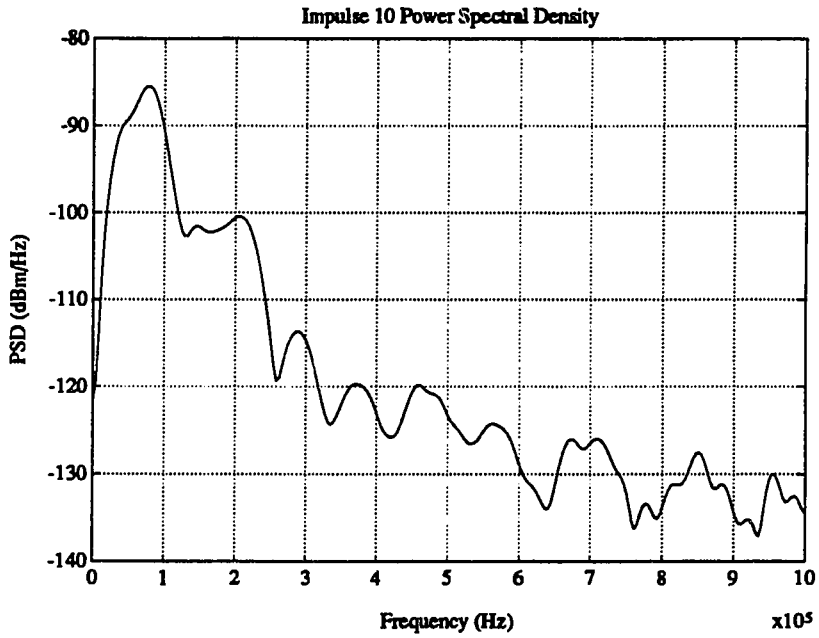

Figure 6.13: NYNEX Impulse 10 Power Spectral Density

89,000 impulses measured by British Telecommunications Ltd [80]. The Cook pulse has been used in the evaluation of (E1-)HDSL transceivers (see [81], [82], and [83]), and it has also been proposed for use in testing the impulse noise immunity of ADSL systems [80]. The Cook pulse is described mathematically by the following equation:

$$V(t) = \begin{cases} V_p \times |t|^{\frac{-3}{4}} & t > 0 \\ 0 & t = 0 \\ -V_p \times |t|^{\frac{-3}{4}} & t < 0 \end{cases} . \tag{6.1}$$

A Cook pulse waveform of peak amplitude 1.0 mV is shown in Figure 6.14, and its power spectral density is given in Figure 6.15.

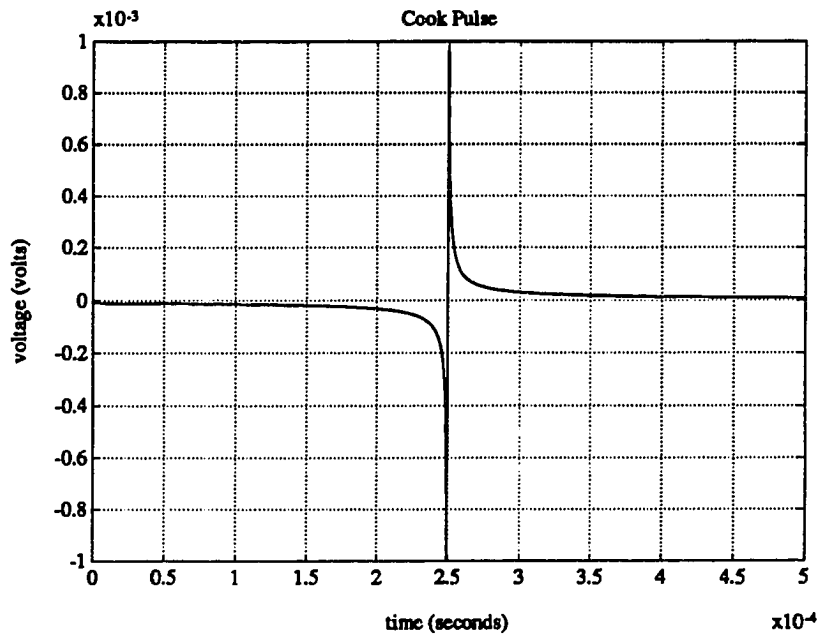

Figure 6.14: Cook Pulse of 1.0 mV Peak Voltage

6.2 Single-Carrier Error Control Techniques

While our emphasis for the remainder of this chapter will be on impulse noise mitigation strategies designed specifically for a multicarrier modulation system (in

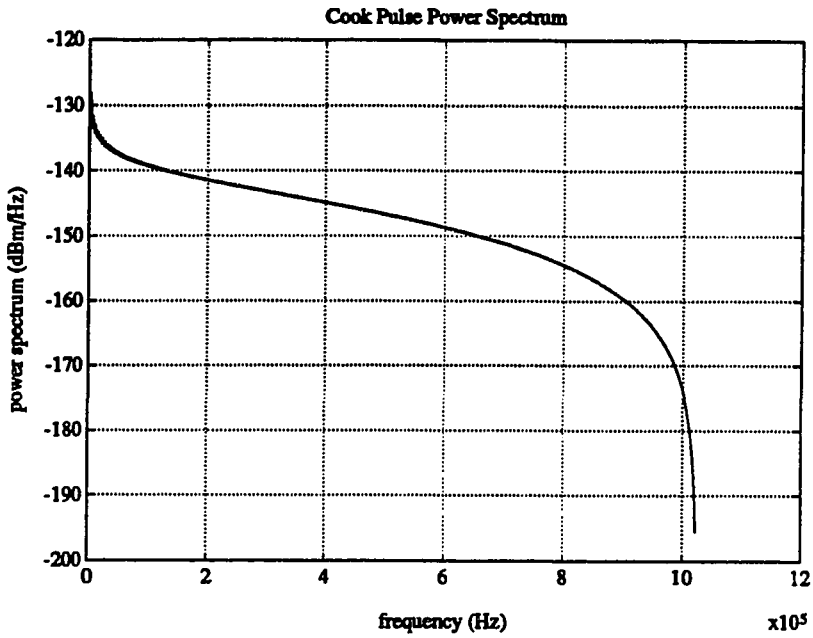

Figure 6.15: Cook Pulse Power Spectrum

particular, a DMT transceiver for ADSL), we will first briefly review some of the single-carrier, impulse noise mitigation methods that have been proposed in the literature for the sake of completeness. Furthermore, some of our ideas for multicarrier mitigation techniques are inspired by their single-carrier counterparts.

As mentioned before, the traditional method of dealing with impulse noise in the telephone network is to place a large margin (usually at least 12 dB) on the system and hope for the best. However, with the advent of advanced DSL applications, such as HDSL and ADSL, we can no longer afford to ignore the presence of impulse noise by blindly assigning a large margin to the system for several reasons. First of all, the BER requirements for these advanced DSL applications are much more strict than traditional telephone network applications; as a result, we can no longer tolerate the occasional errors caused by impulse noise hits that are not absorbed by the extra margin. Secondly, the sampling rates required by ADSL and HDSL are much higher than traditional telephone network applications; therefore, impulse noise hits will now affect a significantly larger number of received time domain samples. This in

turn implies that impulse noise is much more damaging in these high sampling rate applications, and it will be much more difficult for a single-carrier system to recover after an impulse hit, especially in the presence of error propagation when a long DFE or a Viterbi detector is employed. Lastly, these advanced DSL applications are simply more challenging to implement, and there may not be a large performance margin available in the first place.

Spurred by this challenge, there has been a renewed interest in impulse noise mitigation strategies in the recent years by researchers in academia as well as in industry. As mentioned in Section 6.1, a number of impulse noise measurement surveys have been conducted in the past decade, and based on the results of these surveys, better, though still not completely satisfactory, models and characterizations of the impulse noise phenomenon are developed in [84], [85], [86], [87], [64], [88], and [89]. In [90], [91] and [92], straightforward (interleaved) forward error correction (FEC) codes are proposed for use in single-carrier DSL systems. Similar schemes have also been proposed for use with a multicarrier ADSL transceiver, and a more detailed treatment will be given in Section 6.3.1. While these simple forward error correction techniques are effective and readily implementable with current technology, they are rather conservative in the sense that a large interleave matrix is necessary to ensure virtually all impulse noise occurrences can be transparently corrected, which in turn leads to a very long decoding delay that may not be acceptable for many envisioned applications of ADSL and HDSL. In [93], practical, single-carrier, erasure declaration mechanisms that are designed to improve the performance of an applied FEC code and reduce decoding delay are proposed and analyzed. In particular, these erasure declaration schemes provide additional side information to the decoder based on the knowledge of impulse noise available at the receiver. Careful selection of system parameters in these erasure declaration schemes are crucial, since the performance of the applied FEC can actually be degraded if inappropriate system parameters are chosen. In [94] and [95], an adaptive impulse noise cancellation approach is suggested based on the assumption that the main source of impulse noise is relatively constant on a line-by-line basis, resulting in a recurring impulse shape for each individual line. The feasibility

and effectiveness of such an adaptive impulse noise canceler, as well as the optimal structure of such device, have not been fully demonstrated at this point in time, and further studies are warranted. Lastly, in [96], a non-linear equalization technique, known as Self-Correcting Decision Feedback Equalization (SCDFE), is proposed to extend the capabilities of the DFE to detect and correct single errors due to impulse noise in DSL and wireless radio environments. While it is attractive to incorporate impulse noise mitigation capability into the equalization structure, the additional complexity of such a device may become formidable to implement when a large number of consecutive errors due to long impulses needs to be corrected instead of single errors, as in the case of ADSL.

6.3 Multicarrier Error Control Techniques

Fortunately for a multicarrier DMT transceiver, superior impulse noise immunity relative to a single-carrier system is inherent due to its block processing nature. For the ideal case of a true impulse noise occurrence that corrupts only one time domain sample, the total energy of the noise pulse is then spread evenly over every carrier, so in the case of a DMT system implemented with a length 512 FFT, its impulse noise threshold will be approximately $10\ log_{10}\ (512) = 27.1\ dB$ higher than a corresponding single-carrier system. In reality, however, impulse noise occurrences may last for significantly longer than a single sample period at the ADSL sampling rates. As a result, additional protection is necessary to ensure satisfactory system performance. We will now turn our attention to a number of impulse noise mitigation strategies designed specifically for a DMT transceiver.

To evaluate the performance of the various impulse noise mitigation strategies discussed in the remainder of this chapter, we make use of the set of canonical loops proposed in [57] for ADSL transceiver evaluation. The configurations of these loops are given in Figure 6.16, and they fall outside of the Carrier Serving Area. In addition to this set of canonical loops, we will also consider three additional loops; namely, the 12 kft, 24 AWG loop (CSA loop 8), the 9 kft, 26 AWG loop (CSA loop 6), and the 18 kft, 24 AWG loop. For our simulations, we consider a DMT

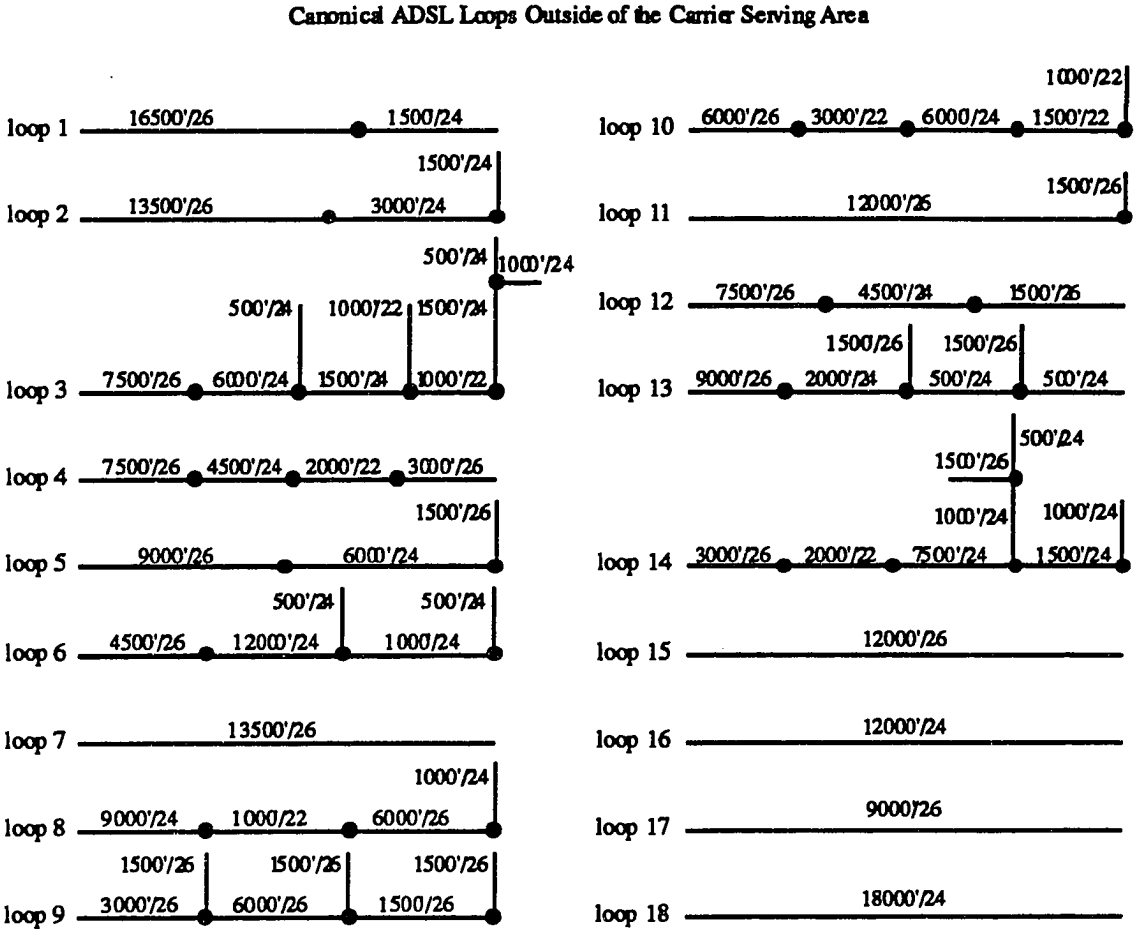

Figure 6.16: Canonical ADSL Loops Outside of the Carrier Serving Area

system with a FFT size of 512, a 4.0 kHz multicarrier block symbol rate, and a 2.048 MHz sampling rate. (We will neglect the additional complexity associated with the cyclic prefix and the time domain equalizer in this chapter.) Because the effect of impulse noise is more pronounced at higher data rates, our analysis focuses on the downstream ADSL channel. For our simulations, we will use an AWGN floor of -143 dBm/Hz (two-sided) plus 49 ADSL far-end crosstalkers, unless otherwise specified.

6.3.1 Basic Multicarrier Error Control

The presence of impulse noise in a multicarrier system leads to the degradation of SNR's over several adjacent subchannels, resulting in burst errors at the decoder output. In addition, if a trellis code with Viterbi detection is employed, burst errors due to error propagation in the decoder are more likely to take place. One technique of providing extra protection against burst errors in a multicarrier system due to impulse noise that has been proposed for ADSL is the application of forward error correction with interleaving [97]. FEC schemes involve efficiently inserting redundancy in the data stream, which can be used at the decoder to correct for any channel errors. A popular class of codes used in many practical applications and for which hardware is readily available is the Reed-Solomon (RS) codes over the finite field $GF(256)$. Each codeword requires $2t$ parity check bytes to correct t random byte errors in a block of n bytes, of which $k = n - 2t$ bytes are information bytes. To enable the correction of long bursts of errors, interleaving is used to spread the burst over many codewords, thus making the correlated errors appear random. For a t random byte error correcting RS code with n bytes per codeword and interleaving depth i, the length in bits of an isolated burst error that can be corrected is simply given by $8ti - 7$, provided that only one impulse occurrence is possible per interleave matrix. As the great majority of impulse noise hits last less than 250 μs, which is also the multicarrier block symbol period of our proposed DMT system, we need to employ a RS code that is designed to correct up to 2 multicarrier block symbols' worth of bits in error in order to ensure perfect protection against these impulses in the absence of other noise sources. This is because the impulse noise hit may straddle two adjacent multicarrier block symbols and cause errors in both

multicarrier block symbols.

6.3.2 Hard Decision Error Control Enhancements

The cost of applying a FEC code is the increased data rate required to meet the same information rate, the additional complexity of encoding and decoding, and the increased latency introduced into the transmission path. Some of these disadvantages can be reduced by enhancing the performance of the error correction scheme with the provision of side information to the decoder. In particular, a RS code of parameters (n, k), in which ρ symbols have been erased (marked as incorrect) and t symbols are in error, will be decoded correctly as long as the following equation is satisfied [21]:

$$n - k \geq 2t + \rho \, . \tag{6.2}$$

For our simulations, we have chosen two sets of code parameters, depending on whether the system is transmitting at a 1.6 Mbps or a 6.4 Mbps uncoded data rate. In the case of 1.6 Mbps, a $(214, 200)$ RS code spanning four multicarrier symbols with an interleaving depth of eight is chosen, enabling the correction of 441 bit bursts (882 with perfect erasure information) or a little over one (two with erasures) multicarrier symbol(s). For the 6.4 Mbps case, a $(212, 200)$ RS code spanning one multicarrier symbol with an interleaving depth of 36 is chosen, enabling the correction of 1721 bit bursts (3442 with erasures), which is again a little over one (two with erasures) multicarrier symbol(s)' worth of data. When these codes are incorporated into the system, the data rates must be increased from 1.6 Mbps and 6.4 Mbps to 1.712 Mbps and 6.784 Mbps, respectively, to allow for the same information rates. We note that these code parameters are chosen in anticipation of the impulse noise mitigation strategies to be discussed in the reminder of this chapter. In particular, we have allowed for the correction of two multicarrier symbols' worth of data under the idealized assumption of perfect erasure information.

Time Domain Monitoring

The first impulse noise mitigation strategy is a simple time domain approach, which is based on the assumption that some of the impulses experienced will be of much larger magnitude than the received ADSL signal. To detect these impulses, the DMT receiver may monitor for sudden drops in the automatic gain control (AGC) level and/or for clipping in the analog-to-digital converter. If this occurs for several time domain samples, the receiver declares that an impulse has occurred and erases the corresponding multicarrier block symbol. The entire symbol is erased because clipping for several samples is likely to result in errors in many of the subchannels. We note that this approach is similar to the one proposed in [98] for erasure decoding in a Raleigh fading environment. In that case, the AGC is, instead, monitored for a large increase in gain, which indicates a sudden drop in signal strength and a fade has most likely occurred.

The time domain clipping technique will be most effective on long loops over which the ADSL signal is severely attenuated and therefore much weaker than the impulses experienced. However, one potential difficulty with this technique rests on the large peak-to-average power ratio of the multicarrier signal. Because of the magnitude of this ratio, the AGC gain is normally set at a value small enough to prevent frequent clippings in the receiver's ADC due to peaks in the DMT signal itself. An appropriate value for the maximum allowable received power is derived by noting that the DMT time domain signal is formed by summing a number of independent, quadrature amplitude modulated signals. Hence, by central limit theorem arguments, the probability distribution function is approximately Gaussian. By setting the AGC threshold at a value far enough out on the tail of the distribution, we can ensure that the probability of clipping due to peaks in the received signal is much less than the desired error rate. For example, an AGC threshold of 15 dB above the average received power corresponds to a probability of clipping of 1.9×10^{-8}, which is below the 10^{-7} BER required for ADSL. Higher AGC levels will lower the probability of clipping due to the DMT signal itself at the expense of allowing larger magnitude impulses into the system. By requiring, for example, that at least three time domain samples exceed the clipping level,

we almost guarantee that a symbol is erased only when an impulse occurs. (The probability of a false erasure is 9.2×10^{-15}.)

Assuming a 15 dB setting for the AGC, the maximum allowable voltage at the DMT receiver can be approximated by the following equation:

$$v_{max} \approx \sqrt{R_{load} 10^{(P_{rcvd}+15)/10}}\,, \tag{6.3}$$

where R_{load} is the load resistance and P_{rcvd} is the average received power in dBW. A value for the average received power in Equation (6.3) is determined by multiplying the power $P(i)$ used in each subchannel by the channel transfer gain $|H(i)|^2$ at the corresponding frequency and summing the products; in other words, $P_{rcvd} = \sum P(i)|H(i)|^2$.

To obtain an estimate of the expected performance of the time domain clipping approach in detecting impulses, we will compare the voltages of the 10 NYNEX impulses presented in Section 6.1 to the maximum allowed voltages for each of the 18 test loops. By focusing only on the impulse noise amplitudes, we neglect the DMT signal and other noise components that add to the impulse in forming the received signal. Since the DMT signal component is zero mean and of a standard deviation 15 dB below the peak allowed voltage, we can assume that the impulse noise dominates whenever the maximum voltage is exceeded. The results for a DMT system with two different levels of transmit power (17 dBm and 20 dBm) at two different data rates (1.6 Mbps and 6.4 Mbps) are presented in Tables 6.1, 6.2, 6.3, and 6.4, respectively, in terms of the number of impulse samples exceeding the peak allowed voltage for the particular test loop. As expected, this scheme is only able to detect the largest impulses on loops for which the ADSL signal is most attenuated. For instance, impulses 7, 8, 9, and 10 are detected in loops 1, 2, and 3 for many of the tested scenarios. Although the performance does not appear too impressive for the selected scenarios, it does represent a relatively simple way to effectively double the capability of a FEC code in the presence of severely damaging impulses over worst case ADSL loops.

A more general characterization of the performance of this time domain clipping technique can be obtained if the distribution of the received signal is known [19].

Impulse Number	1	2	3	4	5	6	7	8	9	10
ADSL Loop 1	0	0	0	0	0	0	17	30	18	12
ADSL Loop 2	0	0	0	0	0	0	0	12	10	10
ADSL Loop 3	0	0	0	0	0	0	0	0	0	5
ADSL Loop 4	0	0	0	0	0	0	0	0	0	0
ADSL Loop 5	0	0	0	0	0	0	0	0	0	0
ADSL Loop 6	0	0	0	0	0	0	0	0	0	0
ADSL Loop 7	0	0	0	0	0	0	0	0	0	0
ADSL Loop 8	0	0	0	0	0	0	0	0	0	0
ADSL Loop 9	0	0	0	0	0	0	0	0	0	0
ADSL Loop 10	0	0	0	0	0	0	0	0	0	0
ADSL Loop 11	0	0	0	0	0	0	0	0	0	0
ADSL Loop 12	0	0	0	0	0	0	0	0	0	0
ADSL Loop 13	0	0	0	0	0	0	0	0	0	0
ADSL Loop 14	0	0	0	0	0	0	0	0	0	0
ADSL Loop 15	0	0	0	0	0	0	0	0	0	0
12 kft 24 AWG	0	0	0	0	0	0	0	0	0	0
9 kft 26 AWG	0	0	0	0	0	0	0	0	0	0
18 kft 24 AWG	0	0	0	0	0	0	0	0	0	0

Table 6.1: Time Domain Clipping - 17 dBm Power; 1.6 Mbps; (214, 200) RS × 8; AWGN + 49 ADSL FEXT

Impulse Number	1	2	3	4	5	6	7	8	9	10
ADSL Loop 1	0	0	0	0	0	0	28	43	25	15
ADSL Loop 2	0	0	0	0	0	0	23	36	21	12
ADSL Loop 3	0	0	0	0	0	0	0	12	10	10
ADSL Loop 4	0	0	0	0	0	0	0	0	0	6
ADSL Loop 5	0	0	0	0	0	0	0	0	0	5
ADSL Loop 6	0	0	0	0	0	0	0	0	0	2
ADSL Loop 7	0	0	0	0	0	0	0	0	0	0
ADSL Loop 8	0	0	0	0	0	0	0	0	0	0
ADSL Loop 9	0	0	0	0	0	0	0	0	0	2
ADSL Loop 10	0	0	0	0	0	0	0	0	0	0
ADSL Loop 11	0	0	0	0	0	0	0	0	0	0
ADSL Loop 12	0	0	0	0	0	0	0	0	0	0
ADSL Loop 13	0	0	0	0	0	0	0	0	0	0
ADSL Loop 14	0	0	0	0	0	0	0	0	0	0
ADSL Loop 15	0	0	0	0	0	0	0	0	0	0
12 kft 24 AWG	0	0	0	0	0	0	0	0	0	0
9 kft 26 AWG	0	0	0	0	0	0	0	0	0	0
18 kft 24 AWG	0	0	0	0	0	0	0	0	0	0

Table 6.2: Time Domain Clipping - 17 dBm Power; 6.4 Mbps; (212, 200) RS $\times$ 36; AWGN + 49 ADSL FEXT

Impulse Number	1	2	3	4	5	6	7	8	9	10
ADSL Loop 1	0	0	0	0	0	0	0	0	0	8
ADSL Loop 2	0	0	0	0	0	0	0	0	0	6
ADSL Loop 3	0	0	0	0	0	0	0	0	0	0
ADSL Loop 4	0	0	0	0	0	0	0	0	0	0
ADSL Loop 5	0	0	0	0	0	0	0	0	0	0
ADSL Loop 6	0	0	0	0	0	0	0	0	0	0
ADSL Loop 7	0	0	0	0	0	0	0	0	0	0
ADSL Loop 8	0	0	0	0	0	0	0	0	0	0
ADSL Loop 9	0	0	0	0	0	0	0	0	0	0
ADSL Loop 10	0	0	0	0	0	0	0	0	0	0
ADSL Loop 11	0	0	0	0	0	0	0	0	0	0
ADSL Loop 12	0	0	0	0	0	0	0	0	0	0
ADSL Loop 13	0	0	0	0	0	0	0	0	0	0
ADSL Loop 14	0	0	0	0	0	0	0	0	0	0
ADSL Loop 15	0	0	0	0	0	0	0	0	0	0
12 kft 24 AWG	0	0	0	0	0	0	0	0	0	0
9 kft 26 AWG	0	0	0	0	0	0	0	0	0	0
18 kft 24 AWG	0	0	0	0	0	0	0	0	0	0

Table 6.3: Time Domain Clipping - 20 dBm Power; 1.6 Mbps; (214, 200) RS × 8; AWGN + 49 ADSL FEXT

Impulse Number	1	2	3	4	5	6	7	8	9	10
ADSL Loop 1	0	0	0	0	0	0	18	32	19	12
ADSL Loop 2	0	0	0	0	0	0	0	16	11	10
ADSL Loop 3	0	0	0	0	0	0	0	0	0	6
ADSL Loop 4	0	0	0	0	0	0	0	0	0	0
ADSL Loop 5	0	0	0	0	0	0	0	0	0	0
ADSL Loop 6	0	0	0	0	0	0	0	0	0	0
ADSL Loop 7	0	0	0	0	0	0	0	0	0	0
ADSL Loop 8	0	0	0	0	0	0	0	0	0	0
ADSL Loop 9	0	0	0	0	0	0	0	0	0	0
ADSL Loop 10	0	0	0	0	0	0	0	0	0	0
ADSL Loop 11	0	0	0	0	0	0	0	0	0	0
ADSL Loop 12	0	0	0	0	0	0	0	0	0	0
ADSL Loop 13	0	0	0	0	0	0	0	0	0	0
ADSL Loop 14	0	0	0	0	0	0	0	0	0	0
ADSL Loop 15	0	0	0	0	0	0	0	0	0	0
12 kft 24 AWG	0	0	0	0	0	0	0	0	0	0
9 kft 26 AWG	0	0	0	0	0	0	0	0	0	0
18 kft 24 AWG	0	0	0	0	0	0	0	0	0	0

Table 6.4: Time Domain Clipping - 20 dBm Power; 6.4 Mbps; (212, 200) RS × 36; AWGN + 49 ADSL FEXT

The received signal, y_k, in the presence of impulse noise can be expressed as:

$$y_k = v_k + u_k + n_k \ , \tag{6.4}$$

where v_k is the desired, channel attenuated, DMT signal component, u_k represents the impulse noise component, and n_k corresponds to an additive colored Gaussian noise component that includes the contributions from crosstalk noise and AWGN. The DMT component, v_k, and the colored Gaussian noise component, n_k, can both be modeled as zero mean, Gaussian random variables. Under this additional assumption, the received signal can then be expressed as:

$$y_k = z_k + u_k \ , \tag{6.5}$$

where $z_k = v_k + n_k$ is normally distributed with variance σ_z^2. The probability that the magnitude of the received signal exceeds the maximum allowable voltage v_{max} given that an impulse is present and conditioned on the impulse amplitude may be expressed as:

$$Pr(|y| > v_{max} \mid u, impulse) = Pr(z + u > v_{max}) + Pr(z + u < -v_{max}) \ . \tag{6.6}$$

Using the fact that z is normally distributed with variance σ_z^2, this expression may be rewritten as:

$$Pr(|y| > v_{max} \mid u, impulse) = Q\left(\frac{v_{max} - u}{\sigma_z}\right) + Q\left(\frac{v_{max} + u}{\sigma_z}\right) \ , \tag{6.7}$$

where the Q function is defined by Equation (2.13) in Section 2.2. The probability of clipping is therefore given by:

$$Pr(|y| > v_{max} \mid impulse) = \int \left[Q\left(\frac{v_{max} - u}{\sigma_z}\right) + Q\left(\frac{v_{max} + u}{\sigma_z}\right)\right] p(u) du \ , \tag{6.8}$$

where $p(u)$ is the amplitude distribution of the impulse noise. As noted in [64] and [79], several surveys have shown that the probability density function of the amplitude u of impulse noise on Digital Subscriber Lines can be approximated by a hyperbolic distribution given by:

$$p(u) = \begin{cases} \frac{u_0^2}{|u|^3} & min\ |u| \le |u| \le max\ |u| \\ 0 & otherwise \end{cases} \ , \tag{6.9}$$

where u_0 is given by:

$$u_0{}^2 = \frac{(max\ |u|)^2 (min\ |u|)^2}{(max\ |u|)^2 - (min\ |u|)^2}\ , \tag{6.10}$$

and $max\ |u|$ and $min\ |u|$ are the maximum and minimum magnitudes of the impulse noise sample, u_k, respectively. Given the parameter u_0 of this distribution and the valid range of voltages, we can determine the probability of the received signal exceeding a particular voltage level on a given loop as:

$$Pr(|y| > v_{max} \mid impulse) = 2 \int_{u_0}^{max\ |u|} \left[Q\left(\frac{v_{max} - u}{\sigma_z}\right) + Q\left(\frac{v_{max} + u}{\sigma_z}\right) \right] \frac{u_0^2}{u^3} du\ . \tag{6.11}$$

If the AGC level is set at 15 dB above the average power level, then Equation (6.11) may be simplified to:

$$Pr(|y| > v_{max} \mid impulse) = 2 \int_{u_0}^{max\ |u|} \left[Q\left(10^{0.75} - \frac{u}{\sigma_z}\right) + Q\left(10^{0.75} + \frac{u}{\sigma_z}\right) \right] \frac{u_0^2}{u^3} du\ . \tag{6.12}$$

By changing the variable of integration, we may rewrite Equation (6.12) as:

$$Pr(|y| > v_{max} \mid impulse) = 2 \int_{1}^{\frac{max\ |u|}{u_0}} \left[Q\left(10^{0.75} - \frac{\bar{u}}{\frac{\sigma_z}{u_0}}\right) + Q\left(10^{0.75} + \frac{\bar{u}}{\frac{\sigma_z}{u_0}}\right) \right] \frac{1}{\bar{u}^3} d\bar{u}\ , \tag{6.13}$$

which indicates that the probability is a function of the AGC level and the ratio $\frac{\sigma_z}{u_0}$. Figure 6.17 presents sample plots of the probability that the received signal plus impulse exceeds the maximum allowable input voltage for two AGC settings; namely, 15 dB and 18 dB.

Frequency Domain Monitoring

Our second approach is a dual to the time domain clipping technique presented in the previous section in that we look for large frequency domain samples for declaring erased tones. In particular, we will erase any tones in which the sliced constellation point exceeds the boundary of the constellation supported by the subchannel of interest. As explained in Chapter 4, the number of bits carried on a subchannel varies from subchannel to subchannel, and to accommodate the various constellation sizes, an embedded labeling scheme is often employed, where the smaller

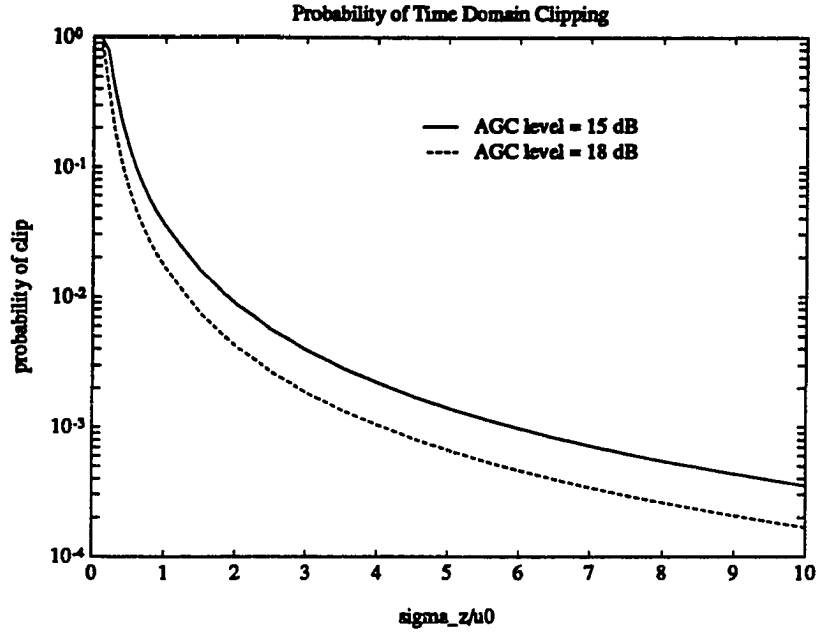

Figure 6.17: Probability of Time Domain Clipping Given an Impulse Occurrence

constellations are subsets of the larger ones. In decoding a particular subchannel, the operations of the decoder typically involve slicing the received point to a point on the two dimensional integer lattice, looking up the corresponding label in a table, and masking off the appropriate number of bits from the label. Thus, by adding an extra step to check the validity of the original sliced point, we are able to extract some side information for the purposes of declaring erasures. At first glance, it may appear somewhat fruitless to check for large values in the frequency domain, especially since multicarrier modulation supposedly spreads the impulse energy over all subchannels. However, this noise energy spreading effect is best realized when the impulse consists of only a few high magnitude time domain samples, which corresponds to a relatively flat spectrum in the frequency domain. In contrast, the 10 NYNEX impulses used in this dissertation are of significant magnitude over a relatively large number of time domain samples.

We use the same scenarios as before to test the performance of the frequency

domain clipping technique with respect to the 10 NYNEX impulses. For simplicity, a tone, or subchannel, is declared as erased when the energy content of the impulse at that particular carrier exceeds the expected received energy. Because each used subchannel carries an integer number of bits ranging from 2 to 10, the peak-to-average power ratio of square and cross QAM constellations are used in calculating the peak energy expected on any one tone. Our simulation results are presented in Tables 6.5, 6.6, 6.7, and 6.8, respectively, in terms of the number of tones in which the impulse noise power exceeds the peak power of the constellation supported by the corresponding subchannel. As in the case of the time domain

Impulse Number	1	2	3	4	5	6	7	8	9	10
ADSL Loop 1	0	0	0	0	0	0	0	0	0	42
ADSL Loop 2	0	0	0	0	0	0	0	0	0	18
ADSL Loop 3	0	0	0	0	0	0	0	0	0	23
ADSL Loop 4	0	0	0	0	0	0	0	0	0	0
ADSL Loop 5	0	0	0	0	0	0	0	0	0	2
ADSL Loop 6	0	0	0	0	0	0	0	0	0	6
ADSL Loop 7	0	0	0	0	0	0	0	0	0	0
ADSL Loop 8	0	0	0	0	0	0	0	0	0	0
ADSL Loop 9	0	0	0	0	0	0	0	0	0	8
ADSL Loop 10	0	0	0	0	0	0	0	0	0	0
ADSL Loop 11	0	0	0	0	0	0	0	0	0	0
ADSL Loop 12	0	0	0	0	0	0	0	0	0	0
ADSL Loop 13	0	0	0	0	0	0	0	0	0	0
ADSL Loop 14	0	0	0	0	0	0	0	0	0	0
ADSL Loop 15	0	0	0	0	0	0	0	0	0	0
12 kft 24 AWG	0	0	0	0	0	0	0	0	0	0
9 kft 26 AWG	0	0	0	0	0	0	0	0	0	0
18 kft 24 AWG	0	0	0	0	0	0	0	0	0	0

Table 6.5: Frequency Domain Clipping - 17 dBm Power; 1.6 Mbps; (214, 200) RS $\times$ 8; AWGN + 49 ADSL FEXT

clipping technique, this approach will only be able to detect the worst case impulse; namely, impulse 10, over some of the longer loops when the system is transmitting at the T1 rate. However, at the higher DS-2 rate transmission, most of the impulses can be detected in many of our test loops. This is because higher rate transmission

Impulse Number	1	2	3	4	5	6	7	8	9	10
ADSL Loop 1	74	68	125	111	110	99	203	100	191	208
ADSL Loop 2	58	41	70	89	61	52	183	62	128	213
ADSL Loop 3	25	17	37	54	22	31	103	31	67	199
ADSL Loop 4	22	11	27	51	13	18	94	33	71	197
ADSL Loop 5	0	1	11	22	4	3	58	12	32	124
ADSL Loop 6	16	11	27	53	15	20	93	22	58	185
ADSL Loop 7	0	0	6	0	2	1	21	5	13	96
ADSL Loop 8	0	2	8	23	3	4	71	26	45	136
ADSL Loop 9	0	0	0	0	0	0	14	2	7	21
ADSL Loop 10	1	0	7	19	2	3	66	23	37	133
ADSL Loop 11	0	0	0	0	0	0	8	2	4	37
ADSL Loop 12	0	0	0	0	0	0	3	2	3	30
ADSL Loop 13	0	0	0	0	0	0	8	1	3	22
ADSL Loop 14	0	0	0	0	0	0	6	3	6	30
ADSL Loop 15	0	0	0	0	0	0	2	0	1	19
12 kft 24 AWG	0	0	0	0	0	0	0	0	0	0
9 kft 26 AWG	0	0	0	0	0	0	0	0	0	0
18 kft 24 AWG	0	0	7	5	2	3	47	13	23	120

Table 6.6: Frequency Domain Clipping - 17 dBm Power; 6.4 Mbps; (212, 200) RS $\times$ 36; AWGN + 49 ADSL FEXT

Impulse Number	1	2	3	4	5	6	7	8	9	10
ADSL Loop 1	0	0	0	0	0	0	0	0	0	22
ADSL Loop 2	0	0	0	0	0	0	0	0	0	12
ADSL Loop 3	0	0	0	0	0	0	0	0	0	0
ADSL Loop 4	0	0	0	0	0	0	0	0	0	0
ADSL Loop 5	0	0	0	0	0	0	0	0	0	0
ADSL Loop 6	0	0	0	0	0	0	0	0	0	0
ADSL Loop 7	0	0	0	0	0	0	0	0	0	0
ADSL Loop 8	0	0	0	0	0	0	0	0	0	0
ADSL Loop 9	0	0	0	0	0	0	0	0	0	4
ADSL Loop 10	0	0	0	0	0	0	0	0	0	0
ADSL Loop 11	0	0	0	0	0	0	0	0	0	0
ADSL Loop 12	0	0	0	0	0	0	0	0	0	0
ADSL Loop 13	0	0	0	0	0	0	0	0	0	0
ADSL Loop 14	0	0	0	0	0	0	0	0	0	0
ADSL Loop 15	0	0	0	0	0	0	0	0	0	0
12 kft 24 AWG	0	0	0	0	0	0	0	0	0	0
9 kft 26 AWG	0	0	0	0	0	0	0	0	0	0
18 kft 24 AWG	0	0	0	0	0	0	0	0	0	0

Table 6.7: Frequency Domain Clipping - 20 dBm Power; 1.6 Mbps; (214, 200) RS $\times$ 8; AWGN + 49 ADSL FEXT

Impulse Number	1	2	3	4	5	6	7	8	9	10
ADSL Loop 1	69	53	112	97	86	78	197	85	172	208
ADSL Loop 2	38	27	52	77	37	40	154	48	96	213
ADSL Loop 3	14	7	26	43	10	15	76	25	51	169
ADSL Loop 4	3	5	12	30	5	9	75	25	51	160
ADSL Loop 5	0	0	7	7	2	1	36	5	19	105
ADSL Loop 6	4	6	12	41	5	10	70	18	41	156
ADSL Loop 7	0	0	0	0	0	0	10	3	6	68
ADSL Loop 8	0	0	6	0	1	1	45	11	20	117
ADSL Loop 9	0	0	0	0	0	0	4	0	3	19
ADSL Loop 10	0	0	2	0	0	0	31	7	16	110
ADSL Loop 11	0	0	0	0	0	0	2	0	1	20
ADSL Loop 12	0	0	0	0	0	0	2	0	1	20
ADSL Loop 13	0	0	0	0	0	0	2	0	1	19
ADSL Loop 14	0	0	0	0	0	0	4	1	4	18
ADSL Loop 15	0	0	0	0	0	0	0	0	0	15
12 kft 24 AWG	0	0	0	0	0	0	0	0	0	0
9 kft 26 AWG	0	0	0	0	0	0	0	0	0	0
18 kft 24 AWG	0	0	2	0	0	0	25	5	14	103

Table 6.8: Frequency Domain Clipping - 20 dBm Power; 6.4 Mbps; (212, 200) RS $\times$ 36; AWGN + 49 ADSL FEXT

generally utilizes a wider bandwidth, and there is significant impulse noise energy located at the higher frequencies, relatively speaking, where the channel transfer functions are severely attenuated. The performance of this frequency domain clipping technique in general depends on the manner in which power is allocated among the carriers, the channel transfer function, and the actual number of carriers used.

MSE Monitoring

The impulse noise mitigation techniques discussed up to this point have focused on the two extremes of large time domain and large frequency domain samples. Many of the impulses not detected under either scheme will still lead to a severe degradation in error rate performance. Another source of side information available to the DMT decoder exists in the form of the squared error between the received signal points and the sliced data points. Figure 6.18 is a diagram of the FEQ and the decision circuit used to decode the QAM signal on each subchannel. The

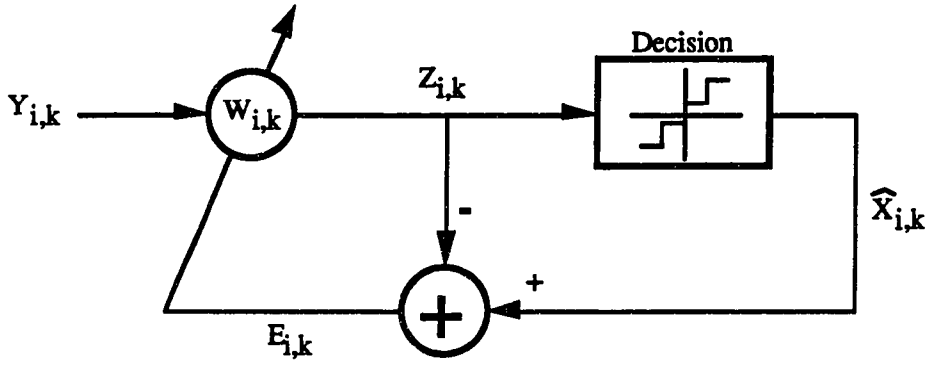

Figure 6.18: One-tap Frequency Domain Equalizer and Decision Element

received constellation point on subchannel i at time k, $Y_{i,k}$, is scaled by a complex multiplier, $W_{i,k}$, to form the input, $Z_{i,k}$, to a slicer. The output of the slicer, $\hat{X}_{i,k}$, is the decoded constellation point and the difference between the slicer output and input, $E_{i,k} = \hat{X}_{i,k} - Z_{i,k}$, is used in adaptively updating the scaling factor by the standard LMS algorithm to track timing and phase jitter. The adaptation algorithm

is given by

$$W_{i,k+1} = W_{i,k} + \mu E_{i,k} Y^*_{i,k} , \tag{6.14}$$

where μ regulates the speed and stability of adaptation [99].

The decoder may, therefore, use a profile of the magnitudes of the mean squared errors, $|E_{i,k}|^2$, across all the carriers to make an estimate as to the reliability of the sliced data points, which in turn can be used to provide erasure information. The simplest scheme is to mark a tone as unreliable if its mean squared error signal exceeds a predetermined threshold, designated as R^2. A picture illustrating this concept is presented in Figure 6.19. The original square decision regions associated

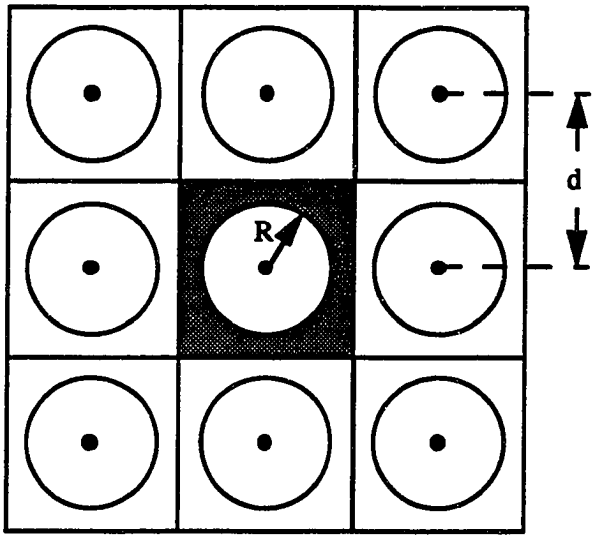

Figure 6.19: Modified Constellation Decision Regions

with each of the constellation points have been replaced by circles of radius R, designating regions in which the scaled point may fall without being erased. The value R represents a tradeoff between the probability of a false erasure in the absence of an impulse and the probability of detecting an unreliable tone. An expression for the probability of false erasure in the absence of impulse noise may be approximated by the probability that the received complex point falls within the shaded region in

Figure 6.19, given that the center point is transmitted; namely,

$$Pr(false\ erasure) \approx \left(1 - 2Q\left(\frac{d}{2\sigma}\right)\right)^2 - \left(1 - e^{-\frac{R^2}{2\sigma^2}}\right), \qquad (6.15)$$

where σ^2 is the one-dimensional noise variance, d is the minimum distance between constellation points (typically normalized to one), and the Q function is again defined by Equation (2.13) in Section 2.2. The first term in Equation (6.15) corresponds to the probability that the received point falls within the original decision square containing the transmitted point, while the second term represents the probability the received point falls within a circle of radius R about the transmitted point. For ADSL, $2Q(\frac{d}{2\sigma}) < 10^{-7}$. Hence, a value of $R^2 = 0.2\ d^2$ will provide a false erasure probability of 7.27×10^{-6} whereas a value of $0.23\ d^2$ gives 10^{-6}, assuming that the system is operating with no margin.

The decoder now has several options in using this side information. One option would be to erase the entire multicarrier symbol if the number of unreliable tones exceeds a threshold. A second option would be to erase all RS symbols containing bits carried by tones marked as unreliable. Yet another option would be to erase all RS symbols containing bits carried by tones either marked as unreliable or surrounded by tones marked as unreliable. All three methods will provide a gain over error correction alone as long as more than half of the bytes marked for erasure would have otherwise been in error.

To obtain an estimate of the performance of this erasure declaration scheme, we will simulate the theoretical operation of a multicarrier demodulator under a test scenario where data at 1.6 Mbps is transmitted through ADSL loop 6 with 17 dBm of power and a noise component consisting of AWGN plus 49 BA-ISDN crosstalkers, for several impulse noise waveforms and erasure thresholds. The impulse waveform selected in each case will be injected at a rate of about one every 100 multicarrier symbols, ensuring that at most one impulse will be present in the interleave matrix, which contains 32 DMT symbols, at any one time. A total of 100 impulses will be injected in each case.

For the first test, we use Cook pulse waveforms of various amplitudes and keep track of the total number of tones in error, number of tones erased, and number

Voltage (mV)	Errors	Thresh = 0.09		Thresh = 0.15		Thresh = 0.2		Thresh = 0.23	
		Erased	Valid	Erased	Valid	Erased	Valid	Erased	Valid
2	0	9	0	0	0	0	0	0	0
5	58	4465	58	1715	57	449	51	172	36
10	4901	5659	4125	4261	3085	3113	2319	2481	1924
15	6131	4839	4142	3158	2726	1928	1629	1288	1051
20	6489	5478	4726	4102	3745	2999	2811	2298	2167
40	7341	6129	5366	4627	3951	3319	2785	2484	2112

Table 6.9: Total Number of Tones in Error, Tones Erased, and Valid Erasures for 100 Injected Cook Pulses

of valid tone erasures. Four different erasure thresholds for the mean squared error signal are used; namely, 0.09 d^2, 0.15 d^2, 0.2 d^2, and 0.23 d^2. We note here that $R = \infty$ corresponds to the case of no erasure mechanism. Simulation results for Cook pulses with peak-to-peak amplitudes of 2 mV, 5 mV, 10 mV, 15 mV, 20 mV, and 40 mV are presented in Table 6.9. The results in Table 6.9 indicate that the erasure mechanism is quite effective in locating tones that are most likely in error, except in the case of the 5 mV Cook pulse. For example, with an erasure threshold of 0.15 d^2 and a 10 mV Cook pulse, 43 tones are erased on average, of which 31 are valid erasures that correspond to a subset of the 49 tones actually in error. For Cook pulses of magnitude greater than or equal to 10 mV peak-to-peak, lowering the erasure threshold from 0.23 d^2 to 0.09 d^2 increases the number of valid erasures without decreasing the ratio of valid erasures to total erasures significantly. In the case of a 5 mV Cook pulse, the number of erasures declared far exceeds the actual number of tones in error, indicating that a Cook pulse of this voltage is very near to the threshold that the system can tolerate without error correction. This fact is further confirmed by noting the dramatic increase in the number of tones erased as the erasure threshold is lowered from 0.23 d^2 to 0.09 d^2. A similar threshold effect for a DMT system tested for impulse noise immunity with the Cook pulse waveform is reported in [81].

The relationship between the tones in error and the RS codeword symbols in

Voltage (mV)	Codeword Errors w/ Erasures	Codeword Errors w/o Erasures
2	0	0
5	0	0
10	0	0
15	0	0
20	0	0
40	0	2

Table 6.10: Total Number of Codeword Errors with and without Erasure Decoding for 100 Injected Cook Pulses

error depends somewhat upon the labeling scheme used for the constellation as well as the bit distribution. For simplicity, we will now obtain an estimate of the RS code performance with interleaving by assuming that any RS symbol containing bits that are carried by a tone decoded incorrectly will in fact be in error. This assumption is slightly pessimistic, but we note that in a straightforward implementation of an embedded constellation labeling scheme, neighboring constellation points may differ by several bits. Furthermore, with large impulse noise waveforms, the transmitted constellation point on some of the tones affected may be driven across several decision region boundaries to the proximity of a constellation point that is not a nearest neighbor. The results are presented for a erasure threshold of $R^2 = 0.15\ d^2$ in Table 6.10, in the form of the number of codewords that will be decoded incorrectly with and without erasure decoding. Interleaving is included in these simulations. The results in Table 6.10 indicate an improved performance offered by the erasure decoding technique in the case of high-amplitude Cook pulses.

Identical simulations are also conducted using each of the 10 NYNEX impulse waveforms. The results for the case of $R^2 = 0.15\ d^2$ are listed in Tables 6.11 and 6.12, respectively. Data in Table 6.11 appear to indicate that the erasure mechanism does not perform extremely well for several of the impulses. For instance, the percentage of tones in error that are erased typically ranges from 50%–70%, while the percentage of erasures that are valid is often below 50%. The large number of invalid erasures demonstrates that when an impulse occurs, the SNR's on many

Impulse	Tones in Error	Tones Erased	Valid Erasures
1	41	96	36
2	41	84	15
3	956	1264	630
4	2371	2624	1466
5	126	323	88
6	212	321	133
7	5002	5383	2812
8	2042	2100	1390
9	1894	2709	1226
10	8362	5137	4486

Table 6.11: Total Number of Tones in Error, Tones Erased, and Valid Erasures for 10 NYNEX Impulses

Impulse	Codeword Errors w/ Erasures	Codeword Errors w/o Erasures
1	0	0
2	0	0
3	0	1
4	0	0
5	0	0
6	0	1
7	78	159
8	32	98
9	15	95
10	20	59

Table 6.12: Total Number of Codeword Errors with and without Erasure Decoding for 10 NYNEX Impulses

of the tones are decreased significantly, although the tones still may be decoded correctly. On the other hand, the tones in error that are not erased correspond to frequency bins in which the impulse spectrum is relatively large, moving the transmitted constellation point into the decoding region of another point. Both occurrences are very reasonable considering the nature of the spectra of the 10 NYNEX impulses. From Table 6.12, we see that in fact, the erasure declaration mechanism often does improve performance in terms of the resulting number of RS codeword errors.

Despite the somewhat improved performance offered by erasure decoding, the results in Table 6.12 show that many of the RS codewords may still be decoded incorrectly in the worst case impulses. With the exception of impulse 10, however, none of these can be detected by the time and frequency domain clipping techniques proposed earlier. An alternative approach to erasing only those tones marked as unreliable is to also erase the entire multicarrier block symbol whenever the number of unreliable tones exceeds a threshold. For the erasure thresholds used in this section and the BER requirement of ADSL, the probability of erasing a multicarrier symbol in the absence of impulse noise is exceedingly small. Tables 6.13 and 6.14 present the results obtained when the alternative erasure mechanism is employed in the same simulations used to generate Tables 6.11 and 6.12. The erasure threshold is set at 0.15 d^2, and in addition to erasing those tones marked as unreliable, the entire multicarrier symbol will be erased whenever more than four tones within the multicarrier symbol are marked as unreliable. As expected, the alternative technique leads to a substantial increase in the number of erasures, but it also enables the correction of all codewords, which is of course our ultimate goal. We note here that without any erasure mechanism, it is readily evident that the applied code needs to correct two multicarrier symbols' worth of data, while with erasure decoding, one multicarrier symbol's worth of data will be sufficient.

Other erasure techniques may be used to compromise between erasing an entire multicarrier symbol and erasing only tones marked as unreliable. For example, the decoder may take advantage of its knowledge of the shape of impulse spectra in declaring erasures. Specifically, we can assume that the impulse noise spectrum is

Impulse	Tones in Error	Tones Erased	Valid Erasures
1	41	96	36
2	41	84	15
3	956	9808	943
4	2371	9709	2370
5	126	976	122
6	212	820	162
7	5002	12363	4998
8	2042	3916	1958
9	1894	10789	1863
10	8362	10260	8362

Table 6.13: Total Number of Tones in Error, Tones Erased, and Valid Erasures with the Alternative Erasure Scheme for 10 NYNEX Impulses

Impulse	Codeword Errors w/ Erasures	Codeword Errors w/o Erasures
1	0	0
2	0	0
3	0	1
4	0	0
5	0	0
6	0	1
7	0	159
8	0	98
9	0	95
10	0	59

Table 6.14: Total Number of Codeword Errors with and without Erasure Decoding with the Alternative Erasure Scheme for 10 NYNEX Impulses

concentrated over a contiguous range of frequencies, and based on this assumption, the decoder may erase all tones between the lowest and highest tones that are marked as unreliable. However, this technique will in general require additional logic; therefore, it may not be as attractive from an implementational standpoint.

6.3.3 Soft Decision Error Control Enhancements

In Section 6.3.2, we have proposed and simulated several practical methods for enhancing the performance of an applied FEC code by providing side information regarding the occurrence of impulse noise events. Increased performance will also be obtained if additional knowledge of impulse characteristics can be exploited. As noted in [94], it may be reasonable to assume that the main source of impulses on a given subscriber loop is relatively constant; thus, the impulses experienced should be of a recurring shape in the frequency and/or time domain on a loop to loop basis. If the DMT transceiver can adaptively learn the spectral shape of the impulse noise and there is sufficient extra margin available, then the extra margin can be placed intelligently on those tones most susceptible to errors due to impulse noise.

The mean squared error monitoring technique discussed in Section 6.3.2 for erasing tones suggests an approach for obtaining a spectral estimate of the impulse noise. Typically, the error signal in Figure 6.18 is quite small as the required BER for ADSL is less than or equal to 10^{-7}. However, when an impulse occurs, most of the tones in which the magnitude of the impulse spectrum is large will show unusually high error signals. (We note that not all of the affected tones will share this property, because some of the received points will be driven well into the decision regions of neighboring points in the constellation.) To obtain an estimate of the impulse (magnitude) spectrum, or more precisely its relative strength across the subchannels, the occurrence of a large number of unusually high error signals over the used carriers in a DMT symbol is monitored. A common threshold is used to determine when the error signal on a particular subchannel is "unusually high", and when more than a predetermined number of tones have unusually high error signals, we declare that an impulse is likely to be present. Each time an impulse is detected, the estimate of the impulse spectrum is updated, using the mean squared

error signals on all of the subchannels. This operation may be expressed by the following running sum:

$$\alpha_{i,j} = \lambda\alpha_{i,j-1} + (1-\lambda)|E_{i,j}|^2 \,, \tag{6.16}$$

where $\alpha_{i,j}$ is the impulse spectral estimate on subchannel i at time j, $|E_{i,j}|^2$ is the mean squared error, and λ is a weighting term that determines the rate at which the estimate is obtained. We note that Equation (6.16) is similar to MSE running sum used in the adaptive bit swap algorithm described in Section 4.3.5. In our current case, however, we only perform the update in Equation (6.16) when an impulse is suspected. The resulting average, $\alpha_{i,j}$, is used to determine how we should optimally distribute the extra margin in an impulse noise environment.

One of the restrictions implied by our assumption of a recurring impulse spectral shape is that the received impulse waveform is normally contained completely within a single multicarrier symbol. If the significant duration of the impulse waveform is relatively small compared to the length of the multicarrier symbol period, then those cases in which the received impulse crosses multicarrier symbol boundaries will be quickly time averaged out in the application of Equation (6.16). Otherwise, longer time averaging or more sophisticated techniques are required.

To test the basic concepts presented in this section, impulses are again injected into a simulated multicarrier demodulator at a rate of about one every 100 DMT symbols. Various values for the "erasure threshold", R^2, are used to declare tones as having unusually large MSE's, and whenever the number of such tones exceeds a value of two, the update procedure given by Equation (6.16) is performed. The value for λ used in the averaging is chosen to be 0.7 for our simulations. We note that for the specified ADSL bit error rate, the probability that more than two tones will be erased is very small in the absence of some form of large noise disturbance. After every suspected 20 impulse occurrences, additional margin will be given to those subchannels with mean squared error estimates, $\alpha_{i,j}$'s, exceed a predetermined threshold, designated as *impthresh*. We will try two different methods for determining how much margin should be added to those subchannels corresponding to large MSE estimates. In the first method, the amount of margin

added will be constant, whereas in the second method, the amount of margin added to a subchannel depends on the MSE estimate associated with that subchannel. In particular, a minimum level of additional margin, *minmarg*, and a maximum level of additional margin, *maxmarg*, are specified, and the amount of margin added to subchannel i at the update time j_u, will be determined by:

$$marginadd_{i,j_u} = \left(\frac{maxmarg - minmarg}{\sigma^2_{maxdB} - \sigma^2_{mindB}}\right)(\alpha_{i,j_u} - \sigma^2_{mindB}) + minmarg\,, \quad (6.17)$$

where $\sigma^2_{maxdB} = \max_i\{\alpha_{i,j_u} \mid \alpha_{i,j_u} > impthresh\}$, $\sigma^2_{mindB} = \min_i\{\alpha_{i,j_u} \mid \alpha_{i,j_u} > impthresh\}$, and the range of i searched is restricted to those tones actually used for data transmission. All terms in Equation (6.17) are expressed in dB. The effect of adding margin to some of the tones is to force a change in the bit distribution by moving bits from carriers most affected by impulse noise to those tones less susceptible, using the adaptive bit swap algorithm presented in Section 4.3.5. This technique is more desirable than merely increasing the transmit power applied to susceptible subchannels and decreasing the transmit power on other subchannels, because that will lead to a wide variation in the level of transmit power across the transmission band.

Results obtained from our simulations are more easily interpreted if the crosstalk component of the noise is eliminated. The reason for this is because we want the impulse (magnitude) spectrum to be indicative of the degradation expected in each of the tones when an impulse occurs. This is not quite the case when spectrally shaped noise is included in the determination of the bit and energy distribution for the DMT system. Therefore, although we find the performance of our proposed techniques to be equally good whether spectrally shaped noise or purely white noise is used, we will only present the results for the latter case in the interest of clarity. Figure 6.20 presents the results obtained using the method of adding a fixed amount of margin on each update when NYNEX impulse 7 is injected under a test scenario where data at a rate of 1.6 Mbps is transmitted through a 18 kft, 24 AWG loop with 17 dBm of input power and a noise component consisting of AWGN only. Since there is a significant amount of margin available for this transmission scenario, we will allow the update process to add 3.0 dB of margin in each iteration and select a value

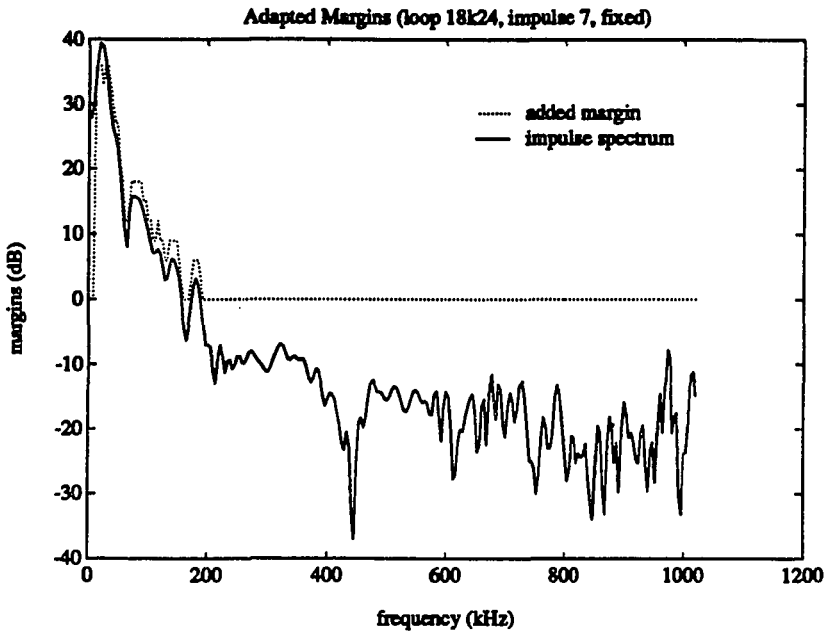

Figure 6.20: Margins for 18 kft, 24 AWG Loop with Impulse 7 and Fixed Updates

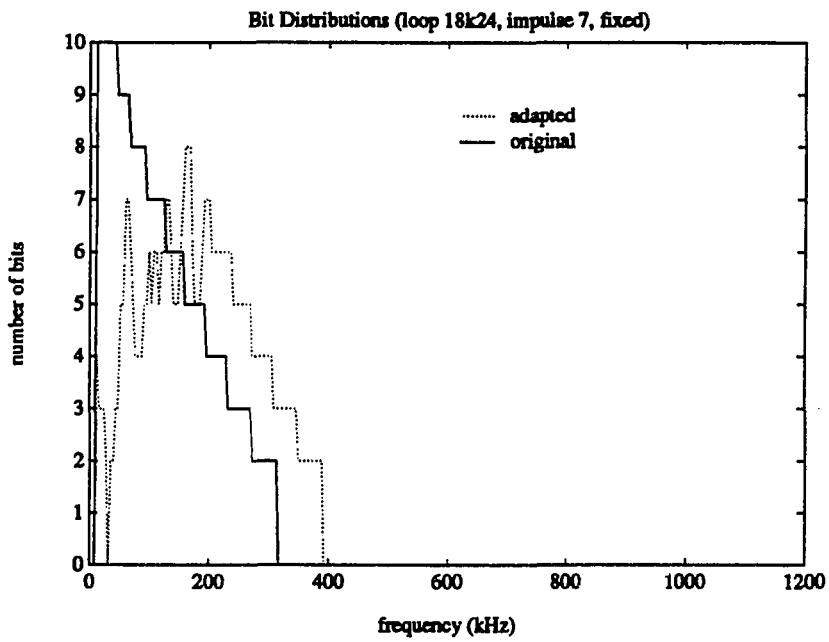

Figure 6.21: Bit Table for 18 kft, 24 AWG Loop, Impulse 7, and Fixed Updates

of 0.05 d^2 for *impthresh*. Furthermore, R^2 is set equal to 0.15 d^2 for determining the reliability of decisions on each of the tones. The dotted line in Figure 6.20 is the resulting distribution of additional margin while the solid line is the impulse spectrum, translated in the vertical direction to allow for an easier comparison. As is evident from the figure, this simple adaptation process will give additional margin to those tones most susceptible to the impulsive disturbance. We note that for this test scenario, the first two carriers are not used, which explains why no margin is added at 4 kHz and 8 kHz tones. Plots of the original bit distribution, before adaptation to the impulse noise spectrum, and the updated bit distribution at the conclusion of the adaptation process are presented in Figure 6.21. This figure clearly demonstrates the ability of a DMT system to move bits from the lower carriers to the higher carriers in order to avoid the large low frequency content of the injected impulse noise. In some instances, the amount of margin required, after adaptation, for a particular carrier that is initially used for data transmission is large enough to force the system to stop using that particular carrier and redistribute those bits among other carriers. For the original bit distribution, the highest carrier used is at 312 kHz, while for the bit distribution after adaptation, it is now at 388 kHz.

A second simulation is conducted in which the same values of R^2 and *impthresh* are used as before, but now Equation (6.17) is employed to determine the amount of update margins to use, instead of a constant amount. Values of 2.0 dB and 5.0 dB are chosen for *minmarg* and *maxmarg*, respectively, and the results are presented in Figures 6.22 and 6.23. Figure 6.22 indicates that updating the margins according to Equation (6.17) provides an improvement over adding fixed additional margin on each update. The resulting distribution of additional margin more closely follows the actual shape of the impulse spectrum than the margin distribution presented in Figure 6.20 for the case of constant updates. Furthermore, by comparing Figures 6.21 and 6.23, we find that the resulting bit distributions are indeed different for the two techniques. Figures 6.20 and 6.22 illustrate that the margin update process successfully increases the amount of error protection on those tones most susceptible to a particular impulse noise. However, as margin is reallocated, the performance of the other carriers will necessarily degrade. This is more clearly illustrated in

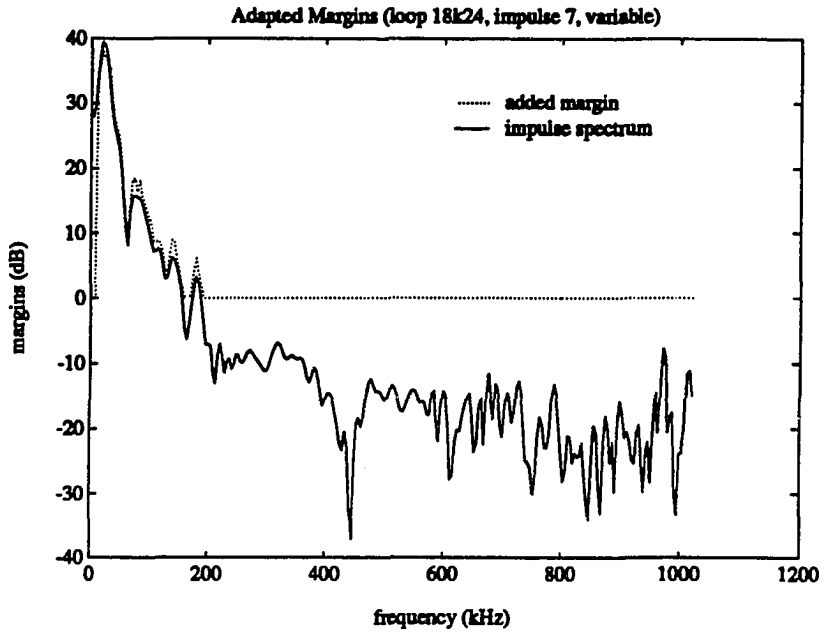

Figure 6.22: Margins for 18 kft, 24 AWG Loop with Impulse 7 and Variable Updates

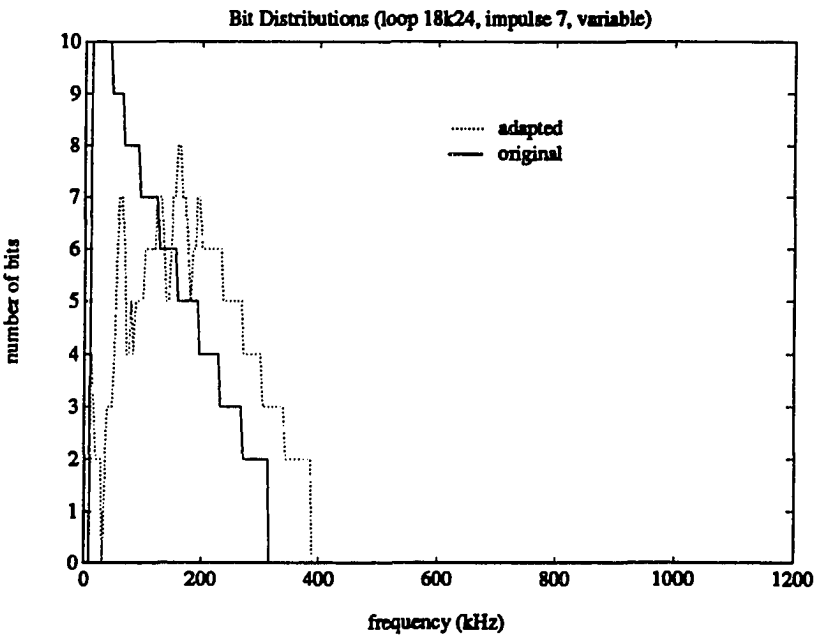

Figure 6.23: Bit Table for 18 kft, 24 AWG Loop, Impulse 7, and Variable Updates

Iteration Number	Fixed Margin: 3.0 dB		Variable Margin: 2.0-5.0 dB	
	Margin (dB)	Tones in Error	Margin (dB)	Tones in Error
1	28.0	318	28.0	312
2	27.0	241	26.8	220
3	26.1	219	25.6	213
4	25.1	206	24.5	197
5	24.3	197	23.6	167
6	23.4	169	22.7	130
7	22.8	146	21.9	100
8	22.2	127	21.2	97
9	21.7	115	20.8	17
10	21.1	92	20.4	0
11	20.7	67	–	–
12	20.2	34	–	–
13	19.9	8	–	–

Table 6.15: Margins and Number of Tones in Error for 18 kft, 24 AWG Loop with Impulse 7

Table 6.15, where we have listed the margin and number of tones in error at the start of each update for the two simulations. The margins in this table represent the margins on those subchannels to which no additional margin is given and are important in determining the overall BER of the system in the absence of impulse noise. In other words, the final margin values listed in this table may be added to the dotted line in Figure 6.20 or Figure 6.22 to obtain a plot of the total amount of margin at the end of the adaptation process, as a function of frequency. From this table, we also find that in both cases, the number of tones in error per impulse hit is driven to below an average value of one within 13 iterations. The case of variable margin updates will provide faster convergence, as well as a slightly better overall performance, than the case of fixed margin updates. However, the cost of this increased performance is the additional complexity of the technique, which may render the fixed margin update scheme more attractive from an implementational standpoint. In particular, the addition of a 3.0 dB margin to a subchannel is essentially equivalent to the reduction by one bit of the number of bits supported

by that subchannel, which in turn implies that a simple bit swap algorithm, as the one presented in Section 4.3.5, can be used with minor modifications.

We performed simulations similar to those discussed above for a test scenario where data transmitting at 1.6 Mbps is passed through ADSL loop 6 with 17 dBm of power, a lower bandedge of 70 kHz, a noise component consisting of AWGN only, and NYNEX impulse 9 injected periodically. Furthermore, we have allowed only 1.0 dB of additional margin per update for the case of fixed updates and a range of 1.0 to 2.0 dB for the variable margin update scheme, because the initial margin is only 8.0 dB for this test scenario. All other parameters have remained the same as before. Figures 6.24 to 6.27 present plots of the margin distributions and bit distributions obtained for the two margin update methods, respectively. The plots in Figures 6.24

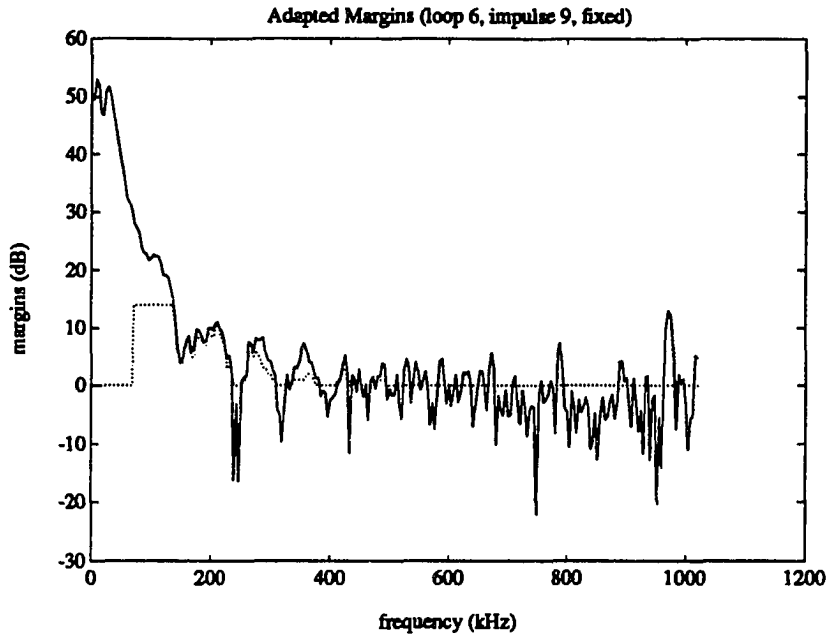

Figure 6.24: Margins for Loop 6 with Impulse 9 and Fixed Updates

and 6.26 further confirm that both techniques for adapting the margin distributions will result in increased margin on those tones most affected by impulse noise, and the technique that allows a range of margins to be added per update will provide better performance in terms of matching the distribution of additional margins to the

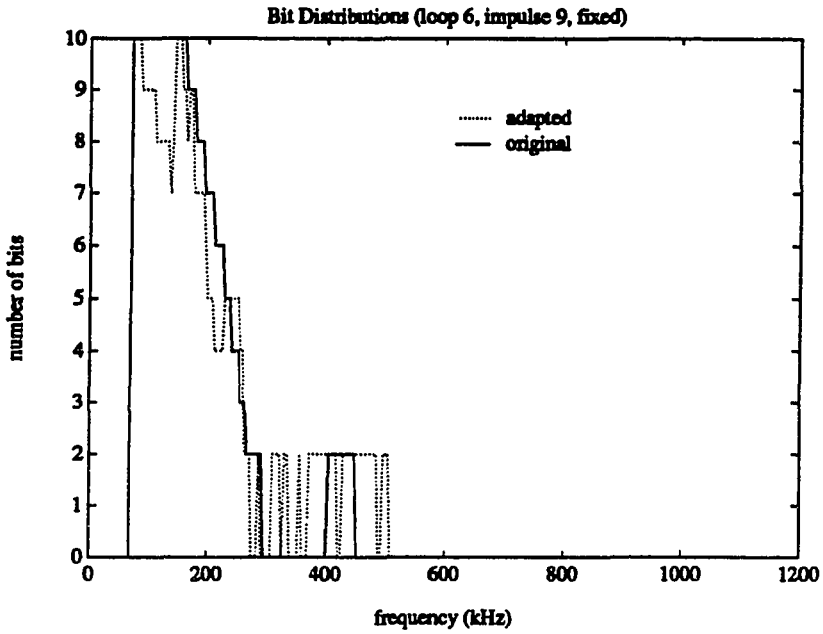

Figure 6.25: Bit Table for Loop 6, Impulse 9, and Fixed Updates

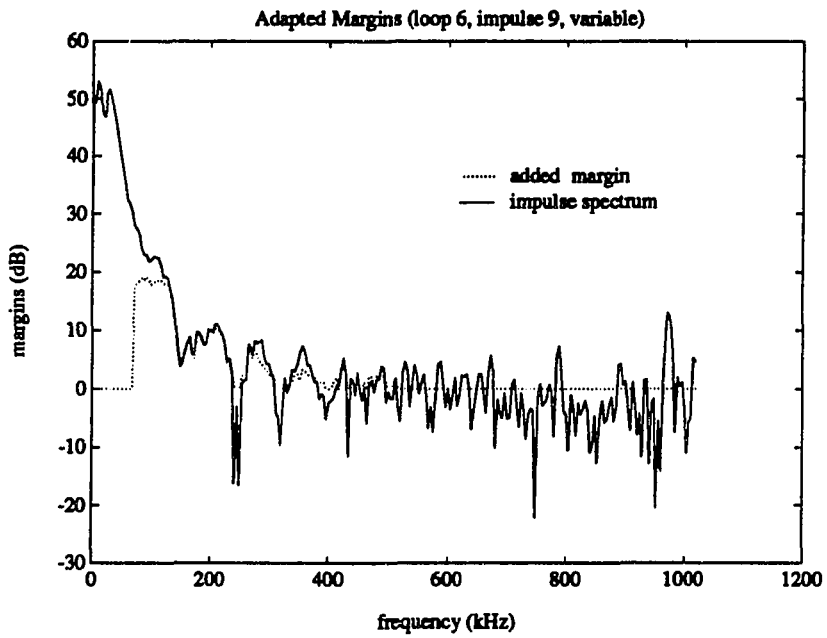

Figure 6.26: Margins for Loop 6 with Impulse 9 and Variable Updates

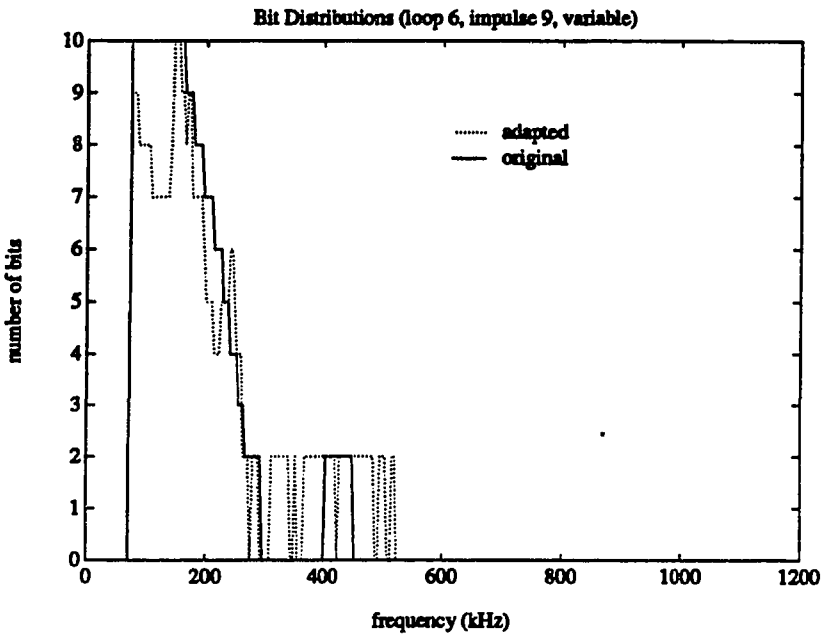

Figure 6.27: Bit Table for Loop 6, Impulse 9, and Variable Updates

actual shape of the impulse spectrum. We note that in this test scenario, carriers below 70 kHz are not used due to the lower bandedge of the system. However, there is still significant impulse noise energy in the frequency band available for transmission, and as is evident from the plots, there is not enough margin available to compensate fully for the large degradation in error rate caused by the impulse noise in the lower frequency tones. Table 6.16 lists the baseline margin and the number of tones in error at the start of each iteration in the margin adaptation process for this test scenario. The iterations are stopped when the baseline margin reached 3.0 dB. Although the limited availability of extra margin precludes the total elimination of errors due to impulse noise in this test scenario, the results in Table 6.16 show that significant performance improvement can be achieved over a system that provides an equal margin (equal bit error rate) across all the tones in an impulse noise environment. This, in turn, may lower the requirements on a FEC code applied to the system.

Iteration Number	Fixed Margin: 1.0 dB		Variable Margin: 1.0-2.0 dB	
	Margin (dB)	Tones in Error	Margin (dB)	Tones in Error
1	8.1	332	8.1	336
2	7.6	334	7.4	325
3	7.2	324	6.8	316
4	6.7	323	6.2	294
5	6.4	312	5.7	275
6	6.0	298	5.1	240
7	5.6	289	4.6	227
8	5.4	282	4.1	188
9	5.1	265	3.6	127
10	4.7	245	3.0	74
11	4.5	221	–	–
12	4.1	201	–	–
13	3.8	180	–	–
14	3.4	144	–	–
15	3.1	106	–	–

Table 6.16: Margins and Number of Tones in Error for Loop 6 with Impulse 9

Chapter 7

Conclusions

We began this dissertation with the goal of designing practical transmission bandwidth optimization algorithms that can be implemented with both multicarrier and single-carrier modulation schemes. We chose to first design bandwidth optimization algorithms following a multicarrier approach because frequency is the natural domain for equalization; therefore, from an implementational perspective, it appeared more convenient and efficient to optimize the transmission bandwidth with multicarrier modulation. By examining and comparing the properties of the two families of modulation and equalization techniques, we observed that virtually the same transmission bandwidth will be used to achieve the asymptotic optimal performance for both systems. This observation encouraged us to propose the use of multicarrier techniques for single-carrier systems as well. Along our development, we applied our proposed algorithms to specific DMT systems designed for advanced Digital Subscriber Line services, and in doing so, we realized that a continuously (that is, even after system initialization) adaptive transmitter is highly desirable, if not necessary, in these DSL transmission environments, where channels are in fact quasi-stationary and slowly time varying. Furthermore, we came across the interesting phenomenon of impulse noise while studying the transmission environment of copper twisted pairs in the current telephone network, which motivated us to develop effective multicarrier mitigation/cancellation strategies for impulse noise.

7.1 Summary of Results

In Chapter 2, we started with the necessary background material on a discrete-time ISI channel, and we described the well known Gap Approximation method of analyzing digital communication systems. We then reviewed the basics of an infinite-length, DMT system and an infinite-length, QAM system implemented with a MMSE-DFE receiver, as the representative structures of multicarrier modulation and single-carrier modulation, respectively. These two systems have been previously shown to achieve virtually the same asymptotic performance level, and we further showed that because nearly the same transmission bandwidth is used by both systems in achieving this asymptotic performance level, multicarrier transmission bandwidth optimization techniques can be applied to single-carrier systems as well.

In Chapter 3, we extended the infinite-length results from Chapter 2 to the finite-length case, and we discussed some practical implications of the finite-length constraint on the two families of modulation and equalization techniques. Materials in this chapter are not new; however, they are necessary for the development of the remaining chapters.

In Chapter 4, we focused on the problem of transmission bandwidth optimization. While a water-pouring energy distribution has previously been shown to achieve the channel capacity, it is generally difficult to implement in practice. We showed that a flat on/off energy distribution will perform virtually as well as a water-pouring energy distribution, as long as the correct transmission bandwidth is used, in many practical applications. We proved that the only independent parameters of optimization for a flat energy, bandwidth optimization algorithm are the data rate and the system performance margin. We presented a number of practical bandwidth optimization algorithms that can be implemented with either a multicarrier or a single-carrier system and that will maximize either the total data rate or the system performance margin. We showed that bandwidth optimization on a line-by-line basis is indeed critical for applications like ADSL and that if the same transmission bandwidth is used for all ADSL loops and data rates, it is possible

to lose up to more than 8 dB in performance relative to a bandwidth optimized transmission system. We extended our flat energy bandwidth optimization algorithms to practically realizable algorithms using only integer bit constellation sizes. We demonstrated that the loss of a practical, integer bit constellation size, bandwidth optimization algorithm with respect to a perfectly flat energy algorithm is relatively small, as long as we adjust the transmit energy levels accordingly on a subchannel-by-subchannel basis. We introduced the idea of adaptive transmitters for quasi-stationary duplex channels, and we proposed a simple bit swap algorithm designed specifically for a Discrete Multitone transceiver.

In Chapter 5, we applied our proposed bandwidth optimized DMT system to three advanced Digital Subscriber Line services: ADSL, E1-HDSL, and VHDSL. We showed that a bandwidth optimized DMT system can reliably deliver more than 6 Mbps over all CSA loops in an ADSL transmission environment, while a fixed symbol rate QAM system implemented with a MMSE-DFE cannot achieve the same performance level for all possible data rate and line combinations without major hardware modifications. We proved that in a FEXT-dominated transmission environment, the achievable data rate will eventually saturate with increasing transmit power level. Moreover, this saturation level is independent of channel characteristics except for the length of the loop. We showed that E1-HDSL service can be delivered reliably with either a dual-duplex mode or a dual-simplex mode of operation over British and German loop plants using a bandwidth optimized DMT transceiver. Finally, we demonstrated that very high data rates; that is, 50 Mbps or higher, are possible over short copper twisted pairs, as those encountered in VHDSL. We determined that the sampling rate is the most crucial system parameter in a DMT system designed for VHDSL and that NEXT is the most damaging impairment.

In Chapter 6, we examined the characteristics and studied the effects of impulse noise on a DMT system operating over an ADSL transmission environment. We proposed a number of impulse noise mitigation strategies designed specifically for a DMT transceiver that exploit both time and frequency domain characteristics of impulse noise and provide side information to the decoder for erasure declarations. Furthermore, we presented a soft decision, multicarrier, error control technique that

continuously adapts both the transmitter and the receiver during normal system operation and adjusts the target system performance margin on a subchannel-by-subchannel basis. Lastly, we tested our proposed impulse noise mitigation schemes through computer simulation and found them to be quite effective in reducing the damage of impulse noise.

7.2 Future Research

In this dissertation we have addressed one small, but key, component of the overall optimization of a digital communication system. Clearly, we have not answered many of the other important questions that are involved in realizing a practical system that approaches the channel capacity predicted by Shannon over forty-five years ago. In fact, we have not answered all of the questions about transmission bandwidth optimization alone. One natural and interesting extension to the work presented in this dissertation is to determine the optimal multirate signal processing structure for a single-carrier system that can efficiently realize variable transmission bandwidth. Another possible enhancement to our work is to coordinate the presently independent bandwidth optimization procedures for the two directions of transmission in a full-duplex system.

In the area of impulse noise mitigation, a complete analysis of impulse noise characteristics may yield valuable insight to the design of better coding schemes for these short-duration, high-amplitude disturbances. Practical impulse noise mitigation strategies that are capable of handling impulses lasting for hundreds of time samples in a single-carrier system are still open for research. Specially designed forward error control codes for either single-carrier or multicarrier systems that exploit the characteristics of the modulation and equalization structure in conjunction with the characteristics of impulse constitute yet another future research topic.

In the area of multicarrier modulation in general, while significant progress has been made in the past seven years at Stanford University within the "coders research group" alone, there are still a number of unanswered questions to be addressed. For

instance, the most cost-effective method of implementing coset codes within the multicarrier modulation structure without introducing unnecessary error propagation during decoding is still an open problem. The phenomenon of high peak-to-average power ratio of a multicarrier modulation system provides yet another challenging problem. Modulating and demodulating basis vectors other than the IDFT/DFT vectors and the channel eigenvectors may also be considered. The application of multicarrier modulation to other transmission environments that are significantly different from copper twisted pairs, such as wireless communication in Digital Audio Broadcast (DAB) and video transmission of High Definition Television (HDTV) signals over coaxial cable, may uncover problems that are of both implementational and theoretical interest as well. While Shannon has shown that source coding and channel coding can be completely separated without affecting performance, there may be implementational advantages in considering them in conjunction with one another, especially in the case of combined equalization and coding with multicarrier modulation, where both time domain and frequency domain signals are available at both the transmitter and the receiver.

Appendix A

Optimal Energy for FEXT+AGN Channels

In this appendix, we derive a closed form solution of the optimal energy allocation for a DMT system in the presence of additive (possibly colored) Gaussian noise and far-end crosstalk (FEXT) interference. This type of transmission environment is encountered in ADSL and merits our attention.

Generally speaking, there are four system parameters to be considered when one tries to optimize system energy (power) allocation; namely the data rate, the noise margin, the total input power, and the probability of bit error. When three out of the four system parameters are held constant, we can optimized the system with respect to the remaining parameter. For example, with a given noise margin, a desired bit error rate, and a total input power constraint, we can derive the optimal energy allocation that will yield the highest data rate. The appropriate parameter to be optimized is application dependent. For instance, the noise margin should be the practical optimization parameter for the current ADSL service, where the total throughput data rate, the minimum acceptable bit error rate (therefore the probability of error), and the maximum input power are precisely defined. On the other hand, for applications where a progressive compression coding scheme is employed, we may want to optimize the system in order to operate at the highest possible data rate with margin, input power, and bit error rate fixed. Furthermore,

if we assume that the gap approximation introduced in Section 2.2 is accurate, then the optimal energy allocation that achieves the minimum probability of error and the optimal solution that obtains the maximum noise margin will be exactly the same, because the resulting energy allocation for both will lead to the maximization of the gap. However, the optimal energy allocation may be different for the other two criteria. In this appendix, we will focus on the case where the optimization parameter is chosen to be the data rate. However, similar procedure can be applied to obtain the optimized bit allocations that will maximize margin (equivalently, minimize the bit error rate) or minimize the input power constraint.

To obtain the optimal energy allocation that maximizes the throughput data rate, we start by examining the noise component within each subchannel of the DMT system, and this noise component can be expressed as[1]:

$$\sigma_i^2 = (K_i \mathcal{E}_i |H_i|^2) + 2\sigma_{AGN_i}^2 \quad , \tag{A.1}$$

where $\sigma_{AGN_i}^2$ is the noise energy or variance per dimension due to the additive Gaussian noise component in the i^{th} subchannel, $\mathcal{E}_i$ is the transmit energy in the i^{th} subchannel, $|H_i|^2$ is the power spectral density of the i^{th} subchannel, and finally, $K_i = K_{FEXT}\ d\ f_i^2$ is a multiplicative constant for the i^{th} subchannel with $K_{FEXT} \approx 8 \times 10^{-20}$, d being the length of the transmission line in feet, and f_i being the center frequency of the i^{th} subchannel in Hz. The $K_i \mathcal{E}_i |H_i|^2$ term represents the FEXT component. Here we have assumed that FEXT is directly proportional to self transmit energy; therefore, as the self transmit energy changes, so does the FEXT component. In reality, this may not be completely accurate, because the FEXT component is really dependent on the transmit energies used by other transmitters at the far-end, which may employ different energy allocation schemes. In fact, if we assume that other far-end transmitters all employ some fixed, known energy allocation schemes regardless of our transmitter, then the noise component within each subchannel can be considered as entirely of AWGN, and the noise component across the entire system bandwidth can be considered as additive colored Gaussian

[1]In this appendix we will use a slightly different notation from earlier chapters in this dissertation in order to more compactly and clearly express certain equations. In particular, all quantities relating to the i^{th} subchannel of a DMT system will be expressed as x_i's instead of $x(i)$'s as in earlier chapters.

noise (ACGN). In that case, the optimization problem is greatly simplified, and the solution is the standard water-pouring energy allocation as shown in [29].

We will now proceed with the assumption that Equation (A.1) accurately models the actual noise component in the i^{th} subchannel[2]. Furthermore, assuming noises are independent between subchannels, then from Section 2.3.2 we know that the i^{th} subchannel can support approximately b_i bits in one block symbol with a gap factor of Γ, where:

$$b_i = log_2\left(1 + \frac{\mathcal{E}_i|H_i|^2}{\sigma_i^2\Gamma}\right) \quad . \tag{A.2}$$

Let the total number of bits per block symbol due to all N subchannels be:

$$B_{total} = \sum_{i=1}^{N} b_i \quad , \tag{A.3}$$

and let the total energy constraint per block symbol be:

$$\mathcal{E}_{total} = \sum_{i=1}^{N} \mathcal{E}_i \quad . \tag{A.4}$$

We are now in position to maximize B_{total} using the standard Lagrange multiplier technique, and we form the following cost function with Lagrange multiplier λ:

$$G = B_{total} + \lambda(\mathcal{E}_{total} - \sum_{i=1}^{N} \mathcal{E}_i) \tag{A.5}$$

$$= \sum_{i=1}^{N} log_2\left(1 + \frac{\mathcal{E}_i|H_i|^2}{\sigma_i^2\Gamma}\right) + \lambda(\mathcal{E}_{total} - \sum_{i=1}^{N} \mathcal{E}_i) \tag{A.6}$$

$$= \sum_{i=1}^{N} log_2\left(1 + \frac{\mathcal{E}_i|H_i|^2}{\Gamma(K_i\mathcal{E}_i|H_i|^2 + 2\sigma_{AGN_i}^2)}\right) + \lambda(\mathcal{E}_{total} - \sum_{i=1}^{N} \mathcal{E}_i) \quad . \tag{A.7}$$

We now take a series of partial derivatives of the cost function G with respect to each of the $\mathcal{E}_i$'s and set each of the resulting equations to zero; that is, $\frac{\partial G}{\partial \mathcal{E}_i} = 0$. We get the following:

$$\frac{\partial G}{\partial \mathcal{E}_i} = \frac{\partial}{\partial \mathcal{E}_i}\left(log_2\left[1 + \frac{\mathcal{E}_i|H_i|^2}{\Gamma K_i\mathcal{E}_i|H_i|^2 + \Gamma 2\sigma_{AGN_i}^2}\right]\right) - \lambda \quad , \tag{A.8}$$

[2]In this case, it turns out that the unique solution, regardless of the optimization parameter that we choose, requires us to solve a set of very complicated quadratic equations. Therefore, these closed form solutions are mainly of theoretical interest and serve as upper bounds in performance when evaluating practical energy allocation algorithms.

$$0 = \frac{\partial}{\partial \mathcal{E}_i}\left(log_2\left[\frac{\Gamma K_i \mathcal{E}_i |H_i|^2 + \Gamma 2\sigma^2_{AGN_i} + \mathcal{E}_i |H_i|^2}{\Gamma K_i \mathcal{E}_i |H_i|^2 + \Gamma 2\sigma^2_{AGN_i}}\right]\right) - \lambda \quad (A.9)$$

$$= \frac{\partial}{\partial \mathcal{E}_i}\left(log_2[\mathcal{E}_i A_i + B_i] - log_2[\mathcal{E}_i C_i + B_i]\right) - \lambda \ , \quad (A.10)$$

where:

$$A_i = |H_i|^2(1 + \Gamma K_i) \ , \quad (A.11)$$

$$B_i = \Gamma 2\sigma^2_{AGN_i} \ , \quad (A.12)$$

$$C_i = \Gamma K_i |H_i|^2 \ . \quad (A.13)$$

In terms of A_i, B_i, and C_i, we get:

$$0 = (log_2\, e)\left[\left(\frac{A_i}{\mathcal{E}_i A_i + B_i}\right) - \left(\frac{C_i}{\mathcal{E}_i C_i + B_i}\right)\right] - \lambda \quad (A.14)$$

$$= \frac{B_i(A_i - C_i)}{(\mathcal{E}_i A_i + B_i)(\mathcal{E}_i C_i + B_i)} - \frac{\lambda}{log_2\, e} \ . \quad (A.15)$$

Now let $\lambda' = \frac{\lambda}{log_2\, e}$, and after some straightforward rearrangement, we get:

$$(\lambda' A_i C_i)\mathcal{E}_i^2 + (\lambda'(A_i + C_i)B_i)\mathcal{E}_i + (\lambda' B_i - A_i + C_i)B_i = 0 \ . \quad (A.16)$$

This is a quadratic equation with variable $\mathcal{E}_i$, and it can be solved with the standard quadratic formula. So let:

$$\alpha_i = \lambda' A_i C_i \ , \quad (A.17)$$

$$\beta_i = \lambda'(A_i + C_i)B_i \ , \quad (A.18)$$

$$\gamma_i = (\lambda' B_i - A_i + C_i)B_i \ , \quad (A.19)$$

and we have:

$$\mathcal{E}_i = \frac{-\beta_i \pm \sqrt{\beta_i^2 - 4\alpha_i\gamma_i}}{2\alpha_i} \ , \quad (A.20)$$

Because $\mathcal{E}_i \geq 0$ and A_i, B_i, C_i are all positive constants, we can discard the solution that results from the negative square root, and our desired solution is given by:

$$\mathcal{E}_i = \frac{-\lambda'(A_i + C_i)B_i + \sqrt{(\lambda'(A_i + C_i)B_i)^2 - 4(\lambda' A_i C_i)(\lambda' B_i - A_i + C_i)B_i}}{2\lambda' A_i C_i} \quad (A.21)$$

$$= \frac{-\lambda'(A_i + C_i)B_i + \sqrt{|H_i|^2 \lambda' B_i(|H_i|^2 \lambda' B_i + 4A_i C_i)}}{2\lambda' A_i C_i} \quad (A.22)$$

$$= \frac{-(A_i + C_i)B_i + \sqrt{|H_i|^2 B_i(|H_i|^2 B_i + \frac{4A_i C_i}{\lambda'})}}{2A_i C_i} \ . \quad (A.23)$$

In conjunction with our original energy constraint, which can be expressed as a function of the Lagrange multiplier λ as:

$$\mathcal{E}_{total}(\lambda) = \sum_{i=1}^{N} \mathcal{E}_i(\lambda) = f(\lambda) \quad , \tag{A.24}$$

we now have a set of $N+1$ equations and $N+1$ unknowns, which can be solved uniquely to yield the optimal energy allocation and the desired λ for a DMT system operating over a noisy channel with FEXT and AGN. However, as it is very difficult to solve for λ and $\mathcal{E}_i$'s directly, we can find the desired solution iteratively by choosing a value for λ', solving for $\mathcal{E}_i$'s from Equation (A.23), summing the $\mathcal{E}_i$'s together to see if the initial energy constraint is met to within some acceptable threshold, and updating the estimate of λ' as required until the initial energy constraint is met to within some acceptable threshold. We caution here that the condition:

$$\mathcal{E}_i \geq 0 \tag{A.25}$$

must also be satisfied for all i's; therefore, we need to discard those worst subchannels with negative $\mathcal{E}_i$'s when summing up the $\mathcal{E}_i$'s.

Appendix B

Two-Port Transmission Line Theory

In this appendix, we review the method that is used to calculate two-port transmission line characteristics.

B.1 Transmission Line Basics

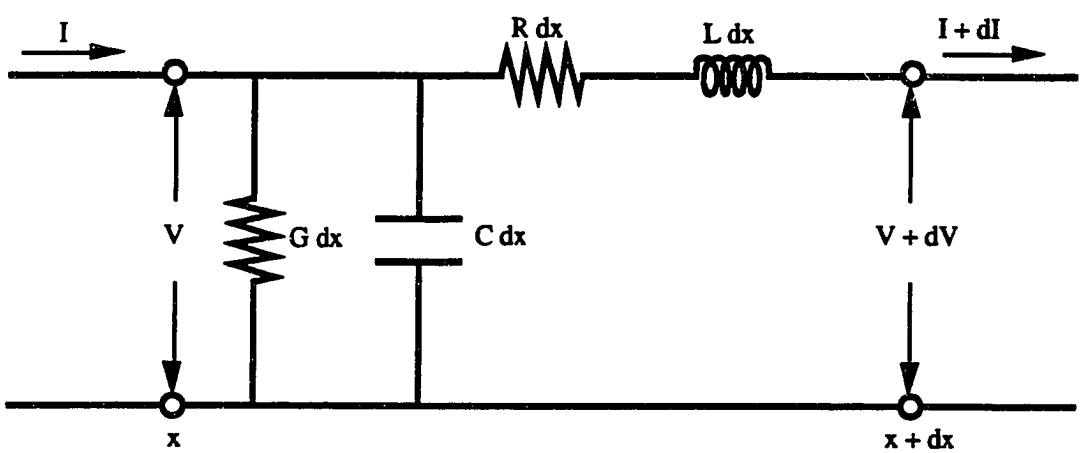

Figure B.1: Section of Loop *dx* in Length

A transmission line can be described in terms of infinitesimally small segments that are modelled as shown in Figure B.1. The line is characterized by its four primary parameters:

1. parallel conductance per unit length G,
2. capacitance per unit length C,
3. series resistance per unit length R, and
4. inductance per unit length L.

These parameters are sometimes called the line's *primary constants*, and they are usually determined by empirical data. Furthermore, they can be functions of frequency themselves. The network section shown is what is known as a *two-port network* and has input current I, input voltage V, output current $I + dI$, and output voltage $V + dV$. The voltage and current are functions of loop length l and of frequency f, and they are denoted by $V(l, f)$ and $I(l, f)$.

We can calculate the two secondary parameters of the line section from the four primary parameters as:

1. propagation constant, $\gamma(\omega)$,

$$\gamma(\omega) = \alpha(\omega) + \jmath\beta(\omega) = \sqrt{(R + \jmath\omega L) \cdot (G + \jmath\omega C)} \quad , \tag{B.1}$$

   where $\omega = 2\pi f$ and f is the frequency in Hz;

2. characteristic impedance, $Z_o(\omega)$,

$$Z_o(\omega) = \sqrt{\frac{R + \jmath\omega L}{G + \jmath\omega C}} \quad . \tag{B.2}$$

Recall that for a perfectly terminated (load impedance $Z_l = Z_o$ and source impedance $Z_s = Z_o$) loop with length l, the steady-state transfer function is given by:

$$\frac{V(l, f)}{V(0, f)} = H(l, f) = e^{-l\gamma(f)} = e^{-l\alpha(f)} \cdot e^{-\jmath l\beta(f)} \quad . \tag{B.3}$$

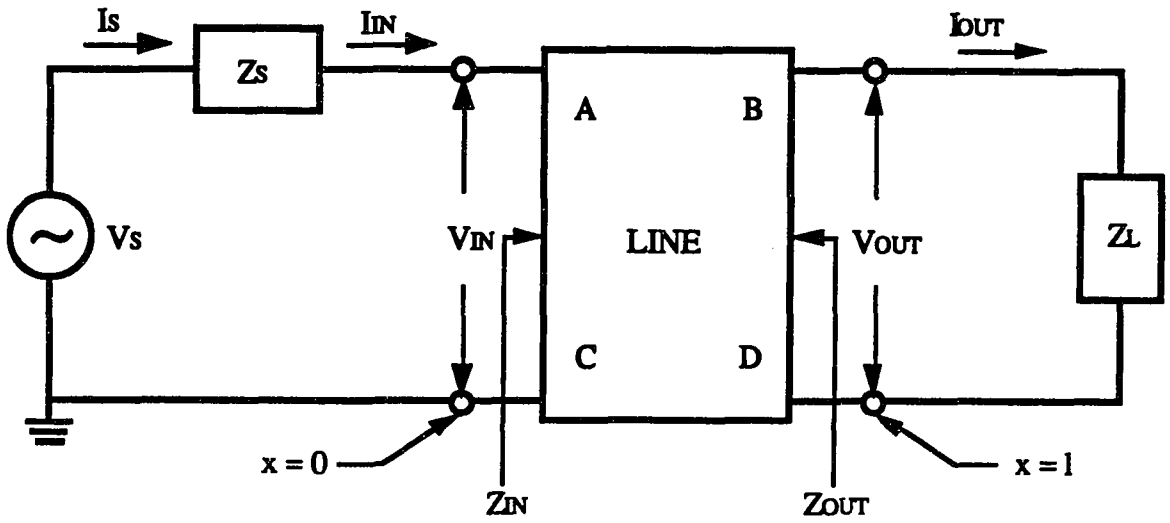

Figure B.2: Two-Port Network

B.2 Steady-State Two-Port Network Analysis

A general two-port network configuration is shown in Figure B.2. The relation between input and output voltages and currents can be written as:

$$\begin{bmatrix} V_s \\ I_s \end{bmatrix} = \begin{bmatrix} 1 & Z_s \\ 0 & 1 \end{bmatrix} \begin{bmatrix} A & B \\ C & D \end{bmatrix} \begin{bmatrix} V_{out} \\ I_{out} \end{bmatrix} \quad . \tag{B.4}$$

For straight transmission line of length l with no gauge changes or bridged taps, these above relations are characterized by:

$$A = D = \cosh(\gamma l) \quad , \tag{B.5}$$

$$B = Z_o \sinh(\gamma l) \quad , \tag{B.6}$$

$$C = Z_o^{-1} \sinh(\gamma l) \quad . \tag{B.7}$$

Some useful relationships are:

$$\begin{bmatrix} V_{in} \\ I_{in} \end{bmatrix} = \begin{bmatrix} A & B \\ C & D \end{bmatrix} \begin{bmatrix} V_{out} \\ I_{out} \end{bmatrix} \tag{B.8}$$

$$= \begin{bmatrix} (AV_{out} + BI_{out}) \\ (CV_{out} + DI_{out}) \end{bmatrix} \quad , \tag{B.9}$$

and

$$\frac{V_{out}}{V_{in}} = \frac{V_{out}}{AV_{out} + BI_{out}} \tag{B.10}$$

$$= \frac{V_{out}}{AV_{out} + BV_{out}Z_L^{-1}} \tag{B.11}$$

$$= \frac{Z_L}{AZ_L + B} \ . \tag{B.12}$$

Also,

$$V_{in} = V_s \frac{Z_{in}}{Z_{in} + Z_s} \ , \tag{B.13}$$

$$Z_{in} = \frac{V_{in}}{I_{in}} \tag{B.14}$$

$$= \frac{AV_{out} + BI_{out}}{CV_{out} + DI_{out}} \tag{B.15}$$

$$= \frac{A + BZ_L^{-1}}{C + DZ_L^{-1}} \tag{B.16}$$

$$= \frac{AZ_L + B}{CZ_L + D} \ , \tag{B.17}$$

and

$$V_{out} = V_{in} \frac{Z_L}{AZ_L + B} \tag{B.18}$$

$$= V_s \left(\frac{Z_{in}}{Z_{in} + Z_s}\right)\left(\frac{Z_L}{AZ_L + B}\right) \tag{B.19}$$

$$= V_s \left(\frac{AZ_L + B}{CZ_L + D}\right)\left(\frac{CZ_L + D}{AZ_L + B + CZ_sZ_L + DZ_s}\right)\left(\frac{Z_L}{AZ_L + B}\right) \tag{B.20}$$

$$= V_s \frac{Z_L}{AZ_L + B + CZ_sZ_L + DZ_s} \ . \tag{B.21}$$

From the expression of V_{out} given above, we are now in position to compute the channel transfer function, $H(f)$, of the loop as follows:

$$H(f) = \frac{V_{out}}{V_s} \tag{B.22}$$

$$= \frac{Z_L}{AZ_L + B + CZ_sZ_L + DZ_s} \ . \tag{B.23}$$

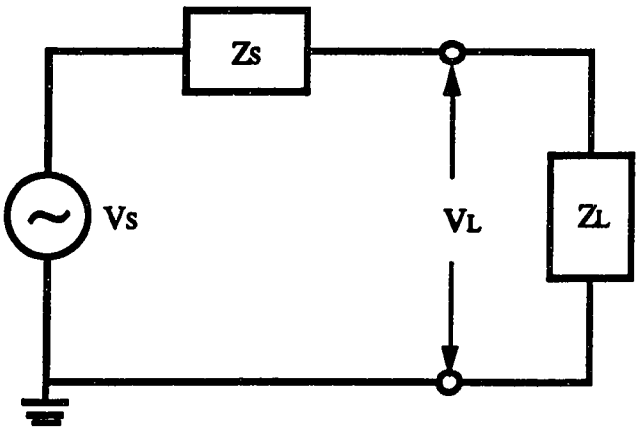

Figure B.3: Network with Line Removed

Instead of channel transfer function, loops for data transmission systems are often specified in terms of their insertion loss, or insertion loss transfer function[1]. We will now derive the expression for insertion loss transfer function in terms of our two-port network ABCD matrix. With reference to Figures B.2 and B.3, insertion loss transfer function, $H_{insert}(f)$ is defined as:

$$H_{insert}(f) = \frac{V_{out}}{V_L} \tag{B.24}$$

$$= \frac{V_s(\frac{Z_L}{AZ_L+B+CZ_sZ_L+DZ_s})}{V_s(\frac{Z_L}{Z_L+Z_s})} \tag{B.25}$$

$$= \frac{Z_L+Z_s}{AZ_L+B+CZ_sZ_L+DZ_s} \quad . \tag{B.26}$$

Therefore, if we have the condition such that $Z_L = Z_s$, then the channel transfer function is related to the insertion loss transfer function by the following simple relationships:

$$H_{insert}(f) = 2H(f) \tag{B.27}$$

$$|H_{insert}(f)| = 2|H(f)| \tag{B.28}$$

$$|H_{insert}(f)|^2 = 4|H(f)|^2 = |H(f)|^2 + 6dB \quad . \tag{B.29}$$

[1]Insertion loss is defined as 20 $log_{10}(\frac{V_L}{V_{out}})$ in dB. However, because this is a "loss", we define the corresponding insertion loss "transfer function" as the inverse, or 20 $log_{10}(\frac{V_{out}}{V_L})$ in dB.

Bibliography

[1] C.E. Shannon. A Mathematical Theory of Communication: Part I. *The Bell Systems Technical Journal*, 27:379–423, July 1948.

[2] C.E. Shannon. A Mathematical Theory of Communication: Part II. *The Bell Systems Technical Journal*, 27:623–657, October 1948.

[3] G. Ungerboeck. Channel Coding with Multilevel/Phase Signals. *IEEE Transactions on Information Theory*, 28(1):55–67, January 1982.

[4] G.D. Forney Jr. Coset Codes - Part I: Introduction and Geometrical Classification. *IEEE Transactions on Information Theory*, 34(5):1123–1151, September 1988.

[5] G.D. Forney Jr. Coset Codes - Part II: Binary Lattices and Related Codes. *IEEE Transactions on Information Theory*, 34(5):1152–1187, September 1988.

[6] G.D. Forney Jr. and A.R. Calderbank. Coset Codes for Partial Response Channels; or Coset Codes with Spectral Nulls. *IEEE Transactions on Information Theory*, 35(5):925–943, September 1989.

[7] M.V. Eyuboglu and G.D. Forney Jr. Trellis Precoding: Combined Coding, Precoding and Shaping for Intersymbol Interference Channels. *IEEE Transactions on Information Theory*, 38(2):301–314, March 1992.

[8] S. Kasturia, J. Aslanis, and J.M. Cioffi. Vector Coding for Partial-Response Channels. *IEEE Transactions on Information Theory*, 36(4):741–762, July 1990.

[9] A. Ruiz, J.M. Cioffi, and S. Kasturia. Discrete Multiple Tone Modulation with Coset Coding for the Spectrally Shaped Channel. *IEEE Transactions on Communications*, 40(6):1012–1029, June 1992.

[10] J.M. Cioffi, G.P. Dudevoir, M.V. Eyuboglu, and G.D. Forney Jr. MMSE Decision-Feedback Equalizers and Coding - Part I: General Results. *IEEE Transactions on Communications*. To appear.

[11] N.A. Zervos and I. Kalet. Optimized Decision Feedback Equalization versus Optimized Orthogonal Frequency Division Multiplexing for High-Speed Data Transmission over the Local Cable Network. In *International Conference on Communications*, pages 1080–1085, Boston, MA, June 1989.

[12] P.S. Chow, J.M. Cioffi, and J.A.C. Bingham. Bandwidth Optimization for Data Transmission over Spectrally Shaped Channels. To be submitted to *IEEE Transactions on Communications*.

[13] P.S. Chow and J.M. Cioffi. Bandwidth Optimization for High Speed Data Transmission over Channels with Severe Intersymbol Interference. In *1992 IEEE Global Telecommunications Conference*, pages 59–63, Orlando, FL, December 1992.

[14] P.S. Chow and J.M. Cioffi. Method and Apparatus for Adaptive, Variable Bandwidth, High-Speed Data Transmission of a Multicarrier Signal over Digital Subscriber Lines. U.S. Patent application, filed May, 1993.

[15] P.S. Chow, J.A.C. Bingham, and J.M. Cioffi. Method for Loading a Multicarrier Signal in a Multicarrier Communication System. U.S. Patent application, in preparation.

[16] P.S. Chow, N. Al-Dhahir, J.M. Cioffi, and J.A.C. Bingham. A Multicarrier E1-HDSL Transceiver System with Coded Modulation. *European Transactions on Telecommunications and Related Technologies*. To appear.

[17] P.S. Chow, J.C. Tu, and J.M. Cioffi. Performance Evaluation of a Multichannel Transceiver System for ADSL and VHDSL. *IEEE Journal on Selected Areas in Communications*, 9(6):909–919, August 1991.

[18] P.S. Chow, J.C. Tu, and J.M. Cioffi. A Multichannel Transceiver System for Asymmetric Digital Subscriber Line Service. In *1991 IEEE Global Telecommunications Conference*, pages 56.5.1–56.5.5, Phoenix, AZ, December 1991.

[19] T.N. Zogakis, P.S. Chow, and J.M. Cioffi. Impulse Noise Mitigation Strategies for Multicarrier Modulation. To be submitted to *IEEE Transactions on Communications*.

[20] T.N. Zogakis, P.S. Chow, J.T. Aslanis, and J.M. Cioffi. Impulse Noise Mitigation Strategies for Multicarrier Modulation. In *1993 International Conference on Communications*, Geneva, Switzerland, May 1993.

[21] R.E. Blahut. *Theory and Practice of Error Control Codes*. Addison-Wesley, Menlo Park, CA, 1983.

[22] I. Kalet and S. Shamai (Shitz). On the Capacity of a Twisted-Wire Pair: Gaussian Model. *IEEE Transactions on Communications*, 38(3):379–383, March 1990.

[23] J.A.C. Bingham. Multicarrier Modulation for Data Transmission : An Idea whose Time has Come. *IEEE Communications Magazine*, 28(5):5–14, May 1990.

[24] I. Kalet. The Multitone Channel. *IEEE Transactions on Communications*, 37(2):119–124, February 1989.

[25] J.W. Lechleider. The Optimum Combination of Block Codes and Receivers for Arbitrary Channels. *IEEE Transactions on Communications*, 38(5):615–621, May 1990.

[26] J.S. Chow, J.C. Tu, and J.M. Cioffi. A Discrete Multitone Transceiver System for HDSL Applications. *IEEE Journal on Selected Areas in Communications*, 9(6):895–908, August 1991.

[27] G.P. Dudevoir. *Equalization Techniques for High Rate Digital Transmission on Spectrally Shaped Channel.* PhD thesis, Stanford University, December 1989.

[28] M.A. Tzannes, M.C. Tzannes, and H. Resnikoff. The DWMT: A Multicarrier Transceiver for ADSL Using M-band Wavelet Transforms. In *ANSI T1E1.4 Committee Contribution, No. 93-67*, Miami, FL, March 1993.

[29] J.C. Tu. *Theory, Design and Application of Multi-Channel Modulation for Digital Communications.* PhD thesis, Stanford University, June 1991.

[30] J.C. Tu and J.M. Cioffi. A Loading Algorithm for the Concatenation of Coset Codes with Multichannel Modulation Methods. In *Global Telecommunications Conference*, pages 1183–1187, San Diego, CA, December 1990.

[31] E.A. Lee and D.G. Messerschmitt. *Digital Communication.* Kluwer, Boston, MA, 1988.

[32] R. Price. Nonlinearly Feedback-Equalized PAM versus Capacity for Noisy Filter Channels. In *International Conference on Communications*, pages 22.12 – 22.17, Philadelphia, PA, June 1972.

[33] J. Salz. Optimum Mean-Square Decision Feedback Equalization. *The Bell System Technical Journal*, 52(8):1341–1373, October 1973.

[34] D.D. Falconer and G.J. Foschini. Theory of Minimum Mean-Square-Error QAM Systems Employing Decision Feedback Equalization. *The Bell System Technical Journal*, 52(10):1821–1849, December 1973.

[35] C.A. Belfiore and J.H. Park Jr. Decision Feedback Equalization. *Proceedings of IEEE*, 67(8):1143–1156, August 1979.

[36] M. Tomlinson. New Automatic Equalizers Employing Modulo Arithmetic. *Electronics Letters*, 7(3):138–139, March 1971.

[37] H. Harashima and H. Miyakawa. Matched-Transmission Technique for Channels with Intersymbol Interference. *IEEE Transactions on Communications*, 20(8):774–780, August 1972.

[38] G.D. Forney Jr. Maximum-Likelihood Sequence Estimation of Digital Sequences in the Presence of Intersymbol Interference. *IEEE Transactions on Information Theory*, 18(3):363–378, May 1972.

[39] W.Y. Chen, G.H. Im, and J.J. Werner. Design of Digital Carrierless AM/PM Transceivers. In *ANSI T1E1.4 Committee Contribution, No. 92-149*, Portland, OR, August 1992.

[40] T. Ericson. Structure of Optimum Receiving Filters in Data Transmission. *IEEE Transactions on Information Theory*, 17(3):353, May 1971.

[41] A. Ruiz. *Frequency-Designed Coded Modulation for Channels with Intersymbol Interference.* PhD thesis, Stanford University, January 1989.

[42] J.S. Chow. *Finite-Length Equalization for Multi-Carrier Transmission Systems.* PhD thesis, Stanford University, June 1992.

[43] A.V. Oppenheim and R.W. Schafer. *Digital Signal Processing.* Prentice-Hall, Englewood Cliffs, NJ, 1975.

[44] J.S. Chow. Private communication. Amati Communications Corporation, August, 1992.

[45] J.S. Chow, J.M. Cioffi, and J.A.C. Bingham. Equalizer Training Algorithms for Multicarrier Modulation Systems. In *1993 International Conference on Communications*, Geneva, Switzerland, May 1993.

[46] J.S. Chow and J.M. Cioffi. Method for Equalizing a Multicarrier Signal in a Multicarrier Communication System. U.S. Patent application, filed June, 1992.

[47] J.M. Cioffi, P.H. Algoet, and P.S. Chow. Combined Equalization and Coding with Finite-Length Decision Feedback Equalization. In *1990 IEEE Global Telecommunications Conference*, pages 807.2.1–807.2.5, San Diego, CA, December 1990.

[48] N.M.W. Al-Dhahir and J.M. Cioffi. MMSE Decision Feedback Equalizers and Coding - Part II: Finite-Length Results. In preparation.

[49] T. Kailath. *Linear Systems.* Prentice-Hall, Englewood Cliffs, NJ, 1980.

[50] N.M.W. Al-Dhahir and J.M. Cioffi. Optimal Transmit Filters for Packet-Based Data Transmission on Dispersive Channels with Application to the FIR MMSE-DFE. To be submitted to *IEEE Transactions on Information Theory.*

[51] R.G. Gallager. *Information Theory and Reliable Communication.* Wiley, New York, NY, 1968.

[52] T.M. Cover and J.A. Thomas. *Elements of Information Theory.* Wiley, New York, NY, 1991.

[53] P.H. Algoet and J.M. Cioffi. How to Achieve the Capacity of a Vector Channel with Additive Gaussian Noise. In preparation.

[54] N.M.W. Al-Dhahir and J.M. Cioffi. Symbol Rate Optimization for the MMSE-DFE on Bandlimited Dispersive Channels. In preparation.

[55] D. Hughes-Hartogs. Emsemble Modem Structure for Imperfect Transmission Media. U.S. Patents Nos. 4,679,227 (July 1987), 4,731,816 (March 1988) and 4,833,706 (May 1989).

[56] J.A.C. Bingham. Private communication. Amati Communications Corporation, July, 1992.

[57] K. Sistanizadeh. Proposed Canonical Loops for ADSL and Their Loss Characteristics. In *ANSI T1E1.4 Committee Contribution, No. 91-116*, August 1991.

[58] D.L. Waring, J.W. Lechleider, and T.R. Hsing. Digital Subscriber Line Technology Facilitates a Graceful Transition from Copper to Fiber. *IEEE Communications Magazine*, 29(3):96–104, March 1991.

[59] J.W. Lechleider. High Bit Rate Digital Subscriber Lines: A Review of HDSL Progress. *IEEE Journal on Selected Areas in Communications*, 9(6):769–784, August 1991.

[60] R.K. Maxwell. Private communication. Amati Communications Corporation, March, 1993.

[61] Bell Communications Research. Generic Requirements for High-Bit-Rate Digital Subscriber Lines. *Bellcore Technical Advisory*, (TA-NWT-001210), October 1991. Issue 1.

[62] K. Sistanizadeh. A Tentative CSA Loop Population for Preliminary Studies of HDSL Transmission Schemes. In *ANSI T1E1.4 Committee Contribution*, September 1990.

[63] AT&T. Digital Data System: Channel Interface Specification. *Bell System Technical Reference*, (Pub. 62310), September 1983.

[64] J.J. Werner. The HDSL Environment. *IEEE Journal on Selected Areas in Communications*, 9(6):785–800, August 1991.

[65] M. Ho, J.M. Cioffi, and J.A.C. Bingham. A High-Speed Full-Duplex Multitone Echo Canceller. In *1993 International Conference on Communications*, Geneva, Switzerland, May 1993.

[66] D.G. Messerschmitt. Design Issues in the ISDN U-Interface Transceiver. *IEEE Journal on Selected Areas in Communications*, 4(8):1281–1293, November 1986.

[67] S.V. Ahamed, P.P. Bohn, and N.L. Gottfried. A Tutorial on Two-Wire Digital Transmission in the Loop Plant. *IEEE Transactions on Communications*, 29(11):1554–1564, November 1981.

[68] G.J. Pottie. Transmission Impairments for Asymmetric Digital Subscriber Lines. In *ANSI T1E1.4 Committee Contribution*, February 1991.

[69] S.H. Lin. Statistical Behavior of Multipair Crosstalk. *Bell Systems Technical Journal*, 59:956–974, July - August 1980.

[70] D.H. Morgen. Expected Crosstalk Performance of Analog Multichannel Subscriber Carrier Systems. *IEEE Transactions on Communications*, 23(2):240–245, February 1975.

[71] D.W. Lin. Wide-Band Digital Subscriber Access with Multidimensional Block Modulation and Decision-Feedback Equalization. *IEEE Journal on Selected Areas in Communications*, 7(6):996–1005, August 1989.

[72] Bell Communications Research. ISDN Basic Access Digital Subscriber Lines. *Bellcore Technical Reference*, (TR-TSY-000393), May 1988. Issue 1.

[73] J.T. Aslanis Jr. *Coding for Communication Channels with Memory.* PhD thesis, Stanford University, November 1989.

[74] P. Mertz. Model of Impulsive Noise for Data Transmission. *IRE Transactions on Communication Systems*, CS-9:130–137, June 1961.

[75] J.H. Fennick. Amplitude Distributions of Telephone Channel Noise and a Model for Impulse Noise. *The Bell System Technical Journal*, 48:3243–3263, December 1969.

[76] R.M. Fano. A Theory of Impulse Noise in Telephone Networks. *IEEE Transactions on Communications*, 25(6):577–588, June 1977.

[77] NYNEX Corp. Characteristics of Impulse Noise on Selected NYNEX Metropolitan Loops. In *ANSI T1D1.3 Committee Contribution, No. 86-144*, 1986.

[78] S.J.M. Tol and W. van der Bijl. Measured Performance of ISDN Transmission in the Dutch Local Telephone Network. In *Proceedings of ISSLS '86*, Tokyo, Japan, September 1986.

[79] K.J. Kerpez. A Model for the Probability Distribution of the Length of Burst Errors Caused by Impulse Noise. In *ANSI T1E1.4 Committee Contribution, No. 91-165*, November 1991.

[80] K.T. Foster and J.W. Cook. A Symbolic Pulse for Impulsive Noise Testing. In *ANSI T1E1.4 Committee Contribution, No. 92-143*, Portland, OR, August 1992.

[81] J.S. Chow and R.R. Hunt. Impulse Nose Measurements for DMT System. In *ANSI T1E1.4 Committee Contribution, No. 92-201*, Anaheim, CA, December 1992.

[82] K.T. Foster. Impulse Noise Test Results for Three Example HDSL Systems. In *ETSI STC TM3 WT1.1 Contribution, Temporary Document, No. 27*, Vienna, Austria, September 1992.

[83] L.M. Smith and H. Zoetman. CAP-Based HDSL Test and Simulation Results - Impulse Noise. In *ETSI STC TM3 WT1.1 Contribution, Temporary Document, No. 33*, Vienna, Austria, September 1992.

[84] P.G. Potter and B.M. Smith. Statistics of Impulsive Noise Crosstalk in Digital Line Systems on Multipair Cable. *IEEE Transactions on Communications*, 33(3):259–270, March 1985.

[85] J.W. Modestino, C.S. Massey, R.E. Bollen, and R.P. Prabhu. Modeling and Analysis of Error Probability Performance for Digital Transmission Over the Two-Wire Loop Plant. *IEEE Journal on Selected Areas in Communications*, 4(8):1317–1330, November 1986.

[86] K. Szechenyi. On the NEXT and Impulse Noise Properties of Subscriber Loops. In *1989 IEEE Global Telecommunications Conference*, pages 1569–1573, Dallas, November 1989.

[87] J.J. Werner. Impulse Noise in the Loop Plant. In *International Conference on Communications*, pages 1734–1737, Atlanta, GA, April 1990.

[88] M. Barton. Impulse Noise Performance of an Asymmetrical Digital Subscriber Lines Passband Transmission System. In *1992 IEEE Global Telecommunications Conference*, pages 32–35, Orlando, FL, December 1992.

[89] K.J. Kerpez. The Channel Capacity in the Presence of Impulse Noise. Submitted to *IEEE Transactions on Information Theory*, 1991.

[90] J.W. Modestino, D.H. Sargrad, and R.E. Bollen. Use of Coding to Combat Impulse Noise on Digital Subscriber Loops. *IEEE Transactions on Communications*, 36(5):529–537, May 1988.

[91] K.J. Kerpez. Forward Error Correction for Asymmetric Digital Subscriber Lines (ADSL). In *1991 IEEE Global Telecommunications Conference*, pages 56.2.1–56.2.5, Phoenix, AZ, December 1991.

[92] K.J. Kerpez. Coding for ADSL. In *ANSI T1E1.4 Committee Contribution, No. 92-153*, Portland, OR, August 1992.

[93] D.H. Sargrad and J.W. Modestino. Errors-and-Erasures Coding to Combat Impulse Noise on Digital Subscriber Loops. *IEEE Transactions on Communications*, 38(8):1145–1155, August 1990.

[94] J.W. Lechleider. Impulse Noise Cancellation for ADSL. In *ANSI T1E1.4 Committee Contribution, No. 92-154*, Portland, OR, August 1992.

[95] J.W. Lechleider. An Adaptive Impulse Noise Canceler for Digital Subscriber Lines. In *1992 IEEE Global Telecommunications Conference*, pages 36–39, Orlando, FL, December 1992.

[96] M.S.B. Romdhane and V.K. Madisetti. Self-Correcting Decision Feedback Equalization (SCDFE) for Impulsive Channels. Submitted to *IEEE Transactions on Communications*, 1993.

[97] J.T. Aslanis, P.T. Tong, and T.N. Zogakis. An ADSL Proposal for Selectable Forward Error Correction with Convolutional Interleaving. In *ANSI T1E1.4 Committee Contribution, No. 92-180*, Portland, OR, August 1992.

[98] J. Hagenauer and E. Lutz. Forward Error Correction Coding for Fading Compensation in Mobile Satellite Channels. *IEEE Journal on Selected Areas in Communications*, 5(2):215–225, February 1987.

[99] B. Widrow and S.D. Stearns. *Adaptive Signal Processing*. Prentice-Hall, Englewood Cliffs, NJ, 1985.